New Operation Tools for Improving Flexibility and Reliability of Systems with Variable Resources and Storage Devices

Final Project Report

M-32

Power Systems Engineering Research Center

Empowering Minds to Engineer
the Future Electric Energy System

New Operation Tools for Improving Flexibility and Reliability of Systems with Variable Resources and Storage Devices

Final Project Report

Project Team
X. Andy Sun, Project Leader
Sakis Meliopoulos
Georgia Institute of Technology

Le Xie
Texas A&M University

Graduate Students
Alvaro Lorca
Evangelos Polymeneas
Orestis Vasios
Georgia Institute of Technology

Anupam Thatte
Sadegh Modarresi
Texas A&M University

PSERC Publication 17-02

September 2017

For information about this project contact:

X. Andy Sun
H. Milton Stewart School of Industrial & Systems
Engineering Georgia Institute of Technology
Atlanta, Georgia 30332-0250
Phone: 404-385-7574
E-mail: andy.sun@isye.gatech.edu

Power Systems Engineering Research Center

The Power Systems Engineering Research Center (PSERC) is a multi-university Center conducting research on challenges facing the electric power industry and educating the next generation of power engineers. More information about PSERC can be found at the Centers website: http://www.pserc.org.

For additional information, contact:

Power Systems Engineering Research
Center Arizona State University
577 Engineering Research
Center Tempe, Arizona
85287-5706
Phone: 480-965-1643
Fax: 480-727-2052

Notice Concerning Copyright Material

Acknowledgments

This is the final report for the Power Systems Engineering Research Center (PSERC) research project M-32 titled New Operation Tools for Improving Flexibility and Reliability of Systems with Variable Resources and Storage Devices.

The authors wish to recognize their postdoctoral researchers and graduate students that contributed to the research and creation of the reports:

Georgia Institute of Technology:
Alvaro Lorca
Evangelos Polymeneas
Orestis Vasios

Texas A & M University:
Anupam Thatte
Mohammad Sadegh Modarresi

The authors thank all PSERC members for their technical advice on the project, especially (the companies shown were as of time of this project work):

Eugene Litvinov, ISO-NE
Tongxin Zheng, ISO-NE
Hong Chen, PJM
Jim Price, CAISO
Aftab Alam, CAISO
Li Zhang, MISO
Nivad Navid, MISO
Harvey Scribner, SPP
Robert Entriken, EPRI
Evangelos Farantatos, EPRI
Eamonn Lannoye, EPRI
Xing Wang, Alstom Grid
Gary Gu, GE Energy Management
Nikhil Kumar, GE Energy
Feng Gao, Ventyx-ABB
Phil Markham, Southern Company Generation
Prashant Kansal, AEP
Zhenhua Wang, AEP

Executive Summary

The real-time economic dispatch (ED) in the current practice relies on a combination of optimization tools and operating rules. The dominant optimization tools used in practice for ED are deterministic models, which dispatch the power system to satisfy a single forecast value of future demand and renewable uncertain output, and keep reserve capacities to account for unexpected disturbance or outages. With the presence of significant variable resources such as wind and solar power, system operators will frequently face undesirable conditions such as lack of reserves, insufficient ramping capabilities, and cycling of thermal units as the variable resources experience sudden strong drop of output. Under these conditions, the real-time electricity markets may suffer temporary price spikes. These risky scenarios have already occurred in the US as well as other major electricity markets in the world. To deal with reserve and ramp shortages, the current operation tools restrict system operators to a limited set of actions such as increasing reserve margins, deploying fast-start units, and out-of-market dispatch. These actions usually incur high costs, create market distortions, and do not guarantee high level of system reliability.

With the recent advances in storage technologies, grid-level storage devices are becoming a viable re- source to participate in system operation. Energy storage systems, such as utility-scale batteries, pumped hydro, and demand-side response can be important resources for providing flexibility into the system. How to best deploy and operate different types of energy storage systems and demand response resources and to assess their economic value in a system with significant variable resources is an important issue for utilities and system operators.

Facing these challenges and opportunities, system operators have recently started looking into new operational models for their economic dispatch and real-time energy markets. This also motivates the central objective of this project to provide a set of new operational tools for operators to improve system flexibility as well as reliability and at the same time to maintain an efficient energy market. This requires us to develop new optimization tools, uncertainty modeling methods, and system flexibility and reliability metrics that can be integrated into the operational model.

In this project, we have focused on adaptive robust optimization as the central paradigm for optimization under uncertainty, and developed new dispatch tools that improve robustness of the dispatch operation for large-scale systems. In particular, robust optimization provides several features that are particularly appealing to applications in power systems. For instance, robust optimization seeks to optimize system performance in a controlled manner against the worst-case scenario, which is consistent with the philosophy of operational practice; robust optimization can provide a rigorous way to identify the worst-case or near worst-case scenarios out of practically infinitely many potential scenarios, rather than restricting to a finite, usually small, number of preselected scenarios; robust optimization also offers a data-driven approach to model uncertainty, which scales well with the increasing dimension of data.

The final report is consisted of three parts, reflecting the three main objectives of the project: 1) Develop new robust optimization models and uncertainty modeling tools for real-time dispatch and day-ahead unit commitment; 2) Develop new metrics for quantifying power system

flexibility in real-time operation and construct new market models for the procurement of flexibility from flexible resources; 3) Develop new and more accurate models for flexible components, including energy storage, responsive demand, distributed energy resources, and ramp-constrained generation, in AC look-ahead OPF, and develop new tools for remedial action and contingency filtering for real-time security analysis.

1. Part I first develops two-stage robust optimization based models for multi-period economic dispatch and proposes a new type of uncertainty modeling method, called the *dynamic uncertainty sets*, for modeling temporal and spatial correlations of wind and solar power. Part I also develops a simulation platform which combines the proposed robust economic dispatch model with statistical prediction tools in a rolling horizon framework. Extensive computational experiments are conducted on this platform using real wind data. The results are promising and demonstrate the benefits of the proposed approach in both reducing cost and increasing system reliability over existing robust optimization models as well as recent look-ahead dispatch models. Part I then turns to the unit commitment problem and studies effective algorithms for solving the two-stage robust optimization model for the unit commitment problem. Part I also provides insight to the worst-case uncertainty scenarios for the robust UC problem both under static and dynamic uncertainty sets.

2. Part II focuses on developing flexibility metrics and market construct for improving flexibility in power systems. It first develops a new probabilistic metrics, called the *lack of ramp probability* (LORP), for quantifying power system flexibility in real-time dispatch. LORP determines the level of risk of ramp capacity shortage associated with a dispatch decision. The LORP metric can also be used independently of the proposed robust dispatch model, to assess the system flexibility under existing and other proposed real-time economic dispatch models, such as conventional dispatch, look-ahead dispatch and dispatch with ramp capability constraints. Part II then proposes a two-step multi-period robust optimization based framework as a market construct for the procurement of flexibility from various flexible resources while observing inter-zonal transmission constraints.

3. Part III focuses on expanding the modeling of the short-term look-ahead dispatch to include new flexible components, such as energy storage, responsive demand, distributed energy resources, and ramp-constrained generation, as well as more accurate network models. Part III also proposes two remedial action schemes to resolve infeasibility in AC OPF with flexible devices. Finally, at a given optimal solution, a filtering & analysis framework is developed for identifying critical outages with a lowered computational cost.

Project Publications:

[1] Lorca, A.; and A. Sun. “Adaptive Robust Optimization and Dynamic Uncertainty Sets for Multiperiod Economic Dispatch with Significant Wind.” IEEE Transactions on Power Systems 2016.

[2] Thatte, A. A.; and L. Xie. “A Metric and Market Construct of Inter-temporal Flexibility in Time- coupled Economic Dispatch.” IEEE Transactions on Power Systems 2015.

[3] Polymeneas, E.; and A.P. Meliopoulos. "Aggregate Equivalent Models of Flexible Distribution Sys- tems for Transmission-Level Studies." IEEE Power and Energy Society General Meeting, Denver, Colorado, July 26-30, 2015.

[4] Meliopoulos, A.P.; E. Polymeneas and R. Huang. "Flexible Resource Optimization to Mitigate Operational Problems from Variable Generation." PowerTech 2015, Eidhoven, Netherlands, June 29-July 2, 2015.

[5] Thatte, A.; A. Sun, and L. Xie. 'Robust Optimization Based Economic Dispatch for Managing System Ramp Requirement." 47th Annual Hawaii International Conference on System Sciences (HICSS-47), pgs. 2344-2352, Waikoloa, Hawaii, January 6-9, 2014.

[6] Thatte, A.; and L. Xie. "A Two-layered Framework for Robust Dispatch with Transmission Constraints." 48th Annual Hawaii International Conference on System Sciences (HICSS-48), Kauai, Hawaii, January 5-8, 2015.

[7] Sun, A; and A. Lorca. "Adaptive Robust Optimization for Daily Power System Operation." Invited paper at 18th Power Systems Computation Conference (PSCC 2014), Wroclaw, Poland, August 18-22, 2014.

[8] Thatte, A. A; Li, Y and Xie, L. "Managing System Ramp Flexibility by Utilizing Price-Responsive Demand: An Empirical Assessment" 48th Annual Hawaii International Conference on System Sci- ences (HICSS-49), Hawaii, January 5-8, 2016.

[9] Sun. A. and A. Lorca. "Robust Optimization in Electric Power Systems Operations", invited chapter in *Integration of Large Scale Renewable Energy into Bulk Power Systems: From Planning to Opera- tion*, Eds. P. Du, R. Baldick, A. Tuohy. Springer. To appear, 2016.

Student Theses:

[1] Alvaro Lorca. *Robust Optimization for Renewable Energy Integration in Power System Operations*, PhD thesis, Georgia Institute of Technology, May 2016.

[2] Evangelos Polymeneas. *Optimal Operation and Security Analysis of Power Systems with Flexible Resources*, PhD thesis, Georgia Institute of Technology, May 2016.

[3] Orestis Vasios. *Optimal control of Thermostatically Controlled Loads*, PhD thesis, Georgia Institute of Technology, expected graduation date, end of 2018.

Part I

Robust Optimization Based New Tools for Improving Flexibility in Economic Dispatch and Unit Commitment

X. Andy Sun
Alvaro Lorca

Georgia Institute of Technology

For information about this project contact:

X. Andy Sun
H. Milton Stewart School of Industrial & Systems
Engineering Georgia Institute of Technology
Atlanta, Georgia 30332-0250
Phone: 404-385-7574
E-mail: andy.sun@isye.gatech.edu

Power Systems Engineering Research Center

The Power Systems Engineering Research Center (PSERC) is a multi-university Center conducting research on challenges facing the electric power industry and educating the next generation of power engineers. More information about PSERC can be found at the Centers website: http://www.pserc.org.

For additional information, contact:

Power Systems Engineering Research
Center Arizona State University
577 Engineering Research
Center Tempe, Arizona
85287-5706
Phone: 480-965-1643
Fax: 480-727-2052

Notice Concerning Copyright Material

PSERC members are given permission to copy without fee all or part of this publication for internal use if appropriate attribution is given to this document as the source material. This report is available for down- loading from the PSERC website.

Table of Contents

List of Figures

List of Tables

1. Adaptive Robust Optimization with Dynamic Uncertainty Sets for Look-ahead Economic Dispatch under Significant Wind

1.1 Introduction

The exceptional benefits of wind power as an environmentally responsible energy resource have led to the rapid increase of wind energy in power systems all over the world. At the same time, wind energy possesses some characteristics drastically different from conventional generating resources in terms of high stochasticity and intermittency in production output. Due to this, deep penetration of wind power will introduce significant uncertainty to the short-term and real-time operation of power systems, in particular, to the day-ahead unit commitment (UC) and the real-time economic dispatch (ED) procedures. If the uncertainty of such variable resources is not managed properly, the system operator may have to face severe operating conditions such as insufficient ramping capabilities from the conventional generating resources due to the sudden strong loss of wind power, complicated by other contingencies, load surge, and transmission congestions [11]. These arising challenges call for new methods and models for power systems operation, and have attracted significant interests from both the electricity industry and academia.

The current UC and ED procedures rely on a combination of optimization tools and operational rules. The main optimization models used for UC and ED are deterministic models, where the uncertainties, such as demand, are assumed to take nominal forecast values. To deal with unexpected contingencies and sudden demand surge, the deterministic optimization model is complemented by operational rules that require extra generation resources, the so-called reserves, to stay available for quick response. The discrepancy between the forecast and realization of uncertainty has been relatively small in power systems composed of conventional load and supply. However, as observed in the recent experience, operating power systems with high penetration of variable resources, especially wind power, requires new methods to deal with uncertainty. See [47] for an overview of the challenges of integrating wind in power systems from the perspective of UC, ED, frequency regulation and planning.

Facing these challenges, both industry and academia have devoted much effort to improving the current ED practice. In particular, dynamic dispatch models with look-ahead capabilities have gained renewed interests. The basic ideas can be traced back to [2] and [35]. Recent works have made significant advancement. [48] presents a look-ahead ED model with new statistical methods for wind forecast. The Midcontinent ISO has proposed look-ahead ED models with ramping products [29]. And [30] studies the selection of spinning reserve requirements under generation outages and forecast errors of demand and wind power. All these models can be characterized as deterministic ED models. Their simple optimization structure, improved performance, and closeness to the current operation make them appealing candidates to impact industry practice. This motivates the present chapter to propose further advances and compare with these promising models.

Stochastic optimization has been a popular approach and extensively studied in the literature especially for the day-ahead unit commitment operation. For example, [39] proposes one of the first stochastic UC models. [41,44] propose security constrained UC models and consider stochastic wind power generation. [8] presents a short-term forward electricity market-clearing model

under net load uncertainty, for the purpose of allowing high penetrations of wind power while keeping the system secure. [27] deals with the selection of spinning and nonspinning reserves through a market-clearing model under stochastic wind power generation. [40] presents a stochastic UC model for significant wind and shows the benefits of more frequent planning and over a deterministic approach. [33] studies reserve requirements for wind integration using a stochastic UC model. [32] proposes multiarea stochastic UC models for high wind penetration. [42] proposes a chance-constrained two-stage stochastic UC for systems with wind power uncertainty.

Regarding stochastic ED, the literature is much less extensive. [20] presents a stochastic programming model without recourse actions for a single-period ED problem. [24] presents a stochastic model of a single-period ED problem under post-contingency frequency constraints. [51] presents a chance-constrained look-ahead ED model where the probability of incurring lost load is constrained and a sampling based scenario approximation approach is used for dealing with wind power randomness, however, transmission constraints are not considered in this work to ease computational burden. We would like to note that UC and ED have quite significant differences in decision structures and therefore modeling considerations: the UC has a relatively clear two-stage decision making structure, whereas for ED, the modeling choices are more diverse. Constructing a stochastic ED model with proper decision structure and desirable computational properties merits further research efforts. The literature in this respect still leaves much room for new contributions.

Recently, robust optimization has emerged as an alternative methodology for optimization under uncertainty [3, 4]. Robust optimization provides several features that are particularly appealing to applications in power systems. In particular, the robust optimization approach seeks to optimize system performance in a controlled manner against the worst-case scenario, which is indeed consistent with the philosophy of the current operational practice; robust optimization provides a data-driven way to model uncertainty, which scales well with the increasing dimension of data and is flexible and practical for many situations; robust optimization models are usually computationally tractable for large-scale systems.

Recent works have proposed robust optimization models for UC problems [5, 16, 37, 54, 56]. [37] provides a robust formulation for the contingency constrained UC problem. [16], [5], [56] present two-stage adaptive robust models, with commitment decisions in the first stage and dispatch decisions in the second stage. In [5] a two-stage robust UC model with security constraints is formulated and tested on the power system operated by ISO New England. [16] deals with a formulation including pumped storage hydro under wind power output uncertainty. Hybrid models and alternative objectives have also been explored to mitigate the conservativeness of the robust solution [18, 52]. Efficient solution methods for the two-stage robust UC have been proposed [5, 16, 23, 50]. Recently, [23] presents acceleration techniques based on cutting planes and column generation for solving the two-stage robust UC problem under full transmission line constraints.

On the other hand, the benefits of robust optimization for the ED operation has not been fully explored. [57] presents a two-stage robust ED model for a single-period regulation dispatch problem, where the first stage corresponds to dispatch and regulation capacity decisions, and the second stage corresponds to the dispatch of automatic generation control (AGC), after observing demand. [15] recently proposes a robust optimal power flow model using affine policies for the AGC dispatch under renewable energy uncertainty. Affine policy is an approximation to the fully adap-

tive policy used in [57]; however, as argued in [15], affine dependence on uncertainty may be a more suitable form for AGC dispatch. The work in [49] applies two advanced statistical methods for wind forecasting, and integrates these models with a robust look-ahead ED. However, their model is of a static robust nature, which lacks the adaptability of a two-stage robust model proposed here; their model also relies on the existing types of uncertainty sets, which will be significantly improved by a new type of uncertainty sets proposed in this chapter.

If we try to summarize the above works, we can draw the following observations: 1) there is a great amount of interests to improve the ED practice; in particular, the recently developed look-ahead ED models have attracted considerable attention in both academia and industry; 2) the existing works on power system operation under uncertainty have focused on UC problems in a day-ahead operating environment, while both stochastic and robust ED models are relatively less explored; 3) the existing robust UC and ED models have used a similar type of uncertainty sets, which we call *static* uncertainty sets, whereas it is important to start considering uncertainty sets that can capture the highly dynamical and correlated variable resources such as wind power.

In this chapter, we propose new robust optimization models for system dispatch under high wind penetration. In particular, the contributions of our work are summarized below:

1. We propose a two-stage adaptive robust optimization model for the multi-period ED, which has a different decision structure from the existing two-stage robust UC and robust ED models. The proposed robust ED model is designed for a rolling-horizon operational framework to model the real time ED process.

2. We introduce a new type of uncertainty sets, the *dynamic uncertainty sets*, as a modeling technique to account for the dynamic relationship between uncertainties across decision stages. Such uncertainty sets explicitly model temporal and spatial correlations in variable sources. We also propose a data-driven approach to construct such dynamic uncertainty sets, which is simple to implement in practice.

3. We develop a comprehensive simulation platform, which integrates the proposed robust ED model with statistical procedures for constructing dynamic uncertainty sets using real-time data. Extensive experiments are performed on this platform.

The chapter is organized as follows. Section 1.2 introduces dynamic uncertainty sets and discusses practical construction methods. Section 1.3 proposes the adaptive robust multi-period ED model and solution methods. Section 1.4 presents the simulation platform and the evaluation framework. Section 1.5 shows extensive computational experiments to demonstrate the effectiveness of our approach. Finally, Section 1.6 concludes.

1.2 Dynamic uncertainty sets

In robust optimization, uncertainty is modeled through uncertainty sets, which are the building blocks of a robust optimization model and have direct impact on its performance. We may summarize three criteria for constructing uncertainty sets as follows. A well constructed uncertainty set

should 1) capture the most significant aspects of the underlying uncertainty, 2) balance robustness and conservativeness of the robust solution, and 3) be computationally tractable.

1.2.1 Static uncertainty sets

Previous works on robust UC have focused on static uncertainty sets, and have treated uncertainty resources of different characteristics in an aggregated, indistinguishing way, see for example [5, 16, 56]. More specifically, consider the following uncertainty set for net demand vector $\boldsymbol{d}_t = (d_{1t}, ..., d_{N^d t})$:

$$\mathcal{D}_t = \Bigg\{ \boldsymbol{d_t} : \sum_{j \in \mathcal{N}^d} \frac{|d_{jt} - \overline{d}_{jt}|}{\hat{d}_{jt}} \leq \Gamma^d \sqrt{N^d}, \\ d_{jt} \in [\overline{d}_{jt} - \Gamma^d \hat{d}_{jt}, \overline{d}_{jt} + \Gamma^d \hat{d}_{jt}] \; \forall \, j \in \mathcal{N}^d \Bigg\}, \tag{1.1}$$

where $\mathcal{N}^d, N^d$ denote the set and the number of loads, and d_{jt} is the net demand of load j at time t. According to (1.1), d_{jt} lies in an interval centered around the nominal value $\overline{d}_{jt}$ with a width determined by the deviation $\hat{d}_{jt}$. Further, the size of the uncertainty set is controled by Γ^d. If $\Gamma^d = 0$, $\mathcal{D}^t = \{\overline{\boldsymbol{d}}_t\}$, corresponding to a singleton set of the nominal demand. As Γ^d increases, more demand vectors are contained in the uncertainty set, thus increasing the protection of the robust solution against larger demand variations.

The above uncertainty set is called *static* uncertainty set, because the uncertainties at later time periods are *independent* of those in earlier periods. That is, the dynamics of uncertainty evolution over time is not explicitly captured. Some recent work proposed additional budget constraints over time periods (e.g. [16, 56]). The modified uncertainty set imposes a coupling of uncertainty between time periods and uncertain sources, however, similar to (1.1), it still does not directly characterize the temporal and spatial correlations of uncertainty; also, by coupling through the entire horizon, the realization of uncertainty breaks the time causality with past depending on the future realization. Yet another drawback of existing models is that uncertain sources of different nature are treated indistinguishably. For example, the uncertainty characteristics of wind power output are different from those of the conventional load, yet the existing proposals consider aggregated net load as the primitive uncertainty [5, 16, 56]. Demand uncertainty is usually much less pronounced and less dynamic than wind, therefore, a static uncertainty set as (1.1) is an appropriate model. However, it is important to explore well suited uncertainty models for wind, specially for high level penetration of such variable resources.

1.2.2 Dynamic uncertainty sets

To explicitly model the correlation between multiple uncertain resources within one time period as well as the dynamics of each uncertain resource evolving over time periods, we propose the

following general form of uncertainty sets, called *dynamic uncertainty sets*: For each time t,

$$\Xi_t(\boldsymbol{\xi}_{[1:t-1]}) = \left\{\boldsymbol{\xi}_t : \exists \boldsymbol{u}_{[t]} \text{ s.t. } f(\boldsymbol{\xi}_{[t]}, \boldsymbol{u}_{[t]}) \leq \mathbf{0}\right\}, \tag{1.2}$$

where $\boldsymbol{\xi}_{[t_1:t_2]} \triangleq (\boldsymbol{\xi}_{t_1}, \ldots, \boldsymbol{\xi}_{t_2})$ and in shorthand $\boldsymbol{\xi}_{[t]} \triangleq \boldsymbol{\xi}_{[1:t]}$. In (1.2), the uncertainty vector $\boldsymbol{\xi}_t$ explicitly depends on uncertainty at stages before time t and the $\boldsymbol{u}$'s are auxiliary variables, $f(\boldsymbol{\xi}_{[t]}, \boldsymbol{u}_{[t]})$ is a vector of convex functions that characterize the dynamics of uncertainty evolution. For the uncertainty set to be computationally tractable, f should be semi-definite representable [3].

As an illustrative example, the dynamic uncertainty set could represent a dynamic interval for $\boldsymbol{\xi}_t$:

$$\boldsymbol{\xi}_t \in \left[\underline{\boldsymbol{\xi}}_t(\boldsymbol{\xi}_{[t-1]}), \overline{\boldsymbol{\xi}}_t(\boldsymbol{\xi}_{[t-1]})\right],$$

where the upper and lower bounds of the interval at time t, namely $\underline{\boldsymbol{\xi}}_t(\boldsymbol{\xi}_{[t-1]})$ and $\overline{\boldsymbol{\xi}}_t(\boldsymbol{\xi}_{[t-1]})$, are functions of uncertainty realizations in previous time periods, rather than fixed values as in static uncertainty sets (1.1).

A simple and useful specialization of (1.2) is the linear dynamic uncertainty set, given as

$$\sum_{\tau=1}^{t} (\boldsymbol{A}_\tau \boldsymbol{\xi}_\tau + \boldsymbol{B}_\tau \boldsymbol{u}_\tau) \leq \mathbf{0}, \tag{1.3}$$

which mimics linear dynamics and is also computationally tractable. In the following, we will propose a specific method for constructing linear dynamic uncertainty sets using time series analysis tools.

1.2.3 Constructing dynamic uncertainty sets for wind power

The proposed dynamic uncertainty set (1.2) is very general. In this section, we present a specific method to construct a dynamic uncertainty set for wind power using linear systems (1.3). The key idea is to fuze time series models with the concept of dynamic uncertainty sets.

We denote the wind speed vector of multiple wind farms at time t as $\boldsymbol{r}_t = (r_{1t}, \ldots, r_{N^w t})$, where r_{it} is the wind speed at wind farm i and time t. Define the dynamic uncertainty set for $\boldsymbol{r}_t$ as:

$$\begin{aligned}
\mathcal{R}_t(\boldsymbol{r}_{[t-L:t-1]}) = \Big\{\boldsymbol{r}_t :\ & \exists\, \widetilde{\boldsymbol{r}}_{[t-L:t]},\ \boldsymbol{u}_t \quad \text{s.t.} \\
& \boldsymbol{r}_\tau = \boldsymbol{g}_\tau + \widetilde{\boldsymbol{r}}_\tau \quad \forall \tau = t-L, \ldots, t && \text{(1.4a)} \\
& \widetilde{\boldsymbol{r}}_t = \sum_{s=1}^{L} \boldsymbol{A}_s \widetilde{\boldsymbol{r}}_{t-s} + \boldsymbol{B}\boldsymbol{u}_t && \text{(1.4b)} \\
& \sum_{i \in \mathcal{N}^w} |u_{it}| \leq \Gamma^w \sqrt{N^w} && \text{(1.4c)} \\
& |u_{it}| \leq \Gamma^w \qquad \forall i \in \mathcal{N}^w && \text{(1.4d)}
\end{aligned}$$

$$\boldsymbol{r}_t \geq \mathbf{0}\Big\}, \tag{1.4e}$$

where vectors $\boldsymbol{r}_{t-L}, \ldots, \boldsymbol{r}_{t-1}$ are the realizations of wind speeds in periods $t-L, \ldots, t-1$. Eq. (2.17a) decomposes wind speed vector $\boldsymbol{r}_\tau$ as the sum of a seasonal pattern $\boldsymbol{g}_\tau$, which is pre-estimated from wind data, and a residual component $\widetilde{\boldsymbol{r}}_\tau$ which is the deviation from $\boldsymbol{g}_\tau$. Eq. (2.17b) is the key equation that represents a linear dynamic relationship involving the residual $\widetilde{\boldsymbol{r}}_t$ at time t, residuals realized in earlier periods $t-L$ to $t-1$, and an error term $\boldsymbol{u}_t$. The parameter L sets the relevant time lags. In Eq. (2.17b), matrices $\boldsymbol{A}_s$'s capture the temporal correlation between $\boldsymbol{r}_t$ and $\boldsymbol{r}_{t-s}$, and $\boldsymbol{B}$ specifically captures the spatial relationship of wind speeds at adjacent wind farms at time t. Eq. (2.17c)-(2.17d) describe a budgeted uncertainty set for the error term $\boldsymbol{u}_t$, where Γ^w controls its size, and (2.17e) avoids negative wind speeds. $\mathcal{N}^w$ and N^w denote the set and number of wind farms, respectively.

Using the above uncertainty sets (2.17) for wind speeds, we can further construct dynamic uncertainty sets for wind power through power curve approximations. In particular, we denote the *available wind power* of wind farm i at time t as $\overline{p}^w_{it}$. Given the wind speed r_{it}, $\overline{p}^w_{it}$ is described by the following constraints

$$\overline{p}^w_{it} \geq h^0_{ik} + h_{ik}\, r_{it} \quad \forall i \in \mathcal{N}^g,\, k = 1, \ldots, K, \tag{1.5}$$

where parameters h^0_{ik}, h_{ik} are determined based on a convex piecewise linear approximation with K pieces of the increasing part of the power curve at wind farm i (in our experiments, we use the power curve of GE 1.5MW wind turbine to approximate the aggregated output of a wind farm). Although (1.5) allows available wind power to exceed $\max_k\{h^0_{ik} + h_{ik} r_{it}\}$, the robust optimization model described in Section 1.3 will always ensure that the available wind power lies on the power curve including the plateau part for wind speed exceeding a cut-off value.

The dynamic uncertainty set of the available wind power $\overline{\boldsymbol{p}}^w_t$ is thus defined as

$$\begin{aligned}\overline{\mathcal{P}}^w_t(\boldsymbol{r}_{[t-L:t-1]}) = \Big\{ \overline{\boldsymbol{p}}^w_t :\ & \exists \boldsymbol{r}_t \in \mathcal{R}_t(\boldsymbol{r}_{[t-L:t-1]}) \\ & \text{s.t. (1.5) is satisfied} \Big\},\end{aligned} \tag{1.6}$$

based on which we can define the uncertainty set for the trajectory of available wind power in time periods 2 through T, namely $\overline{\boldsymbol{p}}^w = (\overline{\boldsymbol{p}}^w_2, \ldots, \overline{\boldsymbol{p}}^w_T)$, as

$$\begin{aligned}\overline{\mathcal{P}}^w = \Big\{ (\overline{\boldsymbol{p}}^w_2, \ldots, \overline{\boldsymbol{p}}^w_T) :\ & \exists (\boldsymbol{r}_2, \ldots, \boldsymbol{r}_T) \text{ s.t. } \boldsymbol{r}_t \in \mathcal{R}_t(\boldsymbol{r}_{[t-L:t-1]}) \\ & \text{and (1.5) is satisfied for } t = 2, \ldots, T \Big\},\end{aligned} \tag{1.7}$$

which is used in the robust ED model.

As a summary, we propose dynamic uncertainty sets (2.17) and (1.6) to capture the intrinsic temporal dynamics and spatial correlations of the wind power. We also distinguish wind power uncertainty from conventional demand uncertainty, which is modeled by traditional uncertainty sets (1.1). The proposed dynamic uncertainty set formulation (1.2) is quite general. The specific models for wind speed (2.17) and wind power (1.6) present one example for its implementation.

Other models may be constructed using more sophisticated statistical tools. For example, the coefficient matrices $\boldsymbol{A}_s$ and $\boldsymbol{B}$ can be made time dependent as $\boldsymbol{A}_{st}$ and $\boldsymbol{B}_t$ using dynamic vector autoregression methods. Also, $\boldsymbol{r}_t$ can be replaced by a nonlinear transformation of wind speed to improve estimation accuracy. However, there is always a tradeoff between model complexity and performance. Our experiments show the above simple models (2.17)-(1.7) achieve a substantial improvement over existing static uncertainty sets. See more discussion in Section 1.4.1 for parameter estimation and possible extensions for the dynamic uncertainty sets.

1.3 Adaptive robust economic dispatch formulation and solution method

1.3.1 Mathematical formulation

In this section, we propose an adaptive robust optimization model for the multi-period ED problem. In particular, the ED problem with T time periods is formulated as a two-stage adaptive robust model in the following way. The first-stage of the robust ED model comprises the current time period $t = 1$, while the second-stage comprises future time periods $t = 2, ..., T$. In the first-stage, the decision maker observes demand and available wind power at the current time period, and determines the dispatch solution, which will be implemented right away for time $t = 1$. Given the first-stage decision, the second-stage of the robust ED model computes the worst-case dispatch cost for the remaining time periods in the dispatch horizon. The overall robust ED model minimizes the total cost of dispatch at the current time period and the worst-case dispatch cost over the future periods.

We denote $\boldsymbol{x} = (\boldsymbol{p}_1^g, \boldsymbol{p}_1^w)$ as the vector of first-stage dispatch decisions, composed of generation of thermal units ($\boldsymbol{p}_1^g$) and wind farms ($\boldsymbol{p}_1^w$). Note that we allow wind generation to be dispatchable. The uncertainty includes both conventional load $\boldsymbol{d} = (\boldsymbol{d}_2, \ldots, \boldsymbol{d}_T) \in \mathcal{D}$ described by (1.1) and the available wind power $\overline{\boldsymbol{p}}^w = (\overline{\boldsymbol{p}}_2^w, \ldots, \overline{\boldsymbol{p}}_T^w) \in \overline{\mathcal{P}}^w$ described by the dynamic uncertainty set (1.7). The second-stage decisions are dispatch solutions $\boldsymbol{y} = (\boldsymbol{p}_t^g, \boldsymbol{p}_t^w, \forall t = 2, \ldots, T)$.

Mathematically, the two-stage robust multi-period ED model is formulated as follows,

$$\min_{\boldsymbol{x} \in \Omega_1^{det}} \left\{ \boldsymbol{c}^\top \boldsymbol{x} + \max_{\boldsymbol{d} \in \mathcal{D}, \overline{\boldsymbol{p}}^w \in \overline{\mathcal{P}}^w} \min_{\boldsymbol{y} \in \Omega(\boldsymbol{x}, \boldsymbol{d}, \overline{\boldsymbol{p}}^w)} \boldsymbol{b}^\top \boldsymbol{y} \right\}, \tag{1.8}$$

where the first and second-stage costs are defined as

$$\begin{aligned} \boldsymbol{c}^\top \boldsymbol{x} &= \sum_{i \in \mathcal{N}^g} C_i^g p_{i1}^g + \sum_{i \in \mathcal{N}^w} C_i^w p_{i1}^w \\ \boldsymbol{b}^\top \boldsymbol{y} &= \sum_{t=2}^{T} \left(\sum_{i \in \mathcal{N}^g} C_i^g p_{it}^g + \sum_{i \in \mathcal{N}^w} C_i^w p_{it}^w \right), \end{aligned}$$

where $\mathcal{N}^g$ denotes the set of generators, and C_i^g, C_i^w denote the variable costs of thermal generators and wind farms. We use linear dispatch costs, but it is straightforward to extend to piecewise linear approximations of nonlinear cost functions.

The feasible region Ω_1^{det} of the first-stage decision variables corresponds to the constraints of a single-period dispatch problem, that is

$$\Omega_1^{det} = \Bigg\{ \boldsymbol{x} = (\boldsymbol{p}_1^g, \boldsymbol{p}_1^w) : \ \underline{p}_{i1}^g \le p_{i1}^g \le \overline{p}_{i1}^g \quad \forall\, i \in \mathcal{N}^g \tag{1.9a}$$

$$0 \le p_{i1}^w \le p_i^{w,max} \quad \forall\, i \in \mathcal{N}^w \tag{1.9b}$$

$$p_{i1}^w \le \overline{p}_{i1}^{w,det} \quad \forall\, i \in \mathcal{N}^w \tag{1.9c}$$

$$-RD_i^g \le p_{i1}^g - p_{i0}^g \le RU_i^g \quad \forall\, i \in \mathcal{N}^g \tag{1.9d}$$

$$-RD_i^w \le p_{i1}^w - p_{i0}^w \le RU_i^w \quad \forall\, i \in \mathcal{N}^w \tag{1.9e}$$

$$\left|\boldsymbol{\alpha}_l^\top (\boldsymbol{E}^g \boldsymbol{p}_1^g + \boldsymbol{E}^w \boldsymbol{p}_1^w - \boldsymbol{E}^d \boldsymbol{d}_1^{det})\right| \le f_l^{max} \ \forall\, l \in \mathcal{N}^l \tag{1.9f}$$

$$\sum_{i \in \mathcal{N}^g} p_{i1}^g + \sum_{i \in \mathcal{N}^w} p_{i1}^w = \sum_{j \in \mathcal{N}^d} d_{j1}^{det} \Bigg\}, \tag{1.9g}$$

where $\underline{p}_{it}^g, \overline{p}_{it}^g$ are the minimum and maximum power outputs of thermal generator i at time t; $p_i^{w,max}$ is the maximum power output at wind farm i, representing the cut-off level of the power curve; $\overline{p}_{i1}^{w,det}$ denotes the available wind power of wind farm i observed at current time $t = 1$; RD_i^g, RU_i^g are the ramp-down and ramp-up rates of thermal generators (similarly, RD_i^w, RU_i^w for wind farms); $\mathcal{N}^l$ is the set of transmission lines; $\boldsymbol{\alpha}_l$ is the network shift factor for line l; $\boldsymbol{E}^d, \boldsymbol{E}^g, \boldsymbol{E}^w$ are the network incidence matrices for loads, thermal generators and wind farms; f_l^{max} is the flow limit on line l; d_{j1}^{det} denotes the observed electricity demand at load j and time $t = 1$. Constraints (1.9a), (1.9b) and (1.9c) enforce generation limits for thermal generators and wind farms, with (1.9c) ensuring that generation of wind farms does not exceed the available wind power at time $t = 1$. (1.9d) and (1.9e) enforce ramping rate limits for thermal generators and wind farms. (1.9f) represents line flow limits. (1.9g) represents energy balance.

Constraints in the second-stage problem are parameterized by the first-stage decision variables and uncertain parameters realized in the uncertainty sets. The feasible region of the second-stage dispatch decison $\boldsymbol{y} = (\boldsymbol{p}_t^g, \boldsymbol{p}_t^w, \forall t = 2, \ldots, T)$ is defined as

$$\Omega(\boldsymbol{x}, \boldsymbol{d}, \overline{\boldsymbol{p}}^w) = \Bigg\{ \boldsymbol{y} : \ \text{s.t.} \ \forall t = 2, \ldots, T$$

$$\underline{p}_{it}^g \le p_{it}^g \le \overline{p}_{it}^g \quad \forall\, i \in \mathcal{N}^g, \tag{1.10a}$$

$$0 \le p_{it}^w \le p_i^{w,max} \quad \forall\, i \in \mathcal{N}^w, \tag{1.10b}$$

$$p_{it}^w \le \overline{p}_{it}^w \quad \forall\, i \in \mathcal{N}^w, \tag{1.10c}$$

$$-RD_i^g \le p_{it}^g - p_{i,t-1}^g \le RU_i^g \quad \forall\, i \in \mathcal{N}^g, \tag{1.10d}$$

$$-RD_i^w \le p_{it}^w - p_{i,t-1}^w \le RU_i^w \quad \forall\, i \in \mathcal{N}^w, \tag{1.10e}$$

$$\left|\boldsymbol{\alpha}_l^\top (\boldsymbol{E}^g \boldsymbol{p}_t^g + \boldsymbol{E}^w \boldsymbol{p}_t^w - \boldsymbol{E}^d \boldsymbol{d}_t)\right| \le f_l^{max} \ \forall\, l \in \mathcal{N}^l \tag{1.10f}$$

$$\sum_{i \in \mathcal{N}^g} p_{it}^g + \sum_{i \in \mathcal{N}^w} p_{it}^w = \sum_{j \in \mathcal{N}^d} d_{jt} \Bigg\}, \tag{1.10g}$$

where (1.10a)-(1.10g) are similar constraints as in (1.9), except that they are enforced for each time period $t = 2, \ldots, T$. Notice that (1.10b)-(1.10c) ensure that the dispatched wind generation is upper bounded by the minimum between the cut-off level $p_i^{w,max}$ and the available wind power $\overline{p}_{it}^{w}$. Also note that the first-stage dispatch decision is involved in constraints (1.10d)-(1.10e) to satisfy ramping constraints.

A few remarks are in order. First, (1.8) is a fully adaptive robust optimization model, namely the second-stage dispatch decision adapts to every realization of the uncertainty in the best possible way, which is similar to the existing robust UC model proposed in [5]. Second, there is a key difference between the two-stage structure of the proposed robust ED (1.8) and the existing two-stage robust UC models. In particular, the decision stages of (1.8) correspond to the actual time periods, so that the first-stage decision can be directly used in the dispatch at the current period, and the dispatch decisions in the second stage can be re-optimized in the following periods. In comparison, the two-stage robust UC models have UC decisions in the first stage and dispatch decisions in the second stage, both for the *entire horizon*. Third, the two-stage structure of the robust ED model makes it convenient to incorporate into the real-time dispatch procedure. In particular, the robust ED model can be implemented in a rolling horizon framework; the dynamic uncertainty sets can also be updated periodically when new information is available. Fourth, the use of the DC power flow is consistent with the industry practice [12] and recent works in robust ED [15, 57]. AC power flow feasibility can be enforced by introducing an AC power flow module. Thus, to emphasize the key proposal of the chapter, we keep with the simple DC power flow model. Fifth, the robust ED model can also readily include convex piecewise linear costs.

1.3.2 Solution method

Several methods have been reported in the literature for solving two-stage adaptive robust optimization problems [5, 16, 50]. In [16], a Benders decomposition approach is proposed to solve the outer level problem and an exact method for the second-stage problem. In [50], a constraint and column generation (C&CG) technique is proposed and rigorously analyzed; an exact method using mixed-integer reformulations is proposed for the second-stage problem. [5] proposes a Benders decomposition framework for the outer level and a heuristic method for the second-stage problem. To speed up the Benders decomposition, [5, Section IV] also proposes a heuristic idea to add extreme points of the uncertainty sets and associated dispatch constraints to the outer level problem, which is similar to the C&CG technique in [50].

Problem (1.8) can be equivalently stated as:

$$\min_{\boldsymbol{x},\eta} \left\{ \boldsymbol{c}^\top \boldsymbol{x} + \eta : \ \eta \geq Q(\boldsymbol{x}), \ \boldsymbol{x} \in \Omega_1^{det} \right\}, \tag{1.11}$$

with

$$Q(\boldsymbol{x}) = \max_{\boldsymbol{\xi} \in \Xi} \ \min_{\{\boldsymbol{y}: \ \boldsymbol{G}\boldsymbol{y} \geq \boldsymbol{h} - \boldsymbol{E}\boldsymbol{x} - \boldsymbol{M}\boldsymbol{\xi}\}} \ \boldsymbol{b}^\top \boldsymbol{y}, \tag{1.12}$$

where $\boldsymbol{\xi} = (\boldsymbol{d}, \overline{\boldsymbol{p}}^w)$, $\Xi = \mathcal{D} \times \overline{\mathcal{P}}^w$, and the feasible region $\{\boldsymbol{y} : \boldsymbol{G}\boldsymbol{y} \geq \boldsymbol{h} - \boldsymbol{E}\boldsymbol{x} - \boldsymbol{M}\boldsymbol{\xi}\}$ represents

the dispatch constraints in (1.10). Problem (1.11) is equivalent to:

$$\min_{\boldsymbol{x}\in\Omega_1^{det},\,\eta,\,\{\boldsymbol{y}_l\}} \quad \boldsymbol{c}^\top\boldsymbol{x}+\eta \tag{1.13a}$$

$$\text{s.t.} \quad \eta \geq \boldsymbol{b}^\top\boldsymbol{y}_l \quad \forall\, l \tag{1.13b}$$

$$\boldsymbol{E}\boldsymbol{x}+\boldsymbol{G}\boldsymbol{y}_l \geq \boldsymbol{h}-\boldsymbol{M}\boldsymbol{\xi}_l^* \quad \forall\, l, \tag{1.13c}$$

where $\{\boldsymbol{\xi}_l^*\}_{l=1}^M$ is the set of extreme points of Ξ, and for each l, $\boldsymbol{y}_l$ is a vector of second-stage decisions associated to $\boldsymbol{\xi}_l^*$. (1.13) is the outer level problem, which shows a nice structure suitable for constraint generation. Indeed, (1.13) can be efficiently solved by adding $(\boldsymbol{\xi}_l^*, \boldsymbol{y}_l)$ and the associated constraints iteratively [50].

In every iteration of this algorithm, $Q(\boldsymbol{x})$ must be evaluated, which involves solving a non-convex max-min problem. Previous work has dealt with this problem using outer-approximation techniques [5] and exact methods based on mixed-integer programming (MIP) reformulations [16, 50, 56]. As will be demonstrated in the computational experiments (Section 1.5.5), the MIP method is time consuming for solving (1.12). Instead, we apply a simple "alternating direction algorithm" [22]. Taking the dual over the inner $\min$ in (1.12) we obtain

$$Q(\boldsymbol{x}) = \max_{\boldsymbol{\xi}\in\Xi,\boldsymbol{\pi}\in\Pi} \quad \boldsymbol{\pi}^\top(\boldsymbol{h}-\boldsymbol{E}\boldsymbol{x}-\boldsymbol{M}\boldsymbol{\xi}), \tag{1.14}$$

where $\Pi = \{\boldsymbol{\pi} \geq \boldsymbol{0} : \boldsymbol{\pi}^\top\boldsymbol{G} = \boldsymbol{b}\}$. For this *bilinear* program with separate polyhedral feasible regions Ξ and Π, the alternating direction algorithm optimizes over $\boldsymbol{\pi}$ with $\boldsymbol{\xi}$ fixed, then over $\boldsymbol{\xi}$ with $\boldsymbol{\pi}$ fixed, and alternates; each of these iterations solves a linear program which achieves the optimum at an extreme point of the corresponding polyhedron Ξ or Π. The alternating algorithm is formally presented below.

Algorithm 1 Alternating Direction (AD) algorithm

```
Start with some ξ' ∈ Ξ
repeat
    Solve (∗): C ← max_{π∈Π} π^⊤(h − Ex − Mξ')
    if C < ∞ then
        Let π' be an optimal solution of (∗)
        Solve C' ← max_{ξ∈Ξ} π'^⊤(h − Ex − Mξ) and let ξ' be its optimal solution
    else
        C' ← ∞
    end if
until C' = ∞ or C' − C ≤ δ
output: C' as estimate of Q(x) with solution ξ'
```

This alternating direction method always converges to a KKT point of (1.14). The proof is omitted to save space. Section 1.5.5 also shows empirical evidence that this heuristic achieves good solution quality and fast convergence on the second-stage problem, comparing to the MIP method.

The overall two-level algorithm is presented in Fig. 1.1.

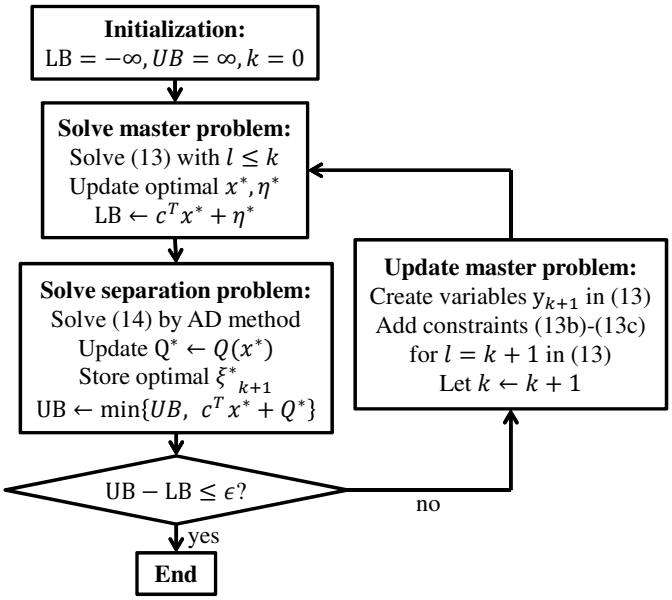

Figure 1.1: Flow chart for the overall two-level algorithm.

1.4 Simulation platform and evaluation metrics

In this Section, we describe the simulation platform and evaluation metrics for the proposed robust model. The motivation is to have a realistic simulation environment that integrates the dispatch optimization model with data analysis procedures which dynamically update the parameters in the optimization and uncertainty models. Fig. 1.2 illustrates the simulation process.

The simulation process is implemented in a rolling horizon framework. At each time period, the robust ED model is solved over a time window of T time periods. The first-stage dispatch solution for the current time period is implemented, while the second-stage dispatch solutions for remaining periods are not materialized; the time horizon rolls forward by one time interval, where new realizations of demand and available wind power are observed, and dynamic uncertainty sets are periodically re-estimated and updated with the new observations (see Section 1.4.1). In order to focus the comparison on the ED policies, the simulation process uses a simplified UC schedule where all thermal generators are on all the time. In the future, we would like to extend the simulation framework to integrate UC decisions into the policy evaluation.

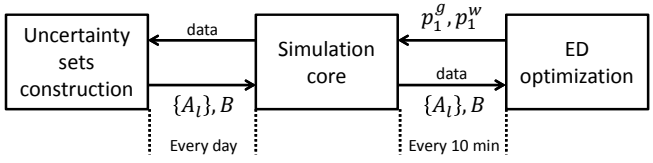

Figure 1.2: Simulation platform integrating ED optimization engine and data analysis tools for uncertainty model construction.

We compare different ED models by evaluating the average and standard deviation (std) of the production cost for every 10 minutes dispatch interval, which includes both generation cost and

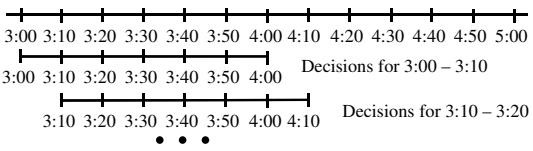

Figure 1.3: Concept of rolling horizon with 10 minute time periods and $T = 6$

penalty cost resulting from the use of expensive fast-start units or load shedding.

1.4.1 Estimating the parameters of the dynamic uncertainty set for wind speeds

In order to estimate the parameters of model (2.17), consider the following time series model:

$$\boldsymbol{r}_t = \boldsymbol{g}_t + \widetilde{\boldsymbol{r}}_t \quad \forall t \tag{1.15a}$$

$$\widetilde{\boldsymbol{r}}_t = \sum_{s=1}^{L} \boldsymbol{A}_s \widetilde{\boldsymbol{r}}_{t-s} + \boldsymbol{\epsilon}_t \quad \forall t, \tag{1.15b}$$

where $\boldsymbol{r}_t$ is the vector of wind speeds at time t, $\boldsymbol{g}_t$ corresponds to a deterministic seasonal pattern, and $\widetilde{\boldsymbol{r}}_t$ corresponds to the deviation of $\boldsymbol{r}_t$ from $\boldsymbol{g}_t$. In this model, $\widetilde{\boldsymbol{r}}_t$ follows a multivariate autoregressive process of order L, determined by the innovation process $\{\boldsymbol{\epsilon}_t\}$, where $\boldsymbol{\epsilon}_t$ is a vector of normal random variables with mean $\mathbf{0}$ and covariance matrix $\boldsymbol{\Sigma}$, and vectors $\boldsymbol{\epsilon}_t$ are independent across different time periods.

Once seasonal patterns have been identified, parameter $\boldsymbol{g}_t$ can be determined. For example, daily and semi-daily seasonalities could be used. In such a case, using a 10 min time interval we would have $g_{it} = a_i + b_i \cos(\frac{2\pi t}{24\times 6}) + c_i \sin(\frac{2\pi t}{24\times 6}) + d_i \cos(\frac{2\pi t}{12\times 6}) + e_i \sin(\frac{2\pi t}{12\times 6})$ (since 24×6 is the number of time periods in a day). Parameters a_i, b_i, c_i, d_i, e_i can be estimated using linear regression [48].

The parameters of the autoregressive component $\widetilde{\boldsymbol{r}}$, namely the matrices $\boldsymbol{A}_s$ and $\boldsymbol{\Sigma}$, can be estimated using statistical inference techniques developed for time series [34], for which many computational packages are available. $\boldsymbol{B}$ in (2.17) is obtained from the Cholesky decomposition of $\boldsymbol{\Sigma}$.

The linear dynamic model (2.17) and the associated estimation method are appealing in their simple structure, which serves well our goal to demonstrate the concept of dynamic uncertainty sets. Computational results also confirm their promising performance. Meanwhile, it is worth noting that the framework of dynamic uncertainty sets is flexible enough to incorporate more sophisticated statistical models, such as the ones proposed in [28], where autoregressive processes are fitted to nonlinearly transformed wind speeds. Using a piecewise linear approximation similar to the one proposed in (1.5), but this time for the transformed wind speed and wind power output, a dynamic uncertainty set can be again constructed using linear constraints.

1.5 Computational experiments

We conduct extensive computational experiments on the simulation platform to compare the proposed robust ED model and dynamic uncertainty sets with existing robust and deterministic dispatch models. The experiments are performed on the 14-bus and 118-bus IEEE test systems, both of which are modified to incorporate significant wind penetration. In the following, we introduce the detailed data for the 14-bus system, and present test results in Sections 1.5.1 to 1.5.5. The test results on the 118-bus system give a similar picture as the 14-bus system. The details are given in Section 1.5.6.

Table 1.1 summarizes P_{min}, P_{max}, 10-min ramping rates, and production costs of all three generators in the 14-bus system. The total generation capacity is 500MW. The system has 20 transmission lines and 11 conventional loads. The daily system demand is between 132.6MW and 319.1MW with an average of 252.5MW. The system has 4 wind farms, each with a capacity of 75MW (equivalent of 50 units of GE 1.5MW wind turbines). The total power output at each wind farm is approximated by a piecewise linear function of wind speed using the power curve data [13].

Table 1.1: Thermal generators in 14-bus system

Gen	**Pmax (MW)**	**Pmin (MW)**	**Ramp (MW/10min)**	**Cost ($/MWh)**
1	300	50	5	20
2	100	10	10	40
3	100	10	15	60

The wind speed data is obtained from [9] for four geographically adjacent locations with a 10-minute data interval. The average wind speeds at the four wind farms are 4.8, 5.6, 5.1, 5.5 m/s, respectively. Using the power curve, the average total available wind power is 104.2 MW, equivalent to a 34.7% capacity factor, which is about 32.7% of peak demand and 20% of conventional generation capacity, representing a realistically high level of wind penetration. After removing stationary components, wind speeds at different sites present strong auto and cross correlation at several lags, which implies that the temporal and spatial dependencies are significant.

The proposed robust ED model has 9 time periods with a 10-min interval for each period (i.e. 1.5-hour look ahead). The robust ED model is evaluated on the simulation platform in the rolling-horizon framework. In particular, it is solved every 10 minutes over 35 days, for which real wind data is used for all wind farms. On each of the 35 days, the simulation engine updates the parameters of the dynamic uncertainty sets (2.17) using the available wind data up to that day. The penalty cost is $C^+ = 6000$ \$/MWh for under-generation, and $C^- = 600$ \$/MWh for over-generation [32, 52].

The simulation platform is implemented in a Python environment, interfaced with Cplex 12.5. Each robust ED takes less than a second to solve, and the entire simulation of 5040 periods takes about 40 minutes on a PC laptop with an Intel Core i3 at 2.1 GHz and 4GB memory.

Before presenting details, we first give a summary of the experiments and main results. We compare the proposed robust ED with dynamic uncertainty sets versus (1) deterministic look-ahead

dispatch and its variant with reserve rules; (2) robust dispatch with static uncertainty sets. The experiments show that adaptive robust ED with dynamic uncertainty sets significantly outperforms both alternative models by substantially reducing average production cost, the variability of the costs, and the probability of shortage events. Our experiments also show that the robust ED provides a *Pareto frontier* for the tradeoff between cost and reliability, which provides an informative guideline for choosing uncertainty set parameters and system operating points.

1.5.1 Robust ED versus look-ahead ED

In this section, we compare the proposed adaptive robust ED (Rob-ED) with the deterministic look-ahead dispatch (LA-ED). The robust ED model uses dynamic uncertainty sets (2.17) and (1.6) with 6 time lags i.e. $L = 6$. The parameter Γ^w controls the size of the uncertainty sets. Notice that when $\Gamma^w = 0$, the uncertainty set contains only one path of the forecasted wind speeds, the robust ED thus reduces to the LA-ED model.

Cost and reliability performance

Table 1.2 shows the performance of the two models: Column 2 for LA-ED, and Columns 3 to 7 for Rob-ED with different Γ^w's. The best average total cost of the Rob-ED model is achieved at $\Gamma^w = 0.5$, where the average cost of Rob-ED is 7.1% lower than that of LA-ED; at the same time, Rob-ED is able to reduce the standard deviation of the cost by 41.2%. We can also see that as Γ^w increases to 1.0, the robust ED can reduce the std of cost by 82.1%, with the average cost reduced by 3.75%. The shortage event frequency of the robust ED model is decreased by up to 80.1% and the associated penalty cost is reduced by 97.3% at $\Gamma^w = 1.0$. The change in penalty costs also implies that Rob-ED incurrs less amount of constraint violation than LA-ED, when penalty occurs. The results show that the robust ED model is effective at improving economic efficiency and reducing risk associated with the dispatch solution, where the risk exactly comes from the highly uncertain wind power. As will be shown in Section 1.5.6, more significant savings on cost and improvement over reliability are achieved for the 118-bus system.

Table 1.2: Performance of robust and deterministic ED

	LA-ED	Rob-ED				
Γ^w	**0.0**	0.1	0.3	**0.5**	0.7	**1.0**
Total Cost Avg ($)	**771.1**	758.5	734.0	**716.0**	718.2	**742.2**
Total Cost Std ($)	**1231**	1172	1000	**723**	513	**221**
Penalty Avg ($)	**88.2**	77.1	54.2	**30.6**	15.8	**2.4**
Penalty Freq (%)	**1.41**	1.21	0.95	**0.67**	0.46	**0.28**

Operational insights

We also want to gain some insights about the operational characteristics of the robust model. Table 1.3 shows average thermal generation (Therm avg) and wind generation (Wind avg) of the two

Table 1.3: Operational Aspects of Robust and Deterministic ED

	LA-ED	Rob-ED				
Γ^w	**0.0**	0.1	0.3	**0.5**	0.7	**1.0**
Therm avg (MW)	**164.6**	165.2	167.5	**171.7**	178.6	**191.1**
Wind avg (MW)	**87.9**	87.2	85.0	**80.8**	74.0	**61.5**

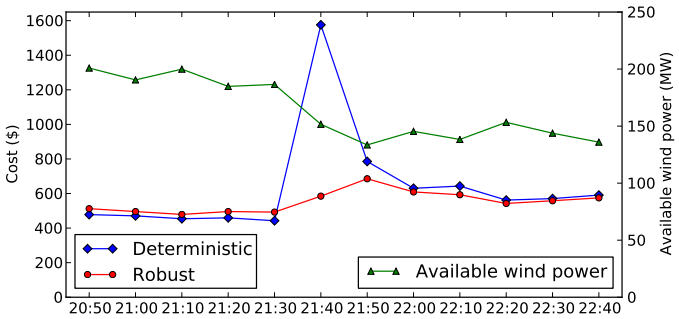

Figure 1.4: A snapshot of the product cost of LA-ED and Rob-ED with $\Gamma^w = 0.5$ when available wind power suddenly drops down.

models. We can see that the robust ED model on average tends to increase the use of thermal generation and curtail wind output: At $\Gamma^w = 0.5$, Therm avg is up by 4.3% and Wind avg down by 8.1%, comparing to LA-ED; at $\Gamma^w = 1.0$, Therm avg is up by 16.1% and Wind avg is down by 24.9%.

Fig. 1.4 shows a typical snapshot from simulation. Available wind power starts a fast and large drop at 21:30PM (green curve), the deterministic LA-ED runs short of ramping capacity and incurs a spike of penalty cost (blue curve), while the system under robust ED is much less affected by this sudden wind event (red curve). The example shows that when the system has significant wind penetration, properly balancing wind and thermal generation becomes very important for system reliability.

The insight is the following. The two-stage robust ED computes wind scenarios over the future periods that are the most detrimental to the system, and makes the optimal dispatch solution to prepare the system against these scenarios. The worst-case wind scenarios often correspond to scenarios with large wind variation between periods as shown in Fig. 1.4. The robust ED model hedges against the potential large swing of wind by increasing thermal generation and moderately curtailing some wind output. In this way, the system maintains enough ramping capability to deal with potential sudden loss of available wind power. The balance between thermal and wind generation is controlled by the value of Γ^w of the uncertainty sets as shown in Table 1.3. In other words, the robust ED determines the optimal ramping schedule of thermal generators, rather than resorting to prefixed operation rules.

Table 1.4: Performance of look-ahead ED with reserve

	LA-ED	Res-LA-ED			Rob-ED
ResFactor (%)	0	2.5	5	10	$\Gamma^w = 0.5$
Cost Avg ($)	771.1	770.0	773.3	790.3	716.0
Cost Std ($)	1231	1223.8	1211.8	1155.1	723
Penalty Avg ($)	88.2	86.7	84.8	71.6	30.6
Penalty Freq (%)	1.41	1.45	1.69	1.35	0.67

Comparing to look-ahead ED with reserve

Reserve is an engineering approach to handle net load uncertainty in a deterministic ED model. Typically, when UC is solved, reserve levels for the next day are co-optimized, and later in real time operation, reserves are used in cases of unexpected net load variations and other contingencies. Consider the following look-ahead ED model with reserve requirement (Res-LA-ED). The LA-ED model is complemented with reserve variables $R_{it} \in [0, \overline{R}_{it}]$, equations (1.9a) and (1.10a) are replaced by

$$\underline{p}^g_{it} \leq p^g_{it} \leq \overline{p}^g_{it} - R_{it} \quad \forall\, i \in \mathcal{N}^g,\, t = 1, \ldots, T,$$

and the following reserve requirement constraints are added:

$$\sum_{i \in \mathcal{N}^g} R_{it} \geq R^{req}_t \quad \forall\, t = 1, \ldots, T.$$

We test the performance of this model for different reserve requirement levels R^{req}_t. We select R^{req}_t as a fraction of the total forecasted net load at time t (i.e. forecast of total demand minus total available wind power), and modify this proportion, denoted as "ResFactor" [32]. Table 1.4 presents the performance of Res-LA-ED under different values of ResFactor, as well as that of Rob-ED with $\Gamma^w = 0.5$.

From these results we can see that this reserve rule can improve the performance of LA-ED in both cost effectiveness and reliability, when the reserve requirement is properly chosen (ResFactor at 2.5%). As ResFactor increases, the reliability (Cost Std) keeps improving with the tradeoff of an increasing Avg Cost; the penalty cost and frequency are also reduced.

If we compare Res-LA-ED with Rob-ED, we can observe that the performance of Rob-ED is significantly better than the best of the three Res-LA-ED test cases: the Cost Avg is reduced by at least 7.14% (against ResFactor $= 2.5\%$); the Cost Std is improved by at least 37.4% (against ResFactor $= 10\%$); the penalty cost is reduced by at least 57.2%, and the penalty frequency is reduced by at least 50.3% (both against ResFactor $= 10\%$).

1.5.2 Dynamic uncertainty sets versus static uncertainty sets

In this section, we compare adaptive robust ED equipped with dynamic uncertainty sets with the same robust ED model using static uncertainty sets. The goal is to study the benefits of dynamic uncertainty sets for modeling dynamic relations of wind power uncertainty across time stages and

spatial locations.

We use dynamic uncertainty sets (2.17) with $L = 6$ as before (denoted as "DUS"), and construct two static uncertainty sets: one ignores the temporal correlation in (2.17) (denoted as "SUS1"), the other further ignores spatial correlations (denoted as "SUS2"). Note that both SUS1 and SUS2 are special cases of the dynamic uncertainty sets for $L = 0$, i.e. the uncertainty sets at different time intervals are independent of each other. To have a fair comparison, both in SUS1 and SUS2, $\boldsymbol{g}_t$ is improved after estimating $\boldsymbol{B}$ to force a persistent forecast of wind speeds for the nominal trajectory (improving the accuracy of the nominal trajectory considered).

Fig. 1.5 plots the standard deviation of the cost per 10 minutes interval (x-axis) versus the average of this cost (y-axis) for DUS, SUS1 and SUS2 with different values of Γ^w. On each curve, the right most point corresponds to $\Gamma^w = 0$, i.e. the deterministic LA-ED model. As Γ^w increases, both the average and std of the cost start to decrease, then after a certain apex value of Γ^w around 0.4 to 0.5, the std keeps decreasing but the average cost starts to increase. This behavior endows a "U" shape for all three curves. Every point on the right half of the "U" shape for Γ^w smaller than the apex value can be strictly improved in both average and std of cost by increasing Γ^w, while every point on the left half of the "U" shape cannot be strictly improved without trading off between average and std of the cost. In other words, on the right half of the curve, each point is dominated by the points to its left, whereas on the left half, no point is dominated by any other. Therefore, the left part of each curve shows the *Pareto frontier* of cost vs std performance of the associated robust ED model. The system should be operated on the Pareto frontier. This provides an informative guideline for choosing a proper Γ^w.

Comparing the Pareto frontiers of the three uncertainty sets in Fig. 1.5, we can see that the dynamic uncertainty set has the lowest Pareto frontier, which means that to retain a same level of average cost, the robust ED with dynamic uncertainty sets achieves the lowest std (i.e. the highest reliability); or, to maintain a same level of std (i.e. reliability), the robust ED with dynamic uncertainty sets incurs the lowest cost. That is, robust ED with DUS *dominates* robust ED with static uncertainty sets. Between the two static uncertainty sets, SUS1 (that considers spatial correlation) dominates SUS2, which has neither temporal nor spatial correlation.

The static uncertainty set SUS2 is the first budgeted uncertainty set proposed in the literature [7] and has inspired its application in modeling net load uncertainty [5]. Works in [16, 56] further introduced budget constraints over time periods to limit the total variations of uncertain demand over the entire or part of the planning horizon. Now, we compare these static uncertainty sets with additional time budgets with DUS. It is worth emphasizing that the fundamental difference between DUS and SUS remains the same for DUS and SUS with time budgets.

We modify the uncertainty sets SUS1 and SUS2 with the following time budget constraint:

$$\sum_{t=2}^{T} \sum_{i \in \mathcal{N}^w} |u_{it}| \leq \Gamma^T \Gamma^w \sqrt{N^w} \sqrt{T-1},$$

where $T = 9$ is the number of periods in the multi-period Rob-ED, and time budget parameter $\Gamma^T = 0.5, 1, 2$. Note that static uncertainty sets without time budget are equivalent to one with very large time budget as $\Gamma^T \geq \sqrt{8}$, the time budget constraint becomes redundant.

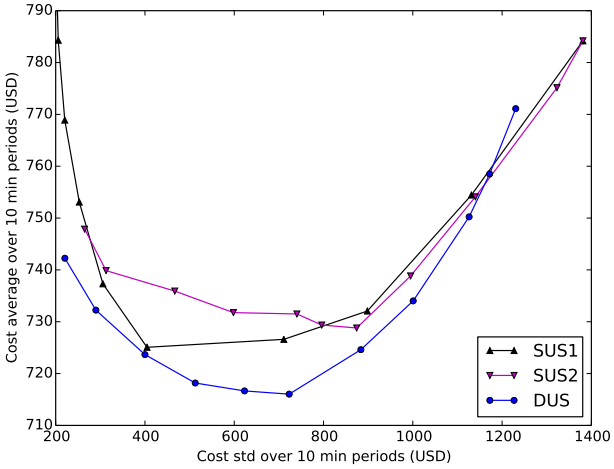

Figure 1.5: Cost std and cost average obtained for the policies determined by the different models with $\Gamma^w = 0.0, 0.1, ..., 1.0$

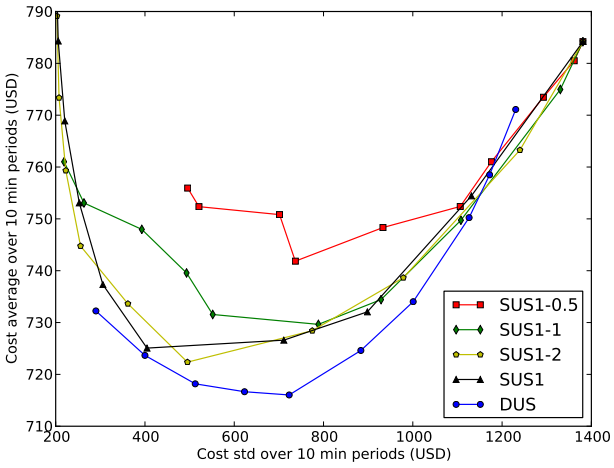

Figure 1.6: Cost std and cost average obtained for the policies determined by DUS and SUS1, with $\Gamma^T = 0.5, 1, 2$ for SUS1 and with $\Gamma^w = 0.0, 0.1, ..., 1.0$.

Fig. 1.6 plots the std of cost per 10 min interval (x-axis) versus the average of that cost (y-axis) for DUS and SUS1 with additional time budgets. The curve denoted by SUS1-0.5 means the SUS1 uncertainty set with time budget $\Gamma^T = 0.5$ and Γ^w varies from 0.0 to 1.0. Among the three curves based on SUS1 with time budgets, we can see that Rob-ED achieves a better Pareto frontier for higher values of time budget (the red curve for SUS1-0.5 is dominated by the green curve for SUS1-1, which is further dominated by SUS1-2). SUS1 without time budget (or equivalently with a time budget $\Gamma^T \geq \sqrt{8}$) has a frontier comparable to the SUS1-2. Furthermore, all four SUS1 based curves are clearly dominated by the DUS curve.

Fig. 1.7 presents a similar comparison for SUS2 with time budgets. Here, the dominance of DUS over static uncertainty sets with time budgets is more eminent.

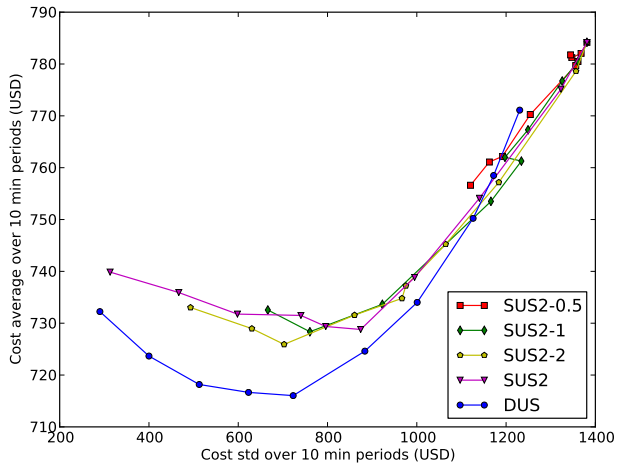

Figure 1.7: Cost std and cost average obtained for the policies determined by DUS and SUS2, with $\Gamma^T = 0.5, 1, 2$ for SUS2 and with $\Gamma^w = 0.0, 0.1, ..., 1.0$ for all policies

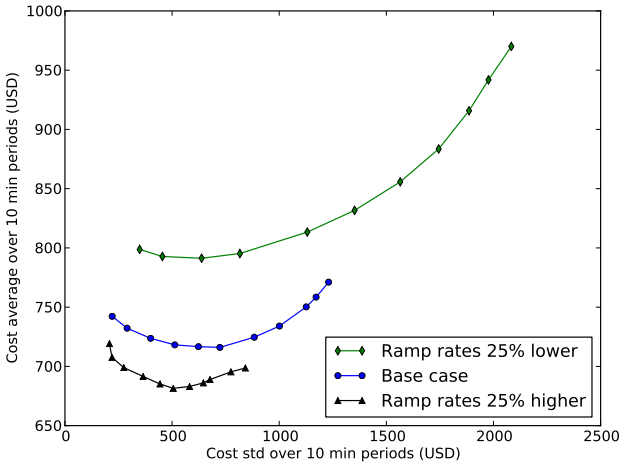

Figure 1.8: Cost std and cost average obtained for the Rob-ED with DUS for $\Gamma^w = 0.0, 0.1, ..., 1.0$, under modified ramping rates.

1.5.3 Impact of system ramping capacity

In this section, we study the relationship between system ramping capacity and the performance of robust ED models. The intuition is that higher ramping rates better prepare the system to deal with high variation of wind output. We want to see how much benefit the robust ED model provides under different system ramping capacities. Fig. 1.8 summarizes the computational results for three scenarios: base case with no change in ramping rates, and -25% or $+25\%$ change on each generator's ramping rates.

We can see that the robust ED model saves the average cost by 7.1% in the base case (the same numbers as in Section 1.5.1) comparing with the look-ahead ED; the saving increases to 21.2% for the reduced ramping case; even for the system with 25% more ramping for every generator, the robust ED still demonstrates a 3.7% saving in average cost over LA-ED. This demonstrates the clear benefit of Rob-ED over a wide range of system ramping conditions.

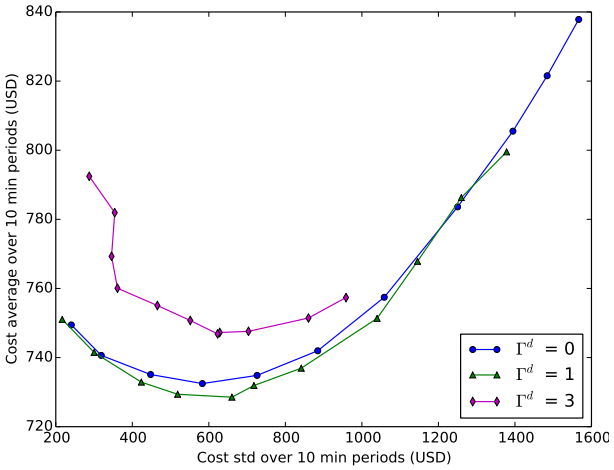

Figure 1.9: Cost std and average obtained by the Rob-ED with $\Gamma^w = 0.0, ..., 1.0$ and $\Gamma^d = 0, 1, 3$.

1.5.4 Considering both demand and wind uncertainty

In this section, we further incorporate traditional demand uncertainty into the robust ED model, using the static uncertainty sets (1.1), where $\overline{d}_{jt}$ and $\hat{d}_{jt}$ are selected as the mean and std of demand from previously realized values. The parameter Γ^d limits the total deviation of demand from its forecast. In simulation, the demand d_{jt} of each load j at each time period t is independently generated as a normal random variable with a std that equals a 5% of its mean, and is truncated to be nonnegative. Therefore, the generated random demand can be outside the uncertainty set. The choice of Γ^d controls the size of the demand uncertainty set.

Fig. 1.9 presents the performance of Rob-ED with dynamic uncertainty set for wind and static uncertainty sets (1.1) for load, at different values of Γ^d, Γ^w. At $\Gamma^d = 0$, the uncertainty set for demand is a singleton containing the forecast value, i.e. only wind uncertainty is considered (blue curve). By considering an uncertainty set for load with $\Gamma^d = 1$, the cost-reliability curve is shifted downward to the green curve, which consistently dominates the blue curve. The two curves are quite close though, which shows that wind is the dominating factor of uncertainty; the dynamic uncertainty set for wind significantly improves the system performance, while further incorporating load uncertainty improves the performance modestly. The purple curve for $\Gamma^d = 3$ shows that too much conservatism in the load uncertainty model leads to inferior solutions. It again demonstrates that properly choosing the level of conservativeness of the uncertainty sets is critical to getting the best performance of the robust ED model. In particular, the best robust ED policy obtained by setting $\Gamma^d = 1, \Gamma^w = 0.6$ reduces the average cost by 13.1% lower than that of the deterministic LA-ED with $\Gamma^d = \Gamma^w = 0$, and reduces the std of the cost by 58.1%. This makes the robust ED model very attractive.

1.5.5 Performance of the alternating direction method for solving the second-stage problem

As discussed in Section 1.3.2, the proposed algorithm requires solving a bilinear program (1.14) in each iteration of the outer master problem. Therefore, to practically tackle large-scale problems, a fast and reliable method for the inner problem is needed. An alternating direction (AD) method

is proposed in Section 1.3.2 for this purpose. In the literature, several exact MIP methods are proposed to solve the second-stage bilinear program (e.g. [16,50,56].) The MIP methods in [16,56] rely on the special structure of the uncertainty sets used in their models, which are not shared by the dynamic uncertainty sets. The exact MIP method proposed in [50] is based on the KKT conditions, which are applicable to general polyhedral uncertainty sets. Thus, we compare the AD algorithm to this MIP method.

In the experiment, we run the Rob-ED model in the rolling-horizon simulator for a 5-day horizon. This involves solving 720 Rob-ED models of the form (1.8), which amounts to 1592 inner bilinear programs (1.14). Every time, the bilinear program is solved by both the AD algorithm and the exact MIP method. We compare both running times and solution qualities.

The AD algorithm achieves convergence for all 1529 instances, and the average running time is 0.12s. The MIP method achieves convergence in 257 instances with an average time of 13.28s; for the remaining 1272 instances (83.2% of the total instances), the MIP method does not converge after 60s, and at that point the solution quality is still worse than the AD solutions (the objective value is on average 1.02% worse than the AD solutions). Those MIP instances exceeding 60s do not achieve much improvement after running for another 10 min. In terms of solution quality, the AD solutions on average obtain an optimality gap of 3.73% compared to the global optimum of the MIP solutions when MIP converges. These comparisons show that the AD algorithm is an effective and efficient heuristic for solving the bilinear program.

1.5.6 Tests on 118-bus system

Extensive simulation is also conducted on the 118-bus system. The results for this larger system support similar conclusions as shown in the 14-bus system. The 118-bus system has 54 generators of total 7220 MW generation capacity and 273.2 MW/10min system ramping capacity. There are 186 lines with flow limits ranging between 280 MW and 1000 MW, and 91 loads. Total electricity demand is between 2485.7 MW (3:30 am) and 5982.9 MW (8:20 pm) with an average of 4735.0 MW. There are 8 wind farms, each with a capacity $p^{w,max} = 750$ MW. The average total available wind power at any time is 1882.7 MW, equivalent to 31.5% of the peak demand. All the wind speeds used in simulation are real data collected from [9]. Each robust ED model can still be quickly solved in about 20 seconds in the laptop described before. For the simulation of 35-day rolling horizon with a 10-min interval, we use a computer cluster [36].

Table 1.5 shows the performance of the deterministic LA-ED and the Rob-ED with dynamic uncertainty sets of lags $L = 6$. From the table, we have the following observations:

(1) Rob-ED reduces the average cost by 43.4% $((15061 - 8528)/15061)$ at a properly chosen $\Gamma^w = 1.5$.

(2) Cost std is reduced by 87.7% at $\Gamma^w = 1.5$ and by 93.9% at $\Gamma^w = 2.0$.

(3) The average penalty cost is reduced by 98.4% or 60.7 times at $\Gamma^w = 1.5$ and is almost eliminated at $\Gamma^w = 2.0$. The frequency of penalty is 7.70% by LA-ED, and is reduced to 0.12% and 0.02% by Rob-ED at $\Gamma^w = 1.5$ and 2.0, respectively.

Table 1.5: Performance of LA-ED and Rob-ED for 118-bus system

	LA-ED	Rob-ED			
Γ^w	0.0	0.5	1.0	1.5	2.0
Cost Avg ($)	15061	12193	8914	8528	9075
Cost Std ($)	38138	30903	14671	4703	2325
Penalty Avg ($)	7775	4835	1214	126	1
Penalty Freq (%)	7.70	4.74	1.45	0.12	0.02
Therm Avg (MW)	2969	3007	3132	3399	3660
Wind Avg (MW)	1758	1723	1602	1336	1075

(4) Rob-ED dispatches more thermal and curtails more wind. On average, the thermal generation is up by 12.7% and 18.9%, and the wind generation is down by 24% and 38.9%, at $\Gamma^w = 1.5$ and 2.0, respectively. This can be explained by a similar reasoning given in Section 1.5.1, namely that the robust ED dispatches the thermal generation anticipating to a potential large drop of wind in the future, optimally balancing thermal and wind generation in the system.

Comparing to the 14-bus system, the above results for the 118-bus system show a more significant benefit of the proposed Rob-ED model: the average operating cost is cut to almost half of the look-ahead ED, the cost variability is reduced by an order of magnitude, and the shortage events and penalty cost are almost eliminated. Table 1.5 also shows a Pareto frontier exists for the range of Γ^w between 1.5 to 2.0.

1.6 Conclusion

In this chapter, we present an adaptive multi-period robust ED model and dynamic uncertainty sets for power system economic dispatch under high penetration levels of wind resources. The adaptive multi-period robust ED model mimics the physical dispatch procedure by using a two-stage decision making structure and a rolling-horizon framework. Dynamic uncertainty sets explicitly model the relationship between uncertainties across decision stages and capture the temporal and spatial correlations of wind power output in multiple wind farms: the proposed dynamic uncertainty sets with linear dynamics in this chapter have general and computationally tractable structure; and the proposed data-driven estimation procedures are easy to implement. We also develop a simulation platform that integrates the optimization engine and data analysis tools for updating uncertainty sets.

Extensive simulation using real wind data shows that the proposed robust ED framework outperforms look-ahead ED models with and without reserves which recently attracted considerable interests in practice, and robust ED models with static uncertainty sets. Both cost efficiency and system reliability are substantially improved. Also, the robust ED model gives an entire Pareto frontier of operating cost and reliability, which provides an informative guideline for choosing uncertainty set parameters and system operating points. The proposed robust ED model and dynamic uncertainty sets are flexible enough to incorporate several extensions, such as using transformed

wind speeds, bids with piecewise linear costs, and including other types of uncertain renewable energy sources.

2. New Algorithms and Worst-Case Analysis for Adaptive Robust Unit Commitment

2.1 Introduction

With the increasing penetration of renewable energy resources, power system operators face new challenges in managing significant generation uncertainty in day-ahead and real-time markets. One of the most critical operational problems facing such challenges is the unit commitment (UC) problem. Great attention has recently been drawn to design new optimization models and algorithms for the UC problem that produce both high economic efficiency and system reliability under increasing uncertainty.

In the current industry practice, the UC problem is modelled and solved as a large-scale deterministic mixed-integer program (MIP). The commitment status of generating units are scheduled to balance the net load forecasted for the next day. Renewable resources such as wind and solar power are intrinsically stochastic and intermittent. As a traditional approach to deal with uncertainties in load forecast and contingencies, system operators require additional generating resources, called reserves, to be online or quickly available [14]. The system operator can also adjust the level of reserves according to the system operating status.

In the recent work [6], we propose a two-stage adaptive robust optimization model and solution methods for the security-constrained unit commitment problem. Computational experiments on the power system operated by the ISO New England demonstrate that the robust UC model can significantly reduce operating costs and improve system reliability, comparing to the widely used deterministic UC model with adjustable reserves. Related models have been studied in several papers, e.g. [17, 43, 53, 55, 56]. For a recent review, see [38]. A significant extension of the two-stage robust model to a general multistage adaptive robust UC model is proposed and systematically studied in [26]. New data-driven approaches for constructing uncertainty sets to model dynamic relationships between uncertainties and decisions are proposed in [25] and [10].

The focus of this chapter is to provide deeper exploration on several important issues in the modeling and solution methods of the two-stage robust UC and economic dispatch (ED) formulation. In particular, Section 2.2 presents the robust UC model. Section 2.3 proposes a general budget uncertainty model and compares exact and heuristic methods for solving the second-stage problem. Section 2.4 explores the properties of the worst case scenarios identified by the robust model. Section 2.5 introduces dynamic uncertainty sets and studies worst case scenarios of wind power in a two-stage robust economic dispatch problem. Section 2.6 concludes the chapter.

2.2 Two-Stage Adaptive Robust Unit Commitment

The two-stage adaptive robust UC model is formulated as follows:

$$\min_{\boldsymbol{x}\in X}\left\{\boldsymbol{c}^\top\boldsymbol{x}+\max_{\boldsymbol{d}\in\mathcal{D}}\min_{\boldsymbol{y}\in Y(\boldsymbol{x},\boldsymbol{d})}\boldsymbol{b}^\top\boldsymbol{y}\right\}. \tag{2.1}$$

In this formulation, X is the feasible region for the unit commitment variables $(x^o_{it}, x^+_{it}, x^-_{it})_{i,t}$:

$$
\begin{aligned}
X = \Big\{ & (\boldsymbol{x}^o, \boldsymbol{x}^+, \boldsymbol{x}^-) \in \{0,1\}^{3N_g T} : \\
& x^o_{it} - x^o_{i,t-1} = x^+_{it} - x^-_{it} \quad \forall\, i \in \mathcal{N}_g,\, t \in \mathcal{T}, && \text{(2.2a)} \\
& \sum_{\tau=t}^{t+UT_i-1} x^o_{i\tau} \geq UT_i x^+_{it} \quad \forall\, i \in \mathcal{N}_g, \\
& \qquad\qquad \forall t \in [L_i + 1 :\, T - UT_i + 1], && \text{(2.2b)} \\
& \sum_{\tau=t}^{t+DT_i-1} (1 - x^o_{i\tau}) \geq DT_i x^-_{it} \quad \forall\, i \in \mathcal{N}_g, \\
& \qquad\qquad \forall t \in [F_i + 1 :\, T - DT_i + 1], && \text{(2.2c)} \\
& \sum_{\tau=t}^{T} (x^o_{i\tau} - x^+_{it}) \geq 0 \quad \forall\, i \in \mathcal{N}_g, \\
& \qquad\qquad \forall t \in [T - UT_i + 1 :\, T], && \text{(2.2d)} \\
& \sum_{\tau=t}^{T} (1 - x^o_{i\tau} - x^-_{it}) \geq 0 \quad \forall\, i \in \mathcal{N}_g, \\
& \qquad\qquad \forall t \in [T - DT_i + 2 :\, T], && \text{(2.2e)} \\
& \sum_{t=1}^{F_i} x^o_{it} = 0, \quad \sum_{t=1}^{L_i} x^o_{it} = L_i \quad \forall\, i \in \mathcal{N}_g \Big\}, && \text{(2.2f)}
\end{aligned}
$$

where x^o_{it} is the on/off commitment status of generator i at time t, x^+_{it} is the start-up decision and x^-_{it} is the shut-down decision. Constraint (2.2a) is the logic relationship between the $\boldsymbol{x}$ variables. Constraints (2.2b)-(2.2e) are the minimum up and down time constraints, together with boundary conditions (2.2f). N_g is the number of generators and T is the length of the horizon. See [31] for details of the above UC formulation.

The set $Y(\boldsymbol{x}, \boldsymbol{d})$ in (2.1) defines the feasible region for the economic dispatch problem with fixed commitment decision $\boldsymbol{x}$ and uncertain net load $\boldsymbol{d}$.

$$
\begin{aligned}
Y(\boldsymbol{x},\boldsymbol{d}) = \Big\{ & (\boldsymbol{p}, \boldsymbol{q}) :\; p^{min}_{it} x^o_{it} \leq p_{it} \leq p^{max}_{it} x^o_{it}, \;\; \forall i, t, && \text{(2.3a)} \\
& p_{it} - p_{i,t-1} \geq -RD_i x^o_{it} - SD_i x^-_{it}, \;\; \forall i, t, && \text{(2.3b)} \\
& p_{it} - p_{i,t-1} \leq RU_i x^o_{i,t-1} + SU_i x^+_{it}, \;\; \forall i, t, && \text{(2.3c)} \\
& \sum_{i \in \mathcal{N}_g} \alpha^p_{li} p_{it} - \sum_{j \in \mathcal{N}_d} \alpha^d_{lj} d_{jt} + q^f_{lt} \geq -f^{max}_l, \;\; \forall l, t, && \text{(2.3d)} \\
& \sum_{i \in \mathcal{N}_g} \alpha^p_{li} p_{it} - \sum_{j \in \mathcal{N}_d} \alpha^d_{lj} d_{jt} - q^f_{lt} \leq f^{max}_l, \quad \forall l, t, && \text{(2.3e)} \\
& \sum_{i \in \mathcal{N}_g} p_{it} + q^+_t - q^-_t = \sum_{j \in \mathcal{N}_d} d_{jt}, \;\; \forall\, t, && \text{(2.3f)}
\end{aligned}
$$

$$q_{lt}^f, q_t^+, q_t^- \geq 0,\ \forall l, t\Big\}, \tag{2.3g}$$

where (2.3a) is the bound on production levels, (2.3b)-(2.3c) are ramping up and down constraints (notice that we distinguish between the normal ramping rates RU_i, RD_i from the starting-up or shutting-down ramping rates SU_i, SD_i), (2.3d)-(2.3e) are transmission line thermal constraints using DC power flows, and (2.3f) is the energy balance constraint for each hour. We have introduced penalty variables q_{lt}^f and q_t^+, q_t^- in the transmission and energy balance constraints, respectively. In this way, the second-stage $\max$-$\min$ problem is guaranteed to be feasible and penalty cost is a measure of infeasibility. This complete recourse property is also important when we reformulate the second-stage problem as a MIP, as will be shown later.

The objective function is assumed to be linear or piecewise linear in the commitment and dispatch variables. Linear cost function is used here for simple exposition. Penalty costs for violations of transmission and energy balance constraints are also considered.

$$\boldsymbol{c}^\top \boldsymbol{x} = \sum_{i\in\mathcal{N}_g} \sum_{t\in\mathcal{T}} \left(c_{it}^o\, x_{it}^o + c_{it}^+\, x_{it}^+ + c_{it}^- x_{it}^-\right), \tag{2.4a}$$

$$\begin{aligned}\boldsymbol{b}^\top \boldsymbol{y} = \sum_{i\in\mathcal{N}_g, t\in\mathcal{T}} C_{it} p_{it} + \sum_{t\in\mathcal{T}} \left(C^+ q_t^+ + C^- q_t^-\right) \\ + \sum_{l\in\mathcal{N}_l, t\in\mathcal{T}} C^f q_{lt}^f.\end{aligned} \tag{2.4b}$$

The formulation (2.1) is a two-stage adaptive robust optimization model. The first-stage decision is the commitment decision $\boldsymbol{x}$, which has to be made before the uncertain net load is realized. The second-stage decision is the dispatch decision $\boldsymbol{y}$, which fully adapts to the observed realization of net load $\boldsymbol{d}$. That is, the second-stage problem produces a solution $\boldsymbol{y}(\boldsymbol{d})$ that is optimal to each specific realization of the uncertainty $\boldsymbol{d}$.

This two-stage adaptive robust UC model has become a fundamental model in the robust UC literature. It explicitly formulates the operational procedure of the unit commitment phase and the real-time dispatch phase into two stages, and models uncertainty of net load using an uncertainty set $\mathcal{D}$. It turns out that solving this two-stage robust UC model heavily depends on the structure of the uncertainty set. In the following, we first discuss solution algorithms to solve the two-stage robust model, then we provide a new exact formulation for a general budget uncertainty set, and compare the exact method and a heuristic for solving the second-stage problem.

2.3 Solution Algorithms: Exact vesus Heuristics

The robust UC model (2.1) can be rewritten as:

$$\min_{\boldsymbol{x}\in X} \boldsymbol{c}^\top \boldsymbol{x} + \mathcal{Q}(\boldsymbol{x}), \tag{2.5}$$

where the second-stage cost function $\mathcal{Q}(\boldsymbol{x})$ is given by

$$\mathcal{Q}(\boldsymbol{x}) = \max_{\boldsymbol{d}\in\mathcal{D}} \min_{\boldsymbol{y}\in Y(\boldsymbol{x},\boldsymbol{d})} \boldsymbol{b}^\top \boldsymbol{y}. \tag{2.6}$$

From the structure of the dispatch problem (2.3), we can see that the feasible set $Y(\boldsymbol{x}, \boldsymbol{d})$ of the inner minimization problem is a polyhedron in $\boldsymbol{y}$ of the following compact form:

$$\boldsymbol{B}\boldsymbol{y} \geq \boldsymbol{g} + \boldsymbol{A}\boldsymbol{x} + \boldsymbol{C}\boldsymbol{d}.$$

In other words, the parameters $\boldsymbol{x}$ and $\boldsymbol{d}$ only appear in the right-hand side of the linear constraints in (2.3). This is a key feature of (2.6) and allows it to be reformulated as a maximization problem. In particular, if we take the dual of the inner minimization problem in (2.6), we have

$$\begin{aligned} \mathcal{Q}(\boldsymbol{x}) = \max_{\boldsymbol{d},\boldsymbol{\pi}} \ & \boldsymbol{\pi}^\top \boldsymbol{C}\boldsymbol{d} + \boldsymbol{\pi}^\top(\boldsymbol{g} + \boldsymbol{A}\boldsymbol{x}) \\ \text{s.t.} \ & \boldsymbol{d} \in \mathcal{D} \\ & \boldsymbol{\pi} \in \mathcal{P} := \{\boldsymbol{\pi}^\top \boldsymbol{B} = \boldsymbol{b}^\top, \ \boldsymbol{\pi} \geq \boldsymbol{0}\}. \end{aligned} \tag{2.7}$$

Since the second-stage problem has complete recourse, the inner minimization is always feasible and achieves its optimum, therefore (2.6) and (2.7) are equivalent by linear programming strong duality. Now, problem (2.7) has a bilinear objective function in variables $\boldsymbol{d}$ and $\boldsymbol{\pi}$; further, the constraints on these two groups of variables are disjoint. We have the following two properties of (2.7):

1. There exists an optimal solution $(\boldsymbol{d}^*, \boldsymbol{\pi}^*)$ of (2.7), where $\boldsymbol{d}^*$ and $\boldsymbol{\pi}^*$ are an extreme point of $\mathcal{D}$ and $\mathcal{P}$, respectively. Note that this extreme point property holds even if $\mathcal{D}$ is a non-polyhedral convex set, e.g. an ellipsoid.

2. $\mathcal{Q}(\boldsymbol{x})$ is a convex function of $\boldsymbol{x}$. If the uncertainty set $\mathcal{D}$ is a polyhedron, then $\mathcal{Q}(\boldsymbol{x})$ is a piecewise linear convex function.

With these properties at hand, we can design an algorithm to solve the overall problem (2.5), which also involves evaluating $\mathcal{Q}(\boldsymbol{x})$ for any given $\boldsymbol{x}$. The fact that $\mathcal{Q}(\boldsymbol{x})$ is a convex function of $\boldsymbol{x}$ suggests that $\mathcal{Q}(\boldsymbol{x})$ can be approximated from below by linear functions, i.e., a two-level algorithmic framework can be developed, where the first level solves the master problem of the form

$$\min_{\boldsymbol{x}\in X} \boldsymbol{c}^\top \boldsymbol{x} + \hat{\mathcal{Q}}(\boldsymbol{x}),$$

where $\hat{\mathcal{Q}}(\boldsymbol{x})$ is a piecewise linear lower approximation of $\mathcal{Q}(\boldsymbol{x})$. The second level evaluates $\mathcal{Q}(\boldsymbol{x})$ and updates the approximation $\hat{\mathcal{Q}}(\boldsymbol{x})$. It turns out that, although $\mathcal{Q}(\boldsymbol{x})$ is a convex function, evaluating its value for any fixed $\boldsymbol{x}$ is a hard problem. This is indicated by the bilinear structure of (2.7).

2.3.1 Two-Level Algorithmic Framework

The two-level algorithm for solving the two-stage robust UC problem consists of writing the problem in the following extended form:

$$
\begin{aligned}
&\min_{\boldsymbol{x}\in X} \quad \boldsymbol{c}^\top \boldsymbol{x} + \mathcal{Q}(\boldsymbol{x}) \\
=&\min_{\boldsymbol{x},\eta} \quad \boldsymbol{c}^\top \boldsymbol{x} + \eta \\
&\text{s.t.} \quad \boldsymbol{x} \in X \\
&\qquad \eta \geq \max_{\boldsymbol{d}\in\mathcal{D}} \min_{\boldsymbol{y}\in Y(\boldsymbol{x},\boldsymbol{d})} \boldsymbol{b}^\top \boldsymbol{y} \\
=&\min_{\boldsymbol{x},\eta} \quad \boldsymbol{c}^\top \boldsymbol{x} + \eta \\
&\text{s.t.} \quad \boldsymbol{x} \in X \\
&\qquad \eta \geq \min_{\boldsymbol{y}\in Y(\boldsymbol{x},\boldsymbol{d})} \boldsymbol{b}^\top \boldsymbol{y} \quad \forall \boldsymbol{d} \in \mathcal{D} \\
=&\min_{\boldsymbol{x},\eta} \quad \boldsymbol{c}^\top \boldsymbol{x} + \eta \\
&\text{s.t.} \quad \boldsymbol{x} \in X \\
&\qquad \eta \geq \min_{\boldsymbol{y}\in Y(\boldsymbol{x},\boldsymbol{d}_m)} \boldsymbol{b}^\top \boldsymbol{y} \quad \forall m \in M \\
=&\min_{\boldsymbol{x},\eta,\{\boldsymbol{y}_m\}_{m\in M}} \quad \boldsymbol{c}^\top \boldsymbol{x} + \eta && \text{(2.8a)} \\
&\text{s.t.} \quad \boldsymbol{x} \in X && \text{(2.8b)} \\
&\qquad \eta \geq \boldsymbol{b}^\top \boldsymbol{y}_m \quad \forall\, m \in M && \text{(2.8c)} \\
&\qquad \boldsymbol{y}_m \in Y(\boldsymbol{x}, \boldsymbol{d}_m) \quad \forall\, m \in M, && \text{(2.8d)}
\end{aligned}
$$

where the third equality follows from the extreme point property discussed in the previous section, and the fourth equality follows from the property of minimization. Here, $\{\boldsymbol{d}_m\}_{m\in M}$ is the set of extreme points of $\mathcal{D}$, which can be infinite or even uncountable, depending on whether $\mathcal{D}$ is a polyhedron or not. The algorithm is convergent for the general case.

The last reformulation (2.8) suggests that the overall two-stage robust UC problem can be solved by gradually generating extreme points $\boldsymbol{d}_m$ and the associated constraints (2.8c)-(2.8d). Therefore, the master problem (MP) at iteration k contains a list of identified extreme points $\hat{M}_k \subseteq M$:

$$
\begin{aligned}
(MP) \qquad &\min_{\boldsymbol{x},\eta,\{\boldsymbol{y}_m\}_{m\in\hat{M}_k}} \quad \boldsymbol{c}^\top \boldsymbol{x} + \eta \\
&\qquad \text{s.t.} \quad \boldsymbol{x} \in X \\
&\qquad\qquad \eta \geq \boldsymbol{b}^\top \boldsymbol{y}_m \quad \forall\, m \in \hat{M}_k \\
&\qquad\qquad \boldsymbol{y}_m \in Y(\boldsymbol{x}, \boldsymbol{d}_m) \quad \forall\, m \in \hat{M}_k.
\end{aligned}
$$

The subproblem is to identify the worst-case demand scenario for the commitment solution generated by the master problem, denoted as $\boldsymbol{x}_k$. That is, the subproblem needs to evaluate $\mathcal{Q}(\boldsymbol{x}_k)$ and

compare it with the solution η_k from the master problem. This overall two-level procedure, Algorithm 2, has been independently proposed in several works including [6] for solving the robust UC model, [1] for solving a defender-attacker model, and analyzed rigorously in [50].

Algorithm 2 Constraint and Column Generation Algorithm

Initialization: $k = 0$ and $\hat{M}_0 = \emptyset$
for $k = 1, 2, 3...$ **do**
  Solve (MP) with $\hat{M}_k$. Denote solution as $(\boldsymbol{x}_k, \eta_k)$.
  Evaluate $\mathcal{Q}(\boldsymbol{x}_k)$ and denote solution as $\boldsymbol{d}_k$.
  if $\mathcal{Q}(\boldsymbol{x}_k) > \eta_k$ **then**
    Update $\hat{M}_{k+1} \leftarrow \hat{M}_k \cup \{\boldsymbol{d}_k\}$
    $k \leftarrow k + 1$
    Go to Step 3.
  else
    Terminate.
  end if
end for

As we already mentioned, it is difficult to solve the min-max problem (2.6). In the following section, we will develop an exact reformulation of (2.6) to a mixed-integer linear program, and compare it with the simple heuristics of alternating direction method proposed in [25].

2.3.2 Exact method for solving the subproblem

After taking the dual of the dispatch problem $\min_{\boldsymbol{y} \in Y(\boldsymbol{x}, \boldsymbol{d})} \boldsymbol{b}^\top \boldsymbol{y}$, the second-stage problem becomes

$$
\begin{aligned}
\max_{\boldsymbol{d}, \boldsymbol{\pi}} \quad & \sum_{i \in \mathcal{N}_g, t \in \mathcal{T}} \Big[p_{it}^{max} x_{it}^o \pi_{it}^{pmax} - p_{it}^{min} x_{it}^o \pi_{it}^{pmin} \\
& + \left(RD_i x_{it}^o + SD_i x_{it}^- \right) \pi_{it}^{RD} + \left(RU_i x_{i,t-1}^o + SU_i x_{it}^+ \right) \pi_{it}^{RU} \Big] \\
& + \sum_{l \in \mathcal{N}_l, t \in \mathcal{T}} \left(f_l^{max} + \sum_{j \in \mathcal{N}_d} \alpha_{lj}^d \, d_{jt} \right) \pi_{lt}^{f+} + \left(f_l^{max} - \sum_{j \in \mathcal{N}_d} \alpha_{lj}^d \, d_{jt} \right) \pi_{lt}^{f-} \\
& + \sum_{t \in \mathcal{T}, j \in \mathcal{N}_d} d_{jt} \pi_t^{bal} && \text{(2.9a)} \\
\text{s.t.} \quad & \pi_{it}^{pmax} - \pi_{it}^{pmin} + \pi_{it}^{RU} - \pi_{i,t+1}^{RU} - \pi_{it}^{RD} + \pi_{i,t+1}^{RD} \\
& + \sum_{l \in \mathcal{N}_l} \alpha_{li}^p \left(\pi_{lt}^{f+} - \pi_{lt}^{f-} \right) + \pi_t^{bal} = C_{it}, \quad \forall \, i, t, && \text{(2.9b)} \\
& - C^- \le \pi_t^{bal} \le C^+, \quad \forall \, t \in \mathcal{T}, && \text{(2.9c)} \\
& - \pi_{lt}^{f-} - \pi_{lt}^{f+} \le C^f, \quad \forall \, l \in \mathcal{N}_l, \, t \in \mathcal{T}, && \text{(2.9d)} \\
& \boldsymbol{\pi}^{pmin}, \boldsymbol{\pi}^{pmax}, \boldsymbol{\pi}^{RD}, \boldsymbol{\pi}^{RU}, \boldsymbol{\pi}^{f-}, \boldsymbol{\pi}^{f+} \le \mathbf{0}, && \text{(2.9e)}
\end{aligned}
$$

$$\boldsymbol{d} \in \mathcal{D}, \tag{2.9f}$$

where C^+, C^- are the penalty cost of violating energy balance constraints and C^f is the penalty cost of violating transmission constraints.

Notice that the objective function involves bilinear terms of the form:

$$\sum_{j \in \mathcal{N}_d, t \in \mathcal{T}} d_j^t \eta_j^t, \tag{2.10}$$

where η_j^t is defined as

$$\eta_j^t = \pi_t^{bal} + \sum_{l \in \mathcal{N}_l} \alpha_{lj}^d \left(\pi_{lt}^{f+} - \pi_{lt}^{f-} \right). \tag{2.11}$$

To reformulate the bilinear term (2.10), we need to use special structures of the uncertainty set $\mathcal{D}$. Consider the following uncertainty set $\mathcal{D}^t$ at each time t:

$$\mathcal{D}^t = \Bigg\{ \boldsymbol{d}^t = (d_1^t, \ldots, d_{N_d}^t) : \sum_{j \in \mathcal{N}_d} \frac{|d_j^t - \overline{d}_j^t|}{\hat{d}_j^t} \leq \Delta, \\ d_j^t \in [\overline{d}_j^t - \hat{d}_j^t, \, \overline{d}_j^t + \hat{d}_j^t] \;\; \forall \, j \in \mathcal{N}_d \Bigg\}. \tag{2.12}$$

This is the so-called budgeted uncertainty set, which is widely used in the robust optimization literature. There are two types of exact reformulations. The first type uses the KKT conditions of the bilinear problem, which is generally applicable to any polyhedral uncertainty sets [50]. However, the observed computation performance is quite slow [25]. The second one assumes the budget parameter Δ to be integer valued. In this case, the extreme points of $\mathcal{D}^t$ have the form of $\overline{d}_j^t \pm \hat{d}_j^t$. Then, the extreme points of $\mathcal{D}^t$ can be expressed with binary variables [19]. Bilinear terms involving a binary variable and a continuous variable can be easily linearized with the big-M method.

In this chapter, we generalize the second approach by allowing Δ to be fractional. We have the following result.

Proposition 1. *For $\Delta \leq |\mathcal{N}_d|$, the set of extreme points of $\mathcal{D}^t$ is given by*

$$\Bigg\{ \boldsymbol{d}^t : \;\; \exists \, \underline{\boldsymbol{u}}^t, \overline{\boldsymbol{u}}^t, \underline{\boldsymbol{v}}^t, \overline{\boldsymbol{v}}^t \text{ s.t.} \tag{2.13a}$$

$$d_j^t = \overline{d}_j^t + \hat{d}_j^t \left(\overline{u}_j^t - \underline{u}_j^t \right) + \left(\Delta - \lfloor \Delta \rfloor \right) \hat{d}_j^t \left(\overline{v}_j^t - \underline{v}_j^t \right) \quad \forall \, j \in \mathcal{N}_d \tag{2.13b}$$

$$\sum_{j \in \mathcal{N}_d} \underline{u}_j^t + \overline{u}_j^t = \lfloor \Delta \rfloor \tag{2.13c}$$

$$\sum_{j \in \mathcal{N}_d} \underline{v}_j^t + \overline{v}_j^t = 1 \tag{2.13d}$$

$$\underline{u}_j^t + \overline{u}_j^t + \underline{v}_j^t + \overline{v}_j^t \leq 1 \quad \forall\, j \in \mathcal{N}_d \tag{2.13e}$$

$$\left.\underline{u}_j^t, \overline{u}_j^t, \underline{v}_j^t, \overline{v}_j^t \in \{0,1\} \quad \forall\, j \in \mathcal{N}_d\right\}. \tag{2.13f}$$

Using this characterization of the extreme points of $\mathcal{D}^t$, each bilinear term in (2.10) involves products of $\overline{u}_j^t\eta_j^t$, $\underline{u}_j^t\eta_j^t$, $\overline{v}_j^t\eta_j^t$, $\underline{v}_j^t\eta_j^t$, where η_j^t is defined in (2.11). These bilinear terms can be linearized. Introduce new continuous variables $\overline{\theta}_j^t$, $\underline{\theta}_j^t$, $\overline{\rho}_j^t$, $\underline{\rho}_j^t$, we have the following linearized terms:

$$-\, M_j\, \overline{u}_j^t \leq \overline{\theta}_j^t \leq M_j\, \overline{u}_j^t, \tag{2.14a}$$

$$-\, M_j\, (1 - \overline{u}_j^t) \leq \eta_j^t - \overline{\theta}_j^t \leq M_j\, (1 - \overline{u}_j^t), \tag{2.14b}$$

$$-\, M_j\, \underline{u}_j^t \leq \underline{\theta}_j^t \leq M_j\, \underline{u}_j^t, \tag{2.14c}$$

$$-\, M_j\, (1 - \underline{u}_j^t) \leq \eta_j^t - \underline{\theta}_j^t \leq M_j\, (1 - \underline{u}_j^t), \tag{2.14d}$$

where (2.14a)-(2.14b) are the linearization of $\overline{u}_j^t\eta_j^t$, (2.14c)-(2.14d) are the linearization of $\underline{u}_j^t\eta_j^t$, and similarly we can linearize $\overline{v}_j^t\eta_j^t$ and $\underline{v}_j^t\eta_j^t$. Then, (2.10) is reformulated as

$$\sum_{j \in \mathcal{N}_d, t \in \mathcal{T}} \left[\overline{d}_j^t \eta_j^t + \hat{d}_j^t (\overline{\theta}_j^t - \underline{\theta}_j^t) + (\Delta - \lfloor \Delta \rfloor)\, \hat{d}_j^t\, (\overline{\rho}_j^t - \underline{\rho}_j^t) \right].$$

Here M_j is a positive constant big enough to bound the dual variables as in (2.14). It is important to choose a value of M_j as tight as possible. From (2.11), (2.9c), (2.9d) and (2.9e) we have that

$$-\, C^- - C^f \sum_{l \in \mathcal{N}_l} |\alpha_{lj}^d| \leq \eta_j^t \leq C^+ + C^f \sum_{l \in \mathcal{N}_l} |\alpha_{lj}^d| \tag{2.15}$$

must hold. Hence, we can take $M_j = \max\{C^-, C^+\} + C^f \sum_{l \in \mathcal{N}_l} |\alpha_{lj}^d|$ to ensure the formulation is correct.

Using the above linearization, the second-stage problem is equivalent to a mixed-integer linear program. Although solving this MIP can obtain the global optimum, its solution time is usually quite long. In the following, we introduce a simple heuristics that can obtain a feasible solution very quickly. Then we will compare the two methods for the solution times and solution quality.

2.3.3 Simple Heuristics for Solving the Subproblem

An outer approximation algorithm is proposed in [6]. Here, we apply another simple heuristic to solve the disjoint bilinear program, namely the alternating direction (AD) method. It optimizes over $\boldsymbol{d}$ with $\boldsymbol{\pi}$ fixed at a given value, then optimizes over $\boldsymbol{\pi}$ with $\boldsymbol{d}$ fixed at the optimal solution obtained from the previous iteration, and alternates. Use the compact representation (2.7), the AD algorithm is outlined below.

The heuristic algorithm in general only identifies a KKT point of the bilinear program. De-

Algorithm 3 Alternating Direction Algorithm

1: **Initialization**: $t = 0$ and $\boldsymbol{d}_0 \in \mathcal{D}$
2: **repeat**
3: Solve $\boldsymbol{\pi}_{t+1} = \arg\max_{\boldsymbol{\pi} \in \mathcal{P}} \boldsymbol{\pi}^\top \boldsymbol{C}\boldsymbol{d}_t + \boldsymbol{\pi}^\top(\boldsymbol{g} + \boldsymbol{A}\boldsymbol{x})$
4: Solve $\boldsymbol{d}_{t+1} = \arg\max_{\boldsymbol{d} \in \mathcal{D}} \boldsymbol{\pi}_{t+1}^\top \boldsymbol{C}\boldsymbol{d}$
5: $t \leftarrow t + 1$
6: **until** convergence criterion is met.

note the objective value obtained by the AD algorithm as $\hat{\mathcal{Q}}(\boldsymbol{x}_k) \leq \mathcal{Q}(\boldsymbol{x}_k)$. It is possible that $\hat{\mathcal{Q}}(\boldsymbol{x}_k) \leq \eta_k < \mathcal{Q}(\boldsymbol{x}_k)$. In this case, the heuristic method would stop the upper level algorithm and potentially find a suboptimal commitment solution. The above AD algorithm is proposed as a first step heuristics in a cutting plane algorithm for solving general bilinear programs to global optimality [21]. However, the cutting plane algorithm again has the same complexity as the exact method.

2.3.4 Computational Experiments

In this section, we study the performance of the exact method using (2.13) and (2.14) and the heuristic method using Algorithm 3. In particular, we want to empirically show how well the exact method performs, how good or bad the heuristics is in solving the second-stage problem, how much it can influence the final solution, and what is the best way to solve the second-stage problem combining the two methods.

We test on the IEEE 30-bus system with nominal demand as is given in [45, 58]. There are 6 generators and 20 loads in the system. The penalty costs C^+, C^-, C^f are set to be \$5000/MW. All the codes are implemented in Python and call CPLEX 12.5. Computation is conducted on a laptop with 2.1GHz CPU and 4GB RAM.

Choosing big-M

The value of M_j gives the upper and lower bounds on the dual variable η_j^t in (2.9). Since the primal polytope of the dispatch problem (2.3) is bounded, by well-known results from LP duality, the dual polytope defined by (2.9b)-(2.9e) is unbounded. However, since the primal problem always obtains an optimal solution by adding penalty variables, the dual optimal solution is always bounded. Thus, there exists a finite M_j, and a tight value of M_j helps speed up the algorithm. Unfortunately, it is not an easy task to pinpoint a tight value for M_j.

For the 30-bus system, we test different values of M_j at 100, 1000, and $50,000$. With $M_j = 100$, the exact MIP can be solved to optimality under 1 minute for different levels of budget varying from $\Delta = 2$ to 18. However, a closer look at the solution reveals that some dual variables hit the upper or lower bounds, which implies $M_j = 100$ is not big enough to bound the optimal dual solution. With $M_j = 1000$, the MIP gap cannot be closed below 3% after 10 minutes for $\Delta \leq 10$; furthermore, some dual variables still hit the upper and lower bounds. Therefore, $M_j = 1000$ is not large enough either, and it already significant increases the computation time. The bounds on

η_j^t given by (2.15) amount to $44,950$. Therefore, setting $M_j = 50,000$ guarantees a valid big-M value. This value might be an over-estimate for M_j, however, it is the only guarantee we have, and the results for $M_j = 1000$ suggest that a smaller M_j may not save much computation time anyway. This tuning procedure is typical for a MIP model with big-M parameters. It is non-trivial to find a tight bound and usually even a tight M value is already large enough to slow down the convergence of the branch-and-bound procedure.

Computation times of solving the second-stage problem

To compare how fast the exact method and the heuristics can solve the second-stage problem, we conduct the following first set of experiments: For budget $\Delta \in [2, 18]$, we solve the two-stage robust UC using Algorithm 1, where the second-stage problem is solved by the exact method, and then again solved by the heuristics under the same commitment solution.

We observe that CPLEX takes a long time to improve lower bounds when solving the second-stage exact MIP formulation. After 10 min, the optimality gaps are still not much improved from those obtained after 1 min. Therefore, in all the experiments, we terminate the second-stage MIP after 1 min. In comparison, the AD algorithm solving the same set of second-stage problems converges on average within 1.52 seconds.

Solution quality

Naturally, the next question is how good the heuristic solutions are. Table 2.1 shows the objective values obtained from the exact and heuristic methods for solving the same second-stage problem at each iteration of the two-level algorithm.

For example, with $\Delta = 2$, the master problem is solved in 3 iterations by Algorithm 1 with the exact method, i.e., the second-stage problem is also solved 3 times. The objective values obtained by the exact method for these three second-stage problems are $[229830, 88633, 88636]$; the heuristic AD algorithm obtains $[214543, 88636, 88636]$ for the same set of problems. From the table we can see that the Heuristics obtains the same or better second-stage costs toward the end of the iterations. But in the beginning one or two iterations, the exact method obtains a better second-stage cost (recall the second-stage problem is maximizing.) This property is also observed for other values of Δ, which suggests that the heuristics works well when the commitment solution is close to optimal, and may get stuck at a bad local solution when the commitment solution is far from optimal, which is the case in the beginning of the master problem iterations.

We conduct the second set of experiments, where the second-stage problem is solved using the Heuristics alone. That is, the two-stage problem is solved by Algorithm 1 and Algorithm 2. The extreme points generated by Algorithm 2 can be different from the ones generated by the exact method. Therefore, the commitment solutions obtained would also be different. We observe that the second-stage cost of the final commitment solution obtained using Algorithm 1 with Heuristics is on average 2% lower than that obtained by Algorithm 1 with the exact method. This shows that the solution obtained from Heuristics is not globally optimal, as is expected. However, the gap is quite small.

Table 2.1: Quality of the Second-Stage Solution

Δ	Exact Method	Heuristics
2	$[229830, 88633, 88636]$	$[214543, 88636, 88636]$
4	$[252040, 90672, 90694, 90707]$	$[225403, 90707, 90707, 90707]$
6	$[264391, 101064, 91835, 91851, 91853]$	$[231442, 91818, 91863, 91863]$
8	$[274884, 111671, 92803]$	$[236582, 92759, 92804]$
10	$[284488, 121382, 93697]$	$[241288, 93690, 93697]$
12	$[292336, 140564, 94450, 94422]$	$[245136, 94398, 94457, 94422]$
14	$[297630, 148011, 94939, 94904]$	$[247735, 94874, 94939, 94904]$
16	$[301445, 155242, 95308, 95273, 95273]$	$[249608, 95263, 95308, 95273]$
18	$[304633, 161472, 95595, 95560]$	$[251174, 95550, 95595, 95560]$

Hybrid method

Combining the results obtained from the first and second sets of experiments, especially the observation that the exact method does well in the initial iterations and the Heuristics can do better in the later iterations, we propose a hybrid method which uses the exact method in the beginning few iterations and then switches to the Heuristics. We conduct the third set of experiments to implement this hybrid approach, where the second-stage problem is solved by the exact methods in the first two iterations of the master problem, then is solved by the Heuristics. For all 9 test cases of $\Delta = 2, ..., 18$, the hybrid approach converges after 1 iteration of Heuristics, and reaches the same solution as obtained using the exact method.

Summary

In this section, we have conducted a detailed study on the performance of the exact method and the Heuristics. The experiments suggest that it is important to obtain good commitment solutions in the beginning iterations of Algorithm 1. Here, it is worth using the exact method to solve the second-stage problem. As the commitment solution is approaching the optimal, it is more economical and does not seem to sacrifice performance to use the Heuristics.

2.4 Worst Case Scenario Analysis

Solving the two-stage robust UC model (2.1) not only produces the robust UC solution, but also identifies the worst-case net load scenario for the UC solution. These worst case scenarios carry useful information for system security analysis. In this section, we study the worst-case uncertainty scenarios for the budget uncertainty set (2.12) for different budget levels. The experiments are conducted on the same IEEE 30-bus system, where all of the 20 loads are uncertain with 10% variation, i.e. $\hat{d}_j^t = 0.1\overline{d}_j^t$. Table 2.2 summarizes the nominal load levels at the peak hour and load distribution factors for the largest 6 loads.

From the previous analysis, we know that the worst-case net load is an extreme point of the

Table 2.2: Nominal Load Levels and Distribution Factors

Bus i	8	7	2	21	12	30
$\overline{d}_j$ (MW)	34.88	26.51	25.23	20.35	13.02	12.33
Factors (%)	15.86	12.05	11.47	9.25	5.92	5.60

uncertainty set $\mathcal{D}$. The question is which extreme point of the uncertainty set will be the worst case. Intuitively, we may expect the largest net load in the uncertainty set to be the worst case, because product cost increases with net load. This is indeed the case when the transmission network is not congested and the ramping limits are not tight. However, if the transmission network is congested, the worst case net load may not be the largest net load any more. In the following, we analyze both cases.

2.4.1 Transmission Network Not Congested

In this case, we have the following characterization of the worst case net load.

Proposition 2. *Consider a single period dispatch problem. Rank the loads from the largest to the smallest according to their nominal values: $\overline{d}_{(1)} \geq \cdots \geq \overline{d}_{(n)}$. If the transmission network is not congested at the worst case net load $\boldsymbol{d}^*$ and there are no ramping limits, then $\boldsymbol{d}^*$ has the following form:*

$$d^*_{(j)} = \begin{cases} \overline{d}_{(j)} + \hat{d}_{(j)}, & \forall j = 1, \ldots, \lfloor \Delta \rfloor, \\ \overline{d}_{(j)} + (\Delta - \lfloor \Delta \rfloor)\hat{d}_{(j)}, & j = 1 + \lfloor \Delta \rfloor, \\ \overline{d}_{(j)}, & \forall j > 1 + \lfloor \Delta \rfloor. \end{cases}$$

Essentially, when there is no transmission congestion and ramping limits, the worst case scenario is the net load whose total deviation from the nominal values exactly reaches the budget, and make the loads with high nominal values deviate to the upper bounds.

For the IEEE 30-bus system, the worst case scenario for $\Delta = 6$ is the one where the six loads with the largest nominal values (i.e., the six loads shown in Table 2.2) reach the upper bounds $\overline{d}^t_j + \hat{d}^t_j$, and all other loads stay at the nominal value.

2.4.2 Transmission Network Congested

This is the more interesting case. Here, the worst case net load may not always be the highest load scenario. To demonstrate, we lower each tranmission limit in the IEEE 30-bus system by half its original capacity, and increase each nominal load by 30%. The transmission network is congested in this case.

Table 2.3 shows the worst case net load scenario for the budget uncertainty set with $\Delta = 12$. Each column denotes an hour, from hour 1 to 12. Each row is the bus number of a load. A 1 in a

cell means the load at that bus and hour reaches the upper limit, i.e. $d_j^t = \overline{d}_j^t + \hat{d}_j^t$; a -1 means it reaches the lower limit, i.e. $d_j^t = \overline{d}_j^t - \hat{d}_j^t$; a 0 means the load stays at the nominal value.

For the budget level $\Delta = 12$, the worst case scenario at each hour has 12 loads deviating to upper or lower bounds, i.e., the total number of 1 and -1 in a column is 12. The table clearly shows that at several hours, it is the lower level demand that causes the worst case dispatch cost. The reason is that in these hours the lower level demand at certain buses can cause more severe transmission congestion than a demand at the upper bound.

Table 2.3: Worst Case Load Scenario

$i\backslash t$	1	2	3	4	5	6	7	8	9	10	11	12
2	1	1	-1	1	-1	-1	1	0	0	0	0	0
3	0	0	0	0	0	0	0	0	0	0	0	0
4	1	0	-1	1	-1	-1	0	1	0	1	1	1
7	1	1	-1	1	-1	-1	1	1	1	1	1	1
8	1	1	1	1	1	1	1	1	1	1	1	1
10	1	1	1	0	1	1	1	1	1	1	1	1
12	1	0	1	1	1	1	0	1	1	1	1	1
14	0	0	0	1	0	0	0	0	0	0	0	0
15	1	-1	1	1	1	1	0	0	0	1	1	1
16	0	0	0	0	1	1	0	0	0	0	0	0
17	1	1	1	1	1	1	1	1	1	1	1	1
18	1	1	0	0	0	0	1	1	1	1	1	1
19	1	1	1	1	1	1	1	1	1	1	1	1
20	0	1	1	0	0	0	1	1	1	0	0	0
21	1	1	1	1	1	1	1	1	1	1	1	1
23	0	0	0	0	0	0	0	0	0	0	0	0
24	0	1	0	1	0	0	1	0	1	0	0	0
26	1	1	1	1	1	1	1	1	1	1	1	1
29	0	0	0	0	0	0	0	0	0	0	0	0
30	0	0	0	0	0	0	-1	1	1	1	1	1

2.5 Dynamic Uncertainty Sets

The budget uncertainty set (2.12) is widely used in the robust optimization literature. In fact, most of the recent works on robust UC use this type of uncertainty sets, where the uncertainty is assumed to lie in a hyper-rectangle defined by the nominal value and the intervals of variation. The budget constraint restricts the total variation of uncertainty sources. A main drawback of the budget uncertainty set is that it does not explicitly model uncertainty correlations. For this reason, we call these *static* uncertainty sets.

In reality, uncertainties such as wind speeds and the resulting available wind power in neighboring wind farms very often exhibit strong temporal and spatial correlations. It is important for a

robust optimization model to consider these correlations in the uncertainty sets. In the following, we discuss a new type of uncertainty sets, we call *dynamic* uncertainty sets, which can model the dynamic relationships between uncertain parameters, and also the interactions between uncertain parameters and decisions. We show the general model first, then show a specific construction for modeling temporal and spatial correlations of available power of wind farms [25]. Another type of dynamic uncertainty set is proposed in [10], which models the dynamics between uncertainty and decisions for demand response resource.

2.5.1 General Definition

Dynamic uncertainty sets can be generally defined as the following:

$$\mathcal{D}_t(\boldsymbol{d}_{[t-1]}) = \left\{\boldsymbol{d}_t : \exists \boldsymbol{u} \text{ s.t. } f(\boldsymbol{d}_t, \boldsymbol{d}_{[t-1]}, \boldsymbol{u}) \leq \boldsymbol{0}\right\} \tag{2.16}$$

where $\boldsymbol{d}_{[t-1]} = (\boldsymbol{d}_1, \boldsymbol{d}_2, \ldots, \boldsymbol{d}_{t-1})$, and f is a function that represents the dynamic relationships between $\boldsymbol{d}_t$, $\boldsymbol{d}_{[t-1]}$, and the auxilliary variable $\boldsymbol{u}$.

The key idea here is that the function f captures the correlations between uncertain resources at different times and locations. A simple example is a dynamic uncertain interval:

$$\mathcal{D}_t(\boldsymbol{d}_{[t-1]}) = \left[\underline{f}(\boldsymbol{d}_{[t-1]}, \overline{f}(\boldsymbol{d}_{[t-1]})\right],$$

where the interval's upper and lower bounds at time t depend on the realizations of uncertainty in the previous periods.

2.5.2 Modeling Temporal and Spatial Correlations for Wind

In the recent paper [25], the authors propose a construction of dynamic uncertainty sets for modeling wind power's temporal and spatial correlations between different wind farms.

First, we introduce the dynamic uncertainty set for wind speed. Denote the wind speed vector of multiple wind farms at time t as $\boldsymbol{r}_t = (r_{1t}, \ldots, r_{N^w t})$, where r_{it} is the wind speed at wind farm i and time t and N^w is the number of adjacent wind farms. Define the dynamic uncertainty set for $\boldsymbol{r}_t$ as:

$$\begin{aligned}
\mathcal{R}_t(\boldsymbol{r}_{[t-L:t-1]}) = \Big\{\boldsymbol{r}_t :\ & \exists\, \widetilde{\boldsymbol{r}}_{[t-L:t]},\ \boldsymbol{u}_t \quad \text{s.t.} \\
& \boldsymbol{r}_\tau = \boldsymbol{g}_\tau + \widetilde{\boldsymbol{r}}_\tau \quad \forall \tau = t-L, \ldots, t && \text{(2.17a)} \\
& \widetilde{\boldsymbol{r}}_t = \sum_{s=1}^{L} \boldsymbol{A}_{t,s} \widetilde{\boldsymbol{r}}_{t-s} + \boldsymbol{B}_t \boldsymbol{u}_t && \text{(2.17b)} \\
& \sum_{i \in \mathcal{N}^w} |u_{it}| \leq \Delta_t && \text{(2.17c)} \\
& |u_{it}| \leq \Gamma_t \qquad \forall i \in \mathcal{N}^w && \text{(2.17d)} \\
& \boldsymbol{r}_t \geq \boldsymbol{0}\Big\}, && \text{(2.17e)}
\end{aligned}$$

where vectors $\boldsymbol{r}_{t-L}, \ldots, \boldsymbol{r}_{t-1}$ are the realizations of wind speeds in periods $t-L, \ldots, t-1$. $\mathcal{N}^w$ denote the set of wind farms. Eq. (2.17a) decomposes wind speed vector $\boldsymbol{r}_\tau$ as the sum of a seasonal pattern $\boldsymbol{g}_\tau$ such as periodicity of wind speeds over days, which is pre-estimated from the wind data. The residual component $\widetilde{\boldsymbol{r}}_\tau$ represents the fluctuation of wind speeds from the seasonal pattern $\boldsymbol{g}_\tau$.

Eq. (2.17b) is the key equation that represents a linear dynamic relationship involving the residual $\widetilde{\boldsymbol{r}}_t$ at time t, residuals realized in earlier periods $t-L$ to $t-1$, and an error term $\boldsymbol{u}_t$. Here, matrices $\boldsymbol{A}_{t,s}$'s and $\boldsymbol{B}_t$ are estimated from a vector autoregressive time series model with time lag L. In particular, $\boldsymbol{A}_{t,s}$'s capture the temporal correlation between $\boldsymbol{r}_t$ and $\boldsymbol{r}_{t-1}, \ldots, \boldsymbol{r}_{r-L}$, and $\boldsymbol{B}_t$ specifically captures the spatial relationship of wind speeds at adjacent wind farms at time t. In the time series model, $\boldsymbol{B}_t$ characterizes the covariance of the estimation error.

Then, the variable $\boldsymbol{u}_t$ is introduced to control the amount of error by a budget uncertainty set defined in Eq. (2.17c)-(2.17d). The meaning of Γ_t is to set how many "standard deviations" we allow the errors to have. The budget constraint (2.17d) controls the total amount of deviations of the wind speed estimation errors across wind farms. Notice here, the budget uncertainty set is slightly different from the one used in [25]. In particular, we introduce two budget parameters Δ_t and Γ_t to control the range of u_{it} and the total deviation of the $|u_{it}|$ separately. This gives more freedom to the uncertainty sets.

It is important to also notice that we need Eq. (2.17e) to avoid negative wind speeds. This constraint further restricts the available range of u_{it} within the budget uncertainty set. In other words, the projection of the dynamic uncertainty set $\mathcal{R}_t$ onto the $\boldsymbol{u}$ variables is different from the budget uncertainty set Eq. (2.17c)-(2.17d).

Worst Case Wind Scenario

Now, we can ask the same questions as for the budget uncertainty sets, namely, in a robust model using the dynamic uncertainty set, what woud the worst case scenarios be? To study this problem, we apply the dynamic uncertainty set Eq. (2.17) to a two-stage robust economic dispatch (ED) model proposed in [25]. The details of the model can be found there. Here we only give a brief overview of the key components of the model.

The two-stage robust ED model has the same generic structure of a two-stage robust optimization model as shown in Eq. (2.1). However, the specific definition of the first- and second-stage decisions are different from the two-stage robust UC we discussed earlier in this chapter. In particular, the first-stage decision of the robust ED model is the dispatch decision of the current decision period. This dispatch decision is to be implemented right now. The second-stage decision is the dispatch decisions in the future periods. The two-stage robust ED model can be viewed as a generalization of deterministic look-ahead dispatch models (e.g. see [46]).

We build a rolling horizon simulation engine to mimic the real-time dispatch operation. In this engine, the robust ED is solved every 10 min with a look-ahead horizon of 90 min. The rolling horizon simulation runs over a 35-day period. The dynamic uncertainty sets $\boldsymbol{A}_{t,s}$'s and $\boldsymbol{B}_t$ are estimated from real-world wind data collected from [9] and updated after every day in the simulation using the newly available data.

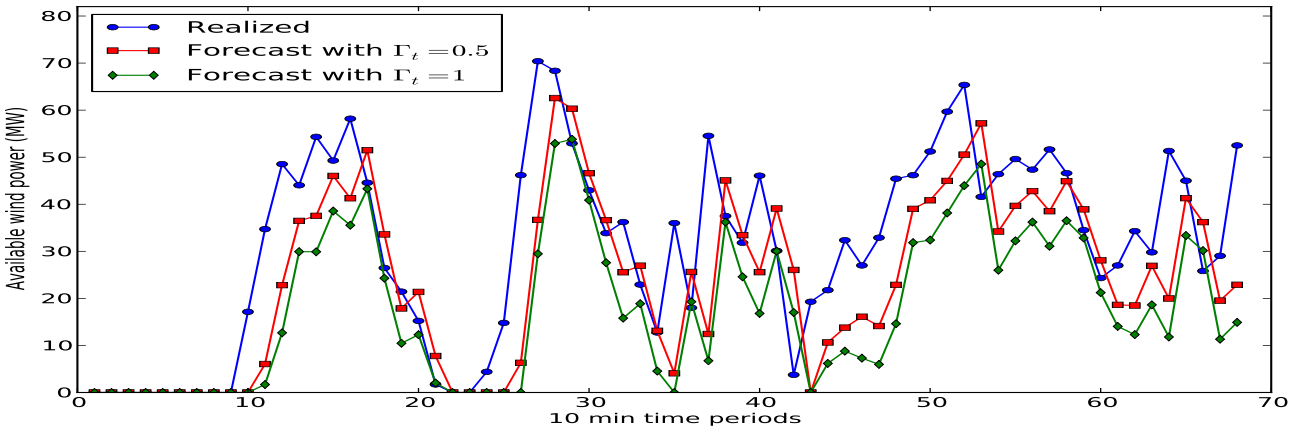

Figure 2.1: Available Wind and Worst Case Wind Scenarios for $\Delta = 0.5$ and $\Delta = 1$.

We test on the IEEE 14-bus system with 4 wind farms and 11 loads. We assume the load forecast is accurate so as to treat the wind uncertainty alone. The wind power is dispatchable in the robust ED model, i.e., wind farm i's production $p^w_{i,t}$ is a decision variable and satisfies $p^w_{i,t} \leq \overline{p}^w_{i,t}$, where $\overline{p}^w_{i,t}$ is the available wind power calculated from wind speed by the power curve of the wind turbines. And $\overline{p}^w_{i,t}$ is the uncertainty in the robust dispatch model, whose uncertainty set is constructed through the uncertainty set of wind speeds (2.17).

At each time t, the robust ED model has the observed wind speeds at time t as the input and generates a worst-case available wind power scenario for all the 4 wind farms during the periods in the look-ahead horizon (in our test, 8 periods ahead). We can point out several interesting properties of the worst-case available wind power scenarios identified by the two-stage robust ED model.

1. Since the wind power can be curtailed in the ED model, high wind scenarios can always be handled by curtailment without additional cost, therefore, the worst case available wind scenario will be the low-wind situaton.

2. If we look at the total available wind power summed over all the wind farms, the total wind power of the worst case scenario in time $t + 1$ is always lower than that at time t, and so on for the next periods in the look-ahead horizon. That is, the worst-case wind scenarios correspond to an overall wind drop from the previous periods.

3. With a more careful study, we can see that the worst-case wind scenario of a period is typically given by the largest possible wind drop from the previous period allowed by the dynamic uncertainty set. This exactly shows the desired property of the dynamic uncertainty set that the temporal and spatial correlations of the wind speeds consistently restrict the range of wind power drop. When there is transmission congestion, the picture is more complicated. Here, the worst-case wind scenario exploits the congested network and may not correspond to the largest drop in total wind.

4. The worst-case wind power of an individual wind farm at a period may not be always a drop from the previous period, although the total wind power of the worst case drops. In other

words, due to the spatial correlation between wind farms, it is possible that some increase of wind power from previous periods can be more costly for dispatch.

Figure 2.1 plots observed and worst-case wind scenarios over 70 periods with 10 min interval, i.e., about 12 hours in total time. In particular, each blue dot is the available wind power observed at time t. Each red and green dot is the total wind power of the worst-case wind scenario for time $t+1$ obtained from solving the robust ED at time t. The red dots are the results of dynamic uncertainty sets with budget 0.5, whereas the green dots are for budget 1. The following are some interesting observations.

1. The red and green curves in general lie below the blue curve. This demonstrates that the worst-case wind scenarios correspond to wind drop events. The red and green curves basically provide a lower limit on the total available wind power above which the system is guaranteed to operate safely.

2. If we look carefully, we can see sometimes the red curve crosses with and go above the blue curve. At these points, the realized wind is even lower than the worst-case wind identified at the previous period. This could happen because the dynamic uncertainty set only allows a certain amount deviation from the forecast wind, controlled by the budget parameters Γ_t and Δ_t. If we want to reduce such "surprise" events of realized wind going below the predicted worst case, we can increase the budget. The green curve is obtained from a higher budget, and it does move the green curve further down below the red curve, which makes the green curve cross with the blue curve much less often. This shows the system operating under the green curve is more conservative and secure.

2.6 Conclusions

In this chapter, we explore several important questions on the robust optimization approach for the UC and ED problems that have not been addressed extensively in the existing literature. This includes the question of how to efficiently solve the second-stage problem in the robust UC model, which is a source of significant computational challenge for fully solving these adaptive robust optimization models. We also discuss with examples the properties of the worst case net load scenarios produced by the budget and dynamic uncertainty sets. Many interesting questions are still open, such as solving the multistage robust UC models, designing new dynamic uncertainty sets for solar power and demand response resources, and applying the adaptive robust optimization framework to medium and long term power system planning.

References

[1] D. L. Alderson, G. G. Brown, W. M. Carlyle, and R. K. Wood, "Solving defender-attacker-defender models for infrastructure defense," in *12th INFORMS Computing Society Conference*. INFORMS, 2011, pp. 28–49.

[2] T. E. Bechert and H. G. Kwatny, "On the optimal dynamic dispatch of real power," *IEEE Transactions on Power Apparatus and Systems*, vol. 91, no. 3, pp. 889–898, 1972.

[3] A. Ben-Tal, L. El Ghaoui, and A. Nemirovski, *Robust optimization*. Princeton University Press, 2009.

[4] D. Bertsimas, D. Brown, and C. Caramanis, "Theory and applications of robust optimization," *SIAM Review*, vol. 53, no. 3, pp. 464–501, 2011.

[5] D. Bertsimas, E. Litvinov, A. X. Sun, J. Zhao, and T. Zheng, "Adaptive robust optimization for the security constrained unit commitment problem," *IEEE Transactions on Power Systems*, vol. 28, no. 1, pp. 52–63, 2013.

[6] D. Bertsimas, E. Litvinov, X. A. Sun, J. Zhao, and T. Zheng, "Adaptive robust optimization for the security constrained unit commitment problem," *IEEE Transactions on Power Systems*, vol. 28, no. 1, pp. 52–63, 2013.

[7] D. Bertsimas and M. Sim, "The price of robustness," *Operations research*, vol. 52, no. 1, pp. 35–53, 2004.

[8] F. Bouffard and F. D. Galiana, "Stochastic security for operations planning with significant wind power generation," *IEEE Transactions on Power Systems*, vol. 23, no. 2, pp. 306–316, 2008.

[9] "RERL wind data," Center for energy efficiency and renewable energy, University of Massachusetts Amherst. [Online]. Available: http://www.ceere.org/rerl/publications/resource_data/index.html

[10] H. Chen, X. A. Sun, and S. Deng, "Robust demand response portfolio management under operational uncertainty," *IEEE Transactions on Smart Grid*, 2014, under review.

[11] E. Ela and B. Kirby, "ERCOT event on February 26, 2008 lessons learned," in *Technical Report NREL/TP-500-43373*. National Renewable Energy Laboratory, 2008.

[12] FERC Staff, "Recent ISO Software Enhancements and Future Software and Modeling Plans," http://www.ferc.gov/industries/electric/indus-act/rto/rto-iso-soft-2011.pdf, 2011.

[13] "GE Energy 1.5 MW wind turbine," General Electric Company, 2009.

[14] H. Gooi, D. Mendes, K. Bell, and D. Kirschen, "Optimum scheduling of spinning reserve," *IEEE Transactions on Power Systems*, vol. 14, pp. 1485–1490, 1999.

[15] R. Jabr, "Adjustable robust OPF with renewable energy sources," *IEEE Transactions on Power Systems*, vol. 28, no. 4, pp. 4742–4751, 2013.

[16] R. Jiang, J. Wang, and Y. Guan, "Robust unit commitment with wind power and pumped storage hydro," *IEEE Transactions on Power Systems*, vol. 27, no. 2, pp. 800–810, 2012.

[17] ——, "Robust unit commitment with wind power and pumped storage hydro," *IEEE Transactions on Power Systems*, vol. 27, no. 2, pp. 800–810, 2012.

[18] R. Jiang, M. Zhang, and Y. Guan, "Two-stage minimax regret robust unit commitment," *IEEE Transactions on Power Systems*, vol. 28, no. 3, pp. 2271–2282, 2013.

[19] R. Jiang, M. Zhang, L. Guang, and Y. Guan, "Two-stage network constrained robust unit commitment problem," *European Journal of Operational Research*, vol. 234, no. 3, pp. 751–762, 2014.

[20] S. N. Keshmiri and W. Gao, "Multi-objective stochastic economic dispatch," in *North American Power Symposium (NAPS)*, 2010, pp. 1–8.

[21] H. Konno, "A cutting plane algorithm for solving bilinear programs," *Mathematical Programming*, vol. 11, pp. 14–27, 1976.

[22] ——, "A cutting plane algorithm for solving bilinear programs," *Mathematical Programming*, vol. 11, no. 1, pp. 14–27, 1976.

[23] C. Lee, C. Liu, S. Mehrotra, and M. Shahidehpour, "Modeling transmission line constraints in two-stage robust unit commitment problem," *IEEE Transactions on Power Systems*, 2013.

[24] Y. Lee and R. Baldick, "A frequency-constrained stochastic economic dispatch model," *IEEE Transactions on Power Systems*, vol. 28, no. 3, pp. 2301–2312, 2013.

[25] A. Lorca and X. A. Sun, "Adaptive robust optimization with dynamic uncertainty sets for multi-period economic dispatch under significant wind," *IEEE Transactions on Power Systems*, 2014, under review.

[26] ——, "Multistage adaptive robust unit commitment problem," Georgia Institute of Technology, Tech. Rep., 2014.

[27] J. M. Morales, A. J. Conejo, and J. Pérez-Ruiz, "Economic valuation of reserves in power systems with high penetration of wind power," *IEEE Transactions on Power Systems*, vol. 24, no. 2, pp. 900–910, 2009.

[28] J. M. Morales, R. Minguez, and A. J. Conejo, "A methodology to generate statistically dependent wind speed scenarios," *Applied Energy*, vol. 87, no. 3, pp. 843–855, 2010.

[29] N. Navid and G. Rosenwald, "Market solutions for managing ramp flexibility with high penetration of renewable resource," *IEEE Transactions on Sustainable Energy*, vol. 3, no. 4, pp. 784–790, 2012.

[30] M. A. Ortega-Vazquez and D. S. Kirschen, "Estimating the spinning reserve requirements in systems with significant wind power generation penetration," *IEEE Transactions on Power Systems*, vol. 24, no. 1, pp. 114–123, 2009.

[31] J. Ostrowski, M. F. Anjos, and A. Vannelli, "Tight mixed integer linear programming formulations for the unit commitment problem," *IEEE Transactions on Power Systems*, vol. 27, no. 1, pp. 39–46, 2012.

[32] A. Papavasiliou and S. Oren, "Multiarea stochastic unit commitment for high wind penetration in a transmission constrained network," *Operations Research*, vol. 61, no. 3, pp. 578–592, 2013.

[33] A. Papavasiliou, S. Oren, and R. P. O'Neill, "Reserve requirements for wind power integration: A scenario-based stochastic programming framework," *IEEE Transactions on Power Systems*, vol. 26, no. 4, pp. 2197–2206, 2011.

[34] G. Reinsel, *Elements of Multivariate Time Series Analysis*. New York: Springer-Verlag, 1997.

[35] D. W. Ross and S. Kim, "Dynamic economic dispatch of generation," *IEEE Transactions on Power Apparatus and Systems*, vol. 99, no. 6, pp. 2060–2068, 1980.

[36] "ISyE High performance computing facility," School of Industrial and Systems Engineering, Georgia Institute of Technology. [Online]. Available: http://www.isye.gatech.edu/computers/hpc/

[37] A. Street, F. Oliveira, and J. M. Arroyo, "Contingency-constrained unit commitment witn $n - k$ security criterion: A robust optimization approach," *IEEE Transactions on Power Systems*, vol. 26, no. 3, pp. 1581–1590, 2011.

[38] X. A. Sun, *Advances and Trends in Optimization with Engineering Applications*. SIAM, To appear in 2014, ch. Robust Optimization in Electric Power Systems.

[39] S. Takriti, J. R. Birge, and E. Long, "A stochastic model for the unit commitment problem," *IEEE Transactions on Power Systems*, vol. 11, no. 3, pp. 1497–1508, 1996.

[40] A. Tuohy, P. Meibom, E. Denny, and M. O'Malley, "Unit commitment for systems with significant wind penetration," *IEEE Transactions on Power Systems*, vol. 24, no. 2, pp. 592–601, 2009.

[41] J. Wang, M. Shahidehpour, and Z. Li, "Security-constrained unit commitment with volatile wind power generation," *IEEE Transactions on Power Systems*, vol. 23, no. 3, pp. 1319–1327, 2008.

[42] Q. Wang, Y. Guan, and J. Wang, "A chance-constrained two-stage stochastic program for unit commitment with uncertain wind power output," *IEEE Transactions on Power Systems*, vol. 27, no. 1, pp. 206–215, 2012.

[43] Q. Wang, J. P. Watson, and Y. Guan, "Two-stage robust optimization for $n - k$ contingency-constrained unit commitment," *IEEE Transactions on Power Systems*, 2013.

[44] L. Wu, M. Shahidehpour, and T. Li, "Stochastic security-constrained unit commitment," *IEEE Transactions on Power Systems*, vol. 22, no. 2, pp. 800–811, 2007.

[45] ——, "Stochastic security-constrained unit commitment," *IEEE Transactions on Power Systems*, vol. 22, no. 2, pp. 800–811, 2007.

[46] L. Xie, P. Carvalho, L. Ferreira, J. Liu, B. Krogh, N. Popli, and M. Ilic, "Wind integration in power systems: Operational challenges and possible solutions," *Proceedings of the IEEE*, vol. 99, no. 1, pp. 214–232, 2011.

[47] L. Xie, P. Carvalho, L. Ferreira, J. Liu, B. H. Krogh, N. Popli, and M. Ilic, "Wind integration in power systems: Operational challenges and possible solutions," *Proceedings of the IEEE*, vol. 99, no. 1, pp. 214–232, 2011.

[48] L. Xie, Y. Gu, X. Zhu, and M. Genton, "Power system economic dispatch with spatio-temporal wind forecasts," in *Energytech, 2011 IEEE*. IEEE, 2011, pp. 1–6.

[49] L. Xie, Y. Gu, X. Zhu, and M. G. Genton, "Short-term spatio-temporal wind power forecast in robust look-ahead power system dispatch," *IEEE Transactions on Smart Grid*, vol. 5, no. 1, pp. 511–520, 2014.

[50] B. Zeng and L. Zhao, "Solving two-stage robust optimization problems using a column-and-constraint generation method," *Operations Research Letters*, vol. 41, no. 5, pp. 457–461, 2013.

[51] Y. Zhang, N. Gatsis, and G. B. Giannakis, "Risk-constrained energy management with multiple wind farms," in *Innovative Smart Grid Technologies (ISGT), 2013 IEEE PES*. IEEE, 2013, pp. 1–6.

[52] C. Zhao and Y. Guan, "Unified stochastic and robust unit commitment," *IEEE Transactions on Power Systems*, vol. 28, no. 3, pp. 3353–3361, 2013.

[53] ——, "Unified stochastic and robust unit commitment," *IEEE Transactions on Power Systems*, 2013.

[54] C. Zhao, J. Wang, J. P. Watson, and Y. Guan, "Multi-stage robust unit commitment considering wind and demand response uncertainties," *IEEE Transactions on Power Systems*, vol. 28, no. 3, pp. 2708–2717, 2013.

[55] ——, "Multi-stage robust unit commitment considering wind and demand response uncertainties," *IEEE Transactions on Power Systems*, 2013.

[56] L. Zhao and B. Zeng, "Robust unit commitment problem with demand response and wind energy," in *Power and Energy Society General Meeting, 2012 IEEE*. IEEE, 2012, pp. 1–8.

[57] T. Zheng, J. Zhao, E. Litvinov, and F. Zhao, "Robust optimization and its application to power system operation," in *CIGRE*, 2012.

[58] R. D. Zimmerman, C. E. Murillo-Sánchez, and R. J. Thomas, "MATPOWER: Steady-state operation, planning and analysis tools for power systems research and education," *IEEE Transactions on Power Systems*, vol. 26, no. 1, pp. 12–19, 2011.

Part II

A Metric and Market Construct for Flexibility in Power Systems

Le Xie
Anupam Thatte
Sadegh Modarresi

Texas A&M University

For information about this project contact:

Le Xie
Department of Electrical and Computer Engineering
Texas A&M University
College Station, TX 77843-3128
Phone: 979-845-7563
Email: le.xie@tamu.edu

Power Systems Engineering Research Center

The Power Systems Engineering Research Center (PSERC) is a multi-university Center conducting research on challenges facing the electric power industry and educating the next generation of power engineers. More information about PSERC can be found at the Centers website: http://www.pserc.org.

For additional information, contact:

Power Systems Engineering Research
Center Arizona State University
577 Engineering Research
Center Tempe, Arizona
85287-5706
Phone: 480-965-1643
Fax: 480-727-2052

Notice Concerning Copyright Material

Table of Contents

List of Figures

List of Tables

1. Introduction

The increasing penetration of variable renewable generation in electrical grids worldwide poses challenges to power system operators [3–5]. The associated increase in uncertainty and variability will impact many aspects of power systems, from planning to operations. In order to maintain system reliability under increasing penetration of renewables more reserve capacity will be needed [6,7]. Moreover, such reserves should be flexible in order to compensate for the variability of wind and thus avoid ramp insufficiency [8]. The lack of *rampable* capacity in a system could lead to curtailment of renewables. This could be a concern when integrating large amounts of variable renewables such as wind and solar. Thus, recently there has been an increased focus on the topic of flexibility in power systems [9].

Research on this topic has been focused on how to define, quantify and procure flexibility for maintaining power system reliability. Menemenlis et al. [10] noted that the notion of flexibility relates to and should be defined within a specific problem formulation, rather than a single general-purpose measure. It uses a flexibility index based upon process control literature and applies it to the selection of level of balancing reserves for maintaining power system reliability under wind generation integration scenario. The North American Electric Reliability Corporation (NERC) has emphasized the need for incorporating flexibility metrics in planning studies to accommodate a greater amount of variable generation in power systems [11]. Lannoye et al. [12] proposed a flexibility metric called insufficient ramping resource expectation (IRRE) for use in long-term planning. It argues that this metric should be included in planning methodology for generator capacity expansion in systems with high penetration of variable generation. Ma et al. [13] proposed an offline index to estimate the technical ability of both individual generators and a portfolio of generating units to provide flexibility. A unit construction and commitment algorithm is presented to consider both investment costs and operational costs in making the optimal generation capacity expansion decision. Ulbig and Andersson [14] characterized the operational flexibility of a power system using the ramp-rate, power capacity and energy capacity. These three metrics, which are related through integration and differentiation operations in time, can be used to determine the amount of renewables that can be integrated into a given system through extensive simulations. However, transmission constraints are not considered in this assessment.

While researchers have focused on designing and procuring flexibility at the *planning* stage [12], there exists an equally if not more pressing need for flexibility at the *operational* stage [15]. From the short-term power system operations perspective, the limited controllability and high variability of renewable power output is a major issue. Net load, which is the difference between electrical load and renewable power, is more variable than electrical load and this variability increases as the penetration of renewables in a system increases. Also, net load has steeper ramps, shorter peaks, and lower turn-downs than load by itself [16]. Several examples have been noted of severe net load ramp events within a one hour timeframe [11].

Failure to meet such steep net load ramp events would cause both physical and market operations volatilities. Several system operators are facing the issue of temporary price spikes in the real-time economic dispatch market [17]. These price spikes are mainly caused by a shortage of system ramp capability and are indicative of a need for greater flexibility in dispatch. Many technological solutions have been proposed to mitigate the lack of ramp flexibility in power systems

with high penetration of renewables. Such solutions include energy storage, demand response, and fast ramping units. While these technologies would provide a portfolio of choices to the system operator, there is an urgent need to design a market mechanism so that different technologies can compete and be valued for their contribution to system flexibility. Some system operators are currently investigating new market products (based on deterministic approach) in order to create additional flexibility in the dispatch, so as to reduce the frequency of ramp shortages and price spikes [18, 19]. However, the deterministic method requires exogenous reserves, leading to a relatively inefficient model. Wang and Hobbs [20] suggest a stochastic approach with endogenously obtained reserves. Papavasiliou and Oren [21] present a day-ahead stochastic unit commitment model and a deterministic economic dispatch model to address the ramping issue due to high wind penetration.

The traditional operation of the grid has focused on controlling generation to follow the stochastic load. The challenge of integrating stochastic renewable generation motivates us to consider partially controlling the load to match the generation. With the integration of advanced communication and control technologies, smart grid operation will allow the participation of loads as resources in energy balancing operations [22]. The energy consumption of individual users can be managed using either direct load control or incentive-based schemes, in order to provide *demand response* (DR). Recent research has focused on the impacts and the benefits of demand response or deferrable demand. Jeon et al. [23] investigates the cost savings from deferrable demand by shifting demand to less expensive periods and providing ramping services to mitigate variability due to wind. Sioshansi and Short [24] uses a detailed unit commitment model to assess the potential of real-time pricing based demand response in managing the increasing integration of wind generation in the grid. In [25] a stochastic security-constrained unit commitment model is considered in which demand response is used as reserve. In [26] the centralized control of deferrable demand by system operator is compared to the decentralized control by aggregators. It shows that the decentralized approach yields benefits that are close to the centralized approach. Varaiya et al. [27] proposed a new operating paradigm called risk-limiting dispatch for the future smart grid. Risk-limiting dispatch uses smart grid information and control technologies to manage the risk of uncertainty from stochastic inputs such as renewable generation and demand response.

There is a need for a ramp centric metric for inter-temporal flexibility assessment in the real-time operations time scale, which can be used by system operators for situational awareness. This report is aimed at creating a rigorous yet intuitive flexibility metric as well as designing a market construct for the procurement of such inter-temporal operational flexibility. Inspired by the commonly used reliability metric, loss of load probability (LOLP), we propose the *lack of ramp probability* (LORP) as an operational metric for flexibility in real-time economic dispatch [1]. It determines the level of risk of ramp capacity shortage associated with a dispatch decision. The LORP metric can also be used independently of the proposed robust dispatch model, to assess the system flexibility under existing and other proposed real-time economic dispatch models, such as conventional dispatch, look-ahead dispatch and dispatch with ramp capability constraints.

Also there is a need for a methodology to predict and quantify DR factoring the uncertainty of response. In order to determine the value of DR we need to develop models for the aggregated attributes of flexible demand resources. A fast responding DR resource that can reduce consumption and thus aid the system energy balancing, should receive an incentive payment based on the quality

as well as impact of its contribution. Therefore, we need an approach to assess the contribution of the DR resources.

In this report, a multi-period robust optimization based framework is proposed as a market construct for the procurement of flexibility from various flexible resources while observing inter-zonal transmission constraints. Researchers have proposed the application of the robust optimization approach to the unit commitment problem in power systems [28–30]. Robust optimization has certain useful features when compared to the stochastic optimization approach which is used in [20, 21]. The stochastic model solves for the expected value by considering a large number of scenarios, leading to a large problem size. Through the use of uncertainty sets rather than a large number of scenarios, the computational effort is reduced in the robust optimization approach. Also, detailed information on the distribution of the uncertain variable is not required. Further, tractability can be maintained through an appropriate choice of the uncertainty set [31]. The robust solution is conservative since the worst case of uncertainty is considered, but this is acceptable in power systems where usually there is a high cost associated with constraint violation. For instance, in real-time electricity markets where Independent System Operators (ISOs) use shortage pricing to incentivize resources to contribute to maintaining the system energy balance. Wang and Hobbs [20] disregard transmission constraints in their work, whereas we consider them. Papavasiliou and Oren [21] consider the commitment and dispatch problems in the day-ahead timeframe. But a lot of ramping challenges are within the timeframe of about an hour, due to uncertainty and variability in renewables. The forecast error on day-ahead horizon for wind production is quite significant. Therefore, it is more appropriate to deal with this issue in real-time economic dispatch than in unit commitment.

We propose a two-step robust economic dispatch approach that considers inter-zonal tie-line flows as well as uncertainty in zonal net load when obtaining the dispatch solution. This allows for the deliverability of procured ramp capability between operating zones. The two-step dispatch method combines the idea of procuring ramp capability on a zonal basis with the economic dispatch on a nodal basis. Currently, in real-time markets system operators procure reserves on a zonal basis. Thus the proposed approach fits well into the current operating procedure of system operators. By using a zonal aggregation in the first step, the two-step approach addresses the challenge of scaling the robust optimization model. Further, the dispatch solution in the proposed approach has lower generator dispatch costs when compared to a single-step nodal robust approach. Our approach allows for dispatch decisions to be made based on updated forecast information through a receding horizon optimization model.

As part of this report we propose an approach that addresses the question of how to procure flexibility from price-responsive DR resources in real-time operations. This approach fits into the current real-time economic dispatch and locational marginal pricing framework. We extend the previous work on the modeling of DR [32], in order to develop a transfer function model of aggregated DR resources. Also we utilize a probability based approach to characterize the contribution of DR to system ramping capability. The flexibility assessment is done based on the proposed Lack of Ramp Probability (LORP) metric [1]. Given uncertainty and variability in renewable generation, the ISO needs to assess the capability of DR resources to contribute to system ramping. Thus our goal is to analyze the participation of DR in energy balancing (and in the future, also potentially ancillary services) in real-time electricity markets.

The rest of this report is organized as follows. Chapter 2 presents an overview of the proposed flexibility metric, its detailed formulation and the robust economic dispatch market construct. Also a case study is presented on a modified 73 bus IEEE Reliability Test System which illustrates both the proposed metric as well as the robust economic dispatch approach. Chapter 3 describes the proposed framework for enabling DR resources to provide flexibility, a methodology for characterizing the net load, the computation of the proposed lack of ramp probability metric and the transfer function model for DR. Also, in Chapter 3 we present a simulation case study on a modified IEEE 24-bus Reliability Test System. Concluding remarks and future work is in Chapter 4.

2. Metric and Market Construct of Inter-temporal Flexibility in Time-coupled Economic Dispatch

In this chapter an *operational* flexibility metric called lack of ramp probability (LORP) is proposed for the real-time economic dispatch. Further, a two-step robust optimization based framework is introduced to simultaneously guarantee LORP flexibility metric and ensure ramp deliverability in a multi-zonal setting. The proposed framework is illustrated on a 3-zone modified IEEE 73 bus (RTS-96) test system. The results show that the proposed framework is better at managing system ramp capability as compared to existing and industry proposed dispatch models.

Table 2.1: Nomenclature

Indices:

n	Index of all buses in the network.
z	Index of all zones in the network.
i	Index of all dispatchable generators.
j	Index of all loads.
k	Index of all inter-zonal tie-lines.
m	Index of all intra-zonal transmission lines.
t	Index of real time dispatch (5 min. intervals).

Sets:

N	Set of buses.
Z	Set of zones.
$I \subset N$	Set of generators.
$J \subset N$	Set of loads.
I^z	Set of dispatchable generators in zone z.
J^z	Set of loads in zone z.
M	Set of intra-zonal transmission lines.

Random Variables:

$\tilde{P}_j^l[t]$	Net load of load j.
u_j	Net load uncertainty of load j.
$\tilde{P}_z^l[t]$	Net load of zone z.
u_z	Net load uncertainty of zone z.

Inputs:

$\hat{P}_j^l[t]$	Net load forecast of load j at time t.

Functions:

$C_i^g()$	Cost function of generator i.
$F_k[t]$	Flow in tie-line k at the time t.

Table 2.2: Nomenclature (continued)

Decision Variables:	
$P_i^g[t]$	Dispatched output of generator i at time t.
Parameters and Constants:	
T	No. of intervals in real-time dispatch horizon.
P_i^{max}	Maximum output of generator i. (MW)
P_i^{min}	Minimum output of generator i. (MW)
R_i	One interval (5 min.) ramp rate of generator i. (MW)
RC_z	Ramp capability (5 min.) for zone z. (MW)
F_k^{max}	Flow limit for tie-line k. (MW)
F_m^{max}	Flow limit for transmission line m. (MW)
U_z	Uncertainty set for net load in zone z.
ΔP_z^l	Maximum deviation of net load in zone z from the point forecast value. (MW)
σ_z	Standard deviation of net load for zone z.
α_z	Constant associated with confidence level in net load forecast for zone z.
H_k^{red}	Row k of the shift factor matrix for equivalent reduced system.
H_m	Row m of the shift factor matrix for original system.
S	Matrix that sums inter-zonal flows.

2.1 Overview of LORP

In power systems operating reserves are used to maintain reliable system operation despite unpredicted events ranging from generator outages to unpredicted variations in load. Operating reserves are divided into different categories based on their usage and technical requirements [33]. Under current industry practice, operating reserves are calculated on a day-ahead basis. Contingency reserves are used in case of events such as outages of generation or transmission lines. Regulation reserves on the other hand deal with deviations from schedules within a dispatch period. Traditionally system operators have used deterministic methods for determining operating reserve requirements. For power systems with significant penetration of renewables, probabilistic methods of calculating the amount of reserves are being favored [7].

Loss of load probability (LOLP) is often used as a reliability metric for generation adequacy. It is the probability that the combination of available generation and reserves will fall short of the system demand. Standard metrics such as the loss of load expectation (LOLE) and the expected energy not served (EENS) are used in planning studies by the power industry [34]. A system may have adequate generation capacity to meet the total demand, but may be unable to match the change in net load due to inadequate ramping capability of available generators. Moreover, the time frame and triggering condition associated with the deployment of contingency reserves does not cover unpredicted changes in net load that occur due to variability of renewables in the real-time dispatch horizon. Thus, the requirement of adequate system-wide ramp capability from controllable generators in the system falls into a separate category from contingency reserves. In the future as the penetration of asynchronous resources increases, in addition to ramping capability, systems may require new Ancillary Services to address the challenge posed by net load variability.

In power systems load forecasting has become fairly accurate with Mean Absolute Error (MAE) of forecast error $\approx$ 1-3% on the day-ahead horizon and MAE $\approx$ 0.5-2% on the hour-ahead horizon [35, 36]. Whereas, for the regional wind power forecast the MAE can be 15% or higher for day-ahead, and as high as 11% for hour-ahead [37]. The causes of unpredicted ramp events include forecast errors in load, renewable power and net interchanges, as well as unscheduled outages of generators. Since net load forecasts depend on the renewable generation forecasts, the system operator may face a challenge due to the fact that the ramping requirement cannot be predicted accurately in advance. In such cases the system operators are not able to dispatch their generation resources effectively, and may require out-of-market actions by the operator in order to maintain power balance. Thus, operational flexibility is critical to the power system operator.

The real-time operational flexibility of a power system depends on the dispatch solution of the economic dispatch model and thus is dependent on the ramping capability of each generation resource. The flexibility metric proposed in this report measures the ability of a system to use its generating resources to meet both expected net load changes as well as forecast errors. Analogous to the way LOLP measures the capacity adequacy of a power system, LORP measures the ability of the power system to meet the net load changes in the real-time operations time frame. LORP depends on the available inter-temporal ramp capability of the system. Further, LORP can be used to quantify the robustness of the dispatch solution, in order to provide guidance to the system operator. Another important issue is the deliverability of ramp capability between operating zones in a system. Thus, the LORP index should be calculated not only on a system-wide basis, but also on a zonal basis taking into account inter-zonal flows and tie-line flow limits.

LORP is independent of the economic dispatch model used by the system operator. It can be used with any existing or proposed economic dispatch model including the conventional security constrained economic dispatch (SCED), look-ahead dispatch or dispatch with ramp capability constraints. Thus, it can be used to compare the robustness of different dispatch methods. The data required to calculate LORP includes the minimum and maximum rated output, ramp up and ramp down rate, and the current dispatch level of each generation resource. While currently conventional generators are considered as providers of ramp capability, other resources such as energy storage or demand response can also provide flexibility, if they meet certain technical requirements specified by the system operator. The total upward or downward ramp capability provided by the resources may be different depending on the state of the resource.

Traditionally system operators have procured reserves on a zonal basis. Due to tie-line congestion deliverability of these reserves between zones is a concern [38]. Inter-zonal tie-line congestion would also have an impact on the operational flexibility of the system. Transmission line ratings can have an impact on the rampable capacity of a zone given that additional ramp power can be transferred over the tie-lines if needed. The available operational flexibility in a system or a zone is also a function of the resource mix. For example, a zone containing several fast ramping units such as natural gas generators would have greater rampable capacity in the short term than a zone primarily containing nuclear and coal generators. Thus, it is important to present a realistic assessment of zonal ramp capability for the system operator to have awareness of the operational flexibility of both the system as a whole as well as the zones comprising the system. The proposed system and zonal LORP metrics represent an attempt at providing such a situational awareness tool to enable a better understanding of the real-time operational flexibility of the system. The metrics

alert the operator to the higher probability of a ramp shortage event. The operator can then act to change the manual load offset in the dispatch system so as to better manage system ramping. For instance the Midcontinent ISO currently uses manual offsets for load as well as for Net Schedule Interchange (NSI), for managing resource flexibility. Thus, the LORP metric can be used with the current conventional real-time economic dispatch model to provide useful information to the system operator. Additionally, in the future as more flexibility providing resources such as energy storage and demand response are included in the system, the dispatch decisions for these could be made based on the LORP metric.

2.2 Detailed Formulations

In this section we present the formulation of the proposed flexibility metric as well as the economic dispatch model for ensuring ramp flexibility in multi-zonal power systems.

2.2.1 Inter-temporal Operational Flexibility Metric

Due to the increasing penetration of variable renewable generation from sources such as wind and solar, power system operators are facing the challenge of managing the system under increased variability and uncertainty in net load. A particular aspect of this challenge is the impact of variable generation on the real-time economic dispatch time scale. At this time horizon it is difficult for system operators to adjust the output profile of their generation resources to handle large unpredicted net load ramp events. The lack of flexibility in dispatch leads to temporary price spikes in the real-time electricity market [17]. It is desirable to have a metric that can indicate when the system may have insufficient ramp capability and the probability of such a price spike occurring.

The system-wide *lack of ramp probability* ($LORP_s$) provides an assessment of the adequacy of the available system ramping capability from dispatched generators to meet both expected changes as well as uncertainty in forecasted net load [1]. It is defined for the ramp up case as follows:

$$LORP_s^{up,\tau}[t] = Pr\left(\sum_{i\in I}\{P_i^g[t] + \min(\tau R_i, P_i^{max} - P_i[t])\} < \tilde{P}_s^l[t+\tau]\right) \tag{2.1}$$

Similarly we can define the LORP index for the availability of system ramp down capability.

$$LORP_s^{dn,\tau}[t] = Pr\left(\sum_{i\in I}\{P_i^g[t] - \min(\tau R_i, P_i[t] - P_i^{min})\} > \tilde{P}_s^l[t+\tau]\right) \tag{2.2}$$

where $\tilde{P}_s^l[t+\tau]$ is the system-wide net load for the interval τ time steps in the future, and is assumed to a Gaussian random variable with known mean and standard deviation. The mean can be taken to be the point forecast value of the net load and the standard deviation can be assumed based on historical data. The distribution is actually conditional, given knowledge of $\hat{P}_s^l[t]$.

If correlation information about load and wind is available then this can be used to improve the calculation of the *pdf* parameters. Further, the LORP concept can be applied to any empirical distribution of net load. Such an empirical distribution can be obtained using the historical data

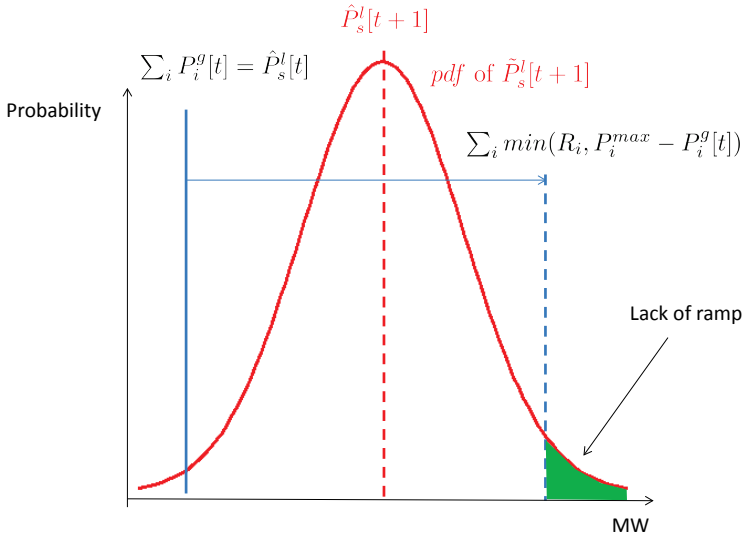

Figure 2.1: Illustration of lack of ramp probability

available to the system operator. The $LORP_s$ value is the probability that given the current dispatch levels the system operator will not be able to ramp up or down the dispatched generation resources to meet the net load in the future time interval. This concept is illustrated in Fig. 2.1 for the case of $\tau = 1$, where the shaded area under the curve represents the $LORP_s^{up}$ value. If the calculated LORP value is below the predetermined target value, the system operator may have to take action to procure additional ramp capability.

Under current ISO practices, reserves are dispatched on a zonal basis. Reserve zones are usually defined on the basis of utility boundaries, geography or significant congested transmission lines. However, deliverability of reserves is a concern due to tie-line congestion. We make an assumption that there is no uncertainty in the short term in the scheduled imports and exports for the zones. Thus we define the ramp up capability for each zone for $\tau = 1$ as follows.

$$RC_z[t] = \text{Zonal Generator Ramp Power[t]+} \\ \text{(Imports[t+1]-Imports[t])} - \text{(Exports[t+1]-Exports[t])} \quad (2.3)$$

where the Zonal Generator Ramp Power is the total available ramp capability from all the dispatched generators in a zone. Based on the definition of zonal ramp capability we can calculate the zonal LORP as:

$$LORP_z^{up}[t] = Pr\left(\sum_{i \in I^z} P_i^g[t] + RC_z[t] < \tilde{P}_z^l[t+1]\right), \forall z \quad (2.4)$$

Unlike the system-wide $LORP$, here inter-zonal tie-line flows are considered. The zonal LORP for the ramp down case can be defined similarly.

For a given grouping of the buses in the system into zones, we can calculate the $LORP_z$ for each zone for a given dispatch solution. The $LORP_z$ value can be used by the system operator as an index for the reliability of the dispatch solution with regards to the ramping capability in a particular zone. If the $LORP_z$ value is too high, the operator may choose to import power from other zones or other ISOs in order to maintain ramp capability.

The difference between $LORP_s$ and $LORP_z$ is that $LORP_z$ uses the zonal ramp capability incorporating inter-zonal tie-line scheduled flows, whereas the system-wide index considers the total system ramp capability ignoring the tie-lines. Since we are not considering the intra-zonal transmission constraints when calculating $LORP_z$, it is an optimistic estimate of the true probability of ramp shortage event. The $LORP_z$ metric enables the system operator to make a decision about sharing of ramping capability between zones. Also, it is not an overly conservative metric. We recognize that procuring ramp at the nodal level may not make physical sense at the nodes where there exists only a fixed/non-controllable demand. Therefore, defining the LORP metric at a nodal level does not provide actionable information to the system operator. Our future work will focus on a metric that includes limits on injections on a nodal basis.

2.2.2 Two Step Robust Economic Dispatch Model

Given the proposed flexibility metric, how does the system operator create a market mechanism to ensure the LORP level? A major consideration is to ensure ramp deliverability in a sub-area/zone of a power system. To accommodate this we have proposed a two-step robust economic dispatch approach. In the first step, each zone is aggregated as an equivalent node with inter-zonal tie-line constraints observed. The ramping capability of the system for the worst case of net load is ensured and the tie-line flows determined. This is fed into the second step dispatch, which is done at the nodal level while maintaining the tie-line flows and zonal ramping capability. The result of the proposed two-step dispatch will (i) ensure zonal level ramping capability, (ii) maintain the tie-line flows, and (iii) observe all transmission constraints.

The two-step robust economic dispatch model with network constraints is as follows:
Step 1: Robust Dispatch Step based on Zonal Aggregated Model

$$\min_{P_i^g[t]} \sum_{t=1}^{T} \sum_{i \in I} C_i^g(P_i^g[t]) \tag{2.5}$$

s.t.

$$\sum_{i \in I} P_i^g[t] = \sum_{j \in J} \hat{P}_j^l[t],\ t = 1 \tag{2.6}$$

$$\sum_{z \in Z} \sum_{i \in I^z} P_i^g[t] \geq \sum_{z \in Z} (\sum_{j \in J^z} \hat{P}_j^l[t] + u_z[t]), \forall t = 2, \ldots, T, \forall u_z[t] \in U_z[t] \tag{2.7}$$

$$P_i^{min} \leq P_i^g[t] \leq P_i^{max}, \forall i, t \tag{2.8}$$

$$-R_i \leq P_i^g[t] - P_i^g[t-1] \leq R_i, \forall i, t \tag{2.9}$$

$$-F_k^{max} \leq H_k^{red}(\sum_{i \in I^z} P_i^g[t] - \hat{P}_z^l[t]) \leq F_k^{max}, t = 1, \forall k \tag{2.10}$$

$$-F_k^{max} \leq H_k^{red}(\sum_{i \in I^z} P_i^g[t] - (\hat{P}_z^l[t] + u_z[t])) \leq F_k^{max}, \forall t = 2, \ldots, T, \forall u_z[t] \in U_z[t], \forall k \tag{2.11}$$

$$U_z[t] = [\hat{P}_z^l[t] - \Delta P_z^l[t], \hat{P}_z^l[t] + \Delta P_z^l[t]], \forall t = 2, \ldots, T, \forall z \tag{2.12}$$

In step 1 a robust optimization based economic dispatch is run on a reduced equivalent network. Using the bus aggregation approach presented in [39] the network can be reduced to one where

each zone is reduced to a single bus with an aggregated net injection. All the generators and loads within an administrative zone are assumed to be co-located at this one bus. The intra-zonal flow limits are ignored and the inter-zonal tie-lines are aggregated to a single equivalent tie-line for each pair of zones. Then the reduced shift factor matrix H^z is obtained for the reduced network.

The objective is to minimize total generation cost over all the time intervals (2.5). The system power balance constraint for the current time interval is given by (2.6). Compared to the conventional dispatch model additional constraints are added in this model in order to ensure that the dispatch solution for future time intervals is feasible even in the worst case of zonal net load uncertainty (2.7). Other constraints include the generator power output limits (2.8) and the inter-temporal ramp rate limits for each generator (2.9). The inter-zonal tie-line flow limits must be satisfied for the equivalent reduced system, namely (2.10) and (2.11). At this step we do not consider the transmission line flow limits within the zones. The inter-zonal tie-lines are aggregated into a single equivalent line which has the combined flow limit of the lines in the original system. This approximation is reasonable given that the approach presented in [39] yields inter-zonal flows in the reduced system that closely match those in the original system for a realistic range of loading. While the limits on the equivalent tie-line are observed, in the case of multiple tie-lines between a given pair of zones, the limits on individual component tie-lines may not be observed for all cases of loading.

For buses without generators we have $P_n^g = 0$, and similarly for buses without loads we have $P_n^l = 0$. The deterministic uncertainty sets (2.12) defines the range of the uncertainty in the net load for the future time intervals. This is the key feature of robust optimization where the uncertainty is modeled using a deterministic set. The zonal net load is assumed to be uncertain, but lies within a defined range around the nominal or forecast value. The parameter $\Delta P_z^l[t]$ controls the size of the uncertainty set. As it increases the solution becomes more conservative and the dispatch considers a higher level of uncertainty in the net load. We can assume that $\Delta P_z^l[t] = \alpha_z \sigma_z$, where α_z is a constant and σ_z is the standard deviation for the zonal net load which can be calculated using historical data. α_z can be selected by the system operator. It can be higher or lower based on the confidence in the net load forecast. For instance, we could select $\alpha_z = 3$ and hence have an uncertainty set spanning $\pm 3\sigma$ i.e., covering 99.73% of cases of uncertainty for a normal distribution. For the assumption of Gaussian distribution of uncertainty, the choice of the uncertainty set for the net load results in a bound on the value of LORP. Thus, the uncertainty set internalizes the desirable LORP requirement.

Step 2: Deterministic Nodal Security Constrained Dispatch Step

$$\min_{P_i^g[t]} \sum_{i \in I} C_i^g(P_i^g[t]) \tag{2.13}$$

s.t.

$$\sum_{i \in I} P_i^g[t] = \sum_{j \in J} \hat{P}_j^l[t],\ t = 1 \tag{2.14}$$

$$P_i^{min} \leq P_i^g[t] \leq P_i^{max}, \forall i, t \tag{2.15}$$

$$-R_i \leq P_i^g[t] - P_i^g[t-1] \leq R_i, \forall i, t \tag{2.16}$$

$$\sum_{i \in I^z} \min(R_i, P_i^{max} - P_i^g[t]) \geq RC_z, \forall z, t \tag{2.17}$$

$$F_k[t] - \varepsilon \leq S.H(P^g_{[1:n]}[t] - \hat{P}^l_{[1:n]}[t]) \leq F_k[t] + \varepsilon, \forall k, t \tag{2.18}$$

$$F_m[t] \leq H(P^g_{[1:n]}[t] - \hat{P}^l_{[1:n]}[t]) \leq F_m[t], \forall m, t \tag{2.19}$$

In step 2 a deterministic optimization based economic dispatch is run on the full system. The inter-zonal flows in this step are constrained by bounds given by $\pm\varepsilon$ around the flows obtained from step 1 (2.18). When the generator re-dispatch occurs, the tie-line flows are not necessarily less than the F_k^{max} limit set in step 1, but could be as high as $F_k^{max} + \varepsilon$. In general, the likelihood of violation of the inter-zonal tie-line limits is related to the net load uncertainty in the system. The value of ε can be selected by the system operator based on acceptable short-term tie-line flow violations. Thus the deliverability of ramp capability is ensured by taking into consideration inter-zonal tie-line flows. The objective is to minimize total generator dispatch cost for the current time interval (2.13). The ramp capability from all committed generators in each zone is maintained at the amount obtained in step 1 (2.17). Other constraints include the demand-supply balance constraint (2.14), generator output constraints (2.15), generator ramp rate limits (2.16) and transmission line flow limits for the intra-zonal lines (2.19).

Procedure for Two Step Robust Dispatch:
The procedure for the two step robust dispatch to be run by the system operator is as follows:

1. The ISO receives the real-time market generator bids ($C_i^g[t]$, $P_i^g[t]$) for all time intervals t in the horizon T.

2. The ISO chooses the value of deviation ΔP_z^l in net load for each zone. Thus the uncertainty sets U_z can be defined using (2.12) based on the confidence level in net load forecast. The uncertainty sets for the net loads for each zone can be defined using $\pm\alpha_z\sigma_z$ deviations from forecast values.

3. The ISO runs the step 1 robust dispatch, namely (2.5)-(2.12), on the reduced equivalent system.

4. The tie-line flows F_k and the zonal ramp capabilities RC_z obtained from step 1 are fed to step 2.

5. In step 2 the tie-line flows obtained from step 1 are allowed to vary by $\pm\varepsilon$. The value of ε can be set based on the acceptable short term deviations in flows.

6. The ISO runs the step 2 deterministic dispatch, namely (2.13)-(2.19), on the original system. The optimization model yields the dispatch solution and the locational marginal prices.

7. The step 2 dispatch solution is implemented. The forecast information for net load is updated and the process is repeated for the next real-time market interval.

Each time the two-step economic dispatch is solved we get generator dispatch solutions for the current time interval ($t = 1$) and future time intervals ($t = 2, 3, \ldots, T$). The current interval solution is implemented while the future interval solutions are considered as advisory. Then we move forward in time and repeat the process, using updated forecast information on load and renewable power generation. This allows the decision maker to use updated forecast information to make dispatch decisions using a receding horizon model.

Since intra-zonal constraints are not considered in step 1 of the dispatch model, the dispatch solution does not consider all realizations of net load uncertainty. Thus, while the dispatch solution will significantly reduce shortage events, it may not eliminate them completely. In order to eliminate the price spikes completely the dispatch solution would have to be very conservative. Our model provides a balanced approach to reducing price spikes while not making the dispatch solution too conservative.

2.3 Case Study

In this section, a case study is presented on a modified 73 bus IEEE Reliability Test System (RTS 96) [40]. There are three identical areas each of which contain three wind farms (bus 15 = 200 MW, bus 18 = 240 MW and bus 23 = 70 MW) which we treat as negative load, while the rest are conventional generators which are controllable. The penetration of wind generation is 13% by capacity. There are 120 transmission lines and the flow limits on all lines are taken from the RTS 96 dataset. The generator costs are calculated using the average of the heat rate data presented in [41] combined with the fuel costs presented in [42].

In the two-step robust dispatch model, in order to ensure deliverability of ramp capability, we consider a reduced equivalent 3 bus network. For the reduced system we aggregate the generation and loads in each zone at a single bus. Thus, the entire 73 bus 3 area system is reduced to 3 buses each representing one zone. In the reduced system the intra-zonal transmission line constraints are ignored while the inter-zonal flow limits are considered. For the numerical example presented in this section we use $T = 2$ for defining the dispatch horizon.

The simulation duration is 24 hours with dispatch performed for 5-min intervals, using scaled real load profile data taken from New York ISO [43]. For each dispatch instance, the net load forecast for the current interval is assumed to be accurate while the forecast for the future intervals has error. Further, it is assumed that within the current time interval any deviation of the actual net load from the schedule can be handled by the frequency regulation control.

The uncertainty set for the net load in each zone is defined by considering deviations of $\pm 2.5\sigma_z$ from the forecast net load values. The standard deviation σ_z for each zone is obtained from the previous day's actual net load data. The standard deviations of the net loads for the zones are $\sigma_1 = 176.29$, $\sigma_2 = 176.29$ and $\sigma_3 = 180.35$. We assume the value of ε to be 5% of the line limits used in the case study.

The robust optimization dispatch is modeled and solved in MATLAB using the CPLEX LP solver *cplexlp* and the YALMIP robust optimization toolbox [44]. The economic dispatch simulation is conducted on a laptop with Intel Core 2 Duo 2.2 GHz CPU with 4 GB RAM.

Fig. 2.2 shows the output of the wind generators, which are considered as non-dispatchable and hence are included in the system net load. Further, it is assumed that there is no curtailment of the wind. The total electrical load and the total net load profiles for the system are shown in Fig. 2.3. The real-time economic dispatch is simulated using the conventional deterministic single-interval model, the deterministic look-ahead model (with look-ahead horizon of one step ahead) and the proposed two-step robust model (with T=2).

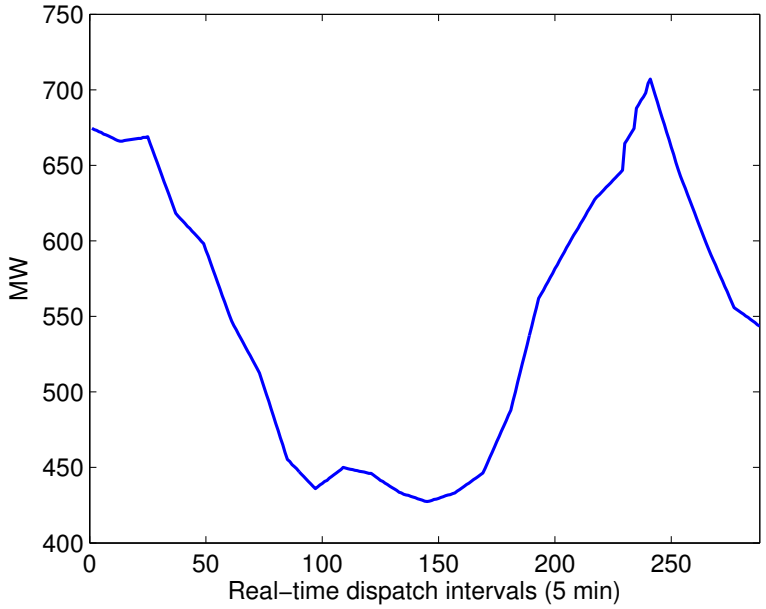

Figure 2.2: System total wind profile for entire day

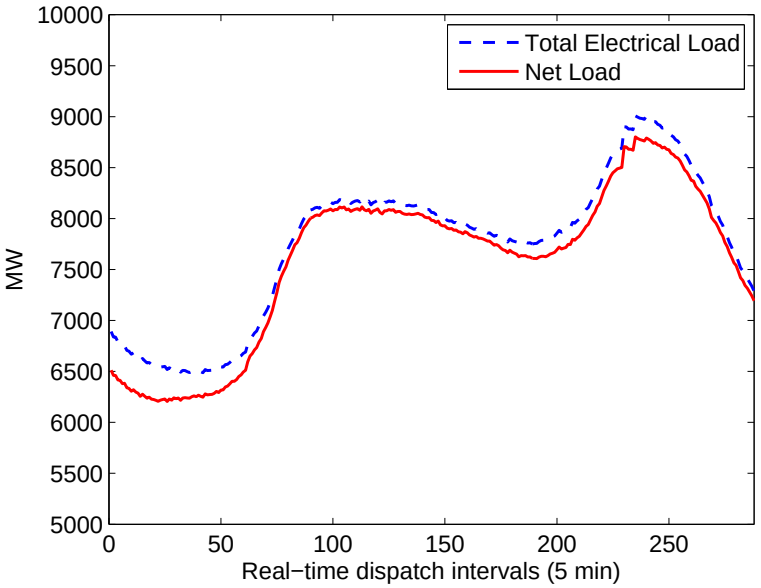

Figure 2.3: System total electrical load and net load profiles for entire day

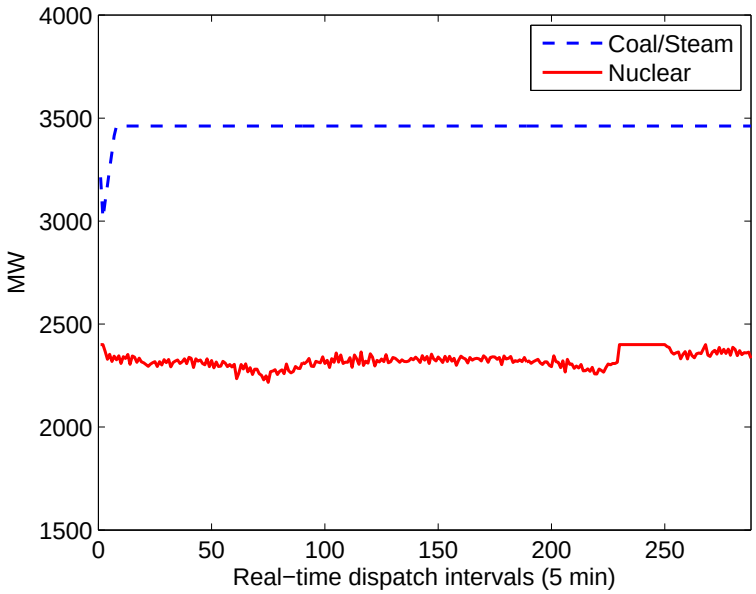

Figure 2.4: System total coal and nuclear generator profile for entire day

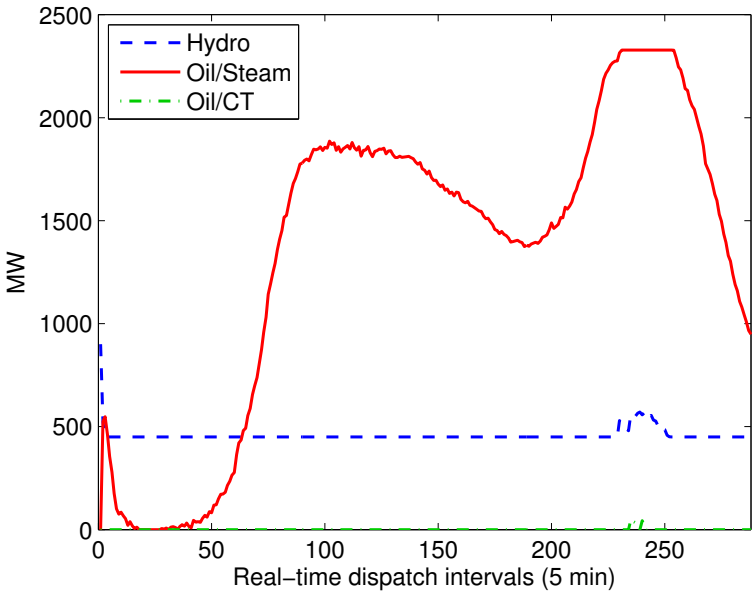

Figure 2.5: System total oil-fired and hydro generator profile for entire day

The generation profiles of the different fuel types using the proposed robust dispatch model are shown in Fig. 2.4 and Fig. 2.5. From these results we observe that both Nuclear and Coal units provide the base load, whereas Oil/Steam units are used for load following. In this scenario the Oil-fired Combustion Turbines (CT) are not dispatched for most of the day since the net load is not high and they are the most expensive generators. Thus the Oil/CT units are used as peaking units.

Fig. 2.6 shows the system-wide LORP as well as the zonal LORP values for the two-step robust dispatch model. The system-wide value does not give a complete picture of the ramp capability

since it does not consider inter-zonal tie-line flows. A situation may occur where the system-wide LORP value is acceptable, but the LORP in a particular zone is too high. In such case the system operator may have to take some action to increase the ramping capability of that zone. Also, it is observed from the difference between $LORP^{up}$ and $LORP^{down}$ values that ramp up is a greater challenge than ramp down. This observation is also seen in operator experience [18].

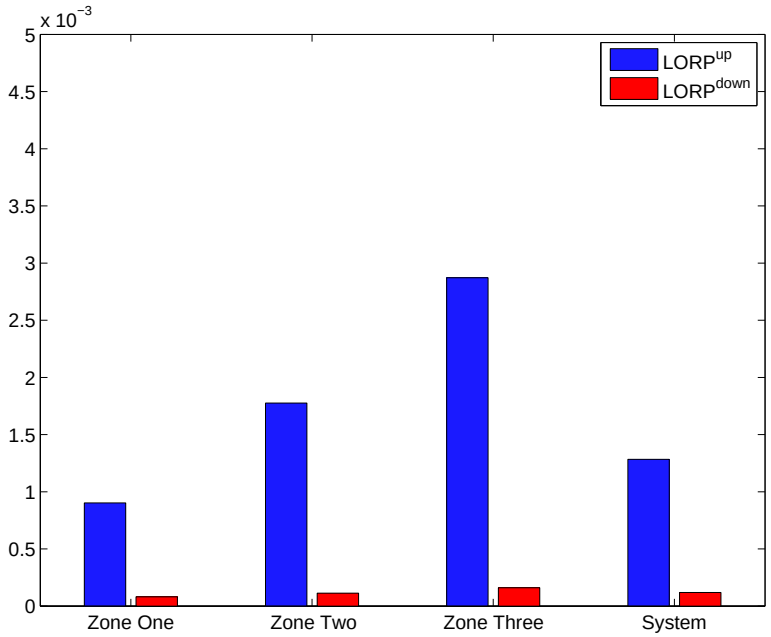

Figure 2.6: Mean LORP comparison for different zones using two-step robust dispatch

Table 2.3 shows the results of running the 3 real-time economic dispatch models for the given day when the net load forecast for the next time interval, namely $\hat{P}^l[t+1]$ has a forecast error of MAE = 0.3766%. The computation time for the deterministic look-ahead model is larger than for the conventional model, due to the increase in the optimization problem size. In the two-step model, the first step (robust optimization) takes up most of the total computation time. The look-ahead model has higher dispatch costs than the conventional, since it sometimes backs down the fast ramping generators based on predicted net load changes and instead uses the more expensive slower units. But, the benefit is that shortage events and price spikes are reduced, as indicated by the reduction in LORP and mean LMPs. The two-step robust dispatch approach results in higher dispatch costs than both the conventional and look-ahead dispatch models. The robust optimization based approach results in a conservative solution which leads to higher dispatch costs. However, this approach leads to a lower number of shortage events and hence reduces the need for out of market manual corrections. These corrections add to the cost of electricity since power may have to be procured from very expensive generators in order to maintain the system energy balance. Thus, the proposed robust approach gives a significantly lower system-wide LORP. Further, this approach yields lower mean of Locational Marginal Prices (LMPs), which is a result of reducing the number of price spikes in the real-time market. These features make the robust approach attractive to system operators.

The conservatism of the solution can be controlled based on the selection of the uncertainty set.

A larger uncertainty set around the nominal net load value will lead to a more conservative solution. Thus, there is a trade-off between dispatch costs and the robustness of the dispatch solution.

Table 2.3: Dispatch results (Forecast MAE = 0.3766%)

Dispatch Model	Conventional	Deterministic Look-ahead	Two-Step Robust
Dispatch Costs (Millions $)	41.77	41.85	50.82
Mean $LORP_s^{up}$	0.0873	0.0821	0.0013
Mean LMP ($/MWh)	70.39	69.53	46.45
Max LMP ($/MWh)	664.05	676.85	464.72
Computation Time (sec)	1.96	2.70	Steps (1) 67.38, (2) 0.70

Table 2.4 shows the economic dispatch results when the net load forecast error is increased to MAE = 0.5069%. In this case with the two-step robust dispatch approach we get mean $LORP_s^{up} = 0.0013$, whereas with the deterministic look-ahead dispatch we get mean $LORP_s^{up} = 0.0821$ and with the conventional dispatch approach we get mean $LORP_s^{up} = 0.0873$. Thus the proposed two-step robust approach is able to ensure the LORP value even with higher net load forecast error. The LORP is ensured by incorporating operating conditions and forecast quality into the procurement of the ramp capability.

Table 2.4: Dispatch results (Forecast MAE = 0.5069%)

Dispatch Model	Conventional	Deterministic Look-ahead	Two-Step Robust
Dispatch Costs (Millions $)	41.77	41.85	50.89
Mean $LORP_s^{up}$	0.0902	0.0847	0.0013
Mean LMP ($/MWh)	70.40	69.74	47.08
Max LMP ($/MWh)	664.05	676.85	464.72
Computation Time (sec)	1.93	2.69	Steps (1) 67.6, (2) 0.69

Fig. 2.7 shows the mean $LORP^{up}$ index values for the entire day for all the 3 zones. The robust approach has lower $LORP^{up}$ values than both conventional as well as look-ahead dispatch. Thus, it is more reliable in terms of zonal ramp capability.

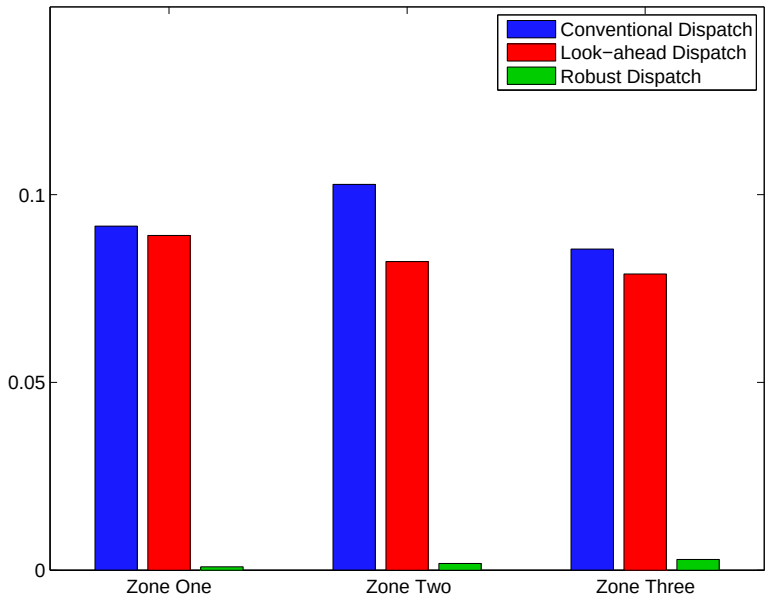

Figure 2.7: Mean LORP comparison for all zones

3. Managing System Ramp Flexibility by Utilizing Price-Responsive Demand: An Empirical Assessment

In this chapter we present an approach to procuring flexibility from price-responsive demand in order to manage system ramp capability. The proposed approach utilizes a metric termed as Lack of Ramp Probability (LORP) to assess the contribution from the demand response to the system ramping flexibility. Our approach fits well into the current real-time economic dispatch framework. We conduct simulations of our proposed approach using real data from price-responsive loads. The impact from the price-responsive demand on the system ramp flexibility is illustrated in a modified IEEE 24-bus Reliability Test System.

3.1 Framework for Flexibility using Demand Response

Traditionally only conventional generation, given its ability to control its power output, has participated in the critical energy balancing operation. However, with the advances in control and communications technologies, and the smart grid paradigm this could change. With smart controls in place, the aggregate load could be shaped such that it contributes to the balancing operation through participating in ISO markets. Depending on the ISO market rules, DR resources could participate in both energy and ancillary service markets [45, 46].

The approaches for DR can be classified into two main categories - direct load control and time varying pricing schemes. In direct load control (DLC) programs, based on an agreement between customers and the aggregator/utility, remote control of certain loads (e.g., air conditioners, pumps etc.) is used to manage their energy consumption [47]. The lack of user privacy is a major barrier to large scale implementation of this approach. There are a number of time-varying pricing schemes for DR including time-of-use pricing (TOU), critical peak pricing (CPP), peak load pricing (PLP), and real-time pricing (RTP) [48, 49]. Under this approach users voluntarily manage their consumption in response to a time-varying retail tariff [50]. The major barrier in this approach is the challenge faced by customers to manually respond to time-varying prices. From the ISO point of view the challenge is to optimally balance the system when uncertainty arises both in supply and demand. Given that procuring larger amounts reserves is an expensive option, utilizing DR to provide the needed flexibility could be cost efficient.

We envision a novel framework for flexible loads that will enable ISOs to integrate demand response for the provision of flexible ramping services, thereby tapping into the aggregated flexibility potential of DR resources (Fig. 3.1). Through the use of smart grid technologies the aggregated load profile could be reshaped over a time horizon of several minutes to hours, without degradation in the end user quality of service level. In this future smart grid, an automated intelligent controller can be fed basic information about user comfort and cost preferences, and then learns to manage the energy consumption schedule of the flexible loads. The controller will receive price signals from the utility or load aggregator. The utility or aggregator will then aim to achieve load shaping of the aggregate load, in order to participate in ISO energy balancing markets. Thus, the aggregate load profile could be reshaped to maintain system energy balancing despite the variability in renewable generation.

Given the large scale deployment of smart meters, utilities now have access to a large amount of empirical high granularity data on customers consumption patterns. This streaming big data can be leveraged for: (1) increasing system ramp flexibility through DR, and (2) the assessment of system ramp issues in real-time dispatch. By utilizing this big data the aggregate behavior of DR resources can be characterized using a transfer function approach [32]. The transfer function model of price responsive demand is better than the traditional econometric models at capturing the salient features of flexible demand. The traditional econometric approach has been to characterize the sensitivity of the load using the concept of elasticity. The preliminary work in [32] shows that price responsive demand exhibits two key features: (1) a nonlinear response to high prices; and (2) a time delay between the high price interval and the resulting reduction in demand. Using real data for one price sensitive load in Texas, a transfer function model of price responsive demand was developed. We build on this work to assess the potential of the price responsive demand to contribute to system *ramp flexibility*. In our work we focus on the probabilistic characterization of DR given a large aggregation of customers. A future avenue of research is the design of the optimal real-time price signal for eliciting ramp flexibility from DR. Thus providing a closed-loop approach for procuring desired amount of ramp flexibility from aggregated DR resources.

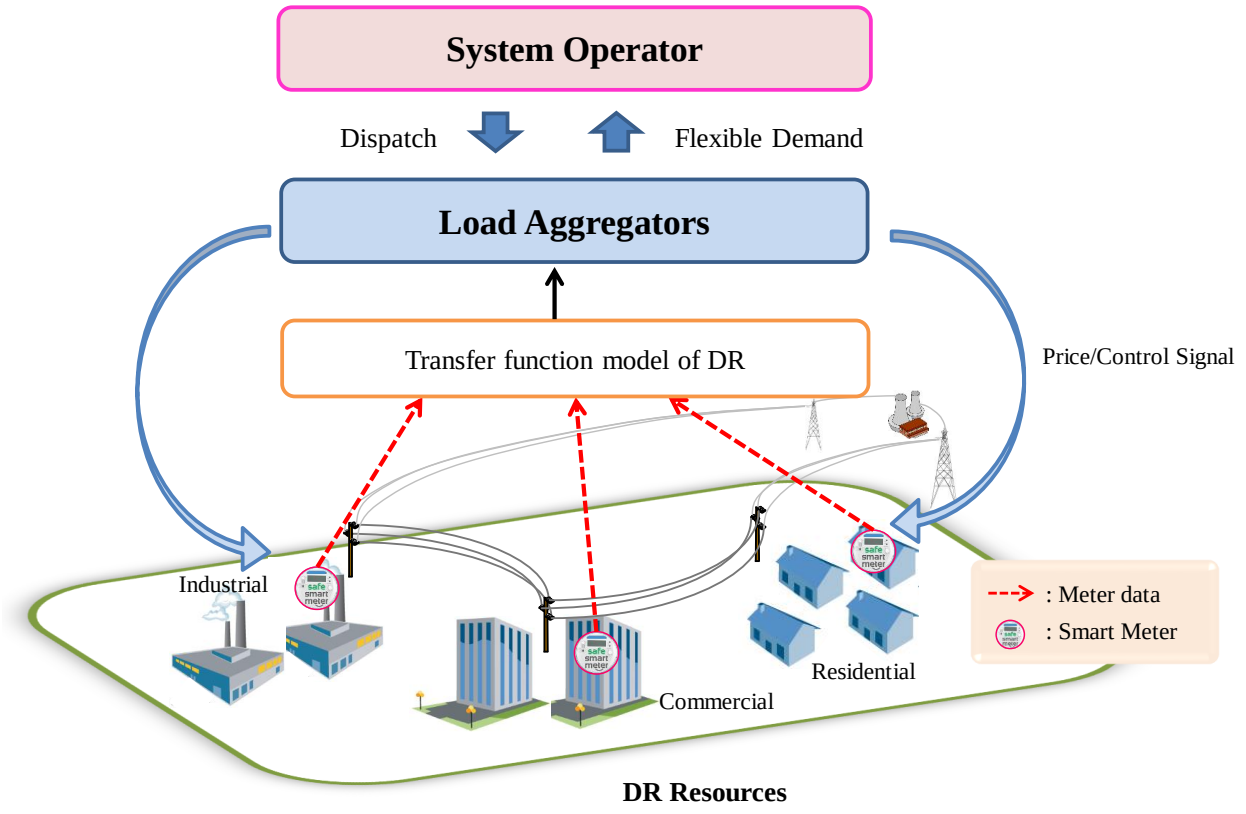

Figure 3.1: Proposed framework for utilizing demand response for ramp flexibility

3.2 Net Load Characterization

In this section we look at characterizing net load when price responsive demand is included. Based on this characterization of net load we obtain an empirical distribution for the net load one-interval into the future. Built upon the recent work of transfer function modeling of demand response [32], we obtain the *controllable* load deviation one step into the future with the excitation of price signals.

3.2.1 Net Load and Flexibility Metric

We consider the net load (NL) as comprised of 3 components:

$$NL[t] = l[t] + d[t] - w[t] \tag{3.1}$$

1. l = aggregation of loads which are not participating in the DR scheme. We assume that this component can be characterized using a Gaussian distribution with known mean and standard deviation. Thus $l \sim N(\mu_l, \sigma_l)$. Also we assume that the point forecast at time $t+1$ is known $\hat{l}[t+1]$.

2. $d(u)$ = aggregation of loads which are participating in DR, i.e., they are receiving a price (or other control) signal, where u is a vector of prices over time. We assume that this component is characterized using the transfer function model. Thus d at time t, namely $d[t]$ is a function of $p[t]$ as well as past prices $p[t-1], \ldots, p[t-T]$. We neglect the impact of prices beyond T intervals in the past.

3. w = total system wind power production. We assume that we have a prediction of the system-wide wind production and that the prediction error is a random variable with known probability distribution.

We can combine the forecasts of the 3 components to get the *net load* forecast. Thus the point estimate of net load at time t is given by $\hat{NL}[t] = \hat{l}[t] + \hat{d}[t] - \hat{w}[t]$. If we neglect the correlation between wind, non participating demand and price responsive demand, we can simply add the errors $e_{NL} = e_l + e_d - e_w$. We assume that the forecast error of wind follows a Cauchy distribution [51], while the demand forecast errors are assumed to be from Gaussian distributions. Thus, we can get the empirical distribution of net load error.

Now that we have a point estimate of net load and its forecast error distribution, we can calculate the flexibility of system ramp using a probabilistic metric. Analogous to the concept of loss of load probability (LOLP) which is used as a metric in system capacity adequacy studies, we have proposed a flexibility metric for system ramp capability called the *lack of ramp probability* (LORP) [1]. We define the LORP metric for both ramp-up and ramp-down cases as follows:

$$LORP^{up}[t] = Pr\left(\sum_{i \in I}\{P_i^g[t] + \min(R_i, P_i^{max} - P_i[t])\} < \tilde{P}_s^l[t+1]\right) \tag{3.2}$$

Similarly we can define a reliability index for the availability of system ramp down capability.

$$LORP^{dn}[t] = Pr\left(\sum_{i\in I}\{P_i^g[t] - \min(R_i, P_i[t] - P_i^{min})\} > \tilde{P}_s^l[t+1]\right) \tag{3.3}$$

where $\tilde{P}_s^l[t+1]$ is the system-wide net load for the next time step, and is assumed to a random variable with an empirically obtained probability distribution. This can be interpreted as the point forecast value of the net load combined with its forecast error.

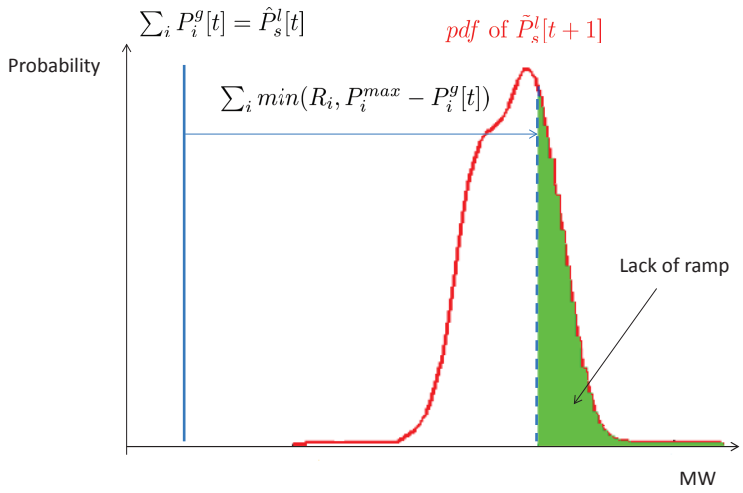

Figure 3.2: Illustration of lack of ramp probability (LORP) for empirical case [1]

The *LORP* index value is the probability that the system will be unable to ramp up or down to ensure energy balancing. In Fig. 3.2 the term $\sum_{i\in I} P_i^g[t]$ represents the total power output of all conventional generators in the system for the interval t of the real-time economic dispatch. In order to balance the system the generation needs to ramp up to the total system load in the next dispatch interval which is given by $P_s^l[t+1]$. However, conventional generators have certain ramp limits (R_i), expressed in MW/min which restrict their ability to change their output. Given the uncertainty in the load forecast we can consider the total system load to be a random quantity with a known probability distribution function (pdf). Thus the shaded area under the curve in Fig. 3.2 represents the probability that the system operator can not ramp up the conventional generation resources to match the demand. A similar case can occur for ramp down as well (3.3). In such circumstance the ISO is forced to take some out-of-market action, such as dispatching a fast-start unit, in order to maintain system power balance. Out-of-market actions should be avoided since they lead to price spikes in the real-time market and also because they distort the market.

Since DR resources enter into this calculation as a component of net load, we can use the LORP metric to evaluate the impact of DR on system ramp flexibility.

3.2.2 Transfer Function Model of DR

To estimate the transfer function (TF) of DR, we use the AutoRegression with eXogenous input (ARX) model. This System Identification tool is widely used for predicting the future values of a given time series of data.

Table 3.1: ARX model notation

z	Delay operator
$y[t]$	Time series of demand
$u[t]$	Time series of price
n_k	Time delay between input and output
$e(t)$	Gaussian noise

The ARX model can be described as follows:

$$A(z)y[t] = B(z)u[t-n_k] + e(t) \tag{3.4}$$

where $A(z) = 1 + a_1 z^{-1} + \ldots + a_{n_a} z^{-n_a}$ and $B(z) = b_1 + b_2 z^{-1} + \ldots + b_{n_b} z^{-n_b+1}$.

The aim of this approach is to estimate the unknown a_i and b_i parameters using the least-squares method. These parameters form the denominator and numerator polynomials of the DR transfer function model. We use the ARX function from the Matlab system identification toolbox. The given data is split into two sets - a training data set and validation data set. The training data set is used to obtain ARX model parameters. The validation data set is used to check the model using the FIT index.

The FIT index can be used to measure the accuracy of the model compared to the training data. For a perfect model the FIT index value is 100. The FIT index is defined as follows:

$$FIT = (1 - \frac{||\hat{y}[k] - y[k]||}{||y[k] - mean(y[k])||}) * 100 \tag{3.5}$$

where $\hat{y}[k]$ is the forecasted data (i.e., output of model), while $y[k]$ is the measured data.

3.2.3 Data Analysis

We have price and demand data for a number of Commercial & Industrial loads in the Houston zone of Electric Reliability Council of Texas (ERCOT) which participate in the DR program. The available data is in intervals of 15 minutes from Nov. 16, 2010 to Oct. 15, 2013. Fig. 3.3 shows the plot of the average price by time of day for each interval for the given range of data. In this plot we see a small peak in the morning and a much larger peak in the evening corresponding to the peak load hours.

Fig. 3.4 shows a particular sample of the price data, for the entire day of Nov. 24, 2010. Usually in the real time market electricity prices lie within a small range. In this example for most

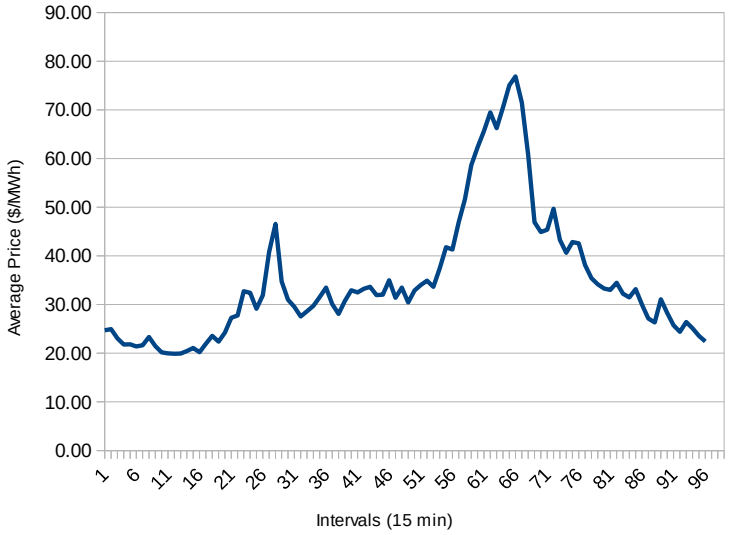

Figure 3.3: Average price by time of day at 15 min intervals for given data

intervals in the day the price is around $20 to 40 per MWh, with price reaching $180 per MWh during peak periods in the evening. However, there are some periods when we observe large spikes in the price series, usually for a short duration such as 15-30 minutes i.e., 1 or 2 intervals. These price spikes can usually be explained by the high marginal cost of fast-responding generators or some reserve shortage event in the system. The fast start units which are typically gas or oil-fired units, are dispatched by the system operator in response to a short-term energy shortage in the system. Alternatively, when the system experiences a shortage in reserves, shortage pricing kicks in, which results in a large increase in the real time electricity price.

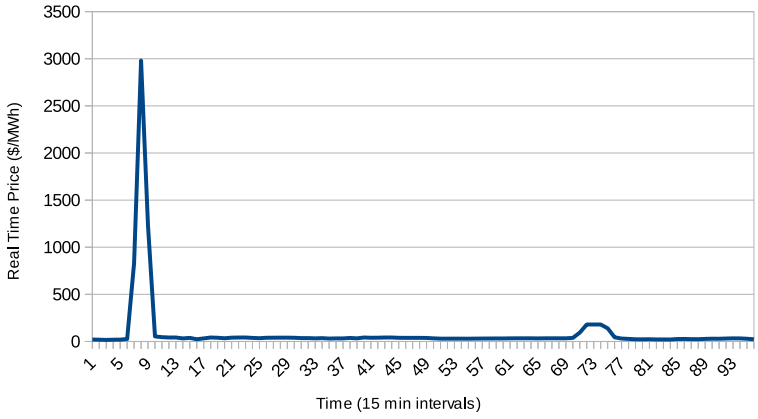

Figure 3.4: Real time price data for Nov. 24, 2010

Fig. 3.5 shows the time series of metered energy consumption data of demand for a DR customer, following a price spike. The price spike occurs at interval T after which in the next few intervals we observe a reduction in the electricity consumption. Each interval is of 15 minutes duration.

We use the price and demand data for a period of close to 3 years, to fit the energy consumption

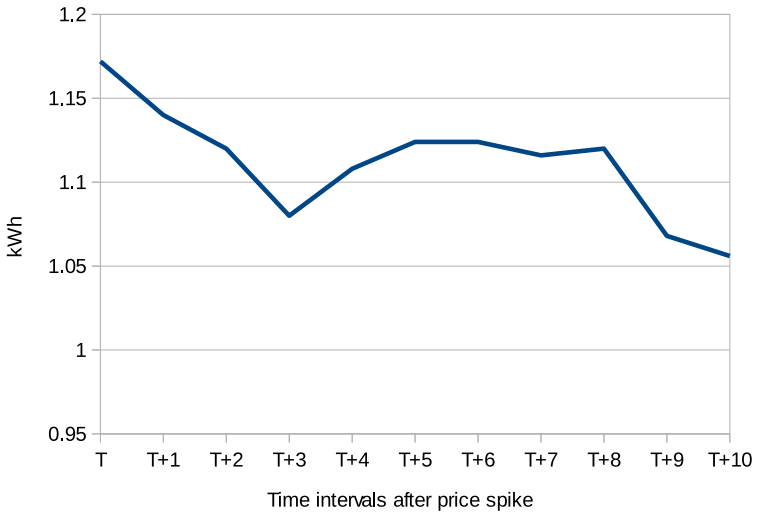

Figure 3.5: Demand response by customer to price spike

profiles of three customers to the ARX model described in the previous subsection. Table 3.2 shows the estimation results of the ARX model for Customer 1. The TF based on the ARX model can be written as follows:

$$TF = \frac{\beta_0 + \beta_1 z^{-1}}{1 - \alpha_1 z^{-1} - \alpha_2 z^{-2}} \tag{3.6}$$

The column *pValue* is the p-value for the t-statistic. If a coefficient has a p-value lower than the threshold of 0.05 we can consider it to be statistically significant. The Table also shows the standard deviation of residuals as well as their mean square error (MSE). Additionally, we perform the F-test to judge the fitting of the transfer function models to the data sets. From the F-test, the p-value of each transfer function is less than 2.2×10^{-16}, which indicates a good fit. The pseudo R-square values of the ARX models are high which indicates the goodness of fit.

Table 3.2: ARX model parameters for Customer 1

Coefficient	Estimate	pValue
α_1	0.9785	2×10^{-16}
α_2	0	n/a
β_0	3.796×10^{-3}	0
β_1	-4.635×10^{-7}	0.03816
Standard Deviation of residual = 0.00495		
MSE of residual = 2.446×10^{-5}		
R^2 value = 0.9831		
p-value of F-test $< 2.2 \times 10^{-16}$		

We observe from the ARX model in Table 3.2 that the demand of the customer in a given time interval has a strong relationship with the demand in the subsequent interval. We also observe from this ARX model that the impact of low to medium prices on the demand in the subsequent time interval is low. However, when we have a price spike, we can see that it will reduce the demand. We can use the transfer function model to predict $d[t+1]$ given a certain $p[t]$ and the vector of past demands and prices. The standard deviation and Mean Square Error (MSE) of the residual are terms that can be used to evaluate how well the ARX model fits the actual data in terms of its predictive ability.

Similarly, Table 3.3 and Table 3.4 shows the estimation results of the ARX models for Customer 2 and Customer 3 respectively.

Table 3.3: ARX model parameters for Customer 2

Coefficient	Estimate	pValue
α_1	1.051	2×10^{-16}
α_2	-0.0696	0.0195
β_0	2.864×10^{-2}	0
β_1	-2.011×10^{-5}	0.03

Standard Deviation of residual = 0.2117
MSE of residual = 0.0447
R^2 value = 0.9668
p-value of F-test $< 2.2 \times 10^{-16}$

Table 3.4: ARX model parameters for Customer 3

Coefficient	Estimate	pValue
α_1	0.9542	2×10^{-16}
α_2	0	n/a
β_0	6.67×10^{-2}	0
β_1	-4.018×10^{-5}	0.011

Standard Deviation of residual = 0.36216
MSE of residual = 0.1309
R^2 value = 0.8896
p-value of F-test $< 2.2 \times 10^{-16}$

The ARX model fitting result for Customer 2 suggests some difference from the other two customers. Namely in this case the demand in a time interval has a relationship with the demand in the past two intervals. Detailed consumption data allows us to model individual customers using a

data driven approach which yields good results in terms of our ability to predict their consumption, at least on the short term horizon. Thus even without knowing the electrical model of the customers we can extract useful information about the demand from the detailed consumption data.

3.3 Case Study

In this section a case study is presented in a modified 24 bus IEEE Reliability Test System (RTS 24) [52]. The generator parameters have been selected to approximate a scaled down version of the generation fuel mix in each zone of the ERCOT system. There are a total of 15 generators of which 3 are wind generators, while the rest are conventional dispatchable generators (Fig. 3.6). As a portion of the total installed capacity in the test system, wind is 12.3%, gas is 60.3% and coal is 27.6%. Table 3.5 gives the parameters for the generators. There are 32 transmission lines and the flow limits are taken from the RTS 24 dataset. The simulation duration is 24 hours with dispatch performed for 15-min intervals using scaled realistic load data from ERCOT. The DR capable load is assumed to be aggregated at Bus 12. Price responsive demand data is obtained from industrial and commercial loads that are exposed to time-varying prices in ERCOT between 2010 and 2013 [53]. To evaluate the impact of price-sensitive load on system flexibility we consider two cases: (i) Case A: without flexible load (i.e., without DR), and (ii) Case B: with price sensitive load (i.e., with DR).

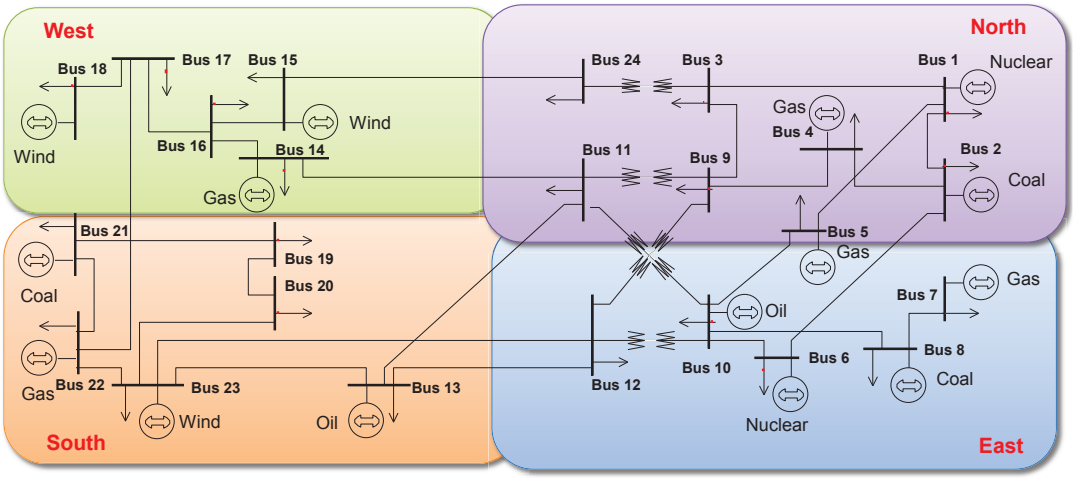

Figure 3.6: IEEE 24 bus RTS system (modified) [2]

Fig. 3.7 shows the total wind power output for the system. The wind production profile shows great variation during the course of the day. Assuming no imports and exports from outside the system the net load faced by the generators is the difference between the electrical load and the wind. The total electrical load and the total net load profiles are shown in Fig. 3.8. Average system net load is 1,252.8 MW and peak net load is 1,434.5 MW. Average system wind output is 94.2 MW and peak wind output is 116.7 MW. As discussed earlier in the report we can see here that there are several periods where the net load ramp is steeper than the electrical load ramp.

For the simulation case study we assume that we have an aggregation of 100 customers at bus 12 in the East zone (Houston zone) of the ERCOT system, of which 50 customers are identical to

Table 3.5: Generator parameters

Bus	Type	P^{max} MW	P^{min} MW	Cost $/MWh	Ramp Rate % MW/min
1	Nuclear	140	50	15	0.8
2	Coal	540	40	20	2
4	Gas	300	30	40	5
5	Gas	510	25	27	6.5
6	Nuclear	150	45	14	0.9
7	Gas	490	24	49	7
8	Coal	165	15	23	1.9
10	Oil	60	0	250	20
13	Oil	90	0	220	20
14	Gas	170	34	48	9
15	Wind	200	0	4	9
18	Wind	240	0	6	10
21	Coal	300	30	21	1.8
22	Gas	725	50	36	11
23	Wind	70	0	5	11

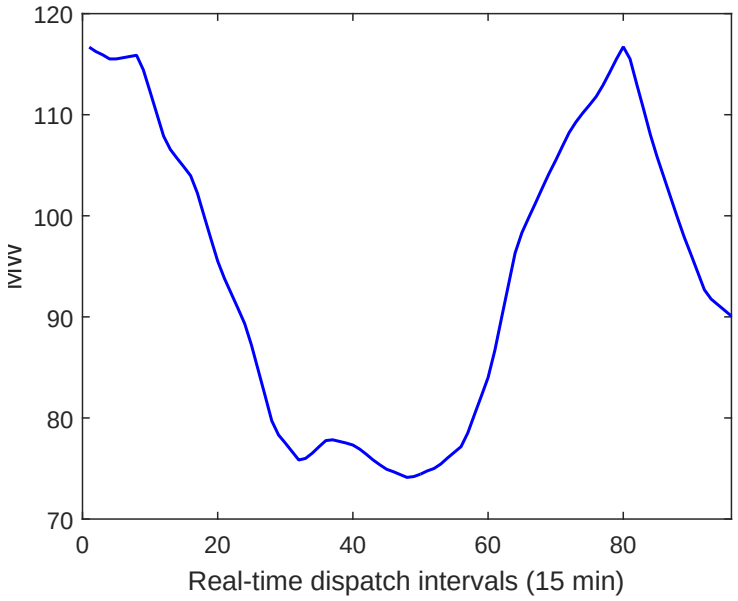

Figure 3.7: System total actual wind profile for entire day

Customer 1, 20 are identical to Customer 2 and 30 are identical to Customer 3.

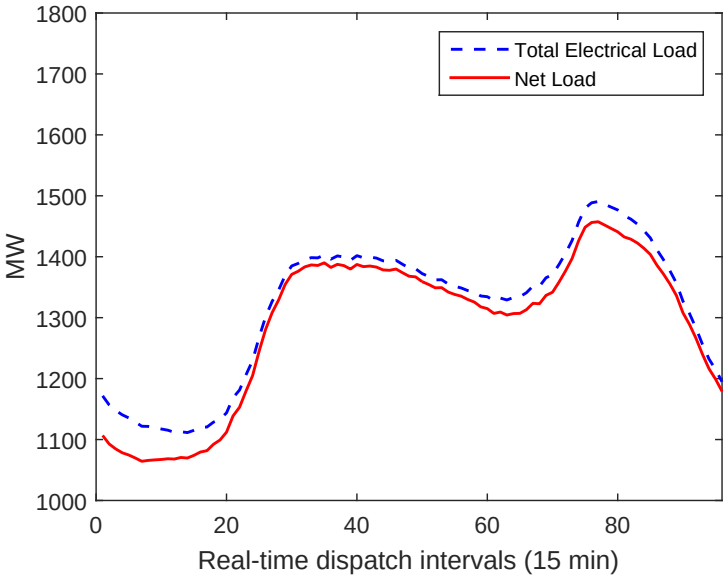

Figure 3.8: System total actual electrical load and net load profiles for entire day

3.3.1 Case A: No flexible load

In this case we assume that there is no price-sensitive load in the system. A simple Auto Regression (AR) model is used to predict the future load from the demand time series. Fig. 3.9 shows the comparison of the actual total load to the prediction using the AR model. The AR model is represented by (3.7).

$$A(z)y[t] = e(t) \tag{3.7}$$

where for this case we obtained $A(z) = 1 - 0.96z^{-1} - 0.05z^{-2}$

3.3.2 Case B: Price-sensitive load

In this case we use the ARX based transfer function models of the 3 customers obtained in the previous section to predict the future load. The total load prediction is the sum of the load prediction from each of the 3 models scaled by the number of customers assumed in each type. Thus we can predict the price-sensitive load.

We run the economic dispatch for both Case A and Case B and then compute the values of the system wide LORP index for each of the 96 fifteen-minute intervals of the day. Fig. 3.10 shows the comparison of the LORP metric using the two cases - without DR and with DR. In the case when we do not have DR, the LORP assesses the ramp flexibility of the system when conventional generation is the only resource the system operator can utilize to balance the net load. In the case when we have DR resources, the LORP metric assesses the ramp flexibility when the system operator can utilize conventional generation as well as through the aggregator

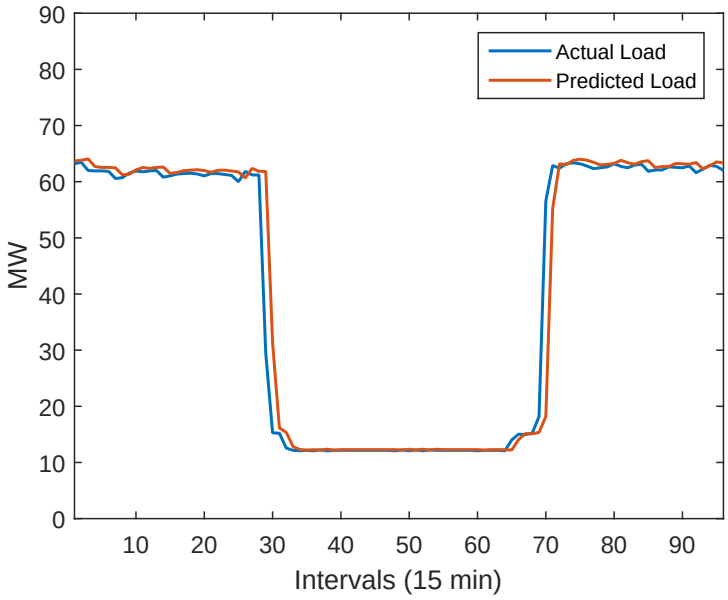

Figure 3.9: Total load prediction for the customers using AR model

it can utilize flexibilty from the DR resources. For most intervals in the day we usually have adequate ramping available to us from conventional generators. However, during a few intervals in the day the system can experience ramp shortage. Utilizing DR resources can help to reduce the probability of shortage events, thereby increasing system reliability, as shown in Fig. 3.10. The system operator can determine if the system is flexible by calculating the LORP and comparing it to a pre-defined target or threshold value for the system. Such a comparison would be useful when it comes to making decisions about the dispatch of various conventional generation units in the system, and also determining the utilization of the DR resources.

The next logical step is to close the loop and design a price signal for DR such that we can achieve a target LORP. This approach will help the system operator to reach its flexibility requirement using price responsive DR as a resource.

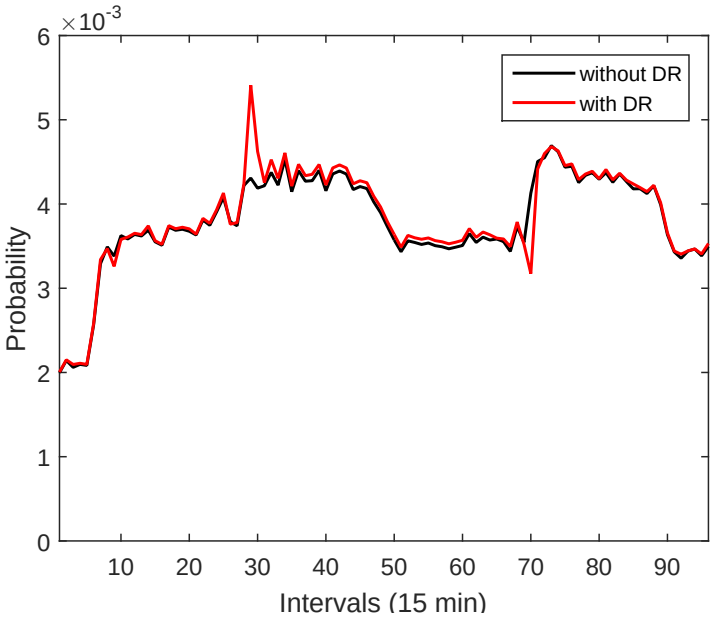

Figure 3.10: Comparison of the LORP metric using the two cases. Case A: without DR and, Case B: with DR

4. Conclusions

This report presents an operational flexibility metric for evaluating system ramp capability in *real-time* economic dispatch. The proposed LORP index can be used by the system operator for situational awareness of the robustness of the economic dispatch solution to uncertainty and variability in the net load. Additionally, this flexibility metric is independent of the dispatch model and can be used to compare different real-time economic dispatch methods.

Also we conduct the empirical study of price responsive demand and assess the potential of providing ramping flexibility from such demand. Built upon the proposed LORP metric for evaluating system inter-temporal flexibility, we evaluate the one interval ramping capability from price responsive demand. Demand data from ERCOT is employed to illustrate the LORP metric. We compare the case of a system without flexible load to the case in which there is price-sensitive demand in the system.

Further, a two-step robust optimization based real-time economic dispatch model is proposed to ensure deliverability of ramp capability between operating zones in multi-zonal systems. The proposed approach meets inter-zonal tie-line flow limits under the worst case of net load uncertainty and thus provides a more reliable zonal ramp capability than in the conventional dispatch model. A case study is presented on a modified 3 zone 73 bus IEEE (RTS-96) test system to illustrate the proposed system and zonal flexibility metrics, as well as the two-step robust dispatch model.

Future work will include the application of the two-stage adaptive robust optimization approach in our proposed two-step dispatch model [28]. We will also study the optimum horizon for the proposed robust dispatch approach when applied to the multi-interval economic dispatch problem. Another avenue of future research will focus on reducing the computational effort and implementation complexity while guaranteeing the operational flexibility. Future work will also include the design of an optimal pricing signal in order to elicit required demand response from large aggregated customers, so as to provide demand side ramp flexibility.

Obtaining a good empirical pdf for the system is a challenging problem. It would be necessary to calculate the correlations between the renewable generation, demand response loads and other system load. In our future work on this topic we will consider this aspect in greater detail.

References

[1] A. A. Thatte, X. A. Sun, and L. Xie, "Robust optimization based economic dispatch for managing system ramp requirement," in *Proc. 47th Hawaii Intl. Conf. on System Sciences*, Hawaii, HI, Jan. 6-9, 2014, pp. 2344–2352.

[2] A. A. Thatte and L. Xie, "A two-layered framework for robust dispatch with transmission constraints," in *Proc. 48th Hawaii Intl. Conf. on System Sciences*, Hawaii, HI, Jan. 5-8, 2015, pp. 2507–2515.

[3] L. Xie, P. M. S. Carvalho, L. A. F. M. Ferreira, J. Liu, B. H. Krogh, N. Popli, and M. D. Ilić, "Wind integration in power systems: Operational challenges and possible solutions," *Proc. IEEE*, vol. 99, no. 1, pp. 214–232, Jan. 2011.

[4] P. Brown, "US renewable electricity: How does wind generation impact competitive power markets?" Congressional Research Service (CRS) Report for Congress, Tech. Rep. R42818, Nov. 2012, available: http://assets.opencrs.com/rpts/R42818_20121107.pdf.

[5] L. E. Jones, "Strategies and decision support systems for integrating variable energy resources in control centers for reliable grid operations," U.S. Department of Energy, Office of Energy Efficiency and Renewable Energy, Tech. Rep., 2011.

[6] M. Milligan, P. Donohoo, D. Lew, E. Ela, B. Kirby, H. Holttinen, E. Lannoye, D. Flynn, M. O'Malley, N. Miller *et al.*, "Operating reserves and wind power integration: an international comparison," in *Proc. 9th Intl. Workshop on Large-Scale Integration of Wind Power Into Power Systems as Well as on Transmission Networks for Offshore Wind Power Plants*, Quebec, Canada, Oct. 18-19, 2010, pp. 18–29.

[7] H. Holttinen, M. Milligan, E. Ela, N. Menemenlis, J. Dobschinski, B. Rawn, R. J. Bessa, D. Flynn, E. Gomez-Lazaro, and N. K. Detlefsen, "Methodologies to determine operating reserves due to increased wind power," *IEEE Trans. Sustain. Energy*, vol. 3, no. 4, pp. 713–723, Oct. 2012.

[8] F. Bouffard and M. Ortega-Vazquez, "The value of operational flexibility in power systems with significant wind power generation," in *Proc. IEEE Power Eng. Soc. Gen. Meet.*, Detroit, MI, Jul. 24-28, 2011, pp. 1–5.

[9] M. O'Malley, "Grid flexibility and research challenges to enhance the integration of variable renewable energy sources," *Stanford Energy Seminar*, Jan. 14, 2013, available: https://energy.stanford.edu/sites/default/files/stanford_january_14th_2013.pdf.

[10] N. Menemenlis, M. Huneault, and A. Robitaille, "Thoughts on power system flexibility quantification for the short-term horizon," in *Proc. IEEE Power Energy Soc. Gen. Meet.*, Detroit, MI, Jul. 2011, pp. 1–8.

[11] J. Adams, M. O'Malley, K. Hanson *et al.*, "Flexibility requirements and potential metrics for variable generation: Implications for system planning studies," *NERC, Princeton, NJ*, Aug. 2010, available: http://www.nerc.com/files/IVGTF_Task_1_4_Final.pdf.

[12] E. Lannoye, D. Flynn, and M. O'Malley, "Evaluation of power system flexibility," *IEEE Trans. Power Syst.*, vol. 27, no. 2, pp. 922–931, May 2012.

[13] J. Ma, V. Silva, R. Belhomme, D. S. Kirschen, and L. Ochoa, "Evaluating and planning flexibility in sustainable power systems," in *Proc. IEEE Power Energy Soc. Gen. Meet.*, Vancouver, BC, Canada, Jul. 21-25, 2013, pp. 1–11.

[14] A. Ulbig and G. Andersson, "On operational flexibility in power systems," in *Proc. IEEE Power Energy Soc. Gen. Meet.*, San Diego, CA, Jul. 22-26, 2012, pp. 1–8.

[15] D. Kirschen, Y. Dvorkin, H. Pandžić, and M. Ortega-Vasquez, "Flexibility management in day-ahead unit commitment," in *FERC Technical Conference: Increasing Real-Time and Day-Ahead Market Efficiency through Improved Software*, Washington DC, Jun. 24-26, 2013, available: http://www.ferc.gov/CalendarFiles/20140411131632-T3-A - Kirschen.pdf.

[16] J. Cochran, M. Miller, O. Zinaman, M. Milligan, D. Arent, B. Palmintier, M. O'Malley, S. Mueller, E. Lannoye, A. Tuohy *et al.*, "Flexibility in 21st century power systems," National Renewable Energy Laboratory (NREL), Golden, CO, Tech. Rep. NREL/TP-6A20-61721, May 2014.

[17] D. B. Patton, "2010 state of the market report Midwest ISO," *Potomac Economics, Midwest ISO Independent Market Monitor*, May 2011.

[18] N. Navid and G. Rosenwald, "Ramp capability product design for MISO markets," MISO, Tech. Rep., Jul. 2013, available: https://www.misoenergy.org/Library/Repository/Communication Material/Key%20Presentations%20and%20Whitepapers/Ramp Product Conceptual Design Whitepaper.pdf.

[19] L. Xu and D. Tretheway, "Flexible ramping products," *CAISO Proposal*, Oct. 2012.

[20] B. Wang and B. F. Hobbs, "Flexiramp market design for real-time operations: Can it approach the stochastic optimization ideal?" in *Proc. IEEE PES General Meeting*, Vancouver, BC, Jul. 21-25, 2013, pp. 1–5.

[21] A. Papavasiliou and S. S. Oren, "Multiarea stochastic unit commitment for high wind penetration in a transmission constrained network," *Operations Research*, vol. 61, no. 3, pp. 578–592, 2013.

[22] F. Rahimi and A. Ipakchi, "Demand response as a market resource under the smart grid paradigm," *IEEE Trans. Smart Grid*, vol. 1, no. 1, pp. 82–88, Jun. 2010.

[23] W. Jeon, A. J. Lamadrid, J. Y. Mo, and T. D. Mount, "Using deferrable demand in a smart grid to reduce the cost of electricity for customers," *Journal of Regulatory Economics*, vol. 47, no. 3, pp. 239–272, 2015, available: http://dx.doi.org/10.1007/s11149-015-9268-0.

[24] R. Sioshansi and W. Short, "Evaluating the impacts of real-time pricing on the usage of wind generation," *IEEE Trans. Power Syst.*, vol. 24, no. 2, pp. 516–524, 2009.

[25] M. Parvania and M. Fotuhi-Firuzabad, "Demand response scheduling by stochastic SCUC," *IEEE Trans. Smart Grid*, vol. 1, no. 1, pp. 89–98, 2010.

[26] H. Lu, W. Jeon, T. Mount, and A. J. Lamadrid, "Can energy bids from aggregators manage deferrable demand efficiently?" in *Proc. 48th Hawaii Intl. Conf. on System Sciences*, Hawaii, HI, Jan. 5-8, 2015, pp. 2530–2539.

[27] P. P. Varaiya, F. F. Wu, and J. W. Bialek, "Smart operation of smart grid: Risk-limiting dispatch," *Proc. IEEE*, vol. 99, no. 1, pp. 40–57, Jan. 2011.

[28] D. Bertsimas, E. Litvinov, X. A. Sun, J. Zhao, and T. Zheng, "Adaptive robust optimization for the security constrained unit commitment problem," *IEEE Trans. Power Syst.*, vol. 28, no. 1, pp. 52–63, Feb. 2013.

[29] R. Jiang, J. Wang, and Y. Guan, "Robust unit commitment with wind power and pumped storage hydro," *IEEE Trans. Power Syst.*, vol. 27, no. 2, pp. 800–810, May 2012.

[30] L. Zhao and B. Zeng, "Robust unit commitment problem with demand response and wind energy," in *Proc. IEEE Power Energy Soc. Gen. Meet.*, San Diego, CA, Jul. 22-26, 2012, pp. 1–8.

[31] D. Bertsimas, D. Brown, and C. Caramanis, "Theory and applications of robust optimization," *Arxiv preprint arXiv:1010.5445*, 2010.

[32] J. An, P. R. Kumar, and L. Xie, "On transfer function modeling of price responsive demand: An empirical study," *Proc. IEEE PES General Meeting*, Jul. 26-30, 2015.

[33] Y. Rebours and D. Kirschen, "A survey of definitions and specifications of reserve services," University of Manchester, Tech. Rep., 2005, available: http://www.ee.washington.edu/research/real/Library/Reports/Survey_of_Reserve_Services.pdf.

[34] R. Billinton and R. N. Allan, *Reliability Evaluation of Power Systems*, 2nd ed. New York, USA: Plenum, 1996.

[35] FERC Staff, "2010 ISO/RTO metrics report," FERC, Washington DC, Tech. Rep., Dec. 2010, available: http://www.isorto.org/Documents/Report/20101207_2010IRCPerformanceMetricsReport_PressRelease.pdf.

[36] C. Y. Tee, J. B. Cardell, and G. W. Ellis, "Short-term load forecasting using artificial neural networks," in *Proc. 41st North American Power Symposium (NAPS)*, Starkville, MS, Oct. 4-6, 2009, pp. 1–6.

[37] K. Porter and J. Rogers, "Status of centralized wind power forecasting in North America," National Renewable Energy Laboratory, Golden, CO, USA, Tech. Rep. NREL/SR-550-47853, 2010.

[38] F. Wang and K. W. Hedman, "Reserve zone determination based on statistical clustering methods," in *Proc. North American Power Symposium (NAPS)*, Champaign, IL, Sep. 9-11, 2012, pp. 1–6.

[39] D. Shi and D. J. Tylavsky, "An improved bus aggregation technique for generating network equivalents," in *Proc. IEEE Power Eng. Soc. Gen. Meet.*, San Diego, CA, Jul. 22-26, 2012, pp. 1–8.

[40] C. Grigg, P. Wong, P. Albrecht, R. Allan, M. Bhavaraju, R. Billinton, Q. Chen, C. Fong, S. Haddad, S. Kuruganty, W. Li, R. Mukerji, D. Patton, N. Rau, D. Reppen, A. Schneider, M. Shahidehpour, and C. Singh, "The IEEE reliability test system-1996. a report prepared by the reliability test system task force of the application of probability methods subcommittee," *IEEE Trans. Power Syst.*, vol. 14, no. 3, pp. 1010–1020, Aug. 1999.

[41] R. D. Christie. (2007) Power system test case archive. Univ. Washington, Dept. Elect. Eng. Available: https://www.ee.washington.edu/research/pstca/rts/pg_tcarts.htm.

[42] K. W. Hedman, M. C. Ferris, R. P. O'Neill, E. B. Fisher, and S. S. Oren, "Co-optimization of generation unit commitment and transmission switching with N-1 reliability," *IEEE Trans. Power Syst.*, vol. 25, no. 2, pp. 1052–1063, May 2010.

[43] New York ISO: Market and operational data - load data. Available: http://www.nyiso.com/public/markets_operations/market_data/load_data/index.jsp. Accessed on: 24 Apr. 2014.

[44] J. Löfberg, "Modeling and solving uncertain optimization problems in YALMIP," in *Proc. 17th IFAC World Congress*, 2008, pp. 1337–1341.

[45] S. Koch, J. L. Mathieu, and D. S. Callaway, "Modeling and control of aggregated heterogeneous thermostatically controlled loads for ancillary services," in *Proc. Power System Computation Conference (PSCC)*, Stockholm, Sweden, 2011, pp. 1–7.

[46] M. D. Galus, S. Koch, and G. Andersson, "Provision of load frequency control by PHEVs, controllable loads, and a cogeneration unit," *IEEE Trans. Ind. Electron.*, vol. 58, no. 10, pp. 4568–4582, Oct. 2011.

[47] D. S. Callaway and I. A. Hiskens, "Achieving controllability of electric loads," *Proc. IEEE*, vol. 99, no. 1, pp. 184–199, Jan. 2011.

[48] FERC Staff, "Assessment of demand response and advanced metering," *Federal Energy Regulatory Commission Staff Report*, Aug. 2006.

[49] S. Borenstein, M. Jaske, and A. Rosenfeld, "Dynamic pricing, advanced metering, and demand response in electricity markets," *Center for the Study of Energy Markets*, Oct. 2002.

[50] A. J. Conejo, J. M. Morales, and L. Baringo, "Real-time demand response model," *IEEE Trans. Smart Grid*, vol. 1, no. 3, pp. 236–242, Dec. 2010.

[51] B. Hodge and M. Milligan, "Wind power forecasting error distributions over multiple timescales," in *Proc. IEEE Power Energy Soc. Gen. Meet.*, Detroit, MI, Jul. 24-28, 2011, pp. 1–8.

[52] P. Wong, P. Albrecht, R. Allan, R. Billinton, Q. Chen, C. Fong, S. Haddad, W. Li, R. Mukerji, D. Patton, A. Schneider, M. Shahidehpour, and C. Singh, "The IEEE reliability test system-1996. A report prepared by the reliability test system task force of the application of probability methods subcommittee," *IEEE Trans. Power Syst.*, vol. 14, no. 3, pp. 1010–1020, Aug. 1999.

[53] L. Xie, S. Puller, M. Ilic, and S. Oren, "Quantifying benefits of demand response and look-ahead dispatch in systems with variable resources," PSERC Final Report M26, Tech. Rep., Aug. 2013.

Part III

Quantification and Optimal Utilization of System Flexibility
The Flexible Optimal Power Flow

Sakis Meliopoulos
Evangelos Polymeneas
Orestis Vasios

Georgia Institute of Technology

For information about this project contact:

Sakis Meliopoulos
School of Electrical & Computer Engineering
Georgia Institute of Technology
Atlanta, Georgia 30332-0250
Phone: 404-894-2926
E-mail: sakis.m@gatech.edu

Power Systems Engineering Research Center

The Power Systems Engineering Research Center (PSERC) is a multi-university Center conducting research on challenges facing the electric power industry and educating the next generation of power engineers. More information about PSERC can be found at the Centers website: http://www.pserc.org.

For additional information, contact:

Power Systems Engineering Research
Center Arizona State University
577 Engineering Research
Center Tempe, Arizona
85287-5706
Phone: 480-965-1643
Fax: 480-727-2052

Notice Concerning Copyright Material

PSERC members are given permission to copy without fee all or part of this publication for internal use if appropriate attribution is given to this document as the source material. This report is available for down- loading from the PSERC website.

Table of Contents

List of Figures

List of Tables

Nomenclature

ACOPF	Optimal Power Flow in phasor domain (without DC assumption)
BESS	Battery Energy Storage Systems
CAISO	California Independent System Operator
DCOPF	Optimal Power Flow with DC assumption
DLR	Dynamic Line Ratings
DOE	Department of Energy
ERCOT	Electric Reliability Council of Texas
ISO	Independent System Operator
MISO	Midwest ISO
NYISO	New York ISO
ODE	Ordinary Differential Equations
OPF	Optimal Power Flow
PDIPM	Primal-Dual Interior Point Method
PHEV	Plug-in Hybrid Electric Vehicle
QCQP	Quadratically Constrained Quadratic Programming
QP	Quadratic Programing
RTS	Reliability Test System (from IEEE)
SDP	Semi-Definite Programming
SOC	Battery State of Charge
TCL	Thermostatically Controlled Loads

1. Introduction

1.1 Problem Statement

A wide range of newly introduced challenges have increased the complexity of power system operations. Increasing renewable power penetration has exacerbated temporal variations and increased the need for load following reserves. Furthermore, it has increased the uncertainty and has given rise to stochastic operations algorithms, especially for day-ahead planning purposes. Given the finite ramp rate of conventional units, these effects have in turn led to higher operational costs and threats to system reliability due to ramping insufficiencies. In addition, gradually increasing system stress combined with aging transmission infrastructure that was designed for system loading and generation technologies that were prevalent decades ago have increased the potential for transmission line congestion issues, leading to high marginal costs. A closely related issue is the threat to power system reliability, due to the gradual aging and retirement of transmission and generation assets, which is not associated with equally active infrastructure investments. Furthermore, the appearance of large wind farm installations has introduced new power flow patterns and in many cases has brought forth unforeseen congestion issues and potentially negative marginal prices. This issue is expected to unfold in ways that are hard to predict especially as system stress increases and as new load types are widely introduced, such as Electric Vehicles. As renewable and distributed generation gains ground in terms of cost effectiveness, the traditional methodologies for designing and operating the power grid are expected to become less relevant and adequate.

One particular manifestation of the upcoming challenges in the scheduling of power system operation is related to the concept of flexibility. The integration of a large capacity of renewable resources in bulk power systems has given rise to step up and down ramps in active power output (MW) from renewable sources, which, combined with already existing load ramps, translate to large ramps in Net System load. The capability of the system to respond to such large deviations in Net Load in short periods of time is known as the system's flexibility. CAISO's projection for a typical Net Load daily profile curve has become famous as the "duck curve" due to its characteristic shape, shown in Figure 1.1 (re-printed from [1]). An additional complication is the timing of these ramping events during the day cannot be accurately predicted in day-ahead studies, and they typically have to be addressed in shorter planning horizons, when the pool of committed generators with sufficient ramping capabilities may be very restricted. Similar ramping phenomena have been recorded or are expected to appear in other systems, such as the Irish [5] as well as the ERCOT, MISO and NYISO systems [9].

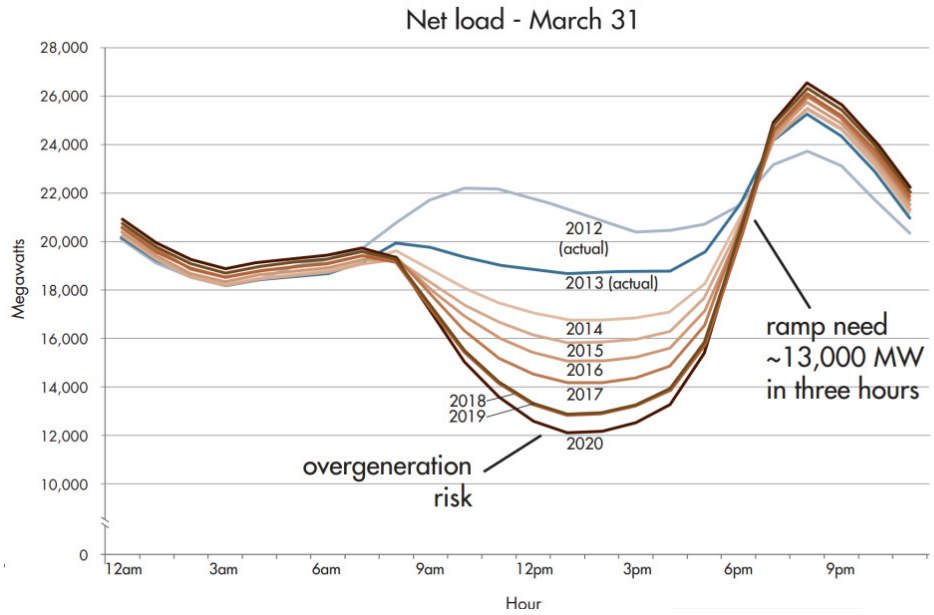

Figure 1.1: The projected duck-curve daily Net Load profile for CAISO [1].

However, ramp-rate related flexibility is not the only challenge for power system operations documented in the literature. With higher renewable penetration, voltage control is expected to become more challenging [5], bringing forth the need for including voltage control to the economic dispatch problem. Hence, voltage-agnostic DC-OPF operational tools that are widely used in practice are fundamentally ill-suited to address this challenge. Reactive power capability is expected to fall due to the displacement of synchronous generators by wind farms with reduced reactive support capability [5], while only 27% of wind farms currently offer reactive control dispatch.

Several studies in the recent years have focused on suggesting institutional, technical and infrastructure improvements to address the challenges from renewable integration. A DOE report [6] highlights the need for short term flexibility of generating units and particularly the need for an operational framework that will allow proper incentives and scheduling for this flexibility to be deployed, especially in the real-time operator action domain. Furthermore, the same study identifies that the additional flexibility may not be easily obtainable from conventional generating units, and suggests alternatives, such as demand side resources, energy storage units and Hybrid Electric Vehicles. A more comprehensive list of flexibility-providing technologies, and their maturity level, has been compiled in Table 1.1 [7].

Table 1.1: Sources of Flexibility, their technical characteristics & maturity level

TECHNOLOGY	RAMP RATE / RESPONSE TIME	MATURITY
Fossil Fuel Generators	From 1.5%/min (coal) to 100%/min (internal combustion engines)	Very Mature
Nuclear	4%-10% per min	Very Mature
Biogas	Very fast	Mature
Co-generation	5-20%/min	Very Mature
Active Control for wind plants	100%/min	Medium
Demand management for industrial installations	20-100%/min	Medium-High
Demand Management for households	100%/min	Low
PHEV's	100%/min	Low-Medium
Pumped Hydro	40%-100%/min	High
Compressed Air Energy Storage	10-20%/min	Low
Flywheels	Milliseconds	Low
Batteries	Seconds	Medium

An IEA study [8] showed that transforming system operation practices and market operation may mitigate the high costs of increases renewable resources integration. Specifically, moving towards real time operations, where the uncertainty is reduced, is considered very important.

A NERC report on flexibility [9], [10] stresses the need for additional flexibility due to the variability of renewable generation. In ERCOT for example, where wind reaches about 25% of load at times, there exist ramps of about 50% of total wind capacity in an hour. The report also highlights the importance of the capability to respond to extreme weather events that may produce wind cut-outs due to very high wind speeds. According the NERC, the sources of flexibility are:

- Conventional Units with ramping capabilities
- Demand Response
- Variable generation Management (renewable curtailment)
- Energy Storage & PHEV's
- Sub-hourly scheduling (look-ahead dispatch)
- Transmission Planning

An NREL report comments on the needs for increased flexibility due to the increasing integration of renewable energy. NREL identifies the following as potential solutions to this issue:

- Flexible Operations: Move decision making closer to real time
- Flexible Demand Side Resources: Responsive distributed storage, customer load
- Flexible Transmission: Optimize transmission usage & improved access to resources
- Flexible Generation: units with high ramp-up & ramp-down capability

The aim of this research is to develop a framework for real-time power system operations that will address some of the challenges put forth by the studies mentioned above. Such a framework would have to:

- Rely on a real-time look-ahead scheduling formulation that is solvable in realistic time windows and schedules the operation of the system for a certain look-ahead horizon. It would be beneficial to model both ramping & voltage control phenomena.
- Model the novel sources of flexibility mentioned above, including energy storage, responsive demand, distributed energy resources, ramp-constrained generation.
- Include remedial action schemes for unforeseen severe events, such as critical component outages
- Have the capability to model & simulate a large number of potential contingency events that threaten the security of power system operations

This research addresses the challenges above by putting forth contributions in all of these areas. A detailed summary of contributions is offered in the next paragraph.

1.2 Research Objectives & Contributions

In order to address the challenges discussed above, especially in the short-term operational time-frame, in this research we focus on expanding the modeling of the short-term look-ahead dispatch to include new flexible components as well as more accurate network models. Once the model formulation has been set up, we modify the model to produce remedial action schemes in infeasible cases. Finally, at a given optimal solution a filtering & analysis framework is developed for identifying critical outages with a lowered computational cost. A summary of contributions in modeling (Distribution, Transmission, Generation & Storage) and in the real time operations & security analysis is given in Figure 1.2.

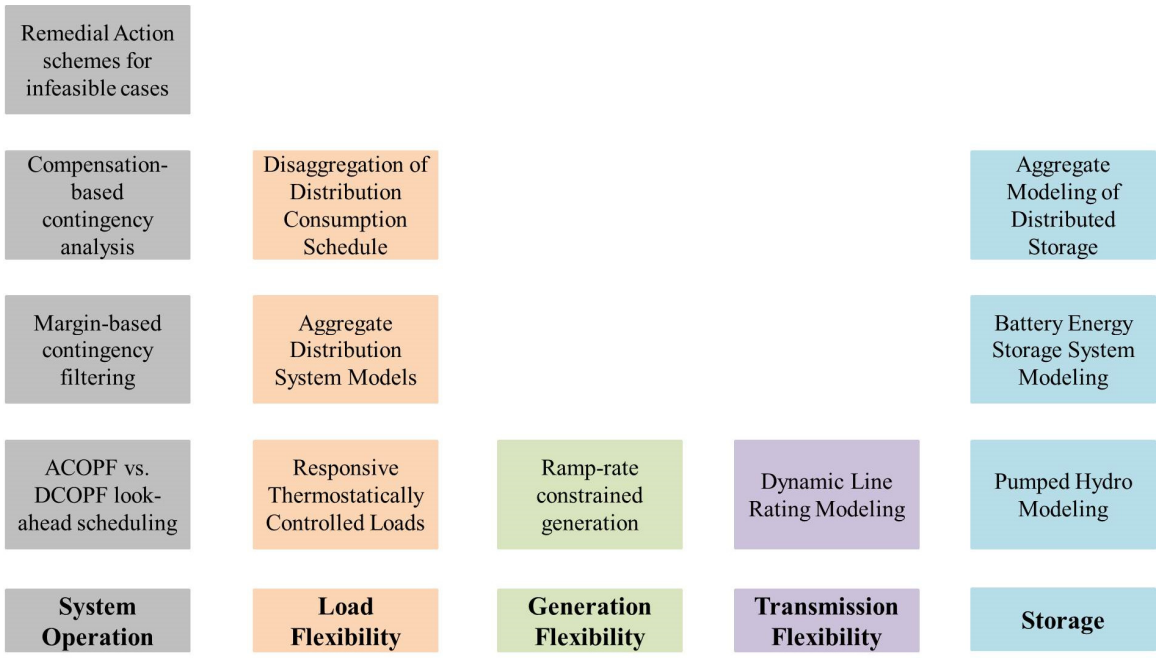

Figure 1.2: Summary of contributions

A summary of the outlined contributions is as follows:

1. An implementation & comparison of AC versus DC look-ahead OPF formulations for scheduling flexible operations in power systems.

A multi-period look-ahead AC-OPF is cast as a Quadratically Constrained Quadratic Programming (QCQP) problem and solved via primal-dual interior method. The non-convexity of the problem may lead to convergence to local minima. For this purpose, a DC-OPF look-ahead formulation is also put forth. This formulation is solved via Quadratic Programming and exhibits desirable convexity properties. In this research, the advantages and disadvantages of using either approach for real time operations are discussed. It should be stressed that the DC-OPF is the current operating practice. In this research, an effort is made to quantify the drawbacks of this practice due to reduced voltage control capabilities and inaccuracy of congestion modeling.

2.a. Development of transmission, generation and load models that are currently disregarded in look-ahead OPF formulations.

It is common for look-ahead scheduling to include standard models such as generators with ramping constraints and static models of network components, such as transmission lines and transformers. However, in this research we introduce physically based models of the following components into the look-ahead OPF:

- Thermal model of transmission line. This model allows for the implementation of dynamic line ratings. The benefits of transitioning from static line ratings to dynamic temperature-based ratings are also quantified.
- Thermostatically Controlled Load with temperature constraints
- Utility-scale Battery Energy Storage System, with separate charge and discharge efficiency

2.b. Aggregate modeling of active distribution systems for transmission-level look-ahead scheduling algorithms & disaggregation of transmission-level commands to individual distributed energy resources.

The effort to enrich the available modeling capabilities is extended to the development of an approximate aggregate dynamic model of an active distribution system that can be used to schedule its operation via the transmission-level look-ahead formulation. This addresses the issue of tractability and scalability for the control of small-scale distributed energy resources. By adding their capabilities to the dispatch procedure, a significant source of flexibility is utilized. Furthermore, a semidefinite programming approach for extracting this aggregate model from Distribution System simulation data is also developed. Finally, a Euclidian distance minimization problem is solved to implement the disaggregation of the aggregate distribution system schedule given by the look-ahead OPF in order to obtain the set of individual device controls that will, in aggregate, produce a consumption pattern as close as possible to the desired one, as given by the look-ahead OPF solution.

3. Remedial action & load shedding scheme formulation, with minimal load shedding

The look-ahead OPF formulation, both in its accurate AC form and its approximate DC form can be an infeasible problem. Two algorithms are put forth for the determination of remedial actions, in the form of load shedding, in cases where they are needed, to restore feasibility. The first is an iterative stepwise de-relaxation algorithm where the equality constraints are initially relaxed but gradually enforced at a given maximum rate per step. The second is a direct & non-iterative minimal load shedding algorithm that identifies minimal load shedding actions by adding the load shedding quantities to the objective function and severely penalizing them. The two methods are compared and their applicability in practical test cases is examined

4. Contingency Filtering & analysis for real time security analysis algorithms

A real-time security analysis approach must be in place to evaluate the security analysis (N-1 or higher) of a given solution to the scheduling algorithm. In this research we develop a two stage (filtering – analysis) framework, where the first step consists of fast contingency filters for critical outages using newly defined margin indices, that quantify overall proximity to constraint violations. A first order Taylor expansion is used to obtain fast margin index estimates after an outage. The second step consists of performing one or more power flow iterations using the Newton method & the post-outage Jacobian matrix. A compensation method, using low-rank Jacobian corrections to increase the speed of these Newton iterations without sacrificing accuracy, is developed and theoretically justified.

The above contributions serve one common goal, whose importance was highlighted in Paragraph 1.1. That goal is to increase available power system flexibility by utilizing a wider range of tools. With the look-ahead dispatch formulation, the security analysis function and the remedial action scheme identification, the decision making is moved closer to real time, which is a key requirement for “flexible operations”. Also, by including more resources to the flexibility pool, the overall system flexibility is extended beyond what conventional fossil fuel plants can offer. In particular, aggregate distribution system & dynamic line rating modeling constitute two important modeling options that have largely been ignored in the literature and their importance is highlighted here.

2. The Flexible Optimal Power Flow

2.1 Introduction

The issue of flexible assets in power systems operations has been studied for quite some time, especially for the provision of ancillary services, such as short-term reserves or ramping. Specifically in the domain of flexible demand response assets, efforts to model aggregate flexibility have been centered around aggregate stochastic battery models (Hao et al, 2013) or Temperature Bin Transition Models (Koch et al, 2011).

Resource flexibility has the potential to reduce OPF optimal cost in two ways:

1. Short term flexibility can offer ramping capabilities (i.e. allow "slower" units to ramp up/down their generation, by temporarily providing the power surplus or deficit). Furthermore it can offer short-term ("spinning") reserve capabilities.
2. Long-term flexibility can offer load shifting and peak shaving services.

Flexible resources exist in both the transmission and the distribution level. A list of flexible resources includes:

In transmission level

- Pumped hydro
- BESS (utility scale)

In distribution level

- House level storage
- Thermostatically controlled load
- PHEV
- Deferrable & schedulable load

The following methodology is proposed in this chapter

- Develop a physically-based aggregate model for the flexible demand response assets in the distribution level
- In the transmission level, solve a multi-period OPF problem, modeling resource flexibility using the above models. The aggregate dispatch of the flexible resources will be obtained solving the system-wide OPF
- In the lower (distribution feeder) level, solve a feeder level problem, to allocate that dispatch amongst individual loads / resources.
- Develop physically based models for **storage, thermostatically controlled loads & dynamic line ratings**

2.2 Quadratized Device Modeling

One of the fundamental challenges in formulating and solving the flexible OPF problem is the capability to model a wide range of power system device models, in addition to the standard

models of generators, transmission lines, transformer and loads. Indeed, an effective flexible OPF framework must include models for a wide range of storage technologies, explicit models of responsive loads with customer convenience constraints, as well as new dynamic models for classical devices, such as ramp-limited generators and dynamic thermal line ratings. In the context of this work, this issue is addressed by introducing "object-oriented" device models that describe the dynamics, algebraic equations and constraints of each device. The device modeling is completely decoupled from the algorithms used to handle the device's connectivity in the network, as well as the algorithms for the synresearch and solution of the optimization problem.

A quadratic device model is adopted, with the syntax as shown in (1):

$$\begin{bmatrix} \mathbf{i}_k \\ \mathbf{0} \end{bmatrix} = \mathbf{g}(\mathbf{x}_{k-1}, \mathbf{u}_{k-1}, \mathbf{x}_k, \mathbf{u}_k \mid \mathbf{p}_k) = \mathbf{a}_{eq}(\mathbf{p}_k) + Y_{eqx}\mathbf{x}_k + Y_{equ}\mathbf{u}_k + \begin{bmatrix} \vdots \\ \mathbf{x}_k^T F_{eqxx}^i \mathbf{x}_k^T \\ \vdots \end{bmatrix} + \begin{bmatrix} \vdots \\ \mathbf{u}_k^T F_{equu}^i \mathbf{u}_k^T \\ \vdots \end{bmatrix} + \begin{bmatrix} \vdots \\ \mathbf{x}_k^T F_{eqxu}^i \mathbf{u}_k^T \\ \vdots \end{bmatrix} - \mathbf{B}_{eq}^{k-1} \tag{1a}$$

$$\mathbf{B}_{eq}^{k-1} = -N_{eqx}\mathbf{x}_{k-1} - N_{equ}\mathbf{u}_{k-1} \tag{1b}$$

$$\mathbf{h}(\mathbf{x}_{k-1}, \mathbf{u}_{k-1}, \mathbf{x}_k, \mathbf{u}_k \mid \mathbf{p}_k) = \mathbf{a}_{ineq}(\mathbf{p}_k) + Y_{ineqx}\mathbf{x}_k + Y_{inequ}\mathbf{u}_k + \begin{bmatrix} \vdots \\ \mathbf{x}_k^T F_{ineqxx}^i \mathbf{x}_k^T \\ \vdots \end{bmatrix} + \begin{bmatrix} \vdots \\ \mathbf{u}_k^T F_{inequu}^i \mathbf{u}_k^T \\ \vdots \end{bmatrix} + \begin{bmatrix} \vdots \\ \mathbf{x}_k^T F_{ineqxu}^i \mathbf{u}_k^T \\ \vdots \end{bmatrix} - \mathbf{C}_{ineq}^{k-1} \tag{1c}$$

$$\mathbf{C}_{ineq}^{k-1} = -N_{ineqx}\mathbf{x}_{k-1} - N_{inequ}\mathbf{u}_{k-1} \tag{1d}$$

$$\mathbf{h}(\mathbf{x}_{k-1}, \mathbf{u}_{k-1}, \mathbf{x}_k, \mathbf{u}_k \mid \mathbf{p}_k) \le \mathbf{0} \tag{1e}$$

$$\mathbf{x}_{\min} \le \mathbf{x}_k \le \mathbf{x}_{\max}, \mathbf{u}_{\min} \le \mathbf{u}_k \le \mathbf{u}_{\max} \tag{1f}$$

$$f(\mathbf{x}_k, \mathbf{u}_k) = \mathbf{a}_f + \mathbf{b}_{fx}^T \mathbf{x}_k + \mathbf{b}_{fu}^T \mathbf{u}_k + \mathbf{x}_k^T C_{fxx} \mathbf{x}_k + \mathbf{x}_k^T C_{fxu} \mathbf{u}_k + \mathbf{u}_k^T C_{fuu} \mathbf{u}_k \tag{1g}$$

The constant vectors $\mathbf{a}_{eq}(p)$ and $\mathbf{a}_{ineq}(p)$ are $n_s \times 1$ and $n_h \times 1$ vector functions respectively. The argument of this function is a vector of device parameters at step *k*, to allow for parameter dependent models. $Y_{eqx}, Y_{equ}, Y_{ineqx}, Y_{inequ}$ are appropriately sized matrices defining the linear terms in equations (1a) and (1c). Furthermore, the quadratic terms, if any, are defined by collections of sparse matrices, such as F_{eqxx}^i. Finally, lower and upper bounds on the participating variables are treated separately from general constraints ***h***. In cases of variables without lower or upper limits, extremely low or large values are set as the lower and upper bounds respectively.

Without loss of generality, this model can be used to represent any flexible resource. Note that constraints (1a) and (1c) include both static and dynamic equalities and inequalities, respectively.

The dynamics are captured by the past history vectors (1b) and (1d). If the equations are static the past history vectors are zero.

The cost of operating the system is assumed to have quadratic structure as well (1g). The matrices C_{fxx}, C_{fxu}, and C_{fuu} are stored in sparse format. In the classical OPF problem, it should be expected that, for most devices, the factors involved in (1g) have zero values, except for generators. However, this formulation allows flexibility for experimentation with other objective functions in different settings (such as customer flexibility markets) & future research.

From an implementation perspective, it is worth noting that, while linear and constant terms (Y_{eqx}, Y_{equ}, Y_{ineqx}, Y_{inequ} e.t.c.) can be stored as full matrices, quadratic terms, such as F^{i}_{eqxx}, must always be stored in sparse form, for computational and storage economy reasons.

This is a quadratic model that accurately represents each device's dynamics. It is obtained by integrating the corresponding differential-algebraic equations (e.g. through quadratic integration). The main advantage of this sparse quadratic syntax is that it allows an efficient algorithmic computation (object oriented) of Jacobeans, Hessians, etc. of the underlying optimization problem, without compromising the capability of utilizing nonlinear device models.

The device interacts with the rest of the network via its through variables. Specifically, the current equations of all devices that are connected to the same node must sum up to zero, in order to enforce Kirchhoff's Current Law. For this purpose, the device model also contains a n_s x 1 connectivity vector to map from the device-level equations to the network-level equations:

$$Ind_d^x(m) = n \tag{2}$$

This signifies that the *m*-th equation of device *d* maps to the *n*-th system-level equation.

2.3 Problem Formulation

The device data structures defined above are adequate to synthesize the system-level look-ahead optimization problem in a concise manner. Specifically, the *n*-th equality constraint for the system level flexible optimal power flow is:

$$g_n(\mathbf{X}_{k-1}, \mathbf{U}_{k-1}, \mathbf{X}_k, \mathbf{U}_k) = \sum_{Ind_d^x(m)=n} g^{(d)}(\mathbf{x}_{k-1}, \mathbf{u}_{k-1}, \mathbf{x}_k, \mathbf{u}_k) \tag{3}$$

A similar process is followed to synthesize the system level inequality constraints *h*. Note that, for this framework to be operational, a mapping between the system-level and the device level states, controls and inequalities must also exist. Namely, the *n*-th system level inequality constraints at each step is:

$$h_n(\mathbf{X}_{k-1}, \mathbf{U}_{k-1}, \mathbf{X}_k, \mathbf{U}_k) = \sum_{Ind_d^h(m)=n} h_m^{(d)}(\mathbf{x}_{k-1}, \mathbf{u}_{k-1}, \mathbf{x}_k, \mathbf{u}_k) \tag{4}$$

The objective function for the system at step *k* is given simply as the summation of the individual cost functions for the N_d devices:

$$c(\mathbf{X}_k, \mathbf{U}_k) = \sum_{i=1}^{N_d} \mathbf{f}^{(d)}(\mathbf{x}_k, \mathbf{u}_k) \tag{5}$$

Given the quadratic structure of the device cost functions (1g), the system cost function is also quadratic.

Using these synthesis rules, the following *K*-step problem is defined:

$$\begin{aligned}
&\min_{\mathbf{X},\mathbf{U}} \sum_{k=1}^{K} c(\mathbf{X}_k, \mathbf{U}_k) \\
&\text{subject to} \\
&\mathbf{g}(\mathbf{X}_{k-1}, \mathbf{U}_{k-1}, \mathbf{X}_k, \mathbf{U}_k \mid \mathbf{P}_k) = 0 \quad k = 1,2,\ldots,K \\
&\mathbf{h}(\mathbf{X}_{k-1}, \mathbf{U}_{k-1}, \mathbf{X}_k, \mathbf{U}_k \mid \mathbf{P}_k) \le 0 \quad k = 1,2,...,K \\
&\mathbf{U}_{\min} \le \mathbf{U}_k \le \mathbf{U}_{\max} \quad k = 1,2,...,K \\
&\mathbf{X}_{\min} \le \mathbf{X}_k \le \mathbf{X}_{\max} \quad k = 1,2,...,K \\
&\mathbf{X}_0 = \mathbf{X}_{init} \\
&\mathbf{U}_0 = \mathbf{U}_{init}
\end{aligned} \tag{6}$$

The flexible OPF problem in (6) is a quadratically constrained quadratic program (QCQP). Note that $\mathbf{X}_k$, $\mathbf{U}_k$ and $\mathbf{P}_k$ are the consolidated system state, control and parameter vectors respectively. The parameter vector depends on the particular device models employed, but typical parameters include load active and reactive consumptions & wind speed values. Hence, (6) needs to be solved independently for each possible scenario in the look-ahead *K*-step horizon. This work is focused on the deterministic look-ahead OPF, i.e. solving (6) for a given scenario of parameters.

2.4 Solution Method

The look-ahead AC-OPF problem is a non-convex Nonlinear Programming (NLP) problem [11]. Numerical solutions to such problems are plagued by sensitivity to initial guess, lack of global optimality guarantees and potentially lack of global convergence guarantees. Given the large scale of the problems under consideration, the class of algorithms used in this research was the Primal Dual Interior Point method, which is widely used for the AC-OPF problem ([12], [13]). The method is amenable to sparse matrix techniques, which is consistent with the sparse structure of network equalities and inequalities.

The solver used in this research is IPOPT [14], which comes with global convergence properties, utilizing an interior point method with a filter line search step that guarantees global convergence under mild regularity conditions. Global optimality is not guaranteed; merely convergence to a stationary point for the problem's Lagrangian. Hence, no global optimality claims are made in this research, whenever the AC-OPF look-ahead algorithm is concerned.

The numerical performance of IPOPT is considerably improved if explicit expressions for the constraint & objective gradients, as well as the Lagrangian's Jacobian are provided. The

quadratic structure of the flexible OPF enables computationally efficient calculation of sparse Jacobian & Hessians. Namely, problem (6) is structured as follows in our framework:

$$\begin{aligned} &\min_{\mathbf{z}} f(z) = \mathbf{z}^{\mathrm{T}} A_f \mathbf{z} + b_f^T \mathbf{z} + c_f \\ &\text{subject to} \\ &\mathbf{z}^T H_{g,i} \mathbf{z} + b_{g,i}^T \mathbf{z} + c_{g,i} + a_{g,i}(\mathbf{P}) = 0 \quad i = 1,...,N_s \\ &\mathbf{z}^T H_{h,i} \mathbf{z} + b_{h,i} \mathbf{z} + c_{h,i} + a_{h,i}(\mathbf{P}) \le 0 \quad i = 1,...,N_h \\ &\mathbf{z}_{\min} \le \mathbf{z} \le \mathbf{z}_{\max} \end{aligned} \tag{7}$$

The problem cast in variables **z**, defined as:

$$\mathbf{z} = \begin{bmatrix} \mathbf{X}_1 \\ \mathbf{U}_1 \\ \vdots \\ \mathbf{X}_k \\ \mathbf{U}_k \end{bmatrix} \tag{8}$$

Hence, the gradients are calculated as follows:

$$\nabla_z f = \mathbf{z}^T (H_f + H_f^T) + b_f^T \tag{9a}$$

$$\nabla_z g_i = \mathbf{z}^T (H_{g,i} + H_{g,i}^T) + b_{g,i}^T \tag{9a}$$

$$\nabla_z h_i = \mathbf{z}^T (H_{h,i} + H_{h,i}^T) + b_{h,i}^T \tag{9c}$$

The Lagrangian hessian is calculated as follows:

$$\nabla_{zz} L(\mathbf{z}, \boldsymbol{\lambda}_g, \boldsymbol{\lambda}_h) = A_f + \sum_{i=1}^{N_s} \lambda_{g,i} H_{g,i} + \sum_{i=1}^{N_h} \lambda_{h,i} H_{h,i} \tag{10}$$

The sparse structure of H_f, H_g, H_h and b_f, b_g, b_h allows for quick calculation of the sparse gradients and hessians This allows, from an implementation perspective, use of IPOPT with relatively small external overhead for obtaining Jacobians and Hessians. This is the primary benefit the Quadratic formulation of the look-ahead AC-OPF developed in this research.

2.5 Comparison with DC-OPF flexible OPF

The DCOPF look-ahead dispatch is a version of the look-ahead problem that relies on the DC Optimal Power Flow at each step. In turn, the DC-OPF is based on the assumption that branch resistances can be neglected, and that voltage magnitudes remain constant at unity. Hence the power flows on lines depend on the voltage phasor angles, which become the only variables in the DC-OPF. In order to implement this approach and compare with the AC-OPF look-ahead dispatch developed in this work, additional dynamic models of devices, consistent with the DC assumptions were developed. In these models:

- The interface variables with the point of connection of each device are the node's angle θ and the incoming (absorbed) active power by the device, instead of I_r^k, I_i^k and V_r^k, V_i^k respectively.
- Kirchoff's current law is enforced by requiring that the sum of active power in a node be zero, instead of currents in the AC-OPF.
- Any reactive power aspects of connected devices are neglected. Indeed, the DC-OPF does not consider reactive power dispatch in any way
- To maintain the main linearity advantage of the DC-OPF, all device models used were linear.

With the above developments, the DC-OPF look-ahead dispatch becomes a Quadratic Programming problem (convex quadratic cost function with linear constraints). This problem is now essentially a succession of DC-OPF's with transition constraints for all dynamic devices:

$$\min_{\theta_i, X_i} \left\{ \sum_{j=1}^{N_g} a_{g,i} P_{g,i}^2 + b_{g,i} P_{g,i} + c_{g,i} \right\}$$

subject to

$$\begin{aligned} \sum_{j \in N_i} P_j(\theta_t^k, X_j^k, \theta_i^{k-1}, X_j^{k-1}) = 0 \qquad & \forall i =\in \{1,\dots N_b\}, \forall k \in \{1,\dots K\} \\ A_j \theta_t^k + B_j X_j^k + C_j \theta_i^{k-1} + D_j X_j^{k-1} \le b_j \quad & \forall j =\in \{1,\dots N_d\}, \forall k \in \{2,\dots K\} \\ E_j \theta_t^k + F_j X_j^k + G_j \theta_i^{k-1} + H_j X_j^{k-1} = 0 \quad & \forall j =\in \{1,\dots N_d\}, \forall k \in \{2,\dots K\} \end{aligned} \tag{11}$$

The DC-OPF look-ahead dispatch problem is a quadratic programming (QP) problem [15]. Assuming the problem is feasible and bounded, as is the case in Optimal Power Flow problems, (11) is solvable by mature Interior Point Methods. Primal-Dual interior point method is a mature method to solve such convex problems to global optimality [15]. The Interior Point solver used in this research is IPOPT [14], however the results are also verified using MIPS, which is part of the MATPOWER package [16], in the MATLAB environment.

Given that the AC-OPF look-ahead dispatch is a non-convex formulation and the PDIPM algorithm may converge to local minima, it is of interest to compare its output with the results of the DC-OPF look-ahead dispatch, which is a convex formulation that uses less accurate linearized models for the system's devices.

Table 2.1: AC-OPF vs. DC-OPF look-ahead dispatch features

FEATURES	DC-OPF LOOK AHEAD DISPATCH	AC-OPF LOOK-AHEAD DISPATCH
TRACTABILITY	Smaller Size QP Problem	Larger Size Non-convex problem
GLOBAL OPTIMALITY	Solved to global optimality	Global optimality not guaranteed
CONVERGENCE GUARANTEES	Always converges (under mild regularity conditions)	Convergence sensitive to initial guess
MODELING ACCURACY	Approximate Models Inaccurate Congestion Modeling	Physically Based & Accurate Models Models non-linear phenomena
QUALITY OF DISPATCH	Only active power dispatch	Full active-reactive dispatch
FEASIBILITY OF REAL-TIME DISPATCH	Static AC-OPF dispatch may be infeasible	Guarantees feasibility

The difference between the two formulations is summarized in Table 2.1. The DC-OPF is a convex problem, with strong convergence and global optimality guarantees. However, unlike the AC-OPF look-ahead dispatch, it utilizes the DC approximation which may misrepresent the actual behavior of the electric grid. As such, if dynamic devices (such as storage or ramp-constrained generation) are scheduled using the DC-OPF, then any errors introduced by the DC approximation will have to be corrected in the clearing of the real-time (static) operation of the system, either through out-of-market actions or a corrective dispatch using more accurate models. These actions may carry more cost or may even be insufficient to restore feasibility, under extreme conditions. Hence, the inaccuracy of the DC-OPF problem may lead to higher costs or even infeasibility of the real-time dispatch. Finally, unlike the AC-OPF, the DC-OPF clearly ignores all non-linear effects and all control variables except for active power dispatch. Thus, it does not perform or account for reactive dispatch, load tap changing mechanisms e.t.c..

In order to explore the tradeoff between the globally optimal DC-OPF and the more accurate AC-OPF model, tests were performed in various standard test cases. The same scenarios (load variation & renewables output) were solved using a DC-OPF and an AC-OPF look-ahead dispatch. In order to consider the corrective dispatch issues of the DC-OPF, the dispatch schedules produced by this method were used to schedule the dynamic resources (ramp-constrained generation and storage in this case) and a static corrective AC-OPF was solved at each step, by keeping the dynamic dispatch fixed to the output of the DC-OPF, in a two stage fashion. On the other hand, the look-ahead flexible AC-OPF output was used for the scheduling of all control variables, and no static dispatch was needed for that case. The comparison methodology for the two different look-ahead formulations is shown in Figure 2.1 .

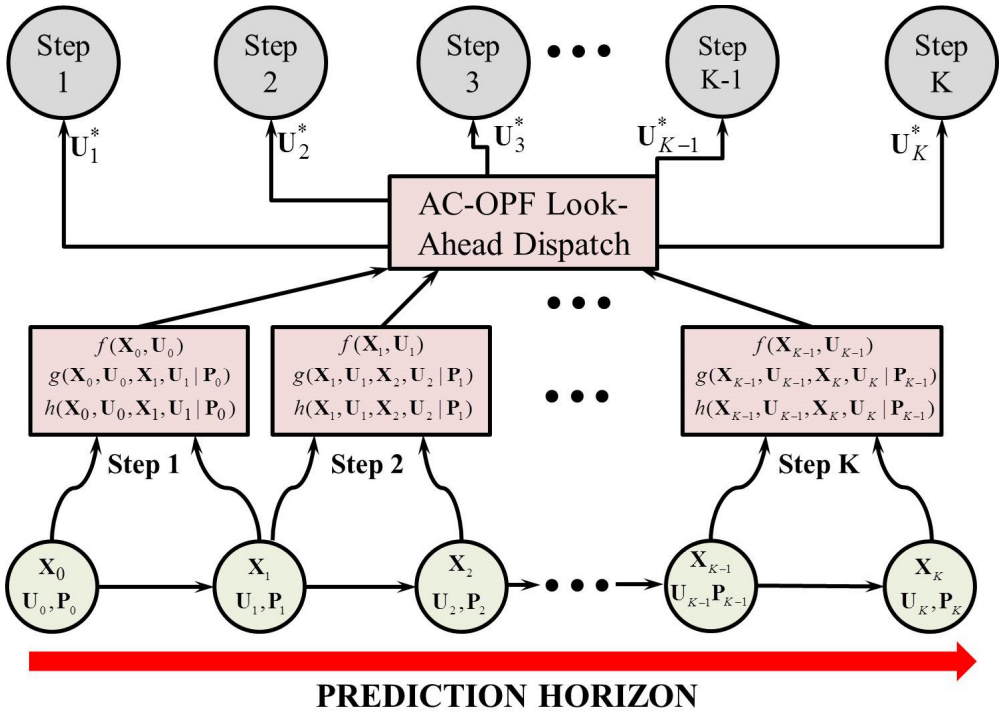

(a)

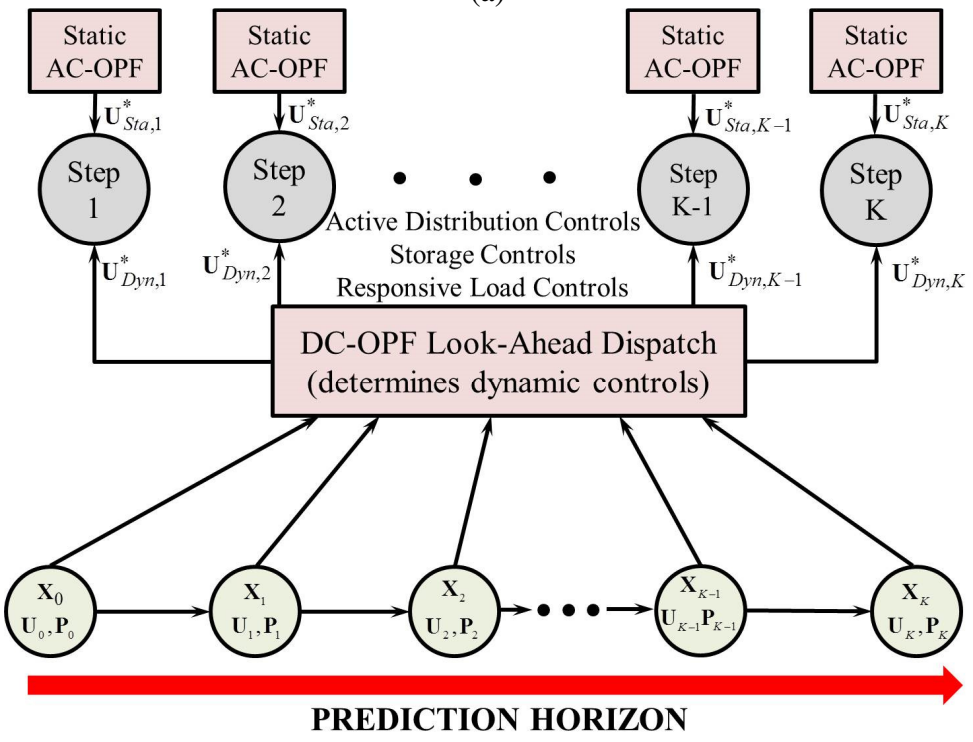

(b)

Figure 2.1: AC-OPF versus DC-OPF evaluation method (a) AC-OPF (b) DC-OPF

The total operating cost of these two different frameworks was recorded for each case. The first case study used was the IEEE 30 bus system (Figure 2.2). A wind farm with a base case capacity of 35MW and a storage unit with base case capacity of 50MW, 100MWh were placed in bus 6. The transmission corridor 6-8, which is a 32MVA, 135KV line, is congested in this particular system. Because of different congestion models used by the AC-OPF and the DC-OPF we expect significant variations in the dispatch results. A summary of different scenarios examined, and the corresponding operating cost yielded by the two different look-ahead dispatch frameworks under examination is given in Table 2.2.

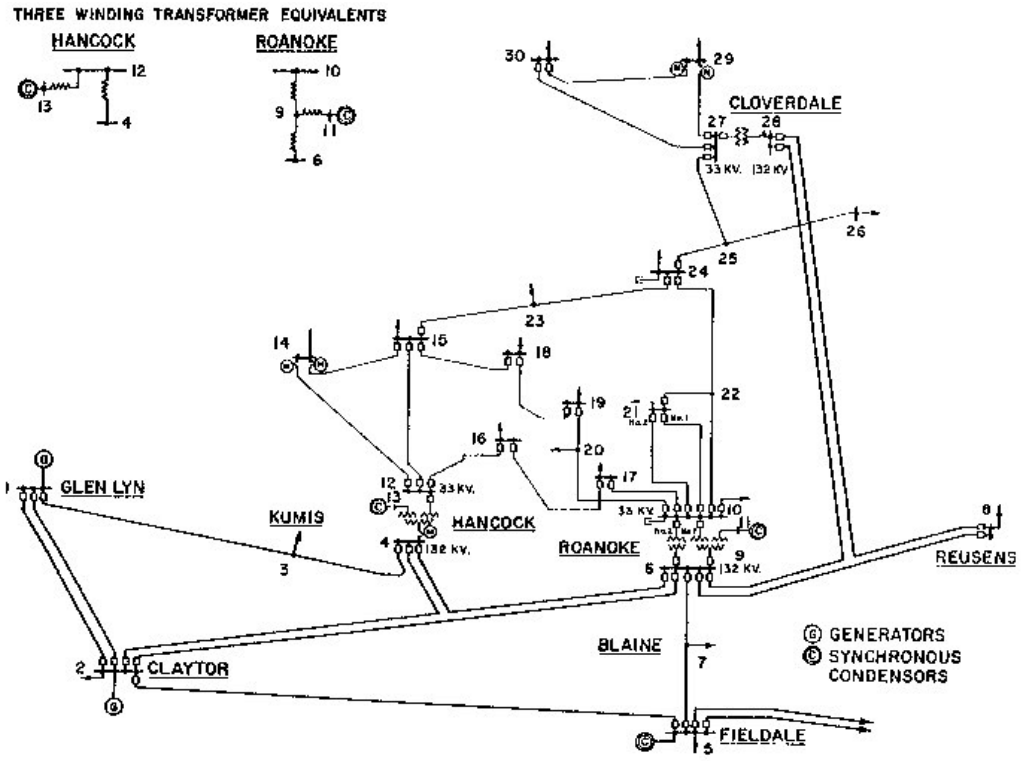

Figure 2.2: IEEE 30-bus system

Table 2.2: AC-OPF versus DC-OPF dispatch operating cost results – IEEE 30 bus

Scenario	Storage Energy	Storage Power	Wind Penetration	DC-OPF Cost	AC-OPF Cost	Cost w/o storage
A	100MWh	50MW	35MW	5.6228e+04	5.5623e+04	5.6381e+04
B	200MWh	100 MW	35MW	5.6095e+04	5.5068e+04	5.6381e+04
C	50MWh	25MW	35MW	5.6313e+04	5.6048e+04	5.6381e+04
D	300MWh	150MW	35MW	5.5479e+04	5.4618e+04	5.6381e+04
E	100MWh	50MW	70MW	4.8897e+04	4.8281e+04	4.9142e+04
F	100MWh	50MW	135MW	4.2105e+04	4.1348e+04	4.2448e+04

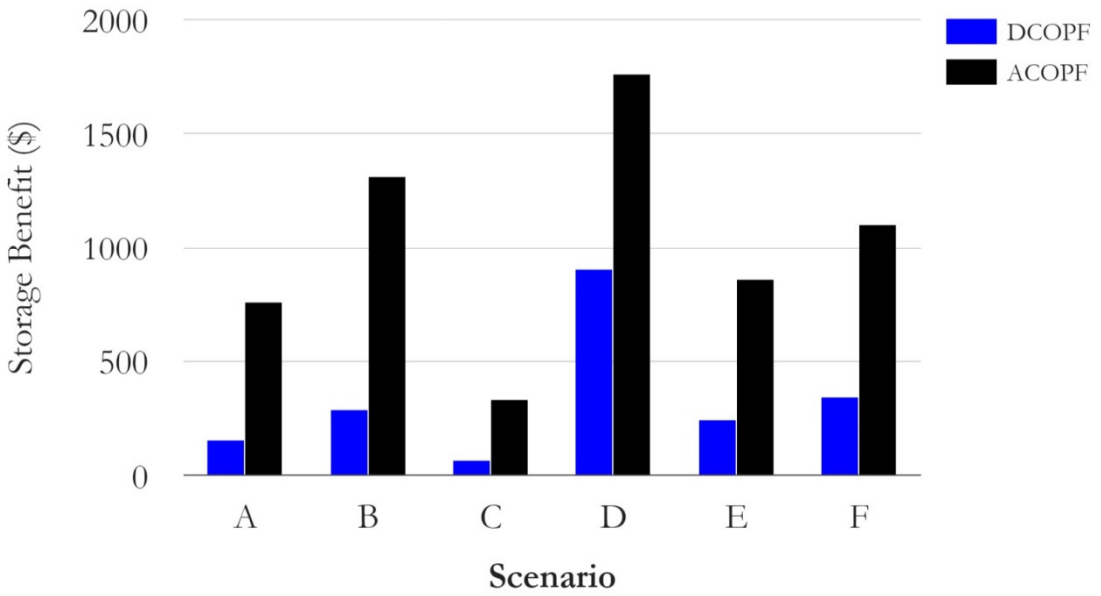

Figure 2.3: Cost Reduction from Battery Operation – ACOPF vs. DCOPF in 30 Bus Case

As shown in Table 2.2, for the scenarios under examination, the AC-OPF dispatch yields lower operational cost than the DC-OPF dispatch with AC-OPF corrective actions. Although this case study does not allow for general conclusions to be drawn, in this particular case the AC-OPF look-ahead dispatch is preferable since it allows more efficient utilization of installed storage capacity. In order to further quantify this, Figure 2.3 shows the *Storage Cost Reduction*, i.e. the reduction in operating cost compared to what the cost would be if storage was completely removed from the system, for the two different look-ahead dispatch procedures. For completeness, that cost value is given in the last column of Table 2.2. It is clear that in all cases the AC-OPF look-ahead dispatch allows better utilization of the storage installed in bus 6. This is attributed mostly to the more accurate modeling of the congestion in line 6-8 in the AC formulation.

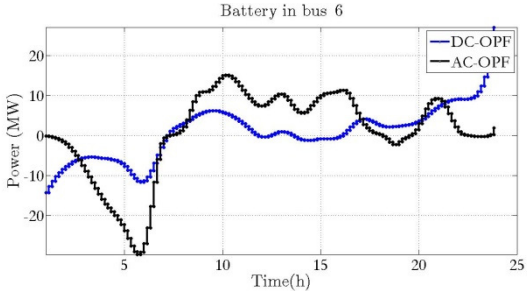

(a) Case A - Battery Power

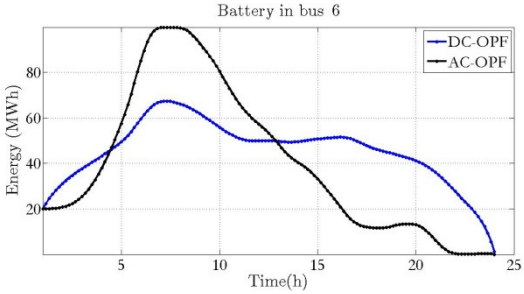

(b) Case A- Battery Energy

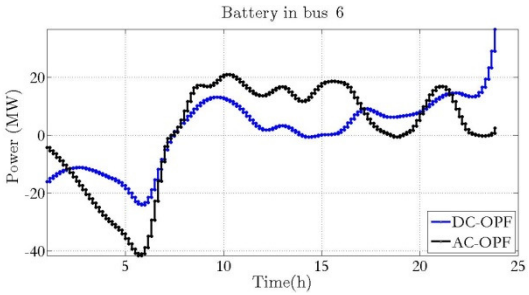

(c) Case B – Battery Power

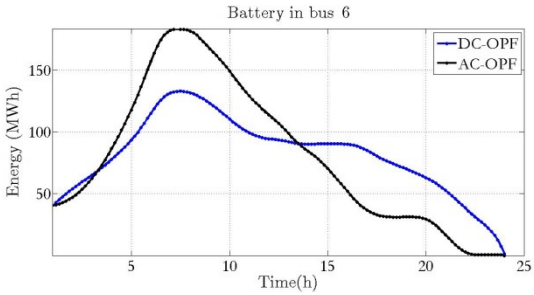

(d) Case B – Battery energy

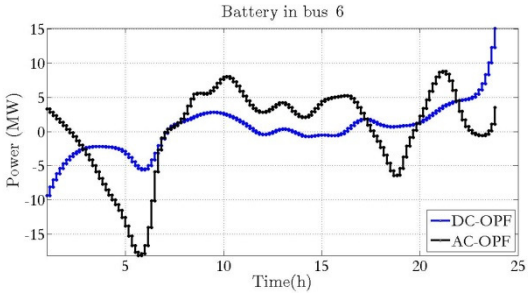

(e) Case C – Battery Power

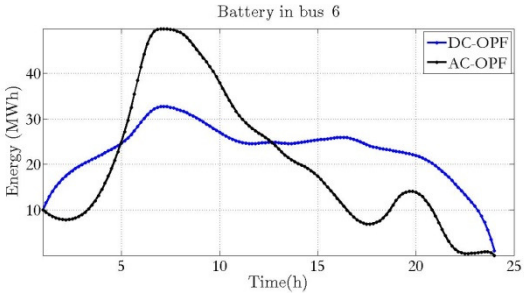

(f) Case C – Battery Energy

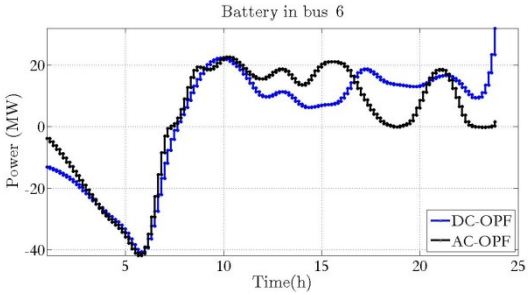

(f) Case D – Battery Power

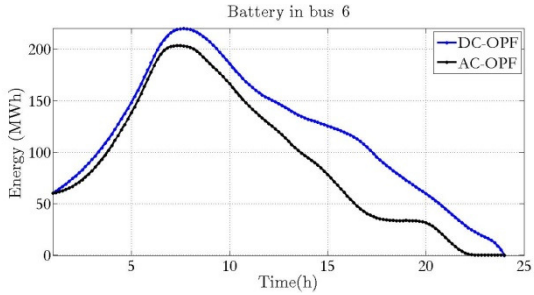

(g) Case D – Battery Energy

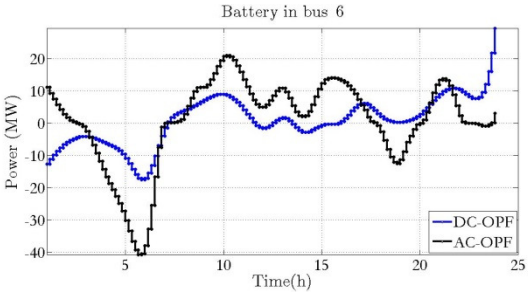

(h) Case E – Battery Power

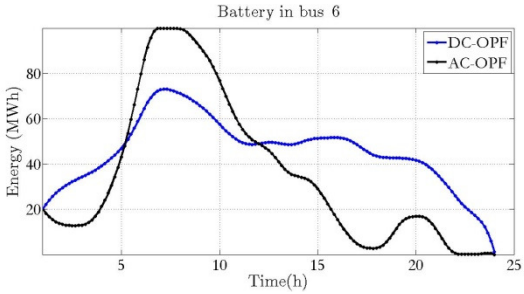

(i) Case E – Battery Energy

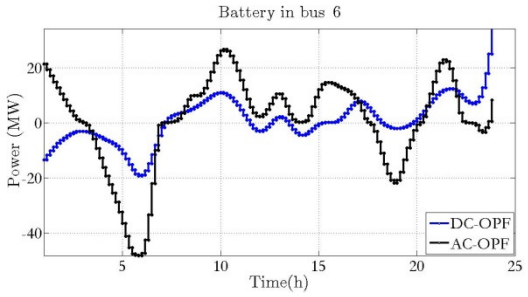

(j) Case F – Battery Power

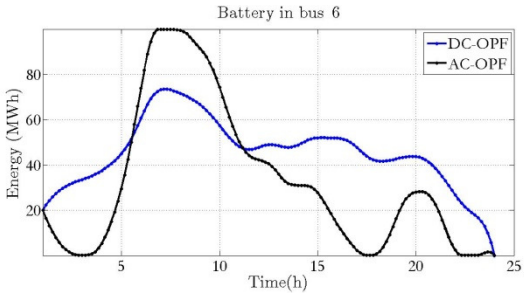

(k) Case F – Battery Energy

Figure 2.4: Storage Dispatch Patterns – Cases A - F

The different dispatch patterns of the storage unit schedules via the look-ahead problems are shown in Figure 2.4, where the differences between the two dispatch results are clearly shown.

However, the IEEE 30 bus system is a small test case and all storage capacity was placed near a congested transmission corridor. By repeating this test in a 2383 bus of the Polish Test system, we can draw some conclusion regarding larger, more realistic systems. The results are shown in Table 2.3 and the cost reduction comparison results are shown in Figure 2.5.

Table 2.3: AC-OPF versus DC-OPF dispatch operating cost results – Polish 2383 bus

Scenario	Storage Energy	Storage Power	Wind Penetration	DC-OPF Cost	AC-OPF Cost	Cost w/o storage
A	24 GWh	8GW	3.21GW	4.2674e+07	4.2568e+07	4.8148e+07
B	46GWh	12 GW	3.21GW	4.1034e+07	4.0886e+07	4.8148e+07
C	12 GWh	4GW	3.21GW	4.4763e+07	4.4700e+07	4.8148e+07
D	46GWh	12GW	4.1730	4.0057e+07	3.9901e+07	4.7169e+07

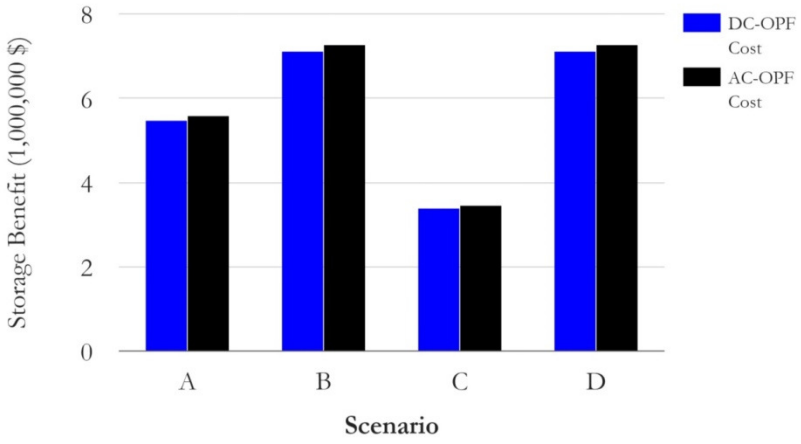

Figure 2.5. Cost Reduction from Battery Operation – ACOPF vs. DCOPF in 2383 Bus Case

From the results in Figure 2.5 it is evident that, while the cost reduction is still greater in the AC-OPF look-ahead case, the difference is much less pronounced (not exceeding 2%) than the 30 bus case.

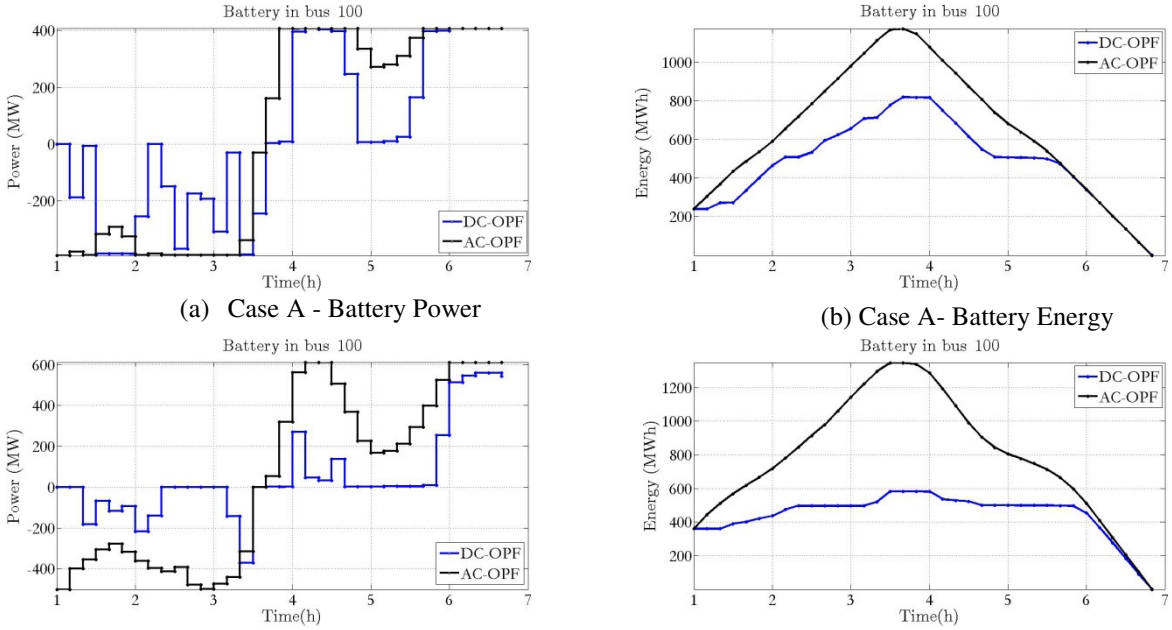

(a) Case A - Battery Power

(b) Case A- Battery Energy

(c) Case B – Battery Power

- Case B – Battery energy

Figure 2.6: Storage Dispatch Patterns – Bus 100

In order to demonstrate a sample of the different dispatch patterns that result from the two look-ahead dispatch paradigms, the power and energy plots for the storage unit in bus 100 are provided in Figure 2.6.

2.6 Sample Timing Results

The AC-OPF look-ahead dispatch was tested on various standard power system test cases, using an 1-hour look-ahead horizon. The timing results, on an un-optimized personal computer with an Intel Core i7-4510U 2GHz processor are reported in Table 2.4. It should be noted that convergence speed relies heavily on initialization and algorithm parameters, such as the Hessian scaling parameter in the PDIPM algorithm. Hence, timing results are only indicative and not definitive.

Table 2.4: Timing Results for Various Case Data – 1 hour look-ahead horizon

SYSTEM CASE	STATE VARIABLES	CONTROL VARIABLES	INEQUALITY CONSTRAINT	AC-OPF EXECUTION TIME (S)	DC-OPF EXECUTION TIME
IEEE 24 Bus	288	396	516	0.1960	0.1050
IEEE 118 Bus	1,416	648	2,532	0.7780	0.0760
IEEE 300 Bus	3,600	828	6,066	2.0280	0.0960
PEGASE 1354	16,248	3,120	28,194	17.1200	0.3030
2383 Polish System (Winter Peak)	28,596	3,924	45,972	53.3560	2.9174
PEGASE 2869	34,428	6,120	61,920	59.5810	0.7120
3120 Polish System (Spring Peak)	37,440	3,576	59,598	48.5290	2.8620
British 2224 System	26,688	4,728	45,930	33.1470	0.8620
PEGASE 9241	110,892	17,340	207,186	235.8153	10.3530

However, timing results serve to indicate that the look-ahead dispatch problem is solvable within reasonable time frames, even in a retail machine, with average computational power. For the larger test case, the PEGASE 9241 system, a 1-hour look-ahead problem was solved within less than 4 minutes. For reference, the DC-OPF look-ahead timing results are also provided. They are obviously advantageous compared to the AC-OPF formulation, given the strong convergence properties of the QP formulation and the smaller size of the problem, due to the modeling restrictions of the DC-OPF formulation.

3. Component Modeling for Flexible OPF

3.1 Introduction

In this Chapter we cover the new component models introduced in the multi-period OPF problem by this research, in order to expand flexibility options. Namely, battery energy storage systems (BESS), thermostatically controlled loads (TCL), dynamic line ratings (DLR) and aggregate control of distribution systems will be addressed.

3.2 Nomenclature

$g_d + jb_d$	**Generator direct-axis admittance**
$\tilde{V}^k = V_r^k + jV_i^k$	Device Terminal Voltage phasor at step k in Cartesian Coordinates
$\tilde{E}^k = E_r^k + jE_i^k$	Generator internal EMF phasor at step k in Cartesian Coordinates
$\tilde{I}^k = I_r^k + jI_i^k$	Device *incoming* current in Cartesian Coordinates
R	Generator Ramp Rate in MW/min
Δt	Chosen step size for look-ahead FOPF
a_g, b_g, c_g	Generator's quadratic cost function coefficients
K_1, K_2, K_3	Line thermal model coefficients
T^k	Line average conductor temperature at step k
T_{amb}^k	Ambient Temperature at step k
Q_{th}^k	Heating / cooling rate from TCL at step k
a_{tcl}	TCL efficiency factor
R_{tcl}, C_{tcl}	TCL parameters – Conditioned Space to Ambient thermal resistance and Conditioned Space thermal capacitance
u_{tcl}	TCL duty cycle
$g_s + jb_s$	Admittance of Battery Energy Storage System
$E_{\max}, E_{\min}$	Maximum and Minimum Energy of Battery Energy Storage System
P_k^+	Battery charge power
P_k^-	Battery discharge power
n_s^+, n_s^-	Battery charging and discharging efficiency respectively
SOC^k	Battery State of Charge, at step k

a_s, b_s, c_s	Storage quadratic cost function coefficients
P_d^k	Active Power Consumed by Aggregate Distribution System at step k
Q_d^k	Reactive Power Consumed by Aggregate Distribution System at step k
B^k	Positive Definite Matrix defining the ellipsoidal feasible region of the Aggregate Distribution System at step k
d^k	Vector defining the ellipsoidal feasible region of the Aggregate Distribution System at step k
$\Delta B_p, \Delta B_q, \Delta B_{par}^+, \Delta B_{par}^-$	2×2 matrices, defining the Active Distribution System state transition model
$\Delta d_p, \Delta d_q, \Delta d_{par}^+, \Delta d_{par}^-$	2×1 vectors, defining the Active Distribution System state transition model
p_j^k	Value of j-th parameter of device model at step k

3.3 Ramp-Rate Constrained Generation

The effect of ramp-up and ramp-down constraints in the economic operation of power systems are very well studied for the unit-commitment problem [17], [18] and the look-ahead dispatch problem [19]. The inclusion of this model is particularly important in systems with high penetration of renewable energy sources. The quadratized model for the ramp-rate constrained generators used in this research is obtained by combining the steady-state single-axis model [20] with the addition of a ramp constraint:

$$\begin{bmatrix} I_r^k \\ I_i^k \\ 0 \\ 0 \end{bmatrix} = \begin{bmatrix} -g_d(E_r^k - V_r^k) + b_d(E_i^k - V_i^k) \\ -b_d(E_r^k - V_r^k) - g_d(E_i^k - V_i^k) \\ g_d E_r^k V_r^k - b_d V_r^k E_i^k + g_d V_i^k E_i^k + b_d V_i^k E_r^k - g_d\left(V_r^k\right)^2 - g_d\left(V_i^k\right)^2 - P_k \\ -g_d V_r^k E_i^k - b_d V_r^k E_r^k + g_d V_i^k E_r^k - b_d V_i^k E_i^k + b_d\left(V_r^k\right)^2 + b_d\left(V_i^k\right)^2 - Q_k \end{bmatrix} \tag{12a}$$

$$\begin{bmatrix} 0 \\ 0 \end{bmatrix} \geq \begin{bmatrix} P_k - P_{k-1} - R\Delta t \\ -P_k + P_{k-1} - R\Delta t \end{bmatrix} \tag{12b}$$

$$\begin{bmatrix} P_{\min} \\ Q_{\min} \end{bmatrix} \leq \begin{bmatrix} P_k \\ Q_k \end{bmatrix} \leq \begin{bmatrix} P_{\max} \\ Q_{\max} \end{bmatrix} \tag{12c}$$

Where the state and controls vectors are given as:

$$\mathbf{x}_k = \begin{bmatrix} V_r^k \\ V_i^k \\ E_r^k \\ E_i^k \end{bmatrix} \tag{13a}$$

$$\mathbf{u}_k = \begin{bmatrix} P_k \\ Q_k \end{bmatrix} \tag{13b}$$

The objective function contribution at each step can be a quadratic cost function of the active power control variable:

$$f(\mathbf{x}_k, \mathbf{u}_k) = a_g P_k^2 + b_g P_k + c_g \tag{14}$$

Where *a*, *b*, *c* are cost coefficients provided by each generator's cost curve.

3.4 Transmission Line with Dynamic Line Rating

Transmission line current magnitude is typically constrained due to the heat generated by Ohmic losses within the conductor. Such thermal limits are considered essential in virtually all Optimal Power Flow formulations and are usually treated as static maximum current magnitude limits. However, the observation has been made that the actual physical constraint with regard to this phenomenon is the transmission line's temperature, and not its current. This gave rise to increasing interest in thermal modeling of transmission lines [21]. More recently, an IEEE Standard [22] was published, detailing a comprehensive line temperature model, including meteorological effects, such as ambient temperature, precipitation, solar irradiation and prevailing winds, all of which affect the dynamic thermal model of the transmission line. It has been recorded that static line ratings often underestimate the actual loading capability of the line by as much as 15% and that higher reliability can be attained if dynamic line ratings of lines are monitored [23]. Further work has focused on actual implementations of real-time dynamic rating monitoring installations [24].

The dynamic thermal model of transmission lines is a good candidate for addition to the flexible dispatch formulation. Benefits in operating cost and reliability have been recorded in cases where dynamic ratings are taken into account in system operation. Furthermore, the dynamic nature of the flexible dispatch procedure outlined above allows the modeling of phenomena such as "temporary" overloading of critical lines, which a static OPF dispatch fails to capture. The hard constraint on line current magnitude can be removed, in favor of the actual conductor temperature limit.

A model for dynamic line rating can be incorporated in the flexible OPF dispatch by using the simplified first-order model put forth in [22] that assumes the conductor temperature model is a first order linear ODE with the line current magnitude as an input. It must be stressed that a fully detailed model of conductor temperature variations is nonlinear and convoluted, but the first order approximation, derived from [21] and [25] and mentioned in the standard is adequate for the purposes of this research. In fact, a linear model is obtained by linearizing the radiation heat losses from the line, which is itself a less significant factor in the model, which strengthens the validity of the approximation used here. The fact that the time constant for the thermal phenomena in a transmission line is approximately 10-15 minutes means that a look-ahead dispatch with 5 minute time steps should be adequate to capture the underlying phenomena.

The thermal model of the transmission line is as follows:

$$\begin{bmatrix} I_{1,r}^k \\ I_{1,i}^k \\ I_{2,r}^k \\ I_{2,i}^k \\ 0 \\ 0 \end{bmatrix} = \begin{bmatrix} (g+g_s)V_{1,r}^k + (-b-b_s)V_{1,i}^k - gV_{2,r}^k + bV_{2,i}^k \\ (b+b_s)V_{1,r}^k + (g+g_s)V_{1,i}^k - bV_{2,r}^k - gV_{2,i}^k \\ -gV_{1,r}^k + bV_{1,i}^k - (g+g_s)V_{2,r}^k + (b+b_s)V_{2,i}^k \\ -bV_{1,r}^k - gV_{1,i}^k + (b+b_s)V_{2,r}^k + (g+g_s)V_{2,i}^k \\ z_1^k - (g^2+b^2)\left[\left(V_{1,r}^k\right)^2 + \left(V_{1,i}^k\right)^2 + \left(V_{2,r}^k\right)^2 + \left(V_{2,i}^k\right)^2\right] + (2g^2+2b^2)\left(V_{1,r}^k V_{2,r}^k + V_{1,i}^k V_{2,i}^k\right) \\ T^k - T^{k-1} - K_1\left(T^{k-1} - T_{amb}^k\right) - K_2 z_1^{k-1} + K_3 \end{bmatrix} \tag{15a}$$

$$T^k \le T^{\max} \tag{15b}$$

The state vector is given as:

$$\mathbf{x}_k = \begin{bmatrix} V_{1,r}^k \\ V_{1,i}^k \\ V_{2,r}^k \\ V_{2,i}^k \\ z_1^k \\ T^k \end{bmatrix} \tag{16}$$

where z_1^k is an auxiliary variable, representing the line current magnitude squared. It was introduced for quadratization purposes. The last equation in (15a) is a simple Euler integration of the simplified thermal dynamics of the line:

$$\frac{dT}{dt} = K_1(T - T_{amb}) + K_2\|I\|^2 + K_3 \tag{17}$$

Note that K_3 depends on solar heating of the line (and hence depends on metrological conditions). Hence, it is treated as a parameter for this model, extracted from the meteorological forecast. The term K_1 depends on convection heat loss of the line, as well as the line's thermal capacitance and a linearized version of radiation heat loss. Hence variable wind speed & direction is to be considered, then K_1 is also a parameter, whose value for the look-ahead horizon depends on the weather forecast, which in turn affects the forced convective heat loss due to the wind. A simplified version of this model, with constant K_1 can be extracted, if constant wind pattern is assumed for the look-ahead horizon, or if the convective losses due to wind are altogether neglected. The latter will result in an overly conservative dynamic line rating model, because forced convection always has a cooling effect for the line. Finally, K_2 is due to ohmic effects within the line and it depends on conductor material only. Hence, it can always be considered constant.

3.5 Thermostatically Controlled Responsive Loads

A responsive TCL load is defined as a power consumption device whose primary purpose is to regulate the temperature of a monitored space so that it lies within a pre-determined tolerable

range: $T_{in} \in [T_{\min}, T_{\max}]$. Space air conditioning, electric water heaters and freezers are some prominent examples. The common characteristic of such loads is that the binding hard constraint on their operation is the minimum and maximum temperature of the regulated space. Hence, their operation can be scheduled by a look-ahead dispatch, so as to consume / refrain from consuming in order to support economic and reliable operation of the system.

It should be noted that the provided system by such loads does not come at the expense of the customer. Since the temperature constraint is explicitly modeled, the load's main function is served without customer inconvenience and any system support provided is within the capabilities of the load.

The model employed for responsive TCL's is:

$$\begin{bmatrix} I_r^k \\ I_i^k \\ 0 \\ 0 \\ 0 \end{bmatrix} = \begin{bmatrix} u_{tcl}^k (g_{tcl} V_r^k - b_{tcl} V_i^k) \\ u_{tcl}^k (b_{tcl} V_r^k + g_{tcl} V_i^k) \\ P_{tcl}^k - g\left(V_r^k\right)^2 - g\left(V_i^k\right)^2 \\ Q_{th}^k - \frac{a_{tcl}}{50}\left[T^k - T_{amb}^k\right] P_{tcl}^k \\ T^k - T^{k-1} - \frac{1}{C_{tcl} R_{tcl}}\left(T_{amb}^k - T^{k-1}\right) - \frac{1}{C_{tcl}} u_{tcl}^k Q_{tcl}^k \end{bmatrix} \tag{18a}$$

$$\begin{aligned} T^{\min} \le T^k \le T^{\max} \\ 0 \le u_{tcl} \le 1 \end{aligned} \tag{18b}$$

Where the state and controls vectors are given as:

$$\mathbf{x}_k = \begin{bmatrix} V_r^k \\ V_i^k \\ P_{tcl}^k \\ Q_{th}^k \\ T^k \end{bmatrix} \tag{19a}$$

$$\mathbf{u}_k = \left[u_{tcl}^k\right] \tag{19b}$$

The ambient temperature is a time-varying parameter for this model, provided by the weather forecast.

For our purposes, the electrical behavior of the TCL is modeled as a constant impedance load $g_{tcl} + jb_{tcl}$. The thermal model includes the effect of ambient temperature and space temperature on the efficiency of the thermodynamic cycle and the temperature dynamics are modeled using a simple first-order model. Note that the duty cycle control variable u_{tcl}^k is factored in when evaluating the device absorbed current, as well as the actual heat/cool rate in (18a). The equations in (18a) are obtained from a quadratization of the following equations:

$$
\begin{aligned}
\tilde{\mathbf{I}} &= u_{tcl} Y \tilde{\mathbf{V}} \\
P_e &= \mathrm{Re}\{\mathbf{V}\mathbf{I}^*\} \\
Q_{th} &= \frac{a}{50}[T_{amb} - T]P_e \\
C\frac{dT(t)}{dt} &= \frac{1}{R}[T_{amb}(t) - T(t)] + u_{tcl}Q_{th}
\end{aligned}
\tag{20}
$$

This model captures both the active and reactive consumption of TCL's, as well as the thermal losses of the house and the effects of control actions on TCL efficiency.

3.6 Battery Energy Storage System

The value of energy storage in addressing issues arising from renewable penetration, and providing ramping, regulation or peak shaving services has been recognized in the literature [26], [27]. Hence, consideration of high-accuracy energy storage models is a salient feature of the look-ahead dispatch framework. The energy storage model considers charging and discharging losses, as well as the capability of the storage plant to provide reactive power support. Obviously, the dynamic aspects of the battery's state of charge, as well as the limitations in active power and energy capacity must be included in the model.

The quadratized model for the battery energy storage system is as follows:

$$
\begin{bmatrix} I_r^k \\ I_i^k \\ 0 \\ 0 \\ 0 \end{bmatrix} = \begin{bmatrix} -g_s(E_r^k - V_r^k) + b_s(E_i^k - V_i^k) \\ -b_s(E_r^k - V_r^k) - g_s(E_i^k - V_i^k) \\ -g_s E_r^k V_r^k - b_s V_r^k E_i^k - g_s V_i^k E_i^k + b_s V_i^k E_r^k + g_s\left(E_r^k\right)^2 + g_s\left(E_i^k\right)^2 - P_k^- + P_k^+ \\ -g_s V_r^k E_i^k + b_s V_r^k E_r^k + g_s V_i^k E_r^k + b_s V_i^k E_i^k - b_s\left(V_r^k\right)^2 - b_s\left(V_i^k\right)^2 - Q_k \\ SOC_k - SOC_{k-1} + \frac{1}{E^{\max}}\frac{1}{n_s^-}P_k^-\Delta t - \frac{1}{E^{\max}}n_s^+ P_k^+ \end{bmatrix}
\tag{21a}
$$

$$
\begin{aligned}
0 \le P_k^+ &\le P^{\max} \\
0 \le P_k^- &\le P^{\max} \\
Q^{\min} \le Q^k &\le Q^{\max} \\
0 \le SOC^k &\le 1
\end{aligned}
\tag{21b}
$$

The state and control vectors for this model are:

$$\mathbf{x}_k = \begin{bmatrix} V_r^k \\ V_i^k \\ E_r^k \\ E_i^k \\ SOC^k \end{bmatrix} \tag{22a}$$

$$\mathbf{u}_k = \begin{bmatrix} P_k^+ \\ P_k^- \\ Q_k \end{bmatrix} \tag{22b}$$

This battery model includes losses in the electrical subsystem (through the admittance $g_s + jb_s$ as well as internal losses in the battery. In fact, discharge efficiency n_s^- may be different from charging efficiency n_s^+, and this phenomenon is appropriately modeled. For this purpose, charging power P_k^+ is treated as a separate control variable from discharge power P_k^-, each with their own control bounds. Note that n_s^- and n_s^+ are constant parameters with a positive value less than one. Furthermore, the state of charge variable *SOC* is between zero and one and expresses the level of charge of the battery. Note that it is simply a scaled version of the battery's currently stored power.

In case it is desirable, the charge/discharge control terms can also participate in the objective function for this device:

$$f(\mathbf{x}_k, \mathbf{u}_k) = a_g \left(P_k^- - P_k^+\right)^2 + b_g \left(P_k^- - P_k^+\right) + c_g \tag{23}$$

Note that the net power output from the battery is $P_k^- - P_k^+$. Also note that, unlike generating plants whose cost is non-negative in every period, storage plants are characterized by a negative cost when they are charging.

3.7 Active Distribution System

A large number of distributed active devices are expected to be connected in the future distribution feeder, including rooftop solar, plug-in hybrid electric vehicles, small scale storage and responsive loads. Each of these devices may be small in rating (a few kW), serving individual residential or small commercial customers. While it would be beneficial to include them in the transmission-level look-ahead dispatch formulation, such a choice is faced with important hurdles:

- The transmission level dispatch is concerned with optimizing large transmission and generation assets, whose typical magnitudes are in the order of several Megawatts. Hence, a scaling issue arises, if all distribution devices are included individually in the dispatch

- Thousands of these devices may be connected to each feeder, and the typical distribution system may be composed of hundreds of such feeders. Hence, individual consideration of every active device will require the full inclusion of millions of state-space models in the look-ahead dispatch, thus increasing considerably the size of the look-ahead dispatch, which is already a computationally challenging problem, as discussed above.
- The devices connected to the distribution system have their own set of binding constraints that need to be considered. Specifically, responsive loads must serve their main function without exception (no customer inconvenience), storage devices must remain within their physical limits etc.

In order to solve the scaling and tractability issues that arise from introducing distributed resources to transmission-level dispatch, one approach is to obtain an aggregate representation of the distribution system. In this paragraph we formulate an aggregate model that relies on the description of the feasible set for the aggregate active and reactive power consumption of the active distribution system. Furthermore, a time-domain model is developed, that provides a description for the feasible *P*-*Q* set in period *t* given the power consumption in period *t*-1. Since this model aggregates a multitude of distributed resources that add up to several Megawatts of capacity, this approach addresses both the scale and the tractability issue.

Ellipsoidal Model for Active Distribution System

The adopted model for the active distribution system represents a compromise between tractability, simplicity and accuracy. To represent the available control capability in terms of active & reactive consumption of the distribution feeder, we assume that the feasible region of this feeder is an ellipsoid in the *P*-*Q* plane:

$$F_{pq} = \left\{ \begin{bmatrix} P_d \\ Q_d \end{bmatrix} \in R^2 : \begin{bmatrix} P_d \\ Q_d \end{bmatrix} = Bu + d, u^T u \le 1 \right\} \tag{24}$$

Where $B \succ 0$ is a 2×2 symmetric matrix and $d \in R^2$.

An example of such a feasible region for a representative feeder with 800 8kW Air-Conditioned Homes and 200 4.4kW, 6kWh batteries is shown in Figure 3.1. The physical meaning of this representation is that the center *d* of the ellipsoid is the "base case" consumption of the feeder – equivalent to a static representation of the feeder as a constant PQ load, and *B* represents the active-reactive control capabilities of the feeder.

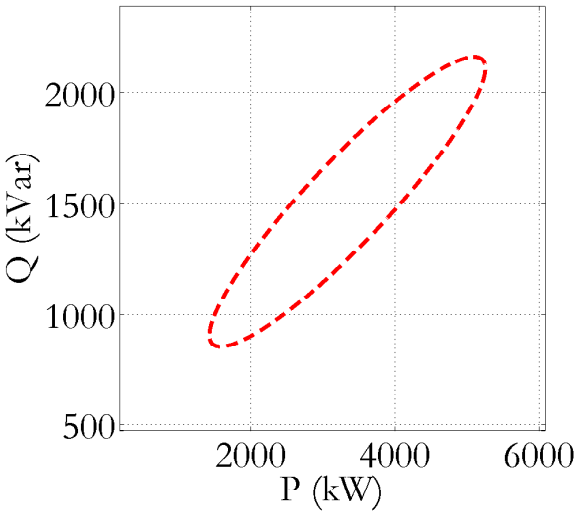

Figure 3.1: *P*-*Q* feasible region for a sample feeder

However, given that dynamic devices are connected to the feeder, the feeder's consumption at one period affects the feasible consumption in the next. Intuitively, in a feeder with responsive loads, increased consumption in one period leads to reduced feasible consumption region in the next step and vice versa. For this purpose, the following time-domain ellipsoidal model for the active distribution feeder is adopted:

$$\begin{bmatrix} P_d^k \\ Q_d^k \end{bmatrix} = B^k u^k + d^k$$

$$B^k = B^{k-1} + P_d^{k-1}\Delta B_p + Q_d^{k-1}\Delta B_q + \sum_{j=1}^{n_p} p_j^{k-1}\Delta B_{par}^- + \sum_{j=1}^{n_p} p_j^k \Delta B_{par}^+ \tag{25a}$$

$$d^k = d^{k-1} + P_d^{k-1}\Delta d_p + Q_d^{k-1}\Delta d_q + \sum_{j=1}^{n_p} p_j^k \Delta d_{par}^- + \sum_{j=1}^{n_p} p_j^k \Delta d_{par}^+$$

$$\left\| u^k \right\|_2 \le 1 \tag{25b}$$

The model defined in (25a)-(25b) defines an ellipsoidal feasible region for the active and reactive power consumption in the *k*-th step, as well as a linear update for the matrix B^k and the vector d^k defining the feasible ellipsoid at step *k*. The linear update depends on the consumptions at step *k*-1, as well as the value of the *exiting parameter* p_j^{k-1} and the *entering parameter* p_j^k. Notice that the exiting parameter models the prevailing conditions determining the feasible region at the previous step, while the entering parameter models the prevailing conditions at the current step, hence it is conceptually reasonable to include both in the state transition model linking the two steps.

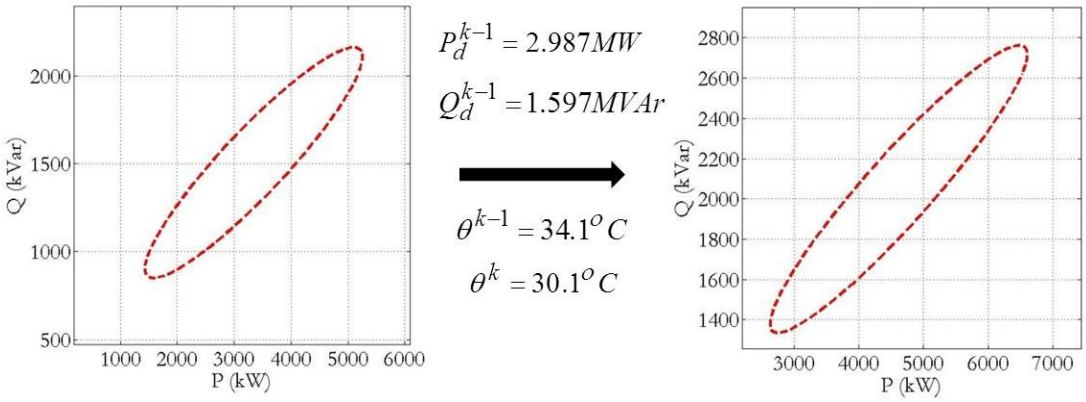

Figure 3.2. Feasible Region Transition for aggregate distribution system

An example of feasible region transition for the same sample feeder is shown in Figure 3.2.

The model of (25a)-(25b) is already in quadratic form. It is not given exactly in the form presented above, as the expressions for the currents are missing. However, these are straight-forward to obtain. Even though the implementation of this model in the look-ahead OPF dispatch includes the current equations, this model is not given here in the interest of conciseness.

The values for $\Delta B_p, \Delta B_q, \Delta B^+_{par}, \Delta B^-_{par}$ and $\Delta d_p, \Delta d_q, \Delta d^+_{par}, \Delta d^-_{par}$ are constant parameters for this model, as well as the initial values for B and d. Their choice seems arbitrary at this point. However, a procedure for their data-driven derivation will be outlined in the upcoming paragraphs.

The inner ellipsoidal approximation of Convex Polyhedra

Let us define the representation of the ellipsoid $E(B,d)$ with B positive semidefinite as the image of the unit ball under an affine mapping.

$$E(B,b) = \{x : x = Bu + d, \|u\|_2 \le 1\} \tag{26}$$

The ellipsoid $E(B,b)$ has a non-empty interior iff $B \succ 0$ [30]. Let $X \subset R^n$ be a nonempty convex set. The inner approximation problem consists of finding the *maximal* ellipsoid contained in X. There can be several measures for "size" of an ellipsoid, including the determinant or the sum of the eigenvalues of B [30].

The following facts are known:

Fact 1 [28]**,** [29]**.** Let $X \subset R^n$ be a nonempty convex set. Then the set of parameters (B,b) of image representation of ellipsoids that are contained in X is convex (i.e. the set $Y = \{(B,d) : E(B,d) \subset X\}$).

Fact 2. The following functions are concave in (B,d):

- $Vol^{\,p}(E) = \prod_{i=1}^{n} \lambda_i(B), 0 < p \le 1/n$

- $\sum_{i=1}^{n} \lambda_i^p(B), 0 < p \leq 1$

Where $\lambda_i^p(B)$ represents the *i*-th eigenvalue of *B*.

The first fact means that the set of image representations of ellipsoids that are contained in *X* is convex, and thus tractable in theory, and the second fact means that some common measures of "size" of an ellipsoid, given its image representation are easy-to-maximize functions of the image representation. This leads us to the following result [28], given without proof:

Fact 3 [28]**.** Let $P = \{x \in R^n : a_i^T x \leq b_i, i = 1, \ldots, m\}$ be a nonempty polyhedral set. Then, the maximal volume ellipsoid $E(B,d)$ contained in *P* can be found by the following problem:

$$\begin{aligned} &\max_{B,d} \mathrm{Det(B)} \\ &\text{subject to} \\ &\left\| Ba_i \right\| + a_i^T d \leq b_i \end{aligned} \tag{27}$$

This is a solvable semi-definite program.

Note that the constraints in (27) guarantee that the ellipsoid $E(B,b)$ is contained in *X* and the maximization of the determinant yields the maximum volume ellipsoid contained in *X*.

Data-Driven Identification of Aggregate Distribution System Model

Consider a simulation of the Active Distribution System for *S* steps. Suppose that for each step we have a polyhedral description of the feasible set in the *P*-*Q* domain, given by $A^{(k)}$ and $b^{(k)}$:

$$F^{(k)} = \left\{ x \in R^2 : A^{(k)} x \leq b^{(k)} \right\} \tag{28}$$

Furthermore, suppose that the consumption of the active distribution feeder between step *k* and *k*+1 is P_d^k for active power and Q_d^k for reactive power, given as the sum of active and reactive power consumption by all devices in the feeder:

$$P_d^k = \sum_{j=1}^{N_d} P_j^k \tag{29a}$$

$$Q_d^k = \sum_{j=1}^{N_d} Q_j^k \tag{29b}$$

Suppose that the parameter vectors p_j^k, the consumption values (29a), (29b) and the polyhedral descriptions of feasible sets (28) are known at each step. Then, the unknown parameters of the aggregate ellipsoidal model can be obtained by the following problem.

$$\max_{B_k, d_k, \Delta B_p, \Delta B_q, \Delta B^-_{par}, \Delta B^+_{par}} \left\{ \sum_{k=1}^{S} \sum_{i=1}^{2} \sqrt{\lambda_i(B_k)} \right\}$$

subject to

$$\begin{aligned}
&\left\| B_k a_i^{(k)} \right\| + a_i^{(k)T} d_k \le b_i^{(k)} && \forall i = 1,2 \ \& \ \forall k \in \{1,\dots S\} \\
&B_k = B_{k-1} + P_d^{k-1} \Delta B_p + Q_d^{k-1} \Delta B_q + \sum_{j=1}^{n_p} p_j^{k-1} \Delta B^-_{par} + \sum_{j=1}^{n_p} p_j^k \Delta B^+_{par} && \forall k \in \{2,\dots S\} \\
&d^k = d^{k-1} + P_d^{k-1} \Delta d_p + Q_d^{k-1} \Delta d_q + \sum_{j=1}^{n_p} p_j^k \Delta d^-_{par} + \sum_{j=1}^{n_p} p_j^k \Delta d^+_{par} && \forall k \in \{2,\dots S\}
\end{aligned} \tag{30}$$

The problem in (30) is semidefinite programming problem, since the added equality constraints with respect to (27) are linear in the decision variables. However, this problem can potentially be infeasible, i.e. such B^k and d^k may not exist. For this purpose, it is best to relax the ellipsoid inclusion constraints using variables μ_{ik} and penalize their value by the norm of μ_k :

$$\max_{B_k, d_k, \Delta B_p, \Delta B_q, \Delta B^-_{par}, \Delta B^+_{par}, \lambda_{ik}} \left\{ \sum_{k=1}^{K} \sum_{i=1}^{2} \sqrt{\lambda_i(B_k)} + \mu \sum_{k=1}^{K} \left\| \mu_k \right\|_1 \right\}$$

subject to

$$\begin{aligned}
&\left\| B_k a_i^{(k)} \right\| + a_i^{(k)T} d_k - \mu_{ik} \le b_i^{(k)} && \forall i = 1,2 \ \& \ \forall k \in \{1,\dots K\} \\
&B_k = B_{k-1} + P_d^{k-1} \Delta B_p + Q_d^{k-1} \Delta B_q + \sum_{j=1}^{n_p} p_j^{k-1} \Delta B^-_{par} + \sum_{j=1}^{n_p} p_j^k \Delta B^+_{par} && \forall k \in \{2,\dots K\} \\
&d^k = d^{k-1} + P_d^{k-1} \Delta d_p + Q_d^{k-1} \Delta d_q + \sum_{j=1}^{n_p} p_j^k \Delta d^-_{par} + \sum_{j=1}^{n_p} p_j^k \Delta d^+_{par} && \forall k \in \{2,\dots K\}
\end{aligned} \tag{31}$$

It is worth noting that, unlike (27), the problems (30) and (31) do not maximize the sum of the determinants of B^k, i.e. are not volume maximization problems. However, since the eigenvalues of B^k are the magnitudes of the half-axes [30], the objective function remains a measure of "size" of the ellipsoid, and hence the purpose of the inner ellipsoidal approximation remains. This choice is made for reasons of numerical stability, since the numerical experiments with the chosen objective function proved much more reliable compared to the ones using the determinant objective.

Hierarchical Receding Horizon Control of Aggregate Distribution System

The linear update assumption for the aggregate distribution system model, used in (25) allows for the formulation of a tractable SDP problem (31), but it is not necessarily accurate. It is, in essence, a simplification of the problem which does not necessarily guarantee accurate modeling of the aggregate behavior of the distribution system. Especially as the prediction horizon increases, larger errors are expected to accumulate due to the approximation. For this reason, a receding horizon control of the distribution system is developed here. The main idea is to use the *K*-step look-ahead OPF problem to determine the control (P-Q commands) of the distribution system over a smaller number of *M* steps. A disaggregation algorithm is used to distribute the P-Q commands to individual devices. Subsequently, the new state of the distribution system is used to re-extract the aggregate model after the *M* steps conclude. This results in an aggregation – dispatch – disaggregation feedback loop.

The aggregate distribution model is used in a multi-step look-ahead optimal power flow problem, which includes AC power flow & dynamic transition constraints and minimizes the cost over a horizon of K steps. Upon convergence, the active and reactive dispatch of a smaller number of M steps ($M<K$) is taken as the distribution system's dispatch for the dispatch horizon. This dispatch is then disaggregated to individual devices in the distribution system by solving an L_2 norm minimization of the distance between the actual consumption of the feeder for the next M steps from the target dispatch, subject to device constraints. This results in individual device-level commands for thousands of devices. The approach is depicted in Figure 3.3. It is important to note that the method has been developed on the assumption that an infrastructure of data acquisition and control capability exists at the distribution level to implement approach [31].

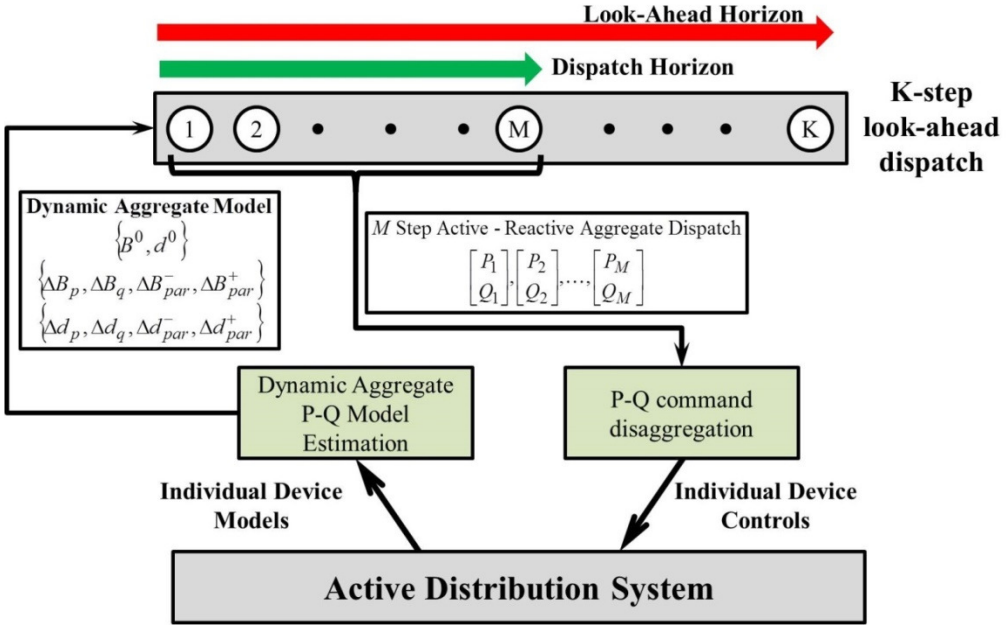

Figure 3.3: Two Level Distribution System Scheduling

The aggregation phase consists of a solution of the SDP problem (31). The data for the problem come from a S-step simulation of the Active Distribution System. While this simulation is performed, the aggregate power consumption P_d^k at step k, the aggregate reactive power consumption Q_d^k as well as the parameters p_j^k are recorded. Furthermore, the feasible P-Q polyhedron for the aggregate consumption of the Distribution Network at each step are also recorded, i.e. a 2x2 matrix $A^{(k)}$ and a 2x1 vector $d^{(k)}$. This simulation is deployed randomly, i.e. the control inputs at each step are drawn randomly from a uniform distribution. Upon collection of that data, an Aggregate Distribution System Ellipsoidal model (25) is fit to this data using (31).

This model is subsequently added to the look-ahead OPF formulation (6) for a chosen look-ahead horizon of K steps. Solution of this problem yields a P and Q time series target for the distribution system for the next K steps, which is the desirable aggregate consumption of the Distribution System. However, only M of these steps are committed as the actual target consumption.

This commitment is realized by solving a disaggregation problem, whereby the aggregate P-Q commands $\hat{P}_d^k$ and $\hat{Q}_d^k$ are distributed to the multitudes of devices connected to the distribution system. Because an approximate aggregate Distribution System P-Q model was used in the look-ahead OPF, there are no guarantees that these P-Q targets are actually feasible. For this reason, the disaggregation problem is cast as an L_2 norm minimization problem, where the normalized distance between the actual consumption and the target consumption over the next M steps is minimized. This problem is formulated as:

$$\min_{\mathbf{x}_j^k, \mathbf{u}_j^k} \left\{ \sum_{k=1}^{M} \left\| \frac{P_d^k - \hat{P}_d^k}{\hat{P}_d^k} \right\|_2 + \lambda \sum_{k=0}^{M} \left\| \frac{Q_d^k - \hat{Q}_d^k}{\hat{Q}_d^k} \right\|_2 \right\}$$

s.t.

$$\begin{aligned}
P_d^k &= \sum_{j=1}^{N_d} P_j^k && \forall k \in \{1,\ldots,M\} \\
Q_d^k &= \sum_{j=1}^{N_d} Q_j^k && \forall k \in \{1,\ldots,M\} \\
\mathbf{x}_j^{k+1} &= A_j \mathbf{x}_j^k + B_j \mathbf{u}_j^k + D_j \mathbf{p}^k && \forall k \in \{1,\ldots,M-1\}, \forall j \in \{1,\ldots,N_d\} \\
\begin{bmatrix} P_j^k \\ Q_j^k \end{bmatrix} &= C_j \mathbf{x}_j^k + E_j \mathbf{u}_j^k + F_j \mathbf{p}^k && \forall k \in \{1,\ldots,M\}, \forall j \in \{1,\ldots,N_d\} \\
H_j \mathbf{x}_j^k + G_j \mathbf{u}_j^k &\le \mathbf{r}_j && \forall k \in \{1,\ldots,M\}, \forall j \in \{1,\ldots,N_d\} \\
\mathbf{x}_j^1 &= \bar{\mathbf{x}}_j^1 && \forall j \in \{1,\ldots,N_d\}
\end{aligned} \tag{32}$$

Where:

$\hat{P}_d^k, \hat{Q}_d^k$	**Target aggregate consumption of active and reactive power at step *k***
λ	Reactive fitting importance parameter
P_j^k, Q_j^k	Active and reactive power consumption of device *j* at step *k*
$\mathbf{x}_j^k$	State vector of device *j* at step *k*
$\mathbf{u}_j^k$	Controls of device *j* at step *k*
$\mathbf{p}^k$	Parameter vector (shared by all devices) at step *k*
A_j, B_j, D_j	Matrices defining the state update model of device *j* in the discrete time domain
C_j, E_j, F_j	Matrices defining the output model of device *j*
$H_j, G_j, \mathbf{r}_j$	Matrices and vector defining the inequality constraint model of device *j*
$\bar{\mathbf{x}}_j^1$	Initial state of device *j*, which is given

A weighting factor λ multiplies the normalized error of the reactive power in (32). This is used to regulate the relative importance of reactive power fitting with respect to active power fitting. Because the two commands are possibly conflicting, it is of interest to explore the tradeoff between them. More importantly, a greater weight should be given to active power, since errors in reactive power dispatch can cause serious mismatches between generation and load in the system, and this power will need to be provided by a standby generator, forcing an out-of-market action. Hence, ensuring perfect tracking of the active power commands provided by the look-ahead OPF is more important than tracking reactive power commands. This is the reason why a value of λ smaller than one is typically chosen in our applications.

Note that all device models in (32) are linear, with linear constraints. This is an obvious simplification. However, it is necessary to maintain the polyhedral assumption for the feasible set $F^{(k)}$ of the active and reactive power at step k, as well as the tractability of the L_2 norm minimization problem. The inequality constraints represent limits of device operation or customer inconvenience constraints. The latter are very important when considering active load devices, such as Thermostatically Controlled Loads of residential houses. Such devices must participate in active-reactive control without disruption of customer temperature requirements.

The formulation in (32) is perhaps too high level and vague. In order to facilitate understanding for the interested reader, we provide a specific example with N_{TCL} air-conditioners and N_{BATT} batteries. A simple linear first-order model is used for both devices. Each house air-conditioner j is assumed to have a constant reactive-to-active power ratio φ_j. For batteries a charging efficiency of $n_{c,i}$ and a discharging efficiency of $n_{d,i}$ is assumed for battery i. A separate active and reactive power control is assumed for each battery device, subject to maximum and minimum active/reactive limits. Note that temperature limits $\theta_{\min}$ and $\theta_{\max}$ are enforced for each house, as well as energy limits $E_{\min}$ and $E_{\max}$ for each battery. The control variables for the air-conditioner is the duty cycle of operation $u_{T,j}^k$ of device j for period k and the control variables for batteries are $u_{P+,j}^k, u_{P-,j}^k$ and $u_{Q,j}^k$, the power charge, power discharge and reactive consumption per period. Negative values for these control variables correspond to active and reactive power generation by the battery. The only parameter involved here is θ_{out}, the ambient temperature, which is common for all thermal house models. The thermal parameters of the first-order thermal model for the residential house are a_j and b_j.

The disaggregation problem now becomes:

$$\min_{\mathbf{x}_j^k,\mathbf{u}_j^k}\left\{\sum_{k=1}^{M}\left\|\frac{P_d^k-\hat{P}_d^k}{\hat{P}_d^k}\right\|_2+\lambda\sum_{k=0}^{M}\left\|\frac{Q_d^k-\hat{Q}_d^k}{\hat{Q}_d^k}\right\|_2\right\}$$

s.t.

$$\begin{aligned}
P_d^k &= \sum_{j=1}^{N_{BATT}} P_{B,j}^k + \sum_{j=1}^{N_{TCL}} P_{T,j}^k && \forall k\in\{1,\ldots,M\}\\
Q_d^k &= \sum_{j=1}^{N_{BATT}} Q_{B,j}^k + \sum_{j=1}^{N_{TCL}} Q_{T,j}^k && \forall k\in\{1,\ldots,M\}\\
\theta_j^{k+1} &= a_j(\theta_{out}-\theta_j^k)+b_j u_{T,j}^k n_j P_j^{rated} && \forall k\in\{1,\ldots,M-1\},\forall j\in\{1,\ldots,N_{TCL}\}\\
P_{T,j}^k &= u_{T,j}^k P_j^{rated} && \forall k\in\{1,\ldots,M\},\forall j\in\{1,\ldots,N_{TCL}\}\\
Q_{T,j}^k &= \phi_j u_{T,j}^k P_j^{rated} && \forall k\in\{1,\ldots,M\},\forall j\in\{1,\ldots,N_{TCL}\}\\
0 &\le u_{T,j}^k \le 1 && \forall k\in\{1,\ldots,M\},\forall j\in\{1,\ldots,N_{TCL}\}\\
\theta_{\min} &\le \theta_j^k \le \theta_{\max} && \forall k\in\{1,\ldots,M\},\forall j\in\{1,\ldots,N_{TCL}\}\\
E_j^{k+1} &= E_j^k + n_{c,j}u_{P+,j}^k\Delta t - \frac{1}{n_{d,j}}u_{P-,j}^k\Delta t && \forall k\in\{1,\ldots,M-1\},\forall j\in\{1,\ldots,N_{BATT}\}\\
P_{B,j}^k &= u_{P,j}^k && \forall k\in\{1,\ldots,M\},\forall j\in\{1,\ldots,N_{BATT}\}\\
Q_{B,j}^k &= u_{Q,j}^k && \forall k\in\{1,\ldots,M\},\forall j\in\{1,\ldots,N_{BATT}\}\\
Q_{\min} &\le u_{Q,j}^k \le Q_{\max} && \forall k\in\{1,\ldots,M\},\forall j\in\{1,\ldots,N_{BATT}\}\\
P_{\min} &\le u_{P,j}^k \le P_{\max} && \forall k\in\{1,\ldots,M\},\forall j\in\{1,\ldots,N_{BATT}\}\\
E_{\min} &\le E_j^k \le E_{\max} && \forall k\in\{1,\ldots,M\},\forall j\in\{1,\ldots,N_{BATT}\}\\
\theta_j^1 &= \overline{\theta}_j^1 && \forall j\in\{1,\ldots,N_{TCL}\}\\
E_j^1 &= \overline{E}_j^1 && \forall j\in\{1,\ldots,N_{BATT}\}
\end{aligned} \tag{33}$$

Note that the above formulation in (33) is consistent with the high-level framework in (32).

Upon solution of (32), the actual controls $\left(\mathbf{u}_j^k\right)^*$ for each device *j* and each step *k* are obtained. These controls minimize the distance between the desired aggregate consumption and the actual consumption of the distribution feeder. This explains the use of the term "disaggregation problem" for (32). The value of the objective is a good metric for the performance of the ellipsoidal approximate model for the aggregate distribution system. Since this model approximates the feasible region of the aggregation, we expect the aggregate commands to be close to feasible. However, such guarantees cannot be provided, since the SDP fitting problem (31) is only a data fitting problem and does not ensure inclusion of the resulting feasible region within the actual polyhedral feasible region of the Distribution System. Hence, infeasibilities of the aggregate commands can and do occur in practice. They manifest as nonzero objective values for (32). The performance of the framework will be evaluated in the results section.

Once the distance-minimizing controls $\left(\mathbf{u}_j^k\right)^*$ for the next *M* steps have been applied, the Distribution System will reside in a new state. Leveraging data acquisition and state estimation techniques that have been described in prior works [31], the new state is extracted, and a new simulation is performed, to obtain data for a new solution of the SDP problem (31). This results

in a new aggregate model for the feasible region of the Distribution Network, and subsequently a new solution of the Transmission-Level look-ahead OPF. Note that each time, the OPF commands after the *M*-th step are discarded and are never applied as Distribution-Level commands.

3.8 Numerical Results and Examples

This paragraph is dedicated to results from the application of the models formulated above. Various test cases, ranging from small instructive examples to larger, more realistic systems, are studied. Emphasis is given in the Active Distribution System Case.

Energy Storage Results

Energy storage system dispatch is, from an applications perspective, one of the most important justifications behind the look-ahead dispatch formulations discussed in this chapter. Detailed results from the dispatching of storage units in the IEEE 30 Bus system and the Polish 2383 Winter Peak systems were presented above, where the comparison of storage dispatch between AC-OPF and DC-OPF methodologies was discussed. Hence, this result section will focus mostly on a sensitivity analysis of System Cost as a function of storage penetration for various renewable energy scenarios.

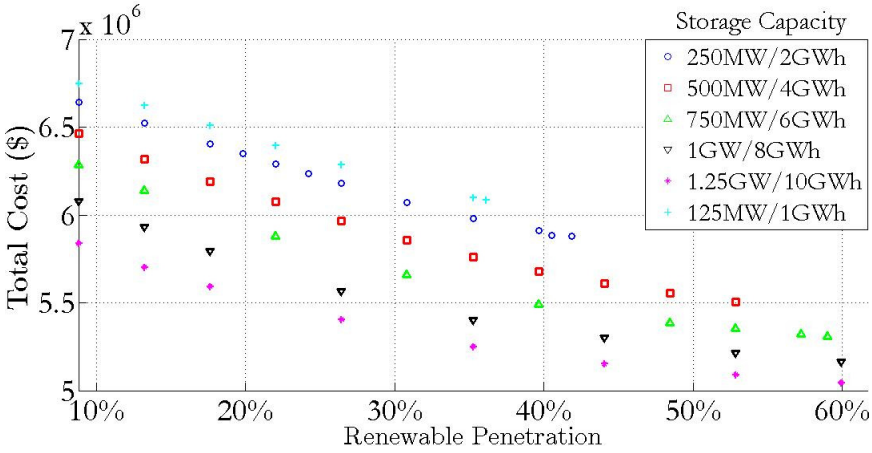

Figure 3.4: IEEE RTS 24 Bus Total System Cost under various storage scenario

The AC-OPF look-ahead methodology was applied to the small-size IEEE 24 Bus test case, for a given loading scenario, and various renewable and storage penetration scenarios. The scatter plot of operating costs for various scenarios is shown in Figure 3.4. Note that, for each storage penetration scenario, renewable penetration was increased up to the point that no feasible solution with full absorption of wind (no wind shedding) could be attained. The maximum feasible wind penetration for each storage penetration scenario is given in Table 3.1

The following conclusions can be drawn from this small case study: 1. Maximum Feasible Wind Penetration increased with wind penetration, but at a decreasing rate, and saturates at some point. This is due to the fact that after a given penetration of storage, issues arise that storage penetration cannot address (for example congestion patterns not affected by the current location of storage). 2. Total cost decreases with storage for all scenarios. The marginal value of storage

(the decrease in total cost for a small change in storage) seems to be initially roughly the same for small renewable capacity (roughly 0.2$/MW/day), but it gradually decreases, in extreme levels of renewable penetration.

Table 3.1: Maximum Feasible Wind as Function of Storage Capacity

STORAGE POWER CAPACITY (MW)	STORAGE ENERGY CAPACITY (MWh)	MAXIMUM FEASIBLE WIND PENETRATION (MW)
126	984	1,230
252	1,968	1,425
504	3,936	1,800
756	5,904	2,010
1,008	7,872	2,040
1,260	9,840	2,040

Thermostatically Controlled Loads

For the purposes of investigating the potential applicability of the Thermostatically Controlled Active load introduced in Paragraph 3.5, we vary the level of penetration of TCL's as a percentage of system load and record the results in terms of total operational cost as well as total energy consumption by thermostatically controlled loads. Subsequently, a version of the dispatch problems were TCL's are passive (not under centralized dispatch) and the same quantities are monitored. The purpose of the comparison is to investigate whether a decrease in cost runs a risk of increase in energy consumption, due to less efficient operation of TCL's.

Table 3.2: Effect of TCL control on Cost & TCL Consumption

	With TCL Control		**Without TCL Control**	
TCL LOAD (%)	**Total Operating Cost ($)**	**TCL Energy Consumption (MWh)**	**Total Operating Cost ($)**	**TCL Energy Consumption (MWh)**
5%	6.9788e+06	959.5052	6.9966e+06	904.1704
7.5%	7.0496e+06	1.4421e+03	7.0711e+06	1.3560e+03
10%	7.1257e+06	1.9269e+03	7.1502e+06	1.8080e+03
12.5%	7.2048e+06	2.4113e+03	7.2344e+06	2.2601e+03
15%	7.2874e+06	2.8950e+03	7.3230e+06	2.7121e+03

The test was run in the 24 Bus IEEE Reliability Test system and the results are shown in Table 3.2. It is interesting to note that centralized TCL dispatch achieves important cost reductions, reaching up to 0.7% reduction in total cost for a 15% penetration of controllable TCL loads. This reduction potential in total cost, coming exclusively from a small change in system operations, i.e. the inclusion of TCL's in centralized dispatch, seems extremely attractive. However, it should be noted that significant investments in real-time TCL monitoring and communication equipment are needed to achieve their inclusion to the dispatch procedure. Nevertheless, the existence of this untapped potential is worth noting.

Another significant observation is that the TCL dispatch comes at a cost of less efficient operation of these loads, as their total energy consumption is evidently higher in all cases, if they are under centralized dispatch. Even though total energy consumed increases, total cost is lower. This means that, while TCL dispatch has value for the system, appropriate incentives must be designed for customers to participate in TCL dispatch, given that their individual consumption will actually increase.

Sample results for the effect of centralized TCL dispatch are shown in Figure 3.5. The total system load with and without centralized dispatch, as shown in Figure 3.5a, is characterized by a smaller peak load in the dispatched case. Of course, increased consumption is required in earlier periods to pre-cool the air-conditioned space and avoid temperature violations. The duty cycle (dispatch decisions) and the corresponding temperatures for three sample TCL's are shown in Figure 3.5b,c, where the pre-cooling effect is evident.

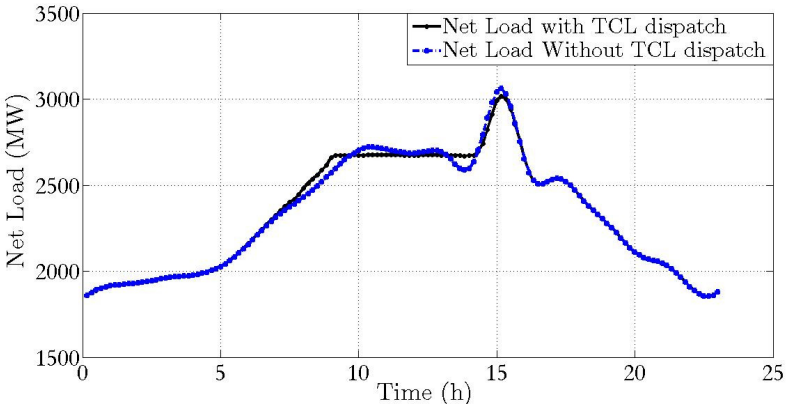

(a)

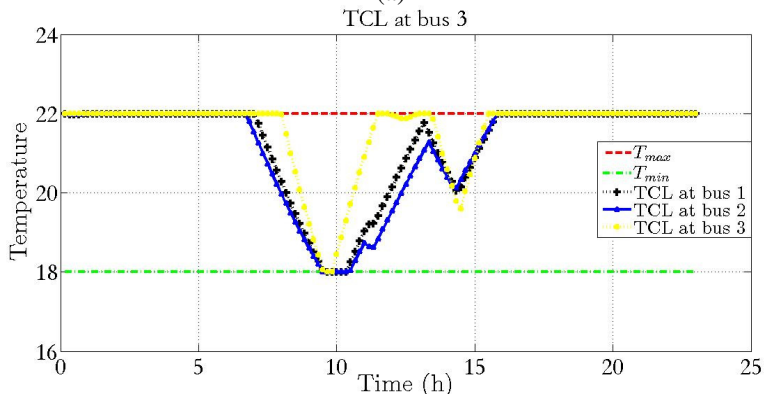

(b)

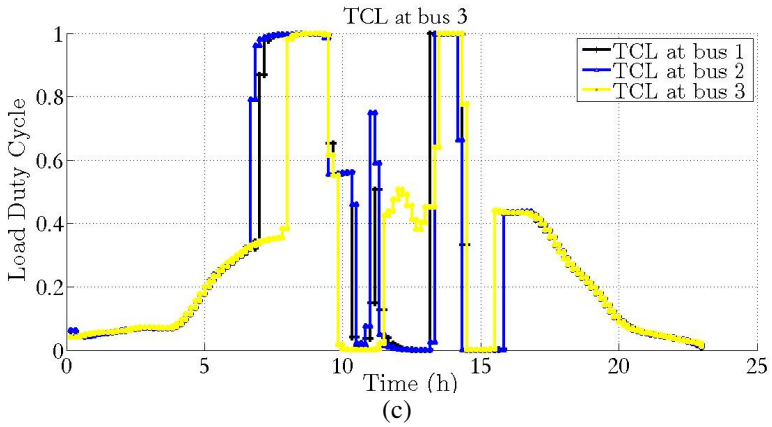

(c)

Figure 3.5: TCL dispatch results (a) Net Load (b) Sample TCL temperatures (c) Sample TCL controls

Dynamic Line Ratings

The purpose of this case study is to investigate the effects of dynamic line rating used in conjunction with the look-ahead AC-OPF formulation. Namely, we will focus on the comparison between static (MVA based) line ratings and dynamic (temperature based) line ratings. Dynamic line ratings provide additional flexibility, since they provide the capability to plan ahead the overload of a certain transmission line, either to maintain feasibility of the OPF, or simply to reduce cost. In this paragraph, we will compare results for two power systems that are identical in all aspects except one: in System A, all transmission line models feature static ratings, whereas in System B, transmission lines are modeled using the dynamic line rating model of Paragraph 3.4.

It should be noted that, whenever feasibility of the OPF cannot be achieved in a certain period, load shedding (rejection) is required in that period to attain a feasible solution. Load shedding consists of selectively reducing loads in specific buses. In order to highlight the capabilities of the Dynamic Line Rating model in guaranteeing feasibility in otherwise infeasible cases, minimal load shedding, for both active and reactive load, will be reported for each system. Minimal load shedding results are obtained a relevant look-ahead AC-OPF formulation that is interesting in its own accord and is discussed in other publications. For feasible cases (where no load shedding is needed), cost results will also be reported.

Table 3.3: Comparison of Static versus Dynamic Line Ratings for IEEE 30 Bus System

	STATIC RATING (SYSTEM A)			**DYNAMIC RATING (SYSTEM B)**		
LOAD (% OF BASE)	**P_{shed} (MW)**	**Q_{shed} (MVAr)**	**Total Operating Cost ($)**	**P_{shed} (MW)**	**Q_{shed} (MVAr)**	**Total Operating Cost ($)**
94	0.0640	0.0306	6.4518e+04	3.3191e-04	1.5907e-04	6.4515e+04
96	0.4301	0.1974	6.6281e+04	0.0015	7.3634e-04	6.6271e+04
98	1.9291	1.6880	N/A	0.0034	0.0016	N/A
100	6.4477	6.1939	N/A	0.0983	0.0951	N/A
102	18.2616	18.0085	N/A	1.9294	1.9291	N/A
104	35.9374	35.6559	N/A	5.4511	5.4506	N/A

Table 3.4: Maximum Lagrange Multiplier – IEEE 30 Bus System

LOAD (% OF BASE)	**STATIC RATING**	**DYNAMIC RATING**
	λ_{max}	λ_{max}
94	535.3731	395.2749
96	712.6980	398.4069
98	988.0519	569.3133
100	1.0088e+03	803.4572
102	1.0297e+03	995.6196
104	1.0506e+03	1.0195e+03

Our first system of interest is the IEEE 30 bus system. The results for System A and System B are presented in Table 3.3 and

Table 3.4. The results verify that the magnitude of load shedding is reduced if Dynamic Line Ratings are used, compared to the static ratings case. Furthermore, the total operating cost, for cases where load shedding is not needed, is reduced in the case of System B. It should be noted that reporting operational cost in cases where load shedding is required would not be meaningful, because the removal of load is bound to lead to reduced operational cost, due to the reduction of net load. Furthermore, the Lagrange multiplier at bus 8, which is the highest Lagrange multiplier for equality constraints, is evidently smaller in the dynamic ratings case.

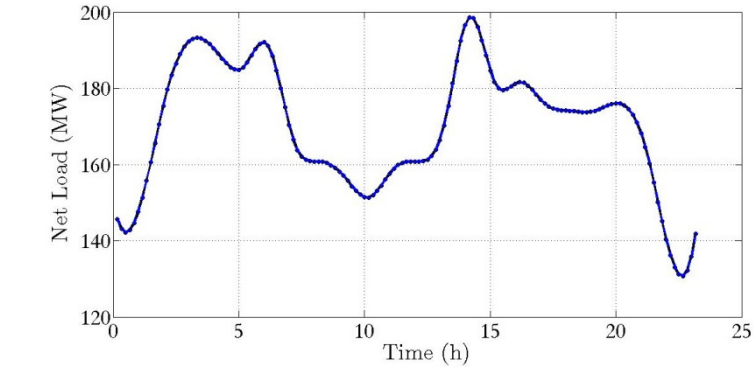

(a)

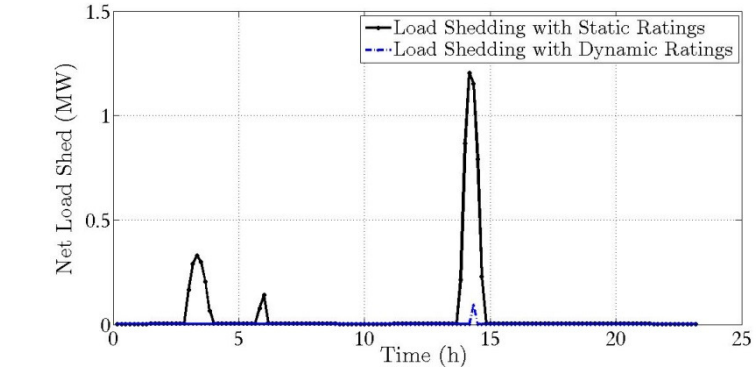

(b)

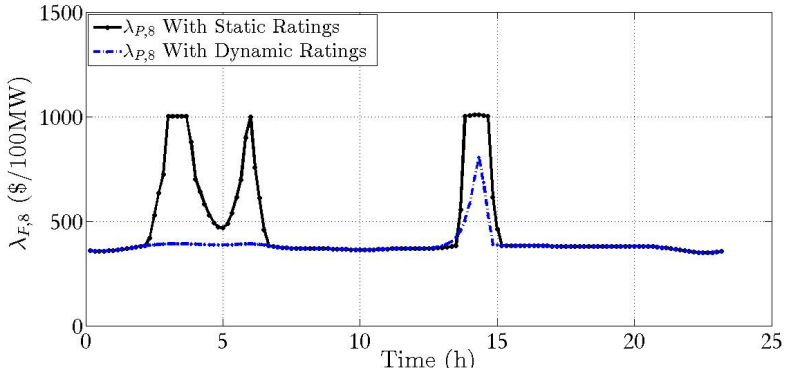

(c)

Figure 3.6: Results for base case scenario a. Load Pattern b. Load Shedding Schedule c. Lagrange Multiplier at bus 8

The reasons behind the results of Table 3.3 and Table 3.4 can be explained with the help of Figure 3.6. In this figure it is evident that, in case A, load shedding is needed during all peak load periods. On the other hand, load shedding is largely avoided in the dynamic rating case, except for a minor load shedding needed during the largest peak. Finally, the Lagrangian multiplier in bus 8, shown in Figure 3.6c, is evidently larger during the critical periods for the static ratings

case. If the interpretation of the Lagrangian multiplier as a marginal cost of electric power is used ($/MW), this means that dynamic line rating has a sizeable effect in reducing the Locational Marginal Price (LMP) in the most constrained region of the system. The reason of the high LMP in bus 8 is due to the congestion of line 6 – 8. Thus Figure 3.6c highlights the capability of this modeling technique to stabilize electricity prices and alleviate the negative effects of congestion.

Some details regarding the first order dynamic transmission line rating model are shown in Figure 3.7. The two congested lines in the system, line 6-8 (135kV, 35 MVA) & line 25-27 (135kV, 16MVA) are examined. As shown in Figure 3.7a,c, use of the dynamic line rating allows temporary overload of both lines, in order to service the load, contrary to the static line rating methodology. As shown in Figure 3.7b,d the first order dynamic line model indicates that this mode of operation will not, in fact, violate the thermal limit of the line.

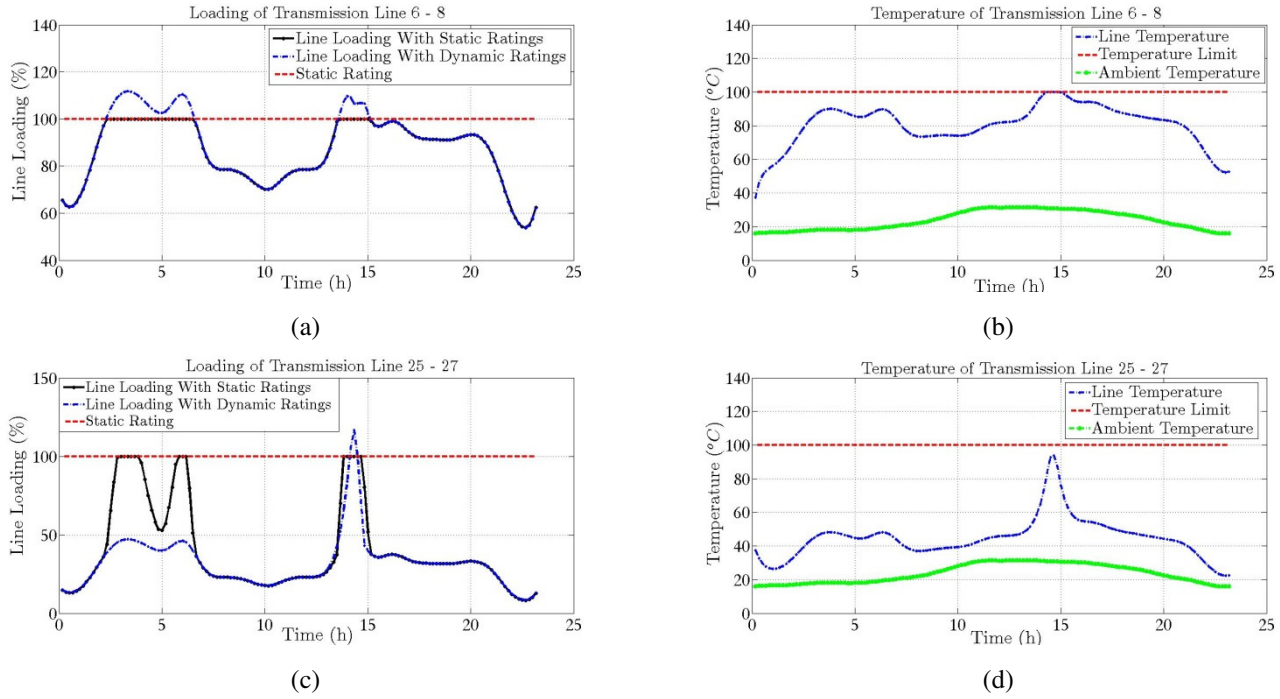

Figure 3.7: Dynamic Line Rating Results in base case scenario

The above observations were made on a rather simplified sample IEEE standard case with a small number of buses. In order to more properly study the benefits of dynamic line rating modeling in a realistic system, a similar testing methodology was applied to the PEGASE 1354 system, a reduced equivalent of the entire European interconnected system, complete with comprehensive line rating data [32]. Unfortunately, dynamic line rating data was not readily available. As a result, realistic line parameters and thermal constant were assumed, using the corresponding IEEE standard [22]. A 7 hour loading scenario, with peak load 80,365MW was tested. This results in a look-ahead AC-OPF model with 223,482 variables and equality constraints and 195,804 inequality constraints. The results are summarized in Table 3.5 and Table 3.6.

Table 3.5: Comparison of Static versus Dynamic Line Ratings for the PEGASE 1354 System

	STATIC RATING (SYSTEM A)			DYNAMIC RATING (SYSTEM B)		
LOAD (% OF BASE)	**P_{shed} (MW)**	**Q_{shed} (MVAr)**	**Total Operating Cost ($)**	**P_{shed} (MW)**	**Q_{shed} (MVAr)**	**Total Operating Cost ($)**
96	1.5245	-0.1705	2.8679e+06	1.6513	-0.2097	2.8678e+06
100	1.6754	-0.1109	2.9893e+06	1.3256	-0.1858	2.9891e+06
104	1.4186	-0.1155	3.1109e+06	1.6530	-0.1069	3.1107e+06
110	3.6608	0.2000	3.2940e+06	2.2641	0.0131	3.2936e+06
115	314.4635	45.4552	N/A	3.7350	0.2812	N/A
120	2.7904e+03	459.3964	N/A	694.0905	136.8818	

Table 3.6: Maximum Lagrange Multiplier – PEGASE 1354 System

LOAD (% OF BASE)	**STATIC RATING**	**DYNAMIC RATING**
	λ_{max}	λ_{max}
96	113.7307	112.9966
100	115.131	114.3696
104	116.7387	115.8559
110	121.6062	120.3828
115	515.8255	190.2477
120	537.3071	523.1247

The results indicate that a negligible amount of load shedding is required in the base case (indicating a feasible solution). The effects of Dynamic Line Ratings in total system operating cost seem to be negligible, less that 0.1%. However, if load is gradually increased (in an effort to increase system stress) the load shedding required in order to restore feasibility is evidently less if Dynamic Line Ratings are considered in the look-ahead formulation. In fact, at 115% loading, load shedding can be largely avoided and at 120% loading it can be greatly reduced by introducing dynamic line ratings. The same picture can be painted by looking at maximum Lagrangian multipliers. Indeed, these multipliers are consistently larger for the static line rating case. As constraints become binding and load shedding is required, Lagrange multipliers in the corresponding buses abruptly rise. If dynamic line rating is modeled, however, congestion can be relieved, thus reducing the Lagrange multipliers in the neighboring buses. If these lagrangian multipliers are used for pricing, the beneficial effect of dynamic line ratings in mitigating price spikes is, once again, apparent.

Active Distribution System

The active distribution system modeling methodology was applied to a sample active distribution system. The distribution system consists of a population of thermostatically controlled loads and battery storage systems, which means that the disaggregation of P-Q commands is eventually cast as the least squares problem given in (32).

To test the generality of results, the parameters of all devices are drawn from a uniform random distribution around certain chosen central values. The various classes of devices are defined as shown in Table 3.7.

Table 3.7: Devices in Sample Feeder

DEVICE	**PARAMETERS**						
Thermostatically controlled loads	**R (kW)**	**C (kWs/^{0}C)**	**P_{rated} (kW)**	**n_{TCL}**	**Power Factor**	**θ_{min} (^{0}C)**	**θ_{max} (^{0}C)**
Class A TCL	2.9±5%	350±10%	8.0±10%	0.95	0.91±10%	18.0	24.0
Class B TCL	3.4±5%	350±10%	8.0±10%	0.95	0.94±10%	17.0	23.0
Class C TCL	2.9±5%	450±10%	8.0±10%	0.95	0.88±10%	18.5	24.5
Class D TCL	3.4±5%	450±10%	8.0±10%	0.95	0.91±10%	17.5	23.5
Batteries	**n_c**	**n_d**	**P_{max} (kW)**	**E_{max} (kWh)**	**E_{min} (kWh)**		
Class A Battery	0.9±1%	0.9±1%	4.4±1%	0.1±1%	6±1%		

A test feeder of 1,000 active devices, consisting of 200 TCL's from each class and 200 batteries was created. The maximum consumption of the feeder is approximately 7MW. A scatterplot with R & C values in the feeder considered in this Chapter is shown in Figure 3.8.

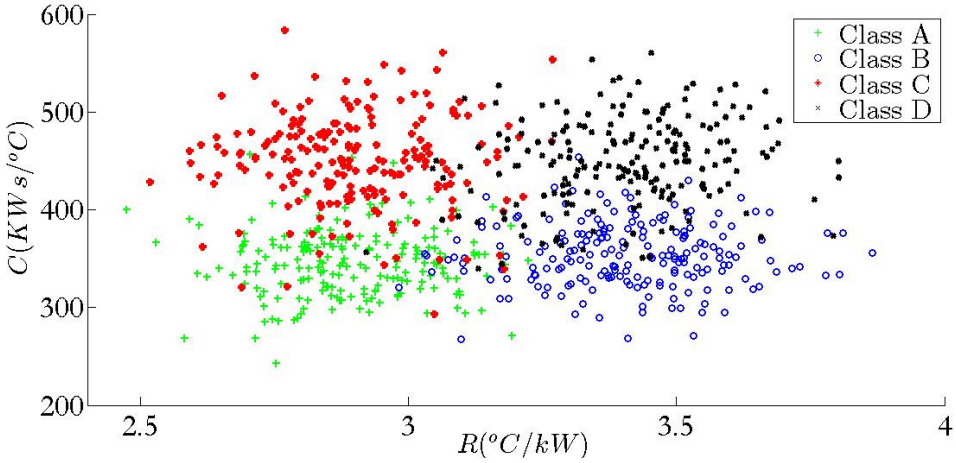

Figure 3.8: TCL Classes in Sample Feeder

The aggregation problem for this feeder is addressed by solving the ellipsoidal feasible region approximation problem (31). The data for this problem comes from a simulation of the feeder, where the inputs for the batteries and TCL's are randomly decided. A sample execution of this "aggregation phase" is shown in Figure 3.9. The choice of penalty factor γ in (31) crucially affects the resulting model. A smaller γ yields a larger feasible ellipsoid, but may overestimate the actual polyhedral feasible region, while the a larger γ will yield a more conservative approximation and may lead to severe contraction of the feasible set if the number of steps increases. We consider erring on the conservative side is always preferred, and a penalty factor $\gamma = 200$ is chosen for the remaining results in this chapter, unless otherwise stated.

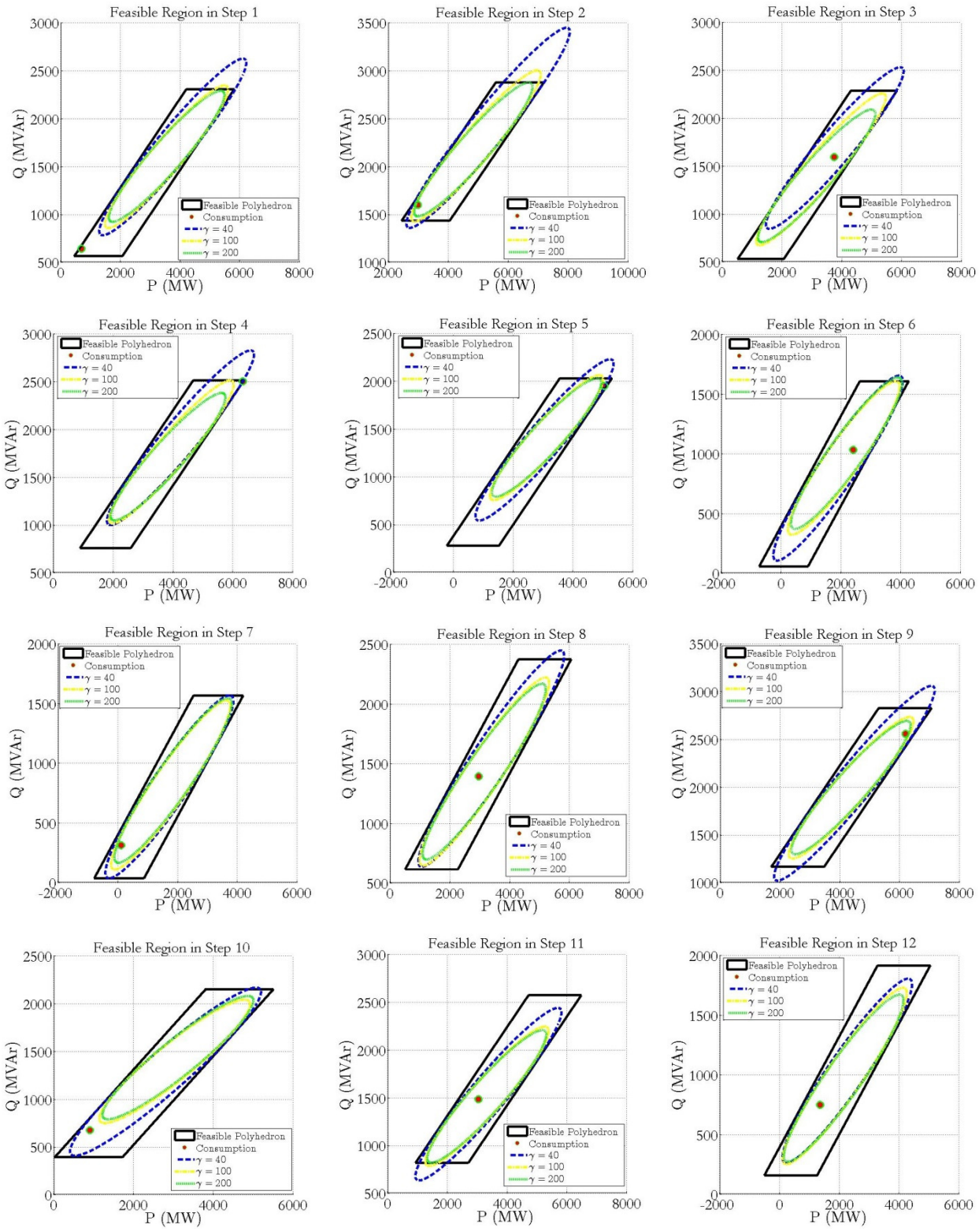

Figure 3.9: Feasible Polyhedron versus Ellipsoidal approximation for various penalty terms

As a first numerical experiment, we run a 100-step random simulation of this feeder and obtain an aggregate model by solving (31). Subsequently, we connect this feeder to bus 17 of the IEEE RTS 24 bus system and run the look-ahead OPF with a 10 minute interval to schedule this distribution system. The results are shown below:

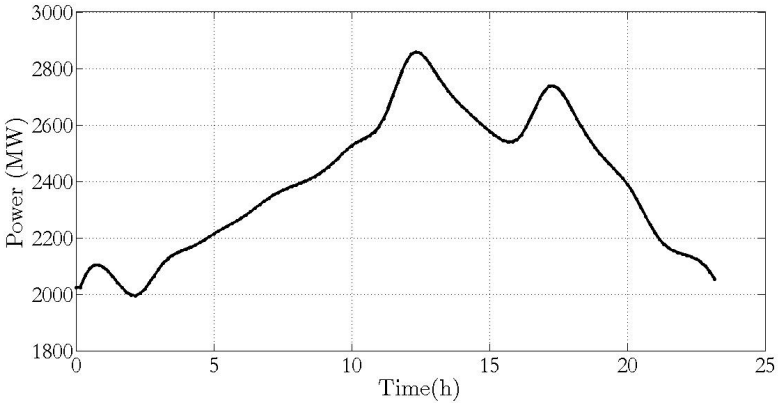

(a)

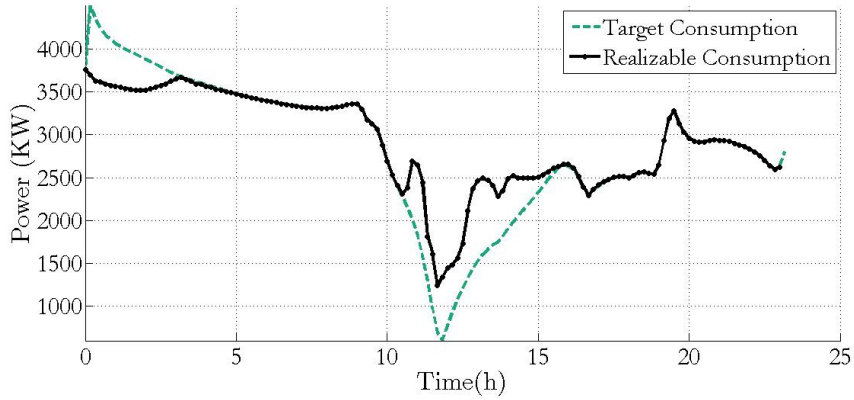

(b)

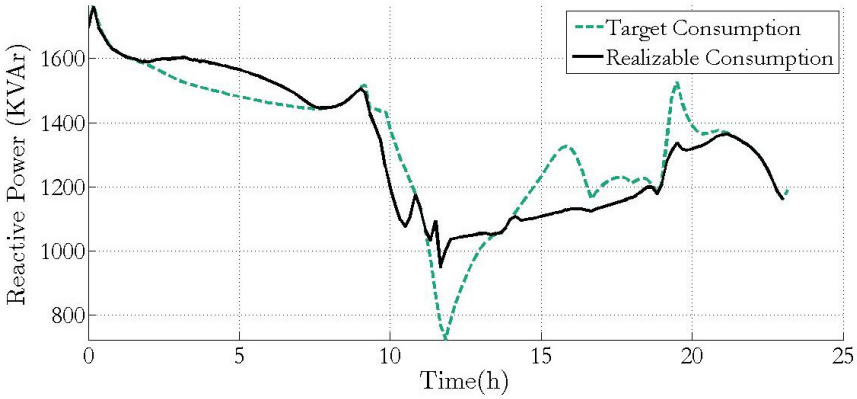

(c)

Figure 3.10. Single-Run Distribution System Scheduling a. Net System Load b. Active Power Schedule c. Reactive Power Schedule

It should be noted that for this first experiment, we do not implement the receding horizon scheme of Figure 3.3. Instead, we perform a single run of the optimization algorithm for the entire day, and then we fit the operation of the feeder to the look-ahead OPF result, using the minimization scheme of (33). As shown in Figure 3.10b, the algorithm manages to schedule the distribution system so that consumption is reduced during the peak load of the system, at around 12pm. The dashed line at Figure 3.10b is the schedule provided by the solution of the look-ahead OPF with the aggregate model obtained by the simulation data, while the solid black line is the closest $L2$ norm fit resulting from the solution of (33). Hence, even though the model proves useful in scheduling the distribution system using the look-ahead algorithm, it does not guarantee feasibility of the target schedule (i.e. the objective of (33) is not zero). This was expected, since our aggregate model is an approximation to allow for transmission system optimization, not an exact modeling approach. This suggests the need for the receding horizon optimization approach of Figure 3.3. The TCL schedules for four TCL's of different classes, which result from the solution of the L2 norm fit problem are shown in Figure 3.11.

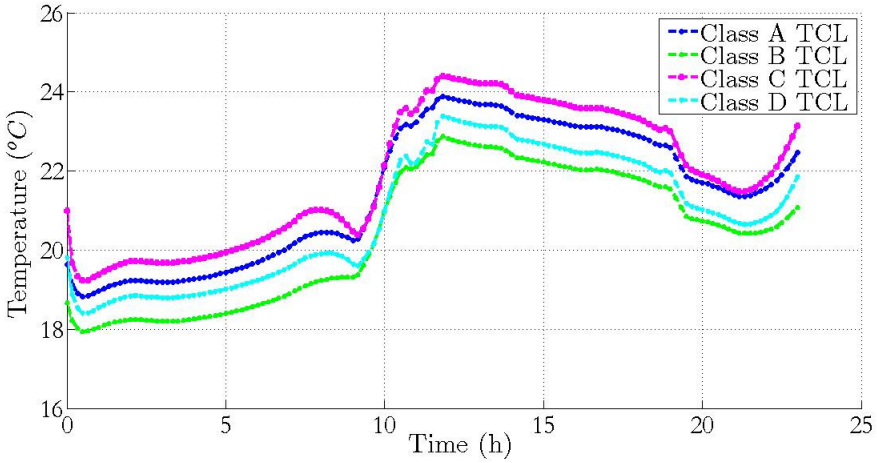

Figure 3.11: TCL temperature for the consumption schedule of Figure 3.10.

Note that, according to Figure 3.11 all TCL's are turned OFF during the peak times, in order to reduce distribution feeder consumption, which explains the temperature rise. Furthermore, their temperature does not violate the maximum temperature settings for each class, which are shown in Table 3.7. This is due to the constraints enforced in the fit problem (33).

If the target dispatch is not realizable, this is a significant problem for the decision-maker (e.g. the balancing authority of the transmission system), especially if the active power consumption is different from the scheduled one. Large errors, such as the one showed in Figure 3.10 should be unacceptable. Use of the receding horizon framework is suggested as a solution of the modeling accuracy problem. Renewal of the model at specified intervals and re-solving of the look-ahead scheduling algorithm will allow a reduction of the inaccuracies, because it allows extraction of renewed state information for all TCL's and Batteries in the system and obtaining of a renewed aggregate model, thus not allowing an accumulation of errors in the aggregate model.

The results for the distribution system scheduling, for the same net load pattern as Figure 3.10a, in the same transmission system (RTS '79) and the same feeder composition as in Figure 3.8, are shown in Figure 3.12. The dashed lines denote the target consumption schedules given for the rest of the day by the look-ahead OPF. There are 10 different dashed lines, each

corresponding to a different target schedule, as the look-ahead OPF is solved every two hours. The black line corresponds to the actual consumption, given by the solution of the L2 norm minimization problem. Note that only two hours of each target set point are committed.

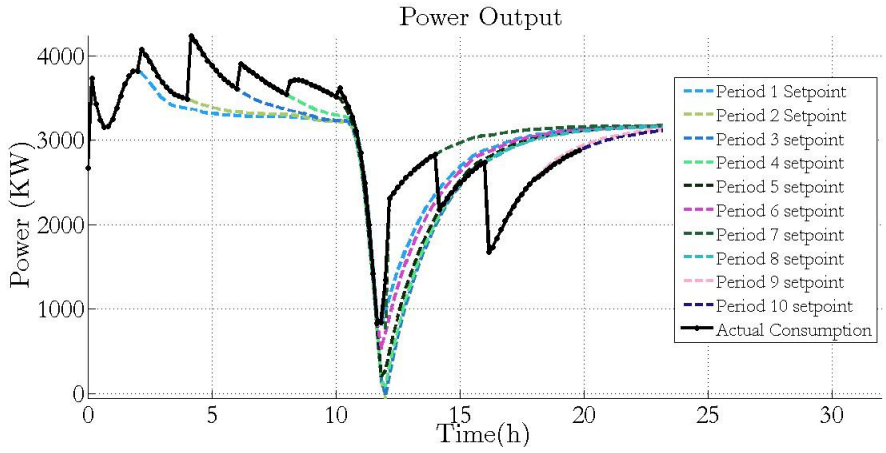

(b)

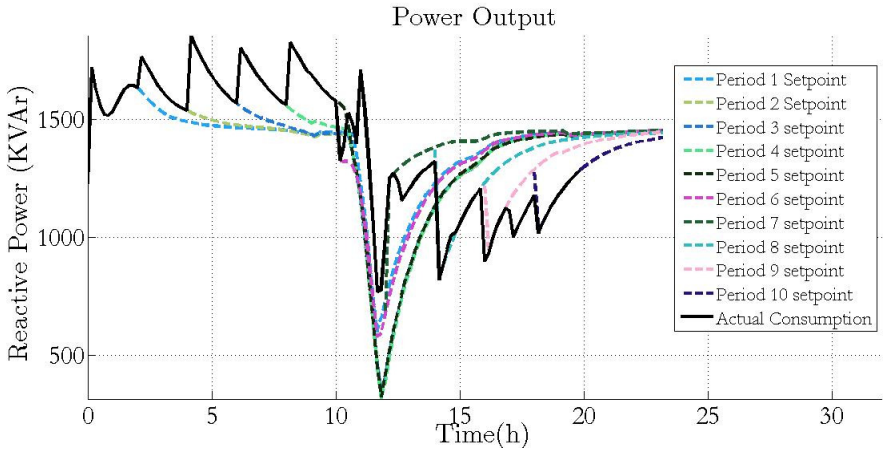

(c)

Figure 3.12: Aggregate Distribution System Scheduling for a 2h Dispatch Horizon

From Figure 3.12a it should be noted that there is no error between the target active power consumption and the actual consumption. However, there is some error in the reactive power consumption, due to the small weight factor λ=0.3 used in (32), to reduce the importance of reactive power fitting. Active power mismatches can be much more threatening to power system operation than reactive power imbalances. It is also of note that, as shown in Figure 3.12, the schedule shows abrupt changes every two hours, as the model is updated, as expected. Note that the general schedule pattern is quite similar to the one yielded by the single-pass approach in Figure 3.10.

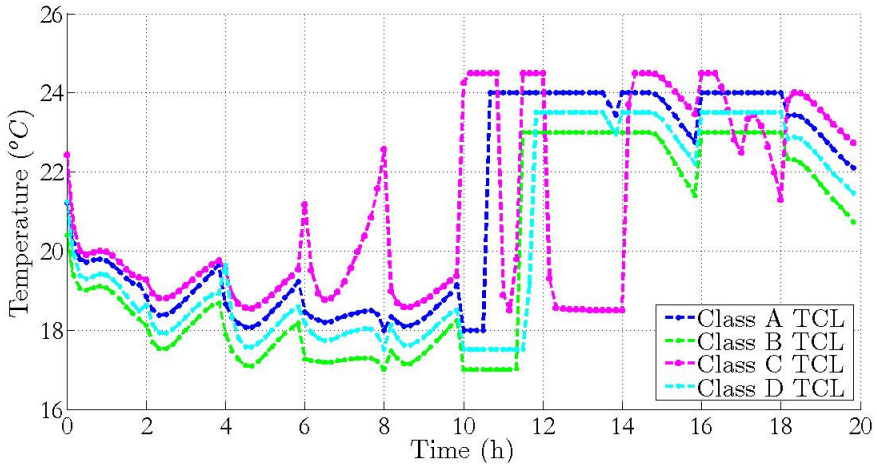

Figure 3.13: TCL temperature for the aggregate consumption of Figure 3.12

Figure 3.13 shows the result of the L2 norm fit problem when it comes to the home temperature for four different TCL classes, in order to get the response shown in Figure 3.12. Note the general pattern of pre-cooling the houses in the early off-peak hours and turning-off the air-conditioners in peak times. Furthermore, note that different TCL classes have different thermal models, and are scheduled in different manners by the L2 norm minimization algorithm.

In the final results for this section, we will show the operation of the distribution system with a receding horizon dispatch, and a 1h dispatch horizon. This results in 20 different dispatch schedules within our 20h period of consideration. The results are shown in Figure 3.14. We see that we achieve a zero error between target and realizable dispatch for active power (Figure 3.14a), but occasional errors exist again in the reactive power scheduling (Figure 3.14b).

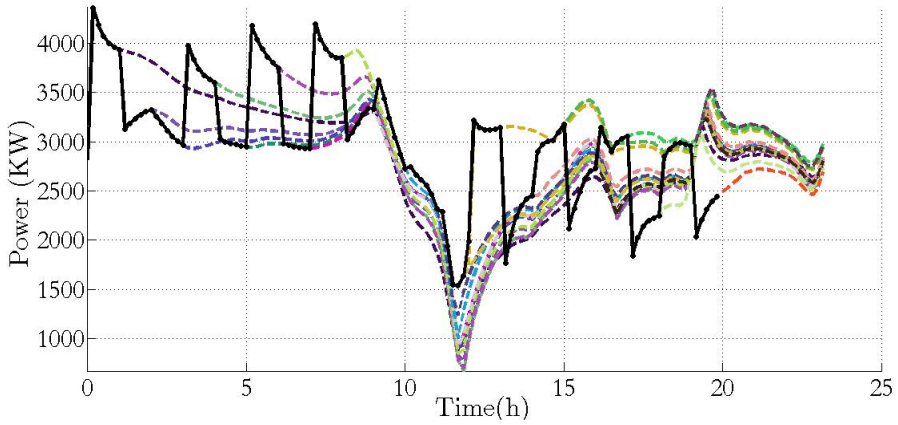

(a)

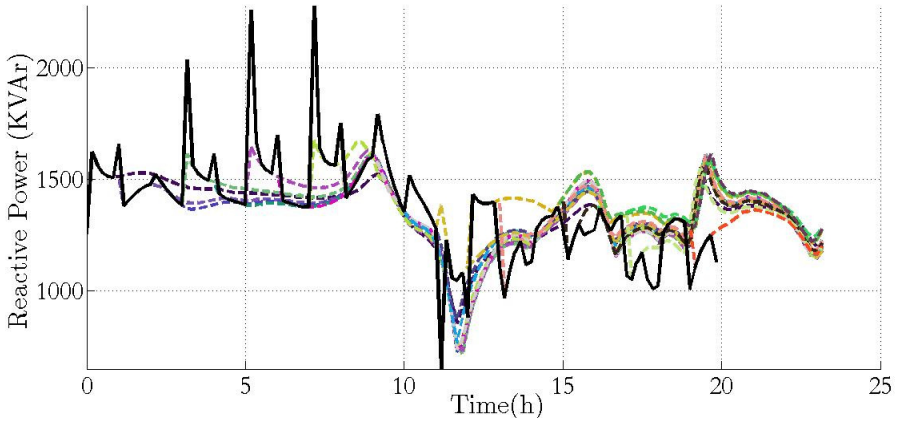

(b)

Figure 3.14: Aggregate Distribution System Scheduling for a 1h Dispatch Horizon

In an effort to explain the operation of this framework, we accompany Figure 3.14 with Figure 3.15. In Figure 3.15 we show the feasible region the approximate aggregate model yields with a dashed black line. The circle shows the look-ahead OPF target consumption, as given by the dashed lines of Figure 3.14, while the square shows the realizable consumption given by the solid black line of Figure 3.14, which is the result of the L2 minimization scheme. Only 12 steps (the first two dispatch horizons) are shown in Figure 3.15.

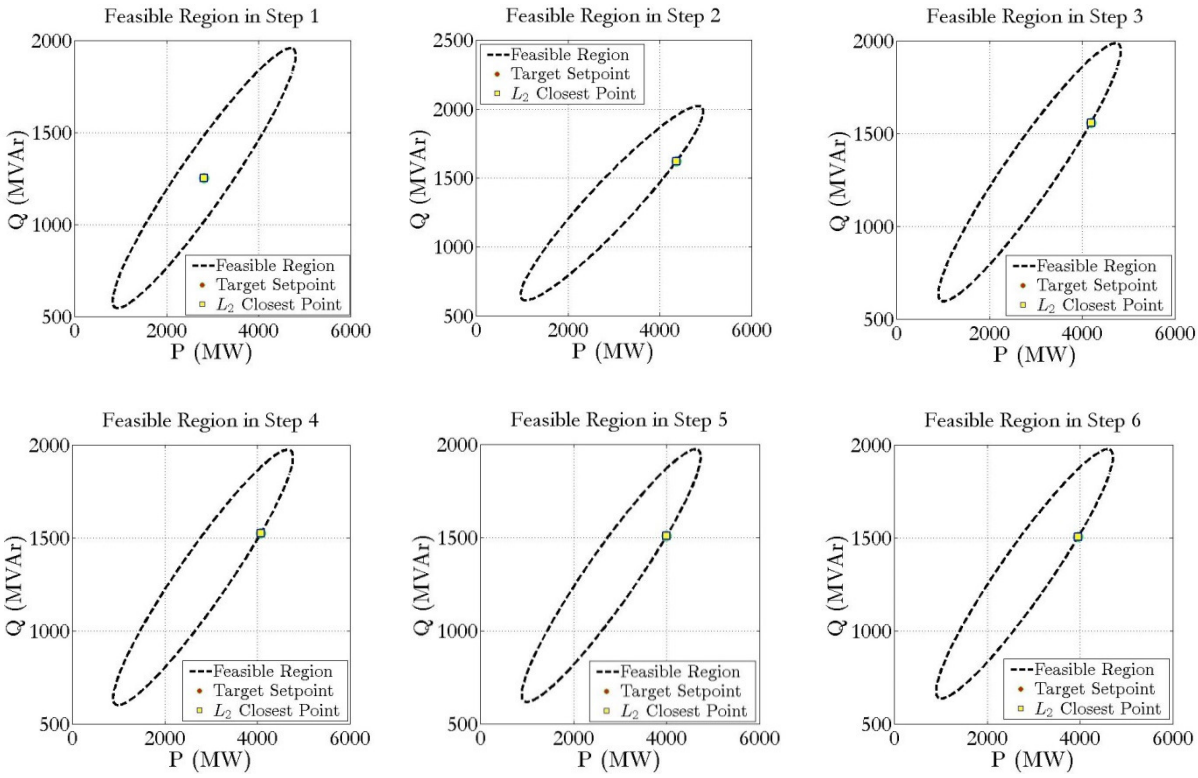

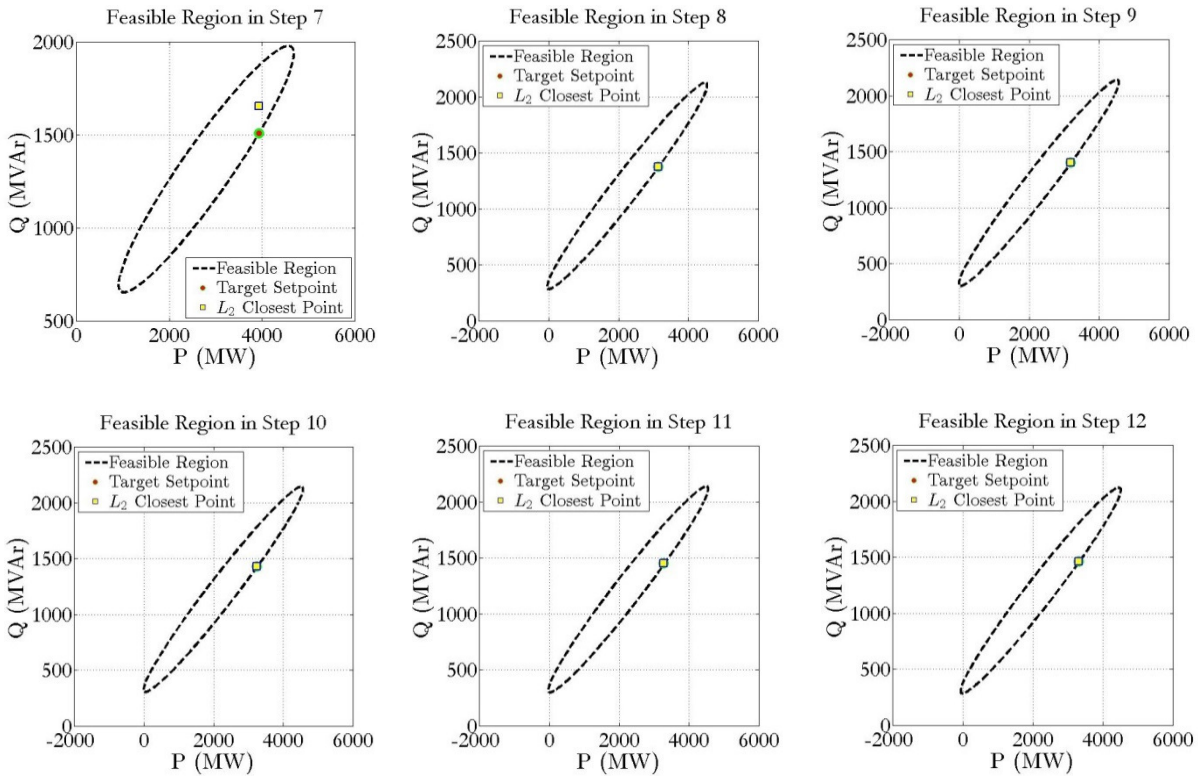

Figure 3.15: Feasible regions of the aggregate model, target consumption & L2 closest consumption per step, for the results of Figure 3.14

It is evident that the two points overlap in most cases, showing a zero error between target consumption and actual consumption, verifying the applicability of the approach. However, in some cases such as step 7, the two points do not overlap, allowing for an error in reactive power consumption, which is also shown in Figure 3.14b.

It should be noted that the following tools were used in this chapter. The L2 norm minimization problem was modeled using YALMIP [33] and the polyhedral feasible regions of distribution systems were obtained using the MPT toolbox [34]. The SDP problem to obtain the parameters for the aggregate modeling of distribution systems was solved using the SDPT solver [35], but the modeling was done using CVX [36] in MATLAB.

4. Company Enterprise Needs

Although the need for this data in operation and control is very sensitive to latency, a much larger set of engineering and business functions need this data not as urgently. Thus, this data needs to be stored in a historical database that can be accessed by many functions and people inside and outside the enterprise.

5. Conclusions & Future Research

5.1 Conclusions

In this research, a real time operations framework for enhancing power system flexibility was presented and modeling of flexible resources was expanded. The following is a summary of the conclusions drawn from this body of work.

With respect to the study of the look-ahead dispatch problem, the AC-OPF and the DC-OPF version of the problem were formulated and studied. It was verified that the AC-OPF version can be substantially more accurate, yielding to decreased costs, mainly due to accurate congestion modeling. However, it was also seen that the DC-OPF is a much more tractable model, with attractive convexity properties, and does not display the sensitivity to initial conditions that is an adverse characteristic of the AC-OPF. This explains its attractiveness for power system operators, who almost exclusively base their operating models on the DC-OPF formulation. While current AC-OPF solvers are not robust enough to justify a transition to AC-OPF look-ahead scheduling, this research provided enough evidence to justify its benefits in terms of producing solutions that are feasible in real time. Furthermore, the proposed AC-OPF formulation is applicable as a necessary operating tool for issues of voltage control which the DC-OPF is incapable of modeling.

As a next step of this research, several models were added to the look-ahead OPF procedure, and their benefits were analyzed. The first model added was a first-order dynamic TCL model for large-scale loads with thermal characteristics and temperature constraints. The resulting analysis showed that, with 15% penetration of thermal loads, cost savings of 0.8% can be achieved simply by scheduling load operation, without violating their temperature constraints. The control did have an adverse effect (increase) in TCL energy consumption, which was around 10%, compared to the non-dispatched case.

Our study of Dynamic Line Ratings resulted in important findings regarding their benefits in multi-step operations algorithms. Specifically, when studying heavily loaded test-cases, it was found that implementing dynamic line ratings in selected critical lines could achieve significant reductions in the amount of load shedding needed to restore feasibility. In many cases, load shedding could be altogether avoided, because critical lines could be temporarily overloaded without violating their temperature constraints. A study of Lagrange multipliers in critical buses showed that dynamic line ratings allow for increased stability in locational marginal prices, by alleviating congestion. The cost benefits of dynamic line ratings, on the other hand, do not seem to be significant. Compared to existing literature, the Thermal Line Model developed here provides a physically-based background for exceeding the very harsh restrictions of static MVA ratings.

In terms of Aggregate Distribution System modeling and controls, a time-dependent ellipsoidal model was developed to capture the time-varying flexibility offered by active Distribution Networks. A model extraction procedure was developed, whereby thousands of small scale DER's were aggregated into a single model by maximizing the resulting feasible region volume. The model's linear nature & unavoidable aggregation gives rise to inaccuracies. However, it was verified that we can obtain a desirable response from aggregate active distribution systems – e.g. curtailed consumption during up-ramps and net load peaks. Also, a

disaggregation algorithm was developed to dispatch the active & reactive consumption targets to each individual distribution-connected device. The aggregation – optimization – disaggregation approach results in a viable hierarchical control scheme and solves the problem of scalability & dimensionality of the look-ahead optimization problem.

5.2 Future Directions

Many open problems associated with this research topic remain open. In the area of AC-OPF formulations, the presented algorithms obviously do not come with global optimality guarantees, and more work should be done towards obtaining a robust look-ahead AC-OPF solver. The benefits for transitioning from the DC-OPF to the AC-OPF have been documented here, but the AC-OPF must reach a maturity level consistent with the operator's current requirements.

In the area of dynamic line ratings, a very important next step would be to design to measurement infrastructure, particularly using PMU data, in order to identify and maintain thermal line models, in order to implement the approach. Dynamic state estimation may be a key element in order to acquire the data required to add dynamic line models to the system's scheduling algorithms. Validation of such models in the field should be an immediate first step, in order for the outlined modeling approach to hold any real value.

Related to aggregate modeling of distribution systems, two areas of research are the most promising: extending the approach to nonlinear models & including the distribution feeder's power flow equations will be important augmentations to the work presented here. It is worth mentioning that the inclusion of all distribution customer models, as well as the feeder three-phase unbalanced power flow equations in the distribution-level optimization will give rise to a formulation with a very large number of constraints and variables. Leveraging high-performance computing methods will be very important in addressing the tractability of this problem. As we suggested in this work, including this level of accuracy of distribution system modeling to the transmission scheduling problem is prohibitive, and aggregate model extraction is of paramount importance.

Furthermore, experimental verification in pilot feeders should be a good first step in demonstrating the applicability of hierarchical optimization. Such a research endeavor would have to cover the very important issues of data acquisition & distribution state estimation, in order to obtain the data and models needed to implement the suggested approach. These issues were not covered in this research, but they are an important area of future research.

In the area of security analysis there is substantial open ground for future research. However, one key element in this topic would be to expand the static security analysis framework that we developed here to dynamic security assessment methods. In many cases, the system may be N-1 secure in terms of static constraints, but it may still be dynamically unstable if a component outage happens. In that case the system is not in a de facto secure state, and thus it does not meet NERC criteria for security. The computational burden for this problem is increased. However, advances in high-performance computing and parallelization, along with decomposition algorithms, should also be leveraged to make such a framework implementable in current real-life systems.

6. Appendix A. Thermal House Model

6.1 A.1. Introduction

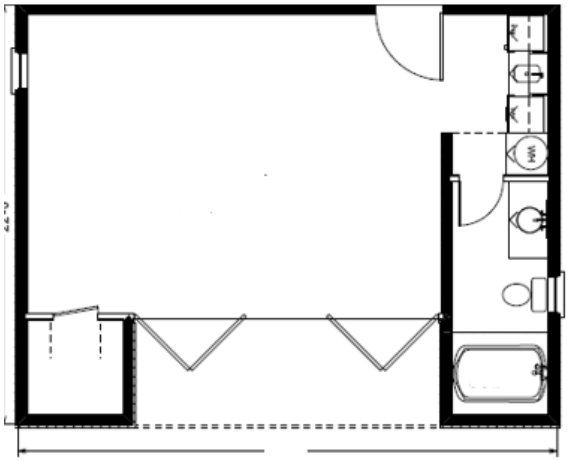

Figure 16.1 Thermal House Model Drawing

This document presents a simplified quadratized electro-thermal model of a house. A quadratized State and Control Algebraic Quadratic Companion Form is derived. As shown in Figure 16.1, the house is modeled as a single – area house with a single air-conditioning source. We assume a **simple constant admittance matrix for the air-conditioner load** (although a motor load should be examined for full detail). The effect of temperature in the efficiency of the air conditioner is also modeled.

A simple first-order model for the house temperature dynamics is assumed, and a constant thermal capacitance and thermal conductance is assumed for the house. The model is assumed to be a "quasi-dynamic" model.

6.2 A.2 Compact Quadratic Form

Here we derive the SCAQCF form of the House Thermal Model

A.2.1 Compact Equations

The device equations in compact form are:

$$\begin{aligned}
&\tilde{\mathbf{I}} = Y\tilde{\mathbf{V}} - h\left[x_s(t) + u(t) - 1/2\right]Y\tilde{\mathbf{V}} \\
&Q = \frac{a}{50}\left(T_a(t) - T_{out}\right)P \\
&P = \mathrm{Re}\left\{\mathbf{V}\mathbf{I}^*\right\} \\
&C\frac{dT_{in}(t)}{dt} = R\left[T_a(t) - T_{in}(t)\right] + Q \\
&x_{s,t} = \left[x_s(t-h) - h(T - T_{high}) + h(T_{low} - T)\right] \\
&0 \le u \le 1
\end{aligned} \tag{34}$$

where:

$\tilde{\mathbf{I}}$	Vector of Current Phasors (A)
$\tilde{\mathbf{V}}$	Vector of Voltage Phasors (V)
Q	Heat Rate (W)
P	Active Power (W)
C	House Thermal Capacitance $Ws/^0C$
R	House – Ambient Thermal Resistance $W/^0C$
$h(x)$	Heaviside step function
$T_{in}(t)$	House indoor temperature
$T_a(t)$	Ambient Temperature
T_{out}	Output air temperature, e.g. 13^0 C.
x_s	$x_s = 0$ if $T_{low} < T < T_{high}$ and T is decreasing
	$x_s = 1$ if $T_{low} < T < T_{high}$ and T is increasing
u	FOPF Control Variable (1: turn OFF AC, 0: AC stays as is)
T_{low}	Thermostat Low Temperature Setting
T_{high}	Thermostat High Temperature Setting

It is worth noting that the efficiency of this AC depends on the difference between the inside and the outside temperature. The control equation is the following:

$$x_{s,t} = \lfloor x_s(t-h) - h(T - T_{high}) + h(T_{low} - T) \tag{35}$$

A.2.2. Quadratized Equations

The quadratized model must look like this

$$i(t) = Y_{eqx1}\mathbf{x}(t) + Y_{equ1}\mathbf{u}(t) + D_{eqxd1}\frac{d\mathbf{x}(t)}{dt} + C_{eqc1}$$

$$0 = Y_{eqx2}\mathbf{x}(t) + Y_{equ2}\mathbf{u}(t) + D_{eqxd2}\frac{d\mathbf{x}(t)}{dt} + C_{eqc2}$$

$$0 = Y_{eqx3}\mathbf{x}(t) + Y_{equ3}\mathbf{u}(t) + \left\{\begin{matrix}\vdots\\ \mathbf{x}(t)^T\left\langle F^i_{eqxx3}\right\rangle\mathbf{x}(t)\\ \vdots\end{matrix}\right\} + \left\{\begin{matrix}\vdots\\ \mathbf{u}(t)^T\left\langle F^i_{equu3}\right\rangle\mathbf{u}(t)\\ \vdots\end{matrix}\right\} + \left\{\begin{matrix}\vdots\\ \mathbf{u}(t)^T\left\langle F^i_{equx3}\right\rangle\mathbf{x}(t)\\ \vdots\end{matrix}\right\} + C_{eqc3}$$

$$\mathbf{h}(\mathbf{x},\mathbf{u}) = Y_{feqx}\mathbf{x} + Y_{fequ}\mathbf{u} + \left\{\begin{matrix}\vdots\\ \mathbf{x}^T\left\langle F^i_{feqxxx}\right\rangle\mathbf{x}\\ \vdots\end{matrix}\right\} + \left\{\begin{matrix}\vdots\\ \mathbf{u}^T\left\langle F^i_{fequu}\right\rangle\mathbf{u}\\ \vdots\end{matrix}\right\} + \left\{\begin{matrix}\vdots\\ \mathbf{u}^T\left\langle F^i_{fequx}\right\rangle\mathbf{x}\\ \vdots\end{matrix}\right\} + C_{feqc}$$

Connectivity: *TerminalNodeName*

$$\textit{subject to}: \quad \mathbf{h}_{\min} \le \mathbf{h}(\mathbf{x},\mathbf{u}) \le \mathbf{h}_{\max}$$

$$\mathbf{u}_{\min} \le \mathbf{u} \le \mathbf{u}_{\max}, \quad \mathbf{x}_{\min} \le \mathbf{x} \le \mathbf{x}_{\max}$$

After the quadratization process, the equations are as follows:

$$\begin{bmatrix} i_{r1}\\ i_{i1}\\ i_{r2}\\ i_{i2}\end{bmatrix} = Y\begin{bmatrix} v_{r1}\\ v_{i1}\\ v_{r2}\\ v_{i2}\end{bmatrix} - \begin{bmatrix} x_1\\ x_2\\ -x_1\\ -x_2\end{bmatrix}$$

$$0 = -C\frac{dT(t)}{dt} + R\left[T_a(t) - T(t)\right] + Q$$

$$0 = Q - \frac{a}{50}\left(T_a(t) - T_{out}\right)P \tag{36}$$

$$0 = x_s(t) - h(T_{low} - T) - \left[h(T - T_{low}) - h(T - T_{high})\right](1-u)x_s(t-h) + u$$

$$0 = P - g\left(v_{r1} - v_{r2}\right)^2 - g\left(v_{i1} - v_{i2}\right)^2 + \left(v_{r1} - v_{r2}\right)x_1 + \left(v_{i1} - v_{i2}\right)x_2$$

$$0 = \begin{bmatrix} x_1\\ x_2\end{bmatrix} - x_s Y\begin{bmatrix} v_{r1}\\ v_{i1}\\ v_{r2}\\ v_{i2}\end{bmatrix} = \begin{bmatrix} x_1\\ x_2\end{bmatrix} - x_s\begin{bmatrix} g(v_{r1} - v_{r2}) - b(v_{i1} - v_{i2})\\ b(v_{r1} - v_{r2}) + g(v_{i1} - v_{i2})\end{bmatrix}$$

where:

$$Y = \begin{bmatrix} g & -b & -g & b \\ b & g & -b & -g \\ -g & b & g & -b \\ -b & -g & b & g \end{bmatrix}$$

The state variables are:

$$x = [v_{r1}, v_{i1}, v_{r2}, v_{i2}, T, Q, P, x_1, x_2, x_s]^T \tag{37}$$

The control variable vector is:

$$u = [u_1] \tag{38}$$

The constraints are:

$$0 \le u_1 \le 1 \tag{39}$$

The matrix assignments are:

Through Variables Equations

$$Y_{eq,x1} = \begin{bmatrix} g & -b & -g & b & 0 & 0 & 0 & -1 & 0 & 0 \\ b & g & -b & -g & 0 & 0 & 0 & 0 & -1 & 0 \\ -g & b & g & -b & 0 & 0 & 0 & 1 & 0 & 0 \\ -b & -g & b & g & 0 & 0 & 0 & 0 & 1 & 0 \end{bmatrix}$$

Linear State Equations

$$Y_{eq,x2} = \begin{bmatrix} 0 & 0 & 0 & 0 & -R & 1 & 0 & 0 & 0 & 0 \\ 0 & 0 & 0 & 0 & 0 & 1 & -\frac{a}{50}(T_a - T_{out}) & 0 & 0 & 0 \\ 0 & 0 & 0 & 0 & 0 & 0 & 0 & 0 & 0 & 1 \end{bmatrix}$$

$$Y_{eq,u2} = \begin{bmatrix} 0 \\ 0 \\ -\left[h(x_5(t-h) - T_{low}) - h(x_5(t-h) - T_{high})\right](-x_9(t-h)+1) \end{bmatrix}$$

$$D_{eq,xd2} = \begin{bmatrix} 0 & 0 & 0 & 0 & -C & 0 & 0 & 0 & 0 & 0 \\ 0 & 0 & 0 & 0 & 0 & 0 & 0 & 0 & 0 & 0 \\ 0 & 0 & 0 & 0 & 0 & 0 & 0 & 0 & 0 & 0 \end{bmatrix}$$

$$C_{eqc2} = \begin{bmatrix} RT_a \\ 0 \\ -h(T_{low} - x_5(t-h)) - \left[h(x_5(t-h) - T_{low}) - h(x_5(t-h) - T_{high})\right]x_9(t-h) \end{bmatrix}$$

Nonlinear State Equations

$$Y_{eq,x3} = \begin{bmatrix} 0 & 0 & 0 & 0 & 0 & 0 & 1 & 0 & 0 & 0 \\ 0 & 0 & 0 & 0 & 0 & 0 & 0 & 1 & 0 & 0 \\ 0 & 0 & 0 & 0 & 0 & 0 & 0 & 0 & 1 & 0 \end{bmatrix}$$

$F^7_{eq,xx3}(0,0) = -g$

$F^7_{eq,xx3}(1,1) = -g$

$F^7_{eq,xx3}(2,2) = -g$

$F^7_{eq,xx3}(3,3) = -g$

$F^7_{eq,xx3}(0,1) = 2g$

$F^7_{eq,xx3}(2,3) = 2g$

$F^7_{eq,xx3}(0,7) = 1$

$F^7_{eq,xx3}(2,7) = -1$

$F^7_{eq,xx3}(1,8) = 1$

$F^7_{eq,xx3}(3,8) = -1$

$$F^{8}_{eq,xx3}(0,9) = -g$$

$$F^{8}_{eq,xx3}(1,9) = b$$

$$F^{8}_{eq,xx3}(2,9) = g$$

$$F^{8}_{eq,xx3}(3,9) - b$$

$$F^{9}_{eq,xx3}(0,9) = -b$$

$$F^{9}_{eq,xx3}(1,9) - g$$

$$F^{9}_{eq,xx3}(2,9) = b$$

$$F^{9}_{eq,xx3}(3,9) = g$$

References

[1] Meliopoulos, A. P., Polymeneas, E., Tan, Z., Huang, R., & Zhao, D. (2013). Advanced distribution management system. IEEE Transactions on Smart Grid, 4(4), 2109-2117.

[2] Meliopoulos, S., Polymeneas, E., & Huang, R. (2015, June). Flexible resource optimization to mitigate operational problems from variable generation. In PowerTech, 2015 IEEE Eindhoven (pp. 1-6). IEEE.

[3] Polymeneas, E., Meliopoulos, S., (2015, July). Aggregate Equivalent Models of Flexible Distribution Systems for Transmission Level Studies. In General Meeting, 2015 IEEE Denver (pp. 1-5). IEEE.

[4] California Independent System Operator (2013). What the duck curve tells us about managing a green grid. Folsom, CA: California ISO. Accessed September 2014: http://www.caiso.com/documents/flexibleresourceshelprenewables_fastfacts.pdf

[5] EirGrid, S. O. N. I. (2011). Ensuring a Secure, Reliable and Efficient Power System in a Changing Environment. A EIRGRID, SONI Report June.

[6] United State Department of Energy (2011). The importance of flexible electricity supply, DOE Solar Integration Series Report, May 2011

[7] Papaefthymiou, G.; Grave, K.; Dragoon, K. (2014), "Flexibility Options in Electricity Systems," ECOFYS report, March 2014

[8] International Energy Agency. (2009). Empowering Variable Renewables-Options for Flexible Electricity Systems. OECD Publishing.

[9] Adams, J., O'Malley, M., & Hanson, K. (2010). Flexibility requirements and potential metrics for variable generation: Implications for system planning studies. Princeton, NJ: NERC.

[10] North American Electric Reliability Corporation (2009). Accommodating High Levels of Variable Generation. Princeton, NJ: NERC., April 2009

[11] D. P. Bertsekas, Nonlinear Programming, 2nd ed. Nashua, NH: Athena Scientific, 1999, pp. 95–97, 397-426.

[12] Wu, Y. C., Debs, A. S., & Marsten, R. E. (1994). A direct nonlinear predictor-corrector primal-dual interior point algorithm for optimal power flows. *Power Systems, IEEE Transactions on*, 9(2), 876-883.

[13] Jabr, R., Coonick, A. H., & Cory, B. J. (2002). A primal-dual interior point method for optimal power flow dispatching. *Power Systems, IEEE Transactions on*, 17(3), 654-662.

[14] Wächter, A., & Biegler, L. T. (2006). On the implementation of an interior-point filter line-search algorithm for large-scale nonlinear programming. *Mathematical programming*, 106(1), 25-57.

[15] Boyd, S., & Vandenberghe, L. (2004). Convex optimization. Cambridge university press.

[16] Zimmerman, R. D., Murillo-Sánchez, C. E., & Thomas, R. J. (2011). MATPOWER: Steady-state operations, planning, and analysis tools for power systems research and education. *Power Systems, IEEE Transactions on*, 26(1), 12-19.

[17] Wang, C., & Shahidehpour, S. M. (1993). Effects of ramp-rate limits on unit commitment and economic dispatch. *Power Systems, IEEE Transactions on*, 8(3), 1341-1350.

[18] Wang, J., Shahidehpour, M., & Li, Z. (2008). Security-constrained unit commitment with volatile wind power generation. *Power Systems, IEEE Transactions on*, 23(3), 1319-1327.

[19] Han, X. S., Gooi, H. B., & Kirschen, D. S. (2001). Dynamic economic dispatch: feasible and optimal solutions. *Power Systems, IEEE Transactions on*, 16(1), 22-28.

[20] Glover, J. D., Sarma, M., & Overbye, T. (2011). Power System Analysis & Design, SI Version. Cengage Learning.

[21] Foss, S. D., Lin, S. H., & Fernandes, R. A. (1983). Dynamic thermal line ratings part I dynamic ampacity rating algorithm. *Power Apparatus and Systems, IEEE Transactions on*, (6), 1858-1864.

[22] IEEE Standard for Calculating the Current-Temperature Relationship of Bare Overhead Conductors," IEEE Std 738-2012 (Revision of IEEE Std 738-2006 - Incorporates IEEE Std 738-2012 Cor 1-2013) , vol., no., pp.1,72, Dec. 23 2013

[23] Douglass, D. A., Lawry, D. C., Edris, A. A., & Bascom, E. C. (2000). Dynamic thermal ratings realize circuit load limits. *Computer Applications in Power, IEEE*, 13(1), 38-44.

[24] Douglass, D. A., & Edris, A. (1996). Real-time monitoring and dynamic thermal rating of power transmission circuits. *Power Delivery, IEEE Transactions on*, 11(3), 1407-1418.

[25] Black, W. Z., & Rehberg, R. L. (1985). Simplified model for steady state and real-time ampacity of overhead conductors. *Power Apparatus and Systems, IEEE Transactions on*, (10), 2942-2953.

[26] Black, M., & Strbac, G. (2007). Value of bulk energy storage for managing wind power fluctuations. *Energy conversion, IEEE transactions on*, 22(1), 197-205.

[27] Ipakchi, A., & Albuyeh, F. (2009). Grid of the future. *Power and Energy Magazine, IEEE*, 7(2), 52-62.

[28] El Ghaoui, L., Feron, E., & Balakrishnan, V. (1994). Linear matrix inequalities in system and control theory (Vol. 15, p. 1). Philadelphia: Society for industrial and applied mathematics.

[29] Vandenberghe, L., Boyd, S., & Wu, S. P. (1998). Determinant maximization with linear matrix inequality constraints. *SIAM journal on matrix analysis and applications*, 19(2), 499-533.

[30] Ben-Tal, A., & Nemirovski, A. (2001). Lectures on modern convex optimization: nalysis, algorithms, and engineering applications (Vol. 2). SIAM.

[31] A. P. Meliopoulos, E. Polymeneas, Zhenyu Tan, Renke Huang, and Dongbo Zhao. (2013). Advanced Distribution Management System. *IEEE Transactions on Smart Grid*, Vol 4, Issue 4, pp 2109-2117, 2013

[32] Fliscounakis, S., Panciatici, P., Capitanescu, F., & Wehenkel, L. (2013). Contingency ranking with respect to overloads in very large power systems taking into account uncertainty, preventive, and corrective actions. *Power Systems, IEEE Transactions on*, 28(4), 4909-4917.

[33] Löfberg, J. (2004, September). YALMIP: A toolbox for modeling and optimization in MATLAB. *In Computer Aided Control Systems Design, 2004 IEEE International Symposium on* (pp. 284-289). IEEE.

[34] Kvasnica, M., Grieder, P., Baotić, M., & Morari, M. (2004). Multi-parametric toolbox (MPT). *In Hybrid systems: computation and control* (pp. 448-462). Springer Berlin Heidelberg.

[35] Toh, K. C., Todd, M. J., & Tütüncü, R. H. (1999). SDPT3—a MATLAB software package for semidefinite programming, version 1.3. Optimization methods and software, 11(1-4), 545-581.

[36] Grant, M., Boyd, S., & Ye, Y. (2008). CVX: Matlab software for disciplined convex programming.